

Influence of Early Bilingual Exposure in the Developing Human Brain

Doctoral dissertation by:
Borja Blanco

Supervised by:
Dr. César Caballero-Gaudes and Dr. Monika Molnar

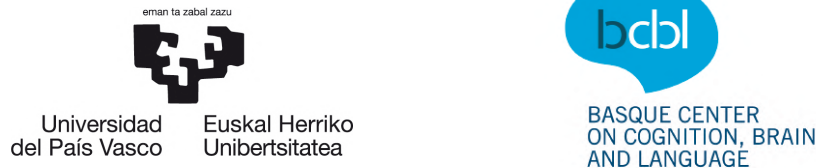


2020

Influence of Early Bilingual Exposure in the Developing Human Brain

Doctoral dissertation by:
Borja Blanco

Supervised by:
Dr. César Caballero-Gaudes and Dr. Monika Molnar



A thesis submitted for the degree of
Doctor of Philosophy (Ph. D.)

Euskal Hizkuntza eta Komunikazio Saila - Euskal Herriko Unibertsitatea
Donostia 2020

Support for this thesis was provided by the Basque Government under the program “Ikertzaile ez doktoreen doktoretza-aurreko formakuntza-programa”. Grant references (PRE-2015_1_0260, PRE-2016_2_0188, PRE-2017_2_0058, PRE-2018_2_0154).

As part of this project, a three-months research stay was conducted at the Biomedical Optics Research Laboratory, University College London (London, UK). This research stay was funded under the program “Egonlabur - ikertzaileak prestatzeko doktoretza-aurreko programako bekak aplikatzeko zentroez bestelakoetan egonaldi laburrak egiteko laguntzak”. Grant reference (EP_2019_1_0026).

I hereby declare that the work presented in this thesis is my own, and where information has been derived from other sources, those sources are credited.

Borja Blanco

Acknowledgments

This journey started almost six years ago, when I was admitted to the Master in Cognitive Neuroscience of Language at the Basque Center on Cognition Brain and Language - BCBL. During these years I have been extremely lucky to interact with the most intelligent, supportive and kind professionals I had ever met, and from which I have learned to be a better scientist, and more importantly a better person. For this reason, I would like to thank all the BCBL family (Admin, IT, Labs and Researchers) for their assistance and encouragement during the development of this research work.

I would like to express my deepest gratitude to my supervisor, Dr. César Caballero-Gaudes, for his knowledge, enthusiasm and patience, and specially for transmitting me his particular way of conducting research, a view that I share and I intend to follow in my future career. I am also extremely grateful to my co-supervisor Dr. Monika Molnar for her expert guidance and support during these years.

I would like to extend my thanks to the DOT-HUB group in University College London, particularly to Dr. Robert J. Cooper from whom I learned a great deal and who I genuinely admire.

Finally, I would like to acknowledge the support provided by my family and friends. Special thanks should be given to Natalia Celestino, for whom this profession and the lifestyle it involves was even more strange than for me, and yet, she has always been by my side becoming my strongest supporter during this process.

Thank you all!

Abstract

Language acquisition is mediated by maturational and experiential mechanisms. It is a remarkably complex process, yet infants show incredible language learning capacities. In a bilingual context this process is even more challenging, since bilingual infants benefit from less day-to-day experience with each language. In addition, they need to perform specific computations such as separating their languages or storing the information of two linguistic inputs. Learning two languages, however, does not negatively affect language acquisition: bilingual infants follow a similar pace to their monolingual peers when main developmental milestones are considered. It has been suggested that bilingualism might elicit cognitive adaptations that allow infants to cope with the increased complexity of their linguistic environment. Distinctive attention allocation skills or an increased perceptual sensitivity are examples of the proposed adaptations. Whether bilingual infants' success is also supported by modulations in the underlying functional systems in charge of these linguistic processes is the question this thesis aims to unravel. This question is addressed using a functional brain imaging technique especially suitable for infant populations: functional near-infrared spectroscopy (fNIRS). This neuroimaging technique offers the potential to study neural activity non-invasively based on cerebral hemodynamics. Because fNIRS is a relatively novel technique to measure infants functional brain activity, the thesis also contains a major methodological component. Particular focus is dedicated to data quality assessment and signal processing.

A series of fNIRS experiments are presented to investigate whether bilingualism might be one factor eliciting experience-induced neural adaptations in 4-month-old infants. First, the brain's functional organization is examined through resting-state functional connectivity. This approach represents a viable strategy to link brain function and cognition, and it offers the potential to simultaneously examine various functional systems. Likewise, functional network activity can be modulated by different prenatal and postnatal conditions. Studying functional connectivity with fNIRS arises some methodological challenges that are inherent to this imaging technique. In particular, whether the fNIRS data preprocessing pipeline should include a step to deal with signal autocorrelation. The second study of this thesis addresses the influence of this step for functional connectivity analyses from a theoretical and empirical point of view. A third study investigates functional differences that might emerge during spoken language processing. Monolingual and bilingual infants' brain responses to speech stimuli are measured to examine the brain areas in support of this cognitive process. The results of these experiments are presented.

Investigating the impact of bilingual exposure on how the brain works, prior to infants even beginning to babble, has remarkable theoretical implications for the field of language acquisition, which had long suspected that brain reorganization for linguistic exposure may begin in-utero, but certainly in the first months of life. This thesis also provides several methodological advancements confirming the suitability of fNIRS imaging for accurately and reliably assessing brain function in developmental populations. The importance of the theoretical and methodological implications of the findings of this thesis are discussed, as is the relevance of transparent and replicable research methodologies for future works in developmental cognitive neuroscience.

Table of Contents

Preface	1
Chapter 1. Bilingual Language Acquisition in Infancy	3
1.1. Language Acquisition in Monolingual and Bilingual Contexts	4
1.2. Neurophysiological Correlates of Bilingual Adaptation	8
1.3. Cognitive and Functional Adaptations Beyond Language	10
1.4. Hypotheses for the Bilingual Adaptation	12
Chapter 2. Fundamentals of Functional Near-Infrared Spectroscopy	15
2.1. Functional Near-Infrared Spectroscopy - fNIRS	16
2.2. fNIRS Signal Processing	24
2.3. fNIRS in Infant Research	28
2.4. Advantages, Limitations and Challenges of fNIRS	31
Chapter 3. Resting-State Functional Connectivity in 4-Month-Old Monolingual and Bilingual Infants	37
3.1. Theoretical Motivation	38
3.2. Methods	43
3.3. Results	51
3.4. Discussion	57
3.5. Summary	60
Chapter 4. Statistical Challenges in Resting-State fNIRS Data Analysis	61
4.1. Theoretical Motivation	62
4.2. Methods	63
4.3. Results	70
4.4. Discussion	77
4.5. Summary	80
Chapter 5. Hemodynamic Correlates of Speech Processing in Bilingual and Monolingual Infants	81
5.1. Theoretical Motivation	82
5.2. Methods	88
5.3. Results	100
5.4. Discussion	106
5.5. Summary	112
Conclusions and Future Work	113
Resumen	117
Appendix A. fNIRS Data Quality Assessment	123
Appendix B. Supplementary Materials Chapter 3	133
Appendix C. Supplementary Figures Chapter 5	149
Bibliography	155

Preface

This thesis is divided into five chapters. The first chapter describes the initial steps of language acquisition during the first year of life in monolingual and bilingual contexts. It establishes the theoretical framework of this thesis, where the presence of bilingualism induced functional brain adaptations are investigated in prelinguistic 4-month-old infants. This chapter reviews existing studies investigating potential behavioural and neural markers of functional adaptations due to an early bilingual experience, and discusses current hypotheses for the potential adaptations that might aid bilingual infants reaching the linguistic milestones at the same pace as their monolingual peers.

The second chapter contains a description of the fundamental principles of the neuroimaging technique employed in the experiments of this thesis, functional near-infrared spectroscopy (fNIRS). The biological basis and the physical principles of this technique are explained, and information about the main steps of the fNIRS signal preprocessing pipeline is provided. A brief literature review on the application of this technique to measure functional brain activity in developmental populations is presented, and the main advantages, limitations and challenges of this technique for its application to infant research are described.

The third chapter examines the effect of an early bilingual exposure on the functional organization of the infant's brain. Behavioural and neuroimaging research attests that monolingual vs. bilingual experience affects cognitive and functional processes already during the first months of life. However, to what extent the intrinsic organization of the infant human brain adapts to monolingual vs. bilingual environments is unclear. In the study presented in this chapter spontaneous hemodynamic brain activity is measured using fNIRS in 4-month-old monolingual and bilingual infants. The final sample includes 99 infants with high-quality data. By implementing state-of-the-art methods for studying functional brain connectivity, the functional organization of the infant brain in large scale cortical networks is described based on fNIRS data, and compared across monolingual and bilingual infants for the first time. Results at the group level revealed functional connectivity networks and components that are consistent with previous literature on functional brain networks in adult and infant populations obtained with other functional neuroimaging modalities, such as functional magnetic resonance imaging. Statistical comparisons between experimental groups reveal no significant differences as a function of language background. Since functional connectivity differences as a function of language background have only been observed in adult populations, this work paves the way for future investigation on the impact of bilingualism on functional brain organization at different stages in development.

Chapter four is a methodological chapter which examines specific statistical challenges of resting-state fNIRS data analysis. In particular, the implications of fNIRS signal autocorrelation for resting-state functional connectivity studies is discussed. This feature of the fNIRS signal is mainly originated by the high sampling frequency of the instruments measuring the signal, and the presence of physiological components related to respiration or cardiac pulse which coexist with the hemodynamic signal of interest. Since the high autocorrelation of the fNIRS signal substantially increases false positive rates,

various methods have been proposed to remove it during data preprocessing. Nevertheless, a detailed evaluation of the implications of applying these methods in fNIRS functional connectivity studies is not available yet. The results of this study show that fNIRS signal autocorrelation can be effectively removed employing prewhitening methods proposed in the literature. Yet, compared with standard preprocessing pipelines, the application of prewhitening methods substantially alters several fundamental neurophysiological properties of the fNIRS signal. These results confirm that more research is needed before mainstream addition of this step into the resting-state fNIRS data preprocessing pipeline.

Chapter five shifts from resting-state to a task-based study in order to investigate the hemodynamic correlates of speech processing in 4-month-old bilingual and monolingual infants using fNIRS. The main goal of this study is to examine how early linguistic experience modulates infants' brain responses to speech stimuli. By testing bilingual and monolingual infants in their shared native language (Spanish), it is assessed whether bilinguals' language experience might elicit neural adaptations that are manifested as dissimilar patterns of early language processing in the brain. An optimized stimulus presentation procedure is implemented in order to efficiently detect brain areas activated by the presentation of speech stimuli, and to accurately estimate the shape of the corresponding hemodynamic response, as well as being able to capture a large number of trials per participant. This optimized experimental design is combined with a large sample of 58 participants. The analyses including the whole group of participants show brain activation patterns over bilateral perisylvian areas classically associated to auditory and language processes. Significant differences between monolingual and bilingual infants are observed, primarily over bilateral auditory regions. These results suggest that early bilingualism might elicit functional adaptations for speech processing, thus confirming the hypotheses anticipated by previous behavioural studies. Nonetheless, these results should be cautiously interpreted, as the observed effects are relatively weak in terms of the statistical procedures applied for multiple comparisons correction.

The last chapter draws the main conclusions of the thesis, framing and linking the different studies, and discusses prospective research directions from the current work.

Finally, in this thesis particular emphasis is drawn to various practical aspects to consider when performing fNIRS studies in infant populations, such as sample size, data quality assessment or recording duration (or number of analysed trials). From a signal processing point of view, several novel and advanced methods for fNIRS data preprocessing and analysis are implemented, such as global signal regression or threshold-free cluster enhancement. Practical materials consisting on Matlab scripts and figures are included throughout the thesis and in Appendix which aim to provide a simple description of the implementation of these methods in order to facilitate their adoption by fNIRS researchers.

Chapter 1

Bilingual Acquisition in Infancy

1.1. Language Acquisition in Monolingual and Bilingual Contexts

To understand the different linguistic milestones across monolingual and bilingual infants, it is important to mention the specific characteristics and challenges faced by infants raised in a bilingual context (Werker, 2012; Byers-Heinlein and Fennell, 2014; Costa and Sebastián-Gallés, 2014; Höhle et al., 2020). The monolingual vs. bilingual experience differs at least in two ways: (i) *amount of exposure* to one language is expected to be less in bilinguals than in monolinguals; (ii) *exposure to the linguistic variability* is expected to be higher in bilinguals than in monolinguals (e.g., Costa and Sebastián-Gallés, 2014). In terms of the amount of exposure, while the total exposure to language is expected to be similar in monolingual and bilingual contexts, it is likely that the experience with each of the languages is reduced in a simultaneous bilingual environment. This is because bilingual infants need to split their exposure time between two linguistic inputs (e.g., if one parent speaks in one language to the infant and the other parent in another language), with the amount and percentage of exposure to each language consequently eliciting some inherent variability within bilingual experiences (e.g., balanced vs. unbalanced bilinguals). Assuming that learning the particular characteristics of a language (e.g., phonemes, words, grammar) requires a certain amount of exposure to that particular language, it might be reasonable to expect that monolingual infants will follow a faster learning trajectory, as they are exposed to just one linguistic code instead of two.

In terms of linguistic variability, the bilingual input contains a higher variability of linguistic regularities. First of all, bilingual infants will probably encounter language switches more regularly in their environment, and also across the same speakers (Byers-Heinlein, 2013). The proficiency on each of the languages of the adults surrounding the infant might further increase the perceptual variability in bilingual infants' environment, as it has been demonstrated that the production of speech sounds by bilingual adult speakers might differ from the formal realization of these sounds by adult monolingual speakers (Sundara et al., 2006; MacLeod et al., 2009). Second, bilingual infants are exposed to more linguistic variability, because their input consists of phonemic categories, lexical items, and syntactic regularities of two languages (Costa and Sebastián-Gallés, 2014).

Despite the above-described differences across the monolingual and bilingual inputs, language acquisition trajectories are not fundamentally different between monolingual and bilingual infants (e.g., Burns et al., 2007; Sundara et al., 2008; for a review see Werker, 2012), which suggests that specific cognitive and/or functional adaptations might take place during the bilingual learning process that help infants compensate the apparent increased learning complexity of the bilingual input. In the upcoming sections of this Chapter, three early language acquisition abilities that have been widely researched across monolingual and bilingual infants during the first year of life are described: (i) language discrimination, (ii) audio-visual speech processing and (iii) phonetic category learning. Reviewing these abilities will highlight the similarities and differences between a monolingual and a bilingual language acquisition. Whether specific computations during bilingual language learning might impact cognitive functions outside the language domain will also be discussed in the next sections of this Chapter.

Language Discrimination

In order to build an accurate representation of the two languages of their environment, bilingual infants first need to notice the presence of two linguistic codes and be able to separate the information they received from each of them (Byers-Heinlein and Fennell, 2014); a specific computation that is not required for infants in a monolingual context. As part of this process, bilingual infants need to learn the properties (e.g., phonological, rhythmical) and rules (e.g., phonotactical, grammatical) of two native languages instead of one, and store the information (e.g., lexicon) of each linguistic code without confusing them (Costa and Sebastián-Gallés, 2014). The peripheral auditory system becomes functional at around 24-28 weeks of gestation, implying that the acquisition of several properties of the native language start while still in the utero (Graven et al., 2008; Jardri et al., 2008). After several weeks of experience, infants are born with established perceptual biases towards, for example, their native language (Moon et al., 1993) or their mother's voice (deRegnier et al., 2000). How this prenatal and postnatal listening experience shapes the cognitive and functional basis of language acquisition in monolingual and bilingual infants is the focus of the current thesis.

Literature on early language discrimination is reviewed in Chapter 5, thus only a brief summary is provided in this Chapter. Language discrimination is a fundamental aspect of language acquisition, especially for bilingual infants who in order to successfully acquire their two native languages must learn to separate them from the start. One of the aspects in which young infants rely the most to perform this distinction is on linguistic rhythm (e.g., Gervain et al., 2010). Traditionally, languages have been categorized into three rhythmic classes based on the duration of specific linguistic units in a particular language (i.e., isochrony principle). For example, stress-timed languages such as English or Dutch show a constant duration between consecutive stressed syllables. On the other hand, languages such as Spanish or Italian are considered syllable-timed languages, as syllable duration is roughly similar in these languages. Lastly, the linguistic unit of equal duration in mora-timed languages such as Japanese is the mora, which is a measure of syllable weight (light-short, heavy-long).

At birth, monolingual infants are able to discriminate between two rhythmically different languages (e.g., Spanish and English), showing a behavioural preference for the one that is familiar to them (Mehler et al., 1988; Moon et al., 1993; Ramus et al., 2000). To perform this distinction, newborns seem to predominantly rely on the rhythmic properties of the language, as it has been demonstrated that they succeed even when presented with low-pass-filtered speech samples, an acoustic modification that only maintains the rhythmical properties of the language (Nazzi et al., 1998). Newborns growing up in a bilingual environment are also capable to perform this distinction, without no preference for any of the two native languages to which they were prenatally exposed (Byers-Heinlein et al., 2010). In another study specifically assessing prosodic grouping preference at birth (Abboub et al., 2016), French monolingual infants showed higher activation responses towards an inconsistent, as compared to a consistent, prosodic cue relevant in French (i.e., durational contrasts), but not to other prosodic cues less salient in this language

(i.e., intensity and pitch). On the other hand, bilingual infants (French and another language) displayed higher activation responses for inconsistent pitch contrasts. This study demonstrated the importance of linguistic rhythm during early language acquisition, and how early prosodic grouping biases can be modulated by prenatal language exposure (Abboub et al., 2016). The ability to discriminate rhythmically similar languages (e.g., Spanish and Italian) is developed at a later age (around 4 months of age) in both monolingual and bilingual infants, although each of these groups seems to rely on different mechanisms to perform this distinction (Bosch and Sebastián-Gallés, 1997; Bosch et al., 2001; Molnar et al., 2014; Nácar-García et al., 2018; see also Chapter 5).

Further evidence of early language discrimination capacities stems from studies of visual language discrimination. In these studies, infants' language discrimination capacities are assessed while watching silent videos of speech stimuli, that is, without auditory information, relying on visual cues from speakers' faces only. Monolingual infants at 4 and 6, but not at 8 months of age were able to visually discriminate two languages from stimuli consisting of silent speech videos (English-French, Weikum et al., 2007; Spanish - Catalan, Sebastián-Gallés et al., 2012). In turn, only bilingual infants preserved the capacity to visually discriminate languages at 6 and 8 months of age (Weikum et al., 2007), even when the languages being tested were not part of the bilingual infants' linguistic environment (Sebastián-Gallés et al., 2012). Overall, these studies demonstrated that monolingual and bilingual infants display similar language discrimination capacities, but particular mechanisms supporting this ability might be modulated by the bilingual input.

Audiovisual Speech Processing

How infants take advantage of relevant audio-visual cues during language acquisition is a research topic that has also attracted great interest. Using eye-tracking techniques several studies have assessed infants' scanning and looking patterns while listening and watching videos of talking faces. Studies on this topic revealed that 4-month-old infants focus their attention primarily on the eye area (Lewkowicz and Hansen-Tift, 2012). At 8 months of age the looking pattern changes, with infants showing increased interest towards the speaker's mouth, which has been interpreted as probably assisting the onset of canonical babbling taking place around this age. At 12 months of age, the primary area of interest appears to change again to the eyes (Lewkowicz and Hansen-Tift, 2012). This change in the looking pattern has been suggested to reflect the increased interest on social communicative information in older infants', which is principally expressed around the eye region. Conversely, other works reported a sustained attention to the speaker's mouth in 1-year-old infants (Frank et al., 2011; Tenenbaum et al., 2013; Tsang et al., 2018), and a positive relationship between this looking pattern and concurrent expressive language development (Tsang et al., 2018).

Some works investigated the potential relationship between infants' scanning patterns for dynamic talking faces and their language background. At 4 months of age, and as opposed to monolinguals (Spanish or Catalan) in which a preference towards the eyes was replicated, studies with bilingual infants (Spanish and Catalan) have not demonstrated a preference for the eyes or the mouth. At 8 and 12 months of age bilingual infants

Bilingual Language Acquisition in Infancy

displayed a marked preference for the mouth, and they did so equally for a native and a non-native language (Pons et al., 2015). Instead, monolingual 12-month-old infants' preference towards the mouth was higher only for the non-native language. Similarly, Spanish-Catalan bilingual infants also showed longer looking patterns to the mouth area in a study using a paradigm involving videos of emotional faces without speech (Ayneto and Sebastián-Gallés, 2017). Altogether, these results might indicate the need of bilingual infants to rely on additional audio-visual cues to successfully separate and learn the specific characteristics of their native languages. However, an effect of language background was not observed in a recent study involving similar tasks (i.e., emotional faces and dynamic talking faces), and which assessed the scanning patterns of 6- and 12-month-old monolingual (English) and bilingual (English and another language) infants (Tsang et al., 2018).

Acquisition of Native Phoneme Categories

Besides being able to distinguish languages based on rhythmic information, infants are also born with the ability to discriminate between a wide variety of speech sound contrasts, independently of whether these distinctions are linguistically relevant in their native or in a non-native language. During the second half of the first year of life, after some months of listening experience, infants become progressively attuned to the speech sounds and phonetic properties of their native language/s. Conversely, their sensitivity to non-native contrasts decreases, an input-driven learning process also known as perceptual narrowing (e.g., Werker, 2018). This trajectory seems to be also influenced by the perceptual salience of the assessed contrast, with the distinction of subtle speech contrasts requiring an increased exposure to the native language (Larraza et al., 2020). Studies assessing perceptual attunement in monolingual infants demonstrated an improved sensitivity towards the sounds of their native language starting at around 6-10 months of age, depending on the frequency distributions and complexity of the employed contrasts (e.g., Kuhl et al., 2006; for a review see Werker, 2018). Monolingual infants' perceptual attunement to vowels typically occurs around 6 months of age (e.g., Polka and Werker, 1994), and to consonants it typically occurs around 11 months of age (e.g., Werker and Tees, 1984).

A few studies have investigated whether an early and simultaneous exposure to two phonological systems influences perceptual attunement in bilingual infants. Early studies on this topic suggested a U-shaped developmental trajectory during perceptual attunement in bilingual infants (Bosch and Sebastián-Gallés, 2003, Sebastián-Gallés and Bosch, 2009). Converging evidence from studies testing Spanish and Catalan monolingual and Spanish-Catalan bilingual infants on different phonetic distinctions (i.e., vowel contrasts) showed that 4-month old infants were able to detect these distinctions, irrespective of their language background. At 8 months of age, only monolingual infants maintained the sensitivity to distinguish the presented vowel contrasts. Whereas bilingual infants at 12 months of age recovered the capacity to perceive these contrasts. These results suggested that the development of phonetic discrimination capacities might be affected by language exposure (Bosch and Sebastián-Gallés, 2003, Sebastián-Gallés and Bosch, 2009). Contrary to these findings, several works have shown that the developmental trajectory of phonetic

discrimination is essentially the same in monolingual and bilingual infants, both groups demonstrating the ability to perceptually discriminate speech sound contrasts of their native language/s at a similar pace, but bilingual infants developing this ability for two parallel phonological systems (Burns et al., 2007; Sundara et al., 2008; Albareda-Castellot et al., 2011). Studies that have examined the functional mechanisms underlying perceptual sensitivity to speech sound contrasts across monolingual and bilingual infants are reviewed in the next section of this Chapter.

1.2. Neurophysiological Correlates of Bilingual Adaptation

A few neuroimaging studies have investigated the potential functional adaptations that might emerge in the developing brain as a consequence of growing up in a bilingual environment. Studies specifically related to speech processing (Nácar-García et al., 2018; Mercure et al., 2020) are described in detail in Chapter 5 of this thesis. In these studies, bilingual infants demonstrated different neural specialization responses during a language discrimination task (i.e., native vs. non-native) (Nácar-García et al., 2018), as well as dissimilar patterns of activated brain regions towards speech stimuli (Mercure et al., 2020).

Measuring event related potentials (ERPs) with electroencephalography (EEG) in English-Spanish bilingual 19- to 22-month-old infants, Conboy and Mills (2006) examined the brain's response to known and unknown words in each of their native languages, and investigated whether these responses were linked with the level of experience in each language (i.e., here determined by vocabulary size). Although this study lacked a monolingual group for comparisons, results were compared with previous studies using the same experimental paradigm with age-matched English monolingual infants (Mills et al., 1993; Mills et al., 1997). In bilingual infants, earlier ERP differences to known vs. unknown words were observed for the dominant language, and were also associated with a higher vocabulary size. The spatial distribution for the ERP effects was broadly distributed across hemispheres, contrasting with previous studies showing a focalized pattern over temporal and parietal regions of the left hemisphere in monolingual infants at this age. Results from this study confirmed that experience and language proficiency modulate the organization of neural systems involved in word recognition. This work also provided the first evidence of a differential resource allocation system related to a simultaneous bilingual experience from birth, which was revealed by the distributed patterns of brain activation and the higher involvement of right hemispheric regions in these infants.

Based also on EEG recordings, a series of studies have measured mismatch responses (MMRs) to vowel contrasts (English) in English monolingual and English-Spanish bilingual infants, and assessed the role of language experience in the exhibited brain response patterns (Shafer et al., 2011; Shafer et al., 2012). The development of discrimination responses followed a similar trajectory across monolingual and bilingual infants, except at 6 months of age, where a higher sensitivity to the language contrasts was observed in bilingual females (Shafer et al., 2011). To elucidate whether a higher attention to the speech sounds might have mediated these outcomes, the same contrasts were tested in a new group of 6-month-old monolingual and bilingual infants, but varying the position of the contrasts within the stimuli sequence (Shafer et al., 2012). When attention to stimuli

Bilingual Language Acquisition in Infancy

was specifically controlled no differences emerged due to language experience, which indicates that monolingual and bilingual infants at this age rely on comparable cognitive systems when processing speech sounds.

Considering a sample of English-Spanish bilingual infants, García-Sierra et al., (2011) tried to replicate the results of a speech sound discrimination study with monolingual infants (English) at 7 and 11 months of age (Rivera-Gaxiola et al., 2005). In this earlier study, monolingual 7-month-old infants showed discriminative ERP responses for consonant contrasts in both familiar and unfamiliar languages, whereas 11-month-old infants only showed discriminative responses for the familiar language, with a more similar pattern to adults. In contrast, García-Sierra et al., (2011) showed that bilingual infants in the younger group (6-9 months of age) did not display discriminatory responses for any of the native contrasts, whereas neural discrimination for both contrasts was observed in the older group (10-12 months of age). As demonstrated by behavioural studies (Bosch and Sebastián-Gallés, 2003, Sebastián-Gallés and Bosch, 2009), these outcomes can be explained by the effect of a reduced language experience, which might increase the time required by bilingual infants to attune to the specific phonetic contrasts of each of their native languages (Kuhl et al., 2008; Byers-Heinlein et al., 2014).

Indeed, the relationship between the amount of language input in the tested language and the amplitude and direction of the MMR (indicators of the degree of perceived difference) was further investigated in García-Sierra et al. (2016) in 11- to 14-month-old monolingual (English) and bilingual (English-Spanish) infants. Results for the native contrasts replicated the previous study (García-Sierra et al., 2011), with monolingual infants showing the expected responses denoting neural commitment towards the sounds of their native language (i.e., negative MMR). Bilingual infants, even those with higher levels of exposure to one of the languages, showed ERP responses (i.e., positive MMR) indicative of a less mature form of linguistic processing. Positive MMRs have been interpreted as being more closely related with lower level attention and acoustic discrimination processes preceding the automatic speech perception response elicited by phonemic representations of the native phonology (i.e., negative MMR). In both groups, the level of neural commitment to the language, as measured by the amplitude and direction of the MMR, was related with the amount of language input or exposure time, which was quantified by means of the Language Environment Analysis System (LENA foundation, Boulder Colorado). This analysis also revealed that the neural responses in the bilingual group were comparable to the neural responses of those monolingual infants regularly receiving a lower language input (García-Sierra et al., 2016).

Similar brain responses towards a native contrast (i.e., negative MMR in English monolingual infants, positive MMR in English-Spanish bilingual infants) have been demonstrated using magnetoencephalography (MEG), a neuroimaging technique that allows a more precise localization of the cortical origin of the observed effects (Ferjan-Ramirez et al., 2017). Interestingly, the origin of the neural responses in monolingual infants was localized over bilateral frontal areas, whereas in bilingual infants the observed neural responses were limited to left auditory regions. The spatial localization of the

responses in each group provided support for the hypothesis arguing that negative MMRs in monolingual infants represent a more complex form of cognitive processing related to language specific memory representations, while positive MMRs in bilingual infants imply a process predominantly based on the acoustic properties of the presented stimuli.

Phonetic processing has been further assessed in monolingual and bilingual infants using functional near-infrared spectroscopy (fNIRS), the neuroimaging technique that has been employed in the studies of this thesis and which will be described in the next Chapter. Concretely, monolingual (English) and bilingual (English-another language) infants were exposed to native (English) and non-native (Hindi) phonetic units and nonlinguistic pure tones (Petitto et al., 2012). Two age groups (younger 4- and older 12-month-old infants) were considered to assess the developmental time-course of early phonetic processing and discrimination. Speech stimuli activated areas in the left superior temporal gyrus, which remained similar across age and language groups, and the inferior frontal cortex, which showed sensitivity to the experimental manipulation. Specifically, the left inferior frontal region showed higher activation in older as compared to younger infants, and the right inferior frontal region showed the opposite pattern. Furthermore, activity in the left inferior frontal cortex in older monolingual infants was restricted to native phonetic contrasts. However, older bilingual infants showed similar activation in this region to both native and non-native contrasts. These results suggest that an early bilingual experience might be related with a sustained sensitivity, or a protracted perceptual attenuation process, towards relevant linguistic stimuli in the environment (e.g., phonetic contrasts), which is not limited to bilingual infants' native languages (Petitto et al., 2012).

In summary, neuroimaging evidence reveals earlier specialized brain responses towards the native language in monolingual infants. The maturational trajectory of these neural responses appears to be influenced by language experience, with bilingual infants showing less mature responses and/or a prolonged sensitivity towards non-native contrasts in some of these studies. Furthermore, each language group seems to recruit different brain regions during this specialization process.

1.3. Cognitive and Functional Adaptations Beyond Language

One of the most discussed topics in the field of bilingual language acquisition is whether the effects of early bilingualism might extend to other cognitive domains beyond language processing and, accordingly, modulate the underlying neural structures in charge of these processes. Relying on the assumption that bilingual infants continuously monitor and track inputs from the two languages of their environment, a series of studies have reported evidence for a more efficient participation of various mechanisms of executive function, such as attentional control, conflict monitoring or inhibitory control, in bilingual infants (Kovacs and Mehler, 2009a; Kovacs and Mehler, 2009b; Comishen et al., 2019), as compared with their monolingually raised peers.

Two studies used eye-tracking to assess cognitive control abilities in monolingual and bilingual infants at 7 and 12 months of age (Kovacs and Mehler, 2009a; Kovacs and Mehler, 2009b). 7-month-old monolingual and bilingual infants were equally able to learn

Bilingual Language Acquisition in Infancy

the association between the presentation of a speech or visual cue, and the subsequent position of a visual reward in a screen. When the rule changed, altering the position of the visual reward with respect to the learning phase, bilingual infants outperformed their monolingual peers on learning the new association and being able to suppress the previously acquired predictive response, a behaviour that monolingual infants were not able to accomplish (Kovacs and Mehler, 2009a). Older bilingual infants at 12 months of age showed a similar pattern of enhanced learning flexibility (Kovacs and Mehler, 2009b). In the task employed in this study, infants were instructed to learn two speech structure - visual cue associations (e.g., ME-ME-BA speech structure was followed by the presentation of a visual cue on the left side of the screen, and LE-NA-LE speech structure was followed by a visual cue presented on the right side). During test trials after the learning phase bilingual infants provided more accurate responses, determined by their first gaze and looking time, indicating that they were able to learn both associations. Monolingual infants, on the other hand, were only able to learn the association for the simplest speech structure (i.e., AAB). These results were also interpreted as evidence of the enhanced cognitive control abilities on the part of bilinguals (Kovacs and Mehler, 2009b). However, a recent study failed to replicate these findings on a group of 9.5-month-old monolingual and bilingual infants (Tsui et al., 2019).

Using a similar experimental paradigm as in Kovacs and Mehler (2009a, 2009b), 6-month-old monolingual and bilingual infants' attention allocation and control abilities were compared during the performance of two tasks involving non-verbal stimuli (Comishen et al., 2019). In the first task infants were exposed to random cue-target location associations during the first half of the trials, a pattern that changed to predictable associations of the target stimulus for the second half of the experiment. Monolingual and bilingual infants showed a similar capability to generate expectations once predictable relationships between cue and target locations could be established. In the second task, a cue-target location association was learned during the first half of the experiment. The association switched during the second half and was contradictory to the one previously learned. In the second part of this task, where updating previously learned expectations of cue-target relationship was required, only bilingual infants succeeded in anticipating the location of the target stimulus, which authors suggested to reflect their increased abilities for attentional control (Comishen et al., 2019). A recent study attempted to replicate these findings in 7-month-old monolingual and Spanish-Basque bilingual infants, by assessing their attentional control capacities using a similar eye-tracking paradigm (Kalashnikova et al., 2020). This study observed no advantage in bilinguals' performance for attentional control, thus failing to replicate previous outcomes.

Lastly, differences in infants' learning and information processing mechanisms as a result of the bilingual input have also been examined. Singh et al. (2015) employed a visual habituation paradigm to test simple learning capacities in 6-month-old monolingual and bilingual infants. During the habituation phase participants were repeatedly presented with an image stimulus (e.g., a picture of a wolf or a bear). During the test phase, infants' recognition ability was assessed by their looking behaviour, which is associated with a preference towards novel stimuli. Bilingual infants fixated longer on the novel stimulus,

which suggests an advantage on basic information processing for bilingual as compared to monolingual infants, and particularly a more efficient capacity for stimulus habituation and a better visual recognition memory (Singh et al., 2015).

1.4. The Bilingual Adaptation Hypotheses

Overall, the above-reviewed evidence converges towards the idea that linguistic development of typically developing monolingual and bilingual infants is comparable. Nonetheless, various cognitive and functional adaptations that might serve bilingual infants to successfully cope with a challenging context during language acquisition have also been consistently reported. Different, not mutually exclusive hypotheses have been proposed to conceptualize the adaptations induced by an early bilingual environment.

One hypothesis proposes a different developmental transition in the perceptual “sensitive periods” during the attunement process to the characteristics of the native language that supports the early stages of language acquisition (Figure 1.1) (Kuhl, 2010a; Kuhl, 2010b; Werker and Hensch, 2015). During the perceptual attunement process, which might start several weeks before birth (Mampe et al., 2009), infants become specialized in the properties of their native language such as rhythm (Mehler et al., 1988; Moon et al., 1993; Byers-Heinlein, 2010) or phoneme categories (Dehaene-Lambertz and Gliga 2004; Mahmoudzadeh et al., 2011). The timing (i.e., onset, offset and duration) of sensitive periods is largely constrained by the maturation of the underlying neural structures and functional circuits, but linguistic experience seems to play a significant role in this process as well (Peña et al., 2010; Peña et al. 2012; Werker and Hensch, 2015). According to this view, as bilingual infants receive a reduced linguistic input in each of the languages of their environment as compared to monolingual infants, they might experience a more flexible timeline where perceptual sensitive periods extend until sufficient experience with the statistical regularities of each language is gained (Kuhl et al., 2008; Kuhl, 2010a). This hypothesis mainly gained support from phonetic and language discrimination studies in which bilingual infants maintained longer their ability to discriminate speech contrasts (Weikum et al., 2007; Burns et al., 2007; Sundara et al., 2008; Petitto et al., 2012; Sebastián-Gallés et al., 2012), or in which the neural responses to native speech contrasts appeared less mature (García-Sierra et al., 2011; García-Sierra et al., 2016; Nácar-García et al., 2018). Further evidence stems from studies assessing word learning capacities in monolingual and bilingual infants, and which showed that bilingual infants demonstrate a delayed capacity for learning specific word-object associations (Fennell et al., 2007) and a lower vocabulary size in each of their native languages (Poulin-Dubois et al., 2013).

Another hypothesis argues that bilingualism enhances, or at least differentially recruits, cognitive mechanisms outside the language domain such as memory, executive functions or perceptual discrimination abilities, even from the earliest stages of language acquisition (Costa and Sebastián-Gallés, 2014; Kovacs et al., 2015; Bialystok, 2015; Bialystok et al., 2017). These differential or improved capacities might allow bilingual infants to efficiently deal with the conflicting linguistic statistical regularities of their environment, and might also reflect differences in the underlying functional networks

Bilingual Language Acquisition in Infancy

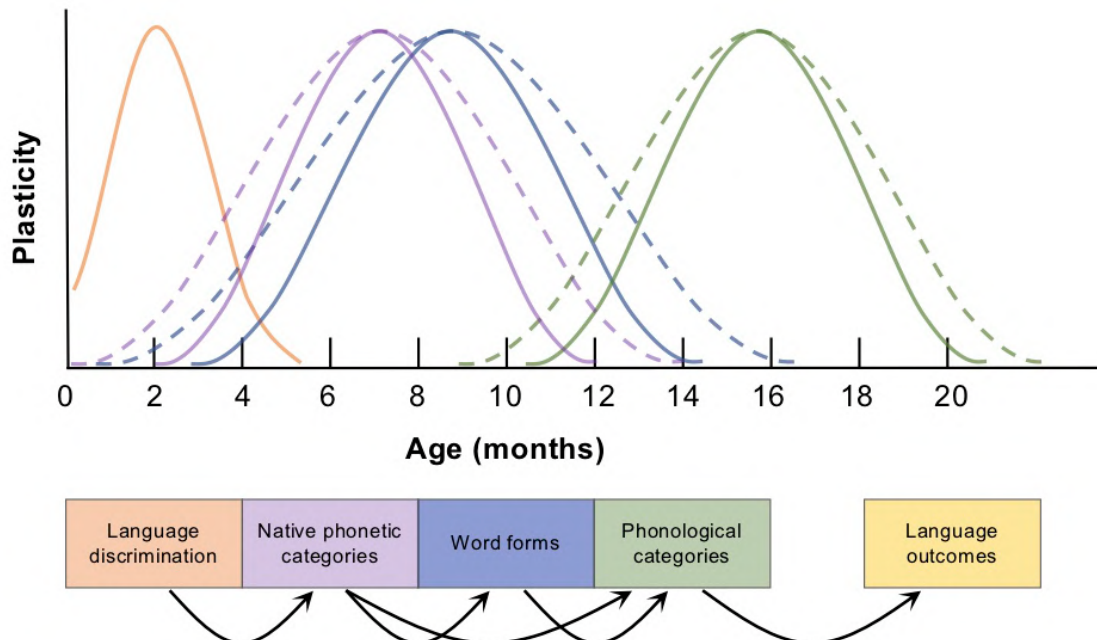


Figure 1.1 Illustration of perceptual sensitive periods during language acquisition (solid curves), and how the timeline of these periods can be modulated by early linguistic experience (e.g., bilingualism) (adapted from Werker and Hensch, 2015).

in charge of these processes. Examples of the reviewed literature that have shown bilingual adaptations in support for this view include the enhanced visual language discrimination abilities (Weikum et al., 2007; Sebastián-Gallés et al., 2012), a differential attention to audio-visual cues during language processing (Pons et al., 2015; Ayneto and Sebastián-Gallés, 2017) or a different allocation of attention during language discrimination tasks (Bosch and Sebastián-Gallés, 1997). Outside the language domain bilingualism has been suggested to improve executive control abilities (e.g., Kovacs and Mehler 2009a;), or to imply a more flexible attention system with a marked preference towards novelty (Singh et al., 2015; Comishen et al., 2019).

Chapter 2

Fundamentals of Functional Near-Infrared Spectroscopy

2.1. Functional Near-Infrared Spectroscopy

Near-infrared spectroscopy (NIRS) is a non-invasive optical imaging technique that uses near-infrared light (650 - 1000 nm) to calculate changes in the optical properties of human tissues, such as the brain or muscles, as result of variations in the concentration and oxygenation state of certain optical absorbers (i.e., chromophores).

The use of NIRS for monitoring brain oxygenation in-vivo was first described by Jöbsis in 1977. Since the scalp and the skull show a high degree of transparency in the NIR spectrum, and the two main chromophores in this range (i.e., oxyhemoglobin - HbO and its reduced equivalent deoxyhemoglobin - HbR) show different absorption spectra, these properties can be conveniently employed to non-invasively track information of blood oxygenation in brain tissues (Jöbsis, 1977). This theory was first probed on animal models, and next on a human subject in which cerebral blood volume changes were measured during voluntary hyperventilation. Results from this work demonstrated the ability of NIRS to detect cerebral vasoconstriction and the progressive reduction of cerebral blood volume during this state (Figure 2.1).

Since this pioneering work the technology and methodology necessary to incorporate NIRS as an advanced imaging modality in neuroscience and clinical research have been under constant development (Villringer and Chance, 1997; Strangman et al., 2002a; Obrig and Villringer, 2003; Elwell and Cooper, 2011; Ferrari and Quaresima, 2012; Obrig et al., 2014; Scholkmann et al., 2014; Pinti et al., 2019). The applicability of NIRS to the study of functional brain activity (functional NIRS - fNIRS) in humans was consolidated in 1993. That year, four independent research groups presented their investigations using fNIRS for the study of different brain functions in international scientific journals (Chance et al., 1993; Hoshi and Tamura, 1993; Kato et al., 1993; Villringer et al., 1993). In these studies, an increase in regional blood supply or local changes in the concentration of HbO and HbR were associated with brain activity during the performance of cognitive tasks (Chance et al., 1993; Hoshi and Tamura, 1993; Villringer et al., 1993), or during visual (Hoshi and Tamura, 1993; Kato et al., 1993; Villringer et al., 1993) and auditory stimulation (Hoshi and Tamura, 1993).

In these first fNIRS studies based on single-channel measurements, mapping of brain activity was limited to the particular cortical region under examination. Nowadays, technological progresses have enabled to simultaneously interrogate multiple cortical regions using multi-channel instruments. Furthermore, the advent of the first wearable high-density diffuse optical tomography systems (HD-DOT) that offer comparable spatial resolution to conventional functional Magnetic Resonance Imaging (fMRI) (Eggebrecht et al., 2012), have broaden the fields of application of fNIRS, consolidating this technique as one of the main non-invasive brain imaging modalities. Nonetheless, all these technologies essentially rely on the same principles: the biological principles governing the physiological phenomena under examination (i.e., neurovascular coupling) and the physical principles describing the interaction of light with biological tissue, both of which are explained in detail below, with emphasis on the specific factors to consider when imaging the infant brain.

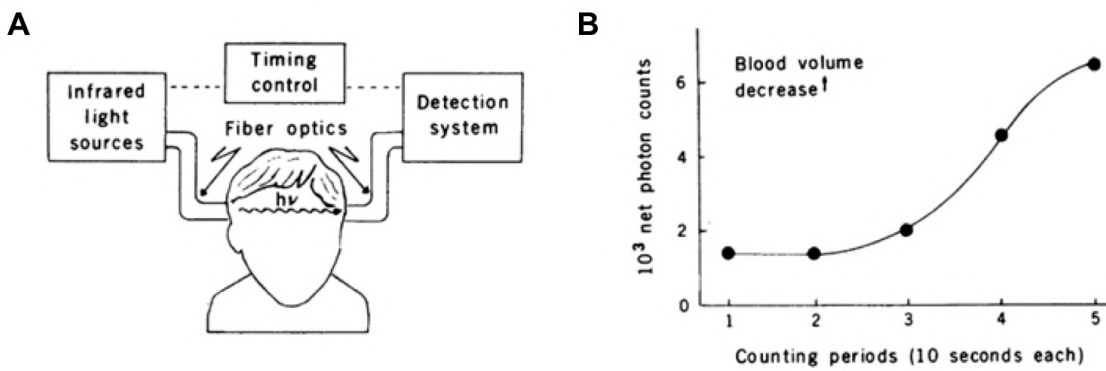


Figure 2.1 A) NIRS experimental setup for the assessment of cerebral hypoxia. B) Blood volume decrease is notable during longer periods of hyperventilation. Note that an increase in the number of photons detected is related with a decrease in absorbance, and therefore a decrease in cerebral blood volume (Adapted from Jöbsis, 1977).

Biological Basis of the fNIRS Signal

Light in the near-infrared (NIR) region of the electromagnetic spectrum (650 – 1000 nm) can be used to monitor changes in hemoglobin concentration and oxygenation in biological tissues. These changes are calculated from variations in the optical properties of the sampled tissue, which in this thesis refer to the head (e.g., scalp, skull and cerebrospinal fluid) and brain tissues, and which are assumed to predominantly result from fluctuations in cerebral and extracerebral hemodynamics. Human tissues such as the scalp or the skull are mostly transparent to NIR light (i.e. they practically do not absorb light in this spectral window), allowing it to penetrate the most superficial layers of the cortex. Other absorbing substances in biological tissues either show a relatively low absorption within the NIR spectral range and a strong absorption of light at other wavelengths (e.g., water and lipids >900 nm, hemoglobin <600 nm), or they are present in comparatively low concentrations (i.e., melanin and cytochrome oxidase). Therefore, any changes in absorption due to these substances are commonly considered negligible (Scholkman et al., 2014).

Conveniently, the main absorbers in the NIR spectral range are HbO and HbR. The absorption spectra of these chromophores in this optical window is significantly different, with an isosbestic point around 800 nm where both show an equivalent absorption coefficient (Figure 2.2). This difference also explains why arterial blood, with higher HbO concentration, presents a bright red color, whereas venous blood, with larger HbR content, appears darker. The simplest NIRS system is formed by a light source, which continuously emits light onto the scalp, and a detector located a few centimeters away, where light attenuation after traversing head tissues (e.g., scalp, skull and cerebral cortex) is measured. The underlying region between a source-detector (SD) pair forms a channel, where changes in the optical properties of tissue (i.e., HbO and HbR chromophore concentration) are examined. Emitting light at two appropriate wavelengths in the “biological window”, and based on the attenuation of NIR light intensity at each wavelength, it is possible to determine the relative concentration changes of HbO and HbR within the sampling volume. Such changes, which reflect the vascular response related to functional brain activation, represent the signal of interest of fNIRS.

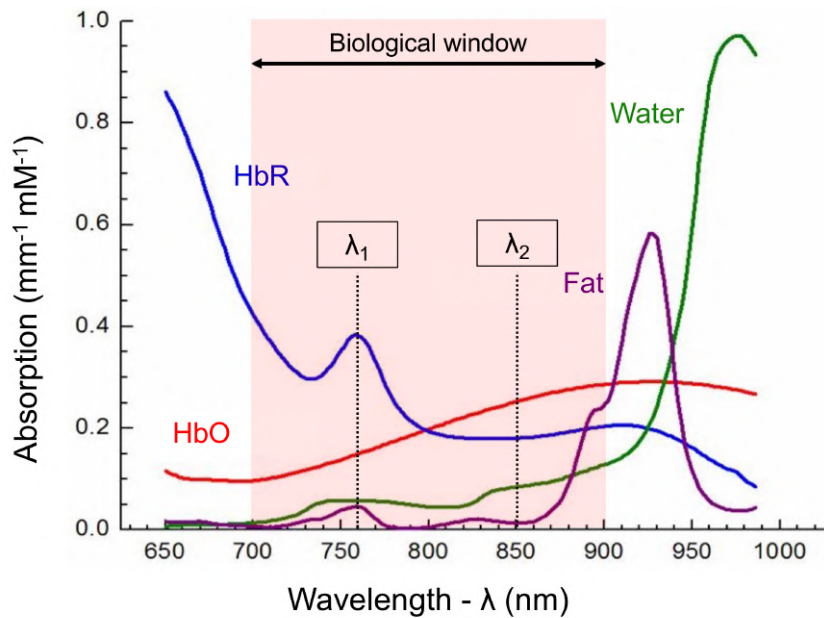


Figure 2.2 The absorption spectra of HbO, HbR, water and fat. Wavelengths λ_1 and λ_2 represent the wavelengths employed by the NIRx NIRScout system used in all the studies of this thesis.

As opposed to other neuroimaging techniques such as electro- and magnetoencephalography (i.e., EEG and MEG), which directly measure the electrical or magnetic fields generated by the synchronized activity of large populations of neurons, fNIRS belongs to the set of neuroimaging techniques assessing the metabolic aspects associated to brain activity, such as positron emission tomography (PET) or fMRI. The slow functional hemodynamic response measured by these techniques lags several seconds behind neuronal activity, and thus, only represents a proxy measurement of brain function.

In brain tissue, regional changes in cerebral blood flow and oxygenation can be employed as surrogate markers of neural activation. The most simplified interpretation of this process considers that changes in cerebral hemodynamics are linked to increases in local neural activity in a process known as neurovascular coupling (Logothetis et al., 2001; Wolf et al., 2002; Steinbrink et al., 2006). This process is however rather complex, and the precise physiological mechanisms that define the link between the hemodynamic response and neural activity are still not completely understood.

The repeated firing of neurons during neural activity, either spontaneously, or internally/externally evoked, elicits an increase in cellular oxygen and glucose consumption. Driven by neurovascular coupling dynamics, this metabolic demand is supplied by a local increase of cerebral blood flow in the activated region, which in turn produces an increase in cerebral blood volume due to the vasodilatation of the local vasculature system (Logothetis et al., 2001; Wolf et al., 2002; Steinbrink et al., 2006). This mechanism known as functional hyperaemia (Nippert et al., 2018), and which requires the participation of several vasoactive agents at different stages along the bloodstream, is one of the main roles of the neurovascular coupling. Autoregulation is another central role filled by neurovascular coupling, keeping blood pressure levels constant during these periods of altered cerebral blood flow (Ward et al., 2012).

Functional Near-Infrared Spectroscopy - fNIRS

Oxygen is transported to cells through the oxygen saturated version of hemoglobin HbO, which after releasing the oxygen molecules leads to the formation of HbR. The amount of HbO delivered to the activated region generally exceeds the metabolic demand, leading to focal hyperoxygenation (i.e., an increase in the local concentration of HbO and a decrease of HbR concentration). This response represents the operational definition of cortical activation on fNIRS measurements, and due to the paramagnetic (i.e., weak attraction by magnetic fields) properties of HbR, it also provides the endogenous contrast responsible for the blood oxygen level dependent (BOLD) effect measured in fMRI (Obrig and Villringer, 2003). The canonical hemodynamic response function (HRF) measured with fNIRS consists of a localized decrease in HbR concentration and a concomitant increase in HbO concentration, which is usually 2 to 3-fold times larger in magnitude than the former in a micro-molar scale (Obrig and Villringer, 2003). This results in an increase in total-hemoglobin (HbT), calculated from the addition of HbO and HbR signals, and which is related with cerebral blood volume (Figure 2.3). An “initial dip” at the early onset of the vascular response characterized by an increase in HbR concentration has been reported in several studies (Frostig et al., 1990; Grinvald et al., 1991; Menon et al., 1995; Malonek and Grinvald, 1996; Hu et al., 1997; Jaszewski et al., 2003; Kamran et al., 2018). The initial dip could be associated to a local increase in the concentration of HbR as activated populations of neurons extract oxygen from the blood. However, contradictory evidence on the existence of this response feature (Lindauer et al., 2001; Fransson et al. 1998; Buxton et al., 2001; Vanzetta et al., 2001) demands further research that may lead to elucidate all the specific dynamics involved in this complex physiological process.

There has been also some controversy over which hemoglobin parameter, either HbO, HbR, HbT or a combination of these parameters, to report when interpreting stimulus induced functional brain activation from fNIRS measurements. Arguments supporting each of them have considered their agreement with the BOLD signal, their

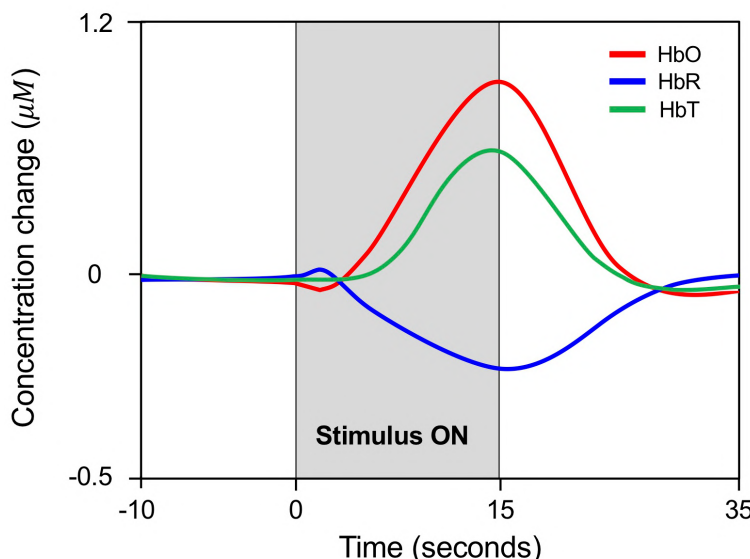


Figure 2.3 A canonical functional hemodynamic response measured with NIRS. Typically, this response is characterized by a decrease in HbR and a concomitant increase in HbO. Total hemoglobin (HbT) is the sum of HbO and HbR and it represents regional cerebral blood volume (adapted from Scholkmann et al., 2014).

signal-to-noise ratio or, alternatively, which of these parameters is more affected by physiological noise. This discussion has yet another consequence, which has to do with the current methodological flexibility when analyzing, reporting and interpreting results derived from fNIRS data. These issues are discussed further in section 2.4.

The signal recorded by fNIRS includes several evoked and spontaneous components with and without neurobiological origin (Scholkmann et al., 2014). Components with neuronal origin (i.e., those originated from neurovascular coupling) represent the main interest for neuroscientific applications. Measuring the evoked response to particular experimental stimuli is the most typical approach to study functional brain activity in fNIRS studies. This is achieved by averaging together the individual HRFs to a common experimental condition (see Chapter 5). Trial averaging also reduces noise, which is assumed to be independent of the experimental effect of interest, providing a clearer temporal and spatial characterization of the HRF evoked by stimuli presentation. Spontaneous cerebral activity measured with fNIRS refers to the hemodynamic activity that is recorded in the absence of any evoked task or stimuli. Spontaneous fluctuations are generally used in functional connectivity analysis to investigate the intrinsic functional organization of the brain (see Chapters 3 and 4). The relevance and impact of components stemming from other sources (i.e., cerebral vs. extracerebral) and origin (neuronal vs. systemic) are discussed in the next sections.

Physical Principles of NIRS Technology

Most commercial NIRS instruments used to investigate the brain's hemodynamic response, as the one employed in the current thesis, rely on continuous-wave (CW) technology (Ferrari et al., 2012; Scholkmann et al., 2014). In these systems, source optodes emit light at two different wavelengths (e.g., 760 and 850 nm) with a constant intensity, and attenuation in light intensity after crossing head tissues is measured at the detector optodes (Figure 2.4). CW systems offer several practical advantages such as low-cost and portability but they only enable the calculation of HbO and HbR concentration changes relative to a baseline, and not an absolute quantification. In contrast, NIRS systems based on spatially resolved spectroscopy combine light intensity measurements from multiple detectors located at various distances, thus providing information on changes in light attenuation with distance (Suzuki et al., 1999; Kovacsova et al., 2018). With this information, tissue optical properties can be computed based on light propagation models, assuming an inverse linear relationship between detected intensity and SD distance (Suzuki et al., 1999; Kovacsova et al., 2018). In frequency domain NIRS systems, light intensity is modulated, and variations in both the amplitude and phase of the re-emerging light are measured (Franceschini et al. 2000; Wolf et al., 2002). Time domain NIRS systems enable measuring the time of flight of individual photons as they traverse through tissues by emitting single and short-duration NIR light pulses (Hebden and Delpy, 1994; Torricelli et al., 2014). The latter three technologies potentially allow the quantification of absolute HbO and HbR concentrations and are essential for the future development of the technique, but fall outside the scope of this thesis. Therefore, the basic physical principles of the NIRS technique are described below with reference to CW systems only.

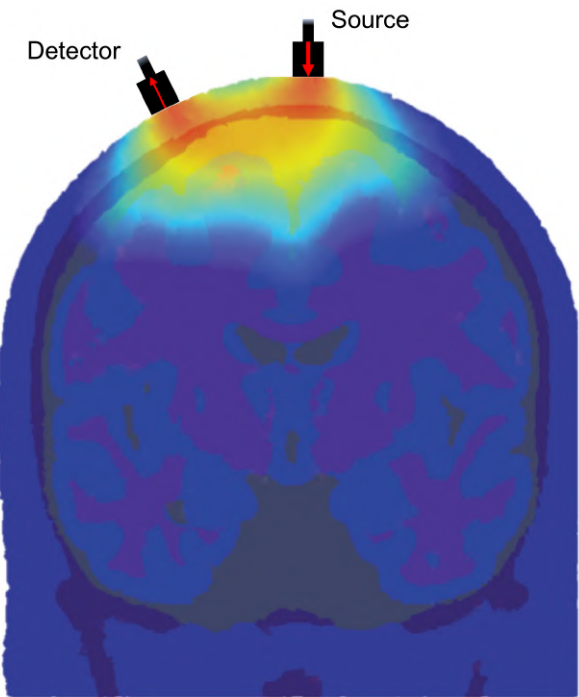


Figure 2.4 Spatial sensitivity profile for a single SD pair, also referred to as photon measurement density function (PMDF). In conventional fNIRS systems the light travels from sources to detectors following a “banana” shaped trajectory, with part of this reflected light having traversed through the cortex. Penetration depth into the cortex is limited by several factors, such as light intensity, SD separation, and the characteristics of the illuminated tissues (e.g., skull thickness is different in adults and infants). Figure courtesy of Dr. Robert J. Cooper.

Light-matter interaction is dominated by two fundamental mechanisms: absorption and scattering. During absorption, light is absorbed by the medium in which it is travelling, and the energy carried by photons is dissipated as heat. In highly-scattering media such as biological tissues, scattering is by far more probable than absorption, and it represents the dominant form of light-matter interaction. This process produces a modification in the direction of photons travelling through the medium, but does not imply a change in the energy of the incoming light. For a particular wavelength λ , the absorption coefficient $\mu_a(\lambda)$, and the reduced scattering coefficient $\mu_s'(\lambda)$ of a medium (e.g., biological tissue) define the probability that the incoming photons will undergo each of these processes per unit length.

In NIRS imaging applications, the most commonly used method to describe the interaction between light and biological tissues is the Beer-Lambert law. According to this law, in a non-scattering media and for a particular wavelength (λ), optical attenuation (or optical density OD) can be expressed as:

$$OD = \frac{I_{out}(t,\lambda)}{I_{in}(t,\lambda)} = e^{-x \mu_a(t,\lambda)},$$

where I_{in} represents the intensity of the light entering the medium, and I_{out} the intensity of the detected light after passing through tissues (Figure 2.5A). The distance travelled by the light x (i.e., source-detector distance) is known as the optical pathlength. Then, it is

possible to determine the absorption coefficient of a material/medium, for a given time point t as follows:

$$\mu_a(t, \lambda) = \frac{1}{x} \ln \frac{I_{in}(t, \lambda)}{I_{out}(t, \lambda)}$$

The absorption coefficient of a medium (e.g., head-brain tissue), for a particular wavelength λ , it is given by the specific extinction coefficients $\varepsilon(\lambda)$ of all the different absorbing substances present in the medium (e.g., water, fat, HbO and HbR) and their concentration C , such that:

$$\mu_a(t, \lambda) = \varepsilon_{water}(\lambda) C_{water}(t) + \varepsilon_{fat}(\lambda) C_{fat}(t) + \varepsilon_{HbO}(\lambda) C_{HbO}(t) + \varepsilon_{HbR}(\lambda) C_{HbR}(t),$$

or alternatively:

$$\mu_a(\lambda, t) = \sum_n \varepsilon_n(\lambda) C_n(t),$$

where $C_n(t)$ represents the time-varying concentration of each of the n^{th} absorbing substances present in the medium. Calculating HbO and HbR chromophore concentration changes from variations in the absorption coefficient of the medium is indeed the effect of interest that fNIRS applications aim to capture. Tabulated values for the specific extinction coefficient $\varepsilon_n(\lambda)$ of each these substances/chromophores at different wavelengths can be found in the literature (Matcher et al., 1995).

Biological tissues are non-homogeneous (i.e., composed of several distinct absorbing and scattering substances) and highly-scattering media. This fact has two direct consequences that must be contemplated when attempting to model light attenuation based on NIRS measurements (Figure 2.5B). First, light intensity losses due to scattering are larger than those related to absorption and must be considered in the general equation. Second, light follows a random walk (i.e., not a linear trajectory), which means that the effective distance X travelled by light from the moment it leaves the source until it reaches the detector is unknown, and it is certainly longer than the SD separation x . The Modified Beer-Lambert law, in which most CW-NIRS imaging approaches are based, introduces two parameters to account for these modifications:

$$OD = \frac{I_{out}(t, \lambda)}{I_{in}(t, \lambda)} = e^{-D(\lambda)x \mu_a(t, \lambda) + G(\lambda)},$$

where the parameter $G(\lambda)$ describes light intensity losses due to scattering, and the differential path length factor (DPF) $D(\lambda)$ denotes the increased distance that light has to travel due to its random walk (i.e., $X = Dx$). DPF values are dependent on several factors such as the age of the participant, wavelength and type of tissue under assessment. Tabulated DPF values exist for a range of wavelengths, ages and tissue types (Essenpreis et al., 1993; Duncan et al., 1995; Duncan et al., 1996). DPF values can also be approximated based on the general equation that was derived after modelling the age and wavelength dependency of this factor (Scholkmann et al., 2013), but they can only be accurately

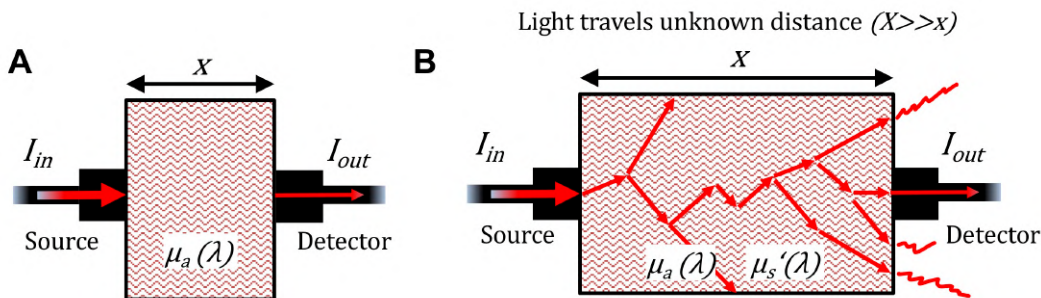


Figure 2.5 Illustration of CW technology, which measures changes in intensity between the emitted light at the source and the detected light after crossing the medium. A) Absorbing, non-scattering medium where changes in intensity are caused by absorption and the distance travelled by the light equals the source-detector (SD) distance (x). B) Absorbing, highly-scattering medium where intensity changes are caused by absorption and scattering processes. This figure also illustrates the effect of scattering on light trajectory, which travels through the medium following a random walk (X), and thus longer than the SD distance ($X \gg x$).

estimated using time or frequency resolved NIRS systems. The parameters G and DPF cannot be determined with CW systems that rely on light intensity measurements only, and therefore measuring the absolute concentrations of HbO and HbR is not feasible.

However, by introducing some assumptions, and allowing certain losses in quantification accuracy, changes in the concentration of HbO and HbR between two time points can be calculated based on attenuation measurements (Obrig and Villringer, 2003; Scholkmann et al., 2013). First, scattering is much more prevalent than absorption, but can be assumed constant within the sampling volume over the duration of the measurement. The implications of this assumption for measuring HbO and HbR concentration changes is that G cancels out, and that DPF can also be considered constant. Second, absorption effects caused by other chromophores (e.g., water, fat) present in the interrogated tissue can be considered time-invariant over the course of a given experiment. Variations in optical attenuation are therefore assumed to stem from variations in the concentration of HbO and HbR only. Measuring changes in optical absorption between two states t_1 and t_2 (i.e., baseline) results in:

$$\begin{aligned}\Delta OD(\lambda) &= \ln \frac{I_{out}(t_2, \lambda)}{I_{in}(t_0, \lambda)} - \ln \frac{I_{out}(t_1, \lambda)}{I_{in}(t_0, \lambda)} = -\ln \frac{I_{out}(t_1, \lambda)}{I_{out}(t_2, \lambda)} \\ &= Dx(\varepsilon_{HbO}(\lambda) \Delta C_{HbO} + \varepsilon_{HbR}(\lambda) \Delta C_{HbR}).\end{aligned}$$

This still leads to a single equation with two unknown values ΔC_{HbO} and ΔC_{HbR} . Using NIRS measurements at two different wavelengths it is then possible to define a system of equations that can be solved in order to measure the relative changes in concentration of HbO and HbR, resulting in the fundamental equations of NIRS.

$$\Delta OD(\lambda_1) = -\ln \frac{I_{out}(t_1, \lambda_1)}{I_{out}(t_2, \lambda_1)} = Dx(\varepsilon_{HbO}(\lambda_1) \Delta C_{HbO} + \varepsilon_{HbR}(\lambda_1) \Delta C_{HbR})$$

$$\Delta OD(\lambda_2) = -\ln \frac{I_{out}(t_1, \lambda_2)}{I_{out}(t_2, \lambda_2)} = Dx(\varepsilon_{HbO}(\lambda_2) \Delta C_{HbO} + \varepsilon_{HbR}(\lambda_2) \Delta C_{HbR}).$$

Optimal wavelength pair selection has been discussed elsewhere (Boas et al., 2004; Scholkmann et al., 2014), but it usually consists of a wavelength either side of the isosbestic point (800 nm), which based on the absorption spectra of these chromophores, helps to maximize sensitivity to HbO and HbR concentration changes and to avoid crosstalk. Multi-spectral or broadband NIRS systems including multiple wavelengths potentially enable calculating the concentration of other functionally relevant parameters such as cytochrome c oxidase (Brigadoi et al., 2017) or tissue oxygen saturation (Phan et al., 2016).

2.2. fNIRS Signal Processing

This section explains the main steps of the fNIRS data preprocessing pipeline employed in this thesis. Due to the lack of standardized procedures for data preprocessing and analysis in the fNIRS community this pipeline might vary between research groups. Importantly, recent reviews highlighted the importance of pre- and post- signal processing methods for meaningful, reliable, and reproducible fNIRS research (Orihuela-Espina et al., 2010; Huppert, 2016; Santosa et al., 2017; Hocke et al., 2018; Pfeifer et al., 2018; Pinti et al., 2019). These works demonstrated that specific choices at different phases of the signal processing pipeline can significantly impact the results and interpretation of fNIRS studies. They also provided recommendations, not only for the best practices regarding fNIRS signal preprocessing and analysis methods, but also on how to report this relevant information in such a way as to ensure that it is useful for other researchers in the field.

Here, only a brief description of the purpose of each preprocessing step is provided. The concrete details of the preprocessing pipeline and the rationale of the parameters applied in the studies of this thesis are provided in each of the experimental chapters (Chapters 3-5, Appendix A and B), together with several MATLAB scripts for its implementation. Data analysis methods employed to investigate spontaneous or evoked functional brain activity from fNIRS measurements are also considered study-specific, and therefore have not been included in this section. Prior to, or parallel to data preprocessing, it is also convenient to perform a data quality assessment, as fNIRS measurements can also be prone to motion artifacts, particularly in infant studies. Several indicators of high fNIRS data quality that can be examined during data preprocessing are described in Appendix A. The specific implementation of the data quality assessment routine employed in the studies of this thesis, including MATLAB scripts and individual examples, is also provided in Appendix A.

- *Conversion from raw intensity data to changes in optical density.*

The first step of the fNIRS preprocessing pipeline requires converting the raw intensity/voltage data, which usually presents different formats between NIRS devices, to changes in attenuation (or optical density) with respect to a baseline level. As derived from the modified Beer-Lambert law, this step is accomplished by computing the negative logarithm of the ratio between the detected light intensity at each time point and the baseline value (e.g., the mean signal).

- Motion artifact correction.

Motion artifacts represent an important source of variability in the fNIRS signal not related to the hemodynamic signal of interest. Abrupt changes in the fNIRS signal can originate from transient losses in coupling between the optodes and the scalp usually caused by head movements. Motion artifacts are frequently observed in data collected from awake infants, and they may appear in various forms (e.g., spikes, low frequency drifts or baseline shifts). The frequency, amplitude and duration of these artifacts is related to different factors, such as the cap fitting into the participant's head, the experimental paradigm under assessment, or the age of the participant. In all cases it is important to identify these artifacts to either correct them, or exclude their contribution for subsequent data analysis, as an insufficient data quality will negatively impact any results derived from fNIRS measurements. Motion detection can be performed by means of automated algorithms, for example by measuring changes in signal amplitude exceeding a prespecified threshold (Huppert et al., 2009), or by visually inspecting channel time series and manually selecting motion affected periods.

Numerous motion correction algorithms based on different principles have been proposed such as wavelet filtering (Molavi and Dumont, 2012), kurtosis-based wavelet filtering (Chiarelli et al., 2015), spline interpolation methods (Scholkmann et al., 2010; Jahani et al., 2018), principal and independent component analysis (Yücel et al., 2014), blind source separation with temporally embedded canonical correlation analysis (von Lühmann et al., 2019; von Lühmann et al., 2020), correlation-based signal improvement (Cui et al., 2010), autoregressive modelling (Barker et al., 2016), down-weighting timepoints based on the distribution of the temporal derivative signal (Fishburn et al., 2019), and sparsity-based regularization algorithms (Selesnick et al., 2014), to mention just a few. The individual and combined efficacy of some of these methods has been evaluated using simulated (Cooper et al., 2012), and real adult (Robertson et al., 2010; Brigadoi et al., 2014), children (Hu et al., 2015) and infant data (Behrendt et al., 2018; Di Lorenzo et al., 2019). However, due to the variable nature of motion artifacts in shape, magnitude and duration, it is problematic to find an algorithm with an adequate performance in all circumstances. Moreover, none of these methods is able to handle highly-contaminated datasets. In some cases, the magnitude and duration of motion-induced noise is so large relative to the underlying hemodynamic fluctuations of interest that this information simply cannot be recovered (Cooper et al., 2012), and these datasets should be discarded.

In this thesis, the wavelet-based despiking approach described in Patel et al., (2014) has been employed for motion artifact correction, which is similar to the one proposed by Molavi and Dumont (2012). Originally developed for denoising fMRI time series, this approach has been optimized to detect, model and remove slow and high frequency noise effects as the ones commonly present in fNIRS data. Briefly, the time series of individual channels are decomposed in the wavelet domain, and coefficients associated with local maxima and minima identified. From this set of coefficients, those that are present simultaneously across multiple frequencies are characterized as non-stationary changes in the signal caused by low and high frequency artifacts. After these coefficients are set to zero, the wavelet-despiked signal is recomposed.

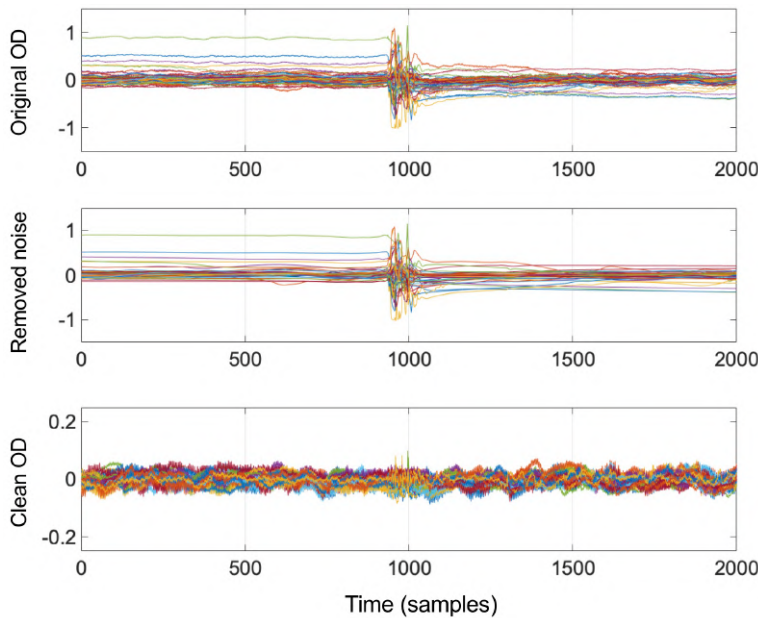


Figure 2.7 Time-series of a representative participant before and after wavelet despike (Patel et al., 2014), and removed noise at this preprocessing step. This wavelet-based method is designed to detect and remove transient events caused by outliers in the signal and low-frequency trends.

Using the inverse approach (i.e., keeping the artifact-related coefficients and making zero the rest) the noise signal can also be reconstructed. This method requires the input of various user-selected parameters, which in this thesis were manually adjusted after evaluating a range of combinations. The outputs of this method are the denoised time series, and the time series of removed noise.

As shown in Figure 2.7, this method effectively reduces motion-related artifacts while keeping clean periods unaffected. Residual noise can still be noticed in the corrected signal although with much smaller amplitude. Throughout all of the experiments described in this thesis, the wavelet-based algorithm outperformed other evaluated methods for motion correction in relatively motion-free data. It should be noted that participants of this thesis have been tested during natural sleep only, and only datasets with an overall good data quality, as determined by visual inspection, have been included for data preprocessing. Moreover, as a first preprocessing step heavily corrupted segments/trials were discarded for the analysis. Data quality was the priority in these studies, and discarding participants/trials was not an issue as the recruitment process was effective and long datasets were recorded. These factors lead to relatively low attrition rates considering the population under study. Nevertheless, these advantageous testing procedures are not always feasible, and a one-size-fits-all solution for dealing with motion artifacts is hardly achievable. In general, a detailed description of the experimental procedures, and transparency when reporting data quality and preprocessing methods, would help advancing the fNIRS community towards unified criteria that facilitate results interpretation and replication.

- Conversion from optical density data to HbO and HbR concentration changes.

In this step HbO and HbR concentration changes are derived by means of the system of equations of the modified Beer-Lambert law described in Section 2.1. At this point, it is also possible to compute HbT by the addition of HbO and HbR time series.

- Physiological noise correction.

Physiological noise represents another major confounding source in fNIRS recordings (Figure 2.8). These components arise from extracerebral and cerebral compartments and can occur naturally (Kirilina et al., 2012; Scholkmann et al., 2013; Scholkmann et al., 2014; Tachtsidis and Scholkmann, 2016) or be evoked by task-related activity (e.g., stressful or physically demanding tasks) (Yücel et al., 2016). In infants, the main physiological noise components are related to spatially global systemic fluctuations, each of them with specific frequency patterns which are usually faster than those observed in adults. For example, cardiac pulse in infants is present at around 2 Hz, and respiratory noise can be found around 0.6 Hz. Slow frequency components associated to blood pressure fluctuations such as Mayer waves (<0.1 Hz) also exist, but are more difficult to identify as they overlap with the frequency content of neurovascular coupling induced hemodynamic activity. These low frequency components exert a negative impact on statistical analysis, as their frequency tends to overlap with task-related hemodynamic responses, thus reducing signal-to-noise ratio (Yücel et al., 2016).

Bandpass filtering is the most commonly implemented method to reduce the impact of physiological components during fNIRS data preprocessing (see Pinti et al., 2019 for a review). In this approach, low and high frequency thresholds are selected (i.e., cut-off frequencies). By bandpass filtering the signal, the frequency content between these thresholds is preserved, and the contribution of frequencies outside this range removed. Due to the high sampling frequency of fNIRS recordings (typically 10 Hz or above), bandpass filtering is well-suited to remove high-frequency physiological components (e.g., cardiac pulse - 2 Hz, and respiration - 0.6 Hz) outside the frequency range of hemodynamic fluctuations of interest (<0.2-0.3 Hz), as well as to reduce very slow frequencies (<0.01 Hz) related to vasomotion regulation and/or instrumental noise. Other global systemic components whose frequencies fall within the frequency range of neuronal related hemodynamic fluctuations, such as Mayer waves, cannot be removed using bandpass filtering approaches without risking removing part of the signal of interest too.

Different approaches have been proposed to reduce fNIRS signal contamination due to systemic components of global origin. First, if short-separation channels, which are expected to largely interrogate extracerebral tissue layers, are incorporated to the fNIRS optode setup, one could potentially regress out the contribution of these channels from standard separation channels that are assumed to sample deeper cerebral tissue layers to a larger extent (Saager and Berger, 2008). In adults, the optimal SD distance that will maximize sensitivity to extracerebral hemodynamics and minimize sensitivity to the brain has been found to be around 10 mm (Gagnon et al., 2011; Brigadoi and Cooper, 2015). In infants, due to their thinner head tissues (i.e., skull, scalp), the optimum SD distance for short-separation channels has been estimated to be much shorter, around 2.15 mm (Brigadoi and Cooper, 2015). In practice though, most NIRS systems do not permit this type of measurements, as they are limited by the physical size of the optodes and/or use a fixed distance optode holder.

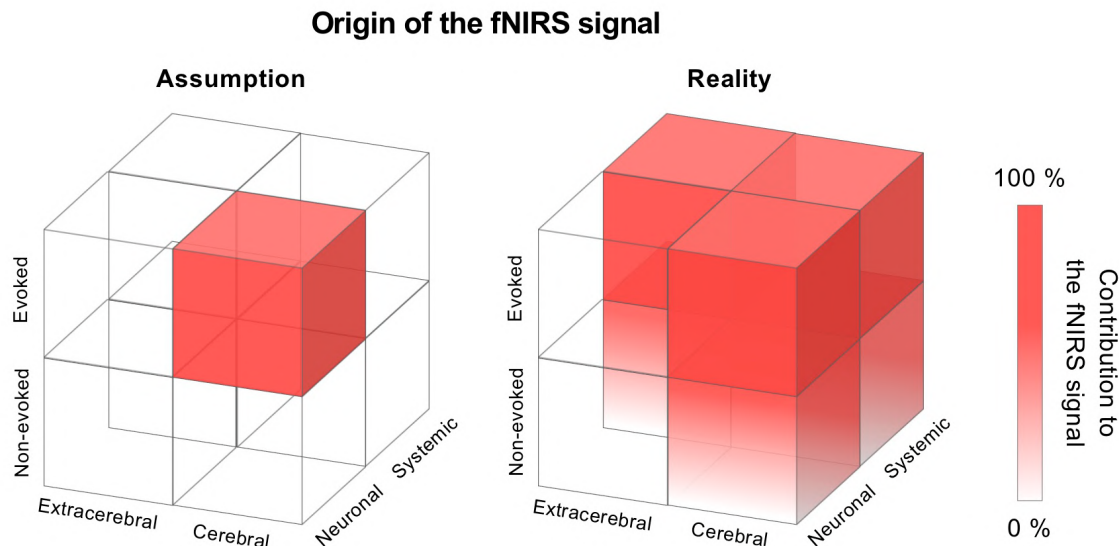


Figure 2.8 Illustration of the different components present in the fNIRS signal. Awareness of the presence of these components is fundamental for signal processing and results interpretation in fNIRS studies (adapted from Tachtsidis and Scholkmann, 2016).

Other signal processing methods exist and should be considered when no short-separation channels are available. Amongst them, global signal regression is perhaps the easiest to implement and the one showing a more straightforward interpretation (Pfeifer et al., 2018). Despite global signal regression has generated substantial controversy in the fMRI community (Murphy and Fox, 2017), its use has been more positively advocated in fNIRS studies (Pfeifer et al., 2018). The average, or global, fNIRS signal is assumed to largely reflect systemic, globally occurring hemodynamic fluctuations, as this signal is usually present across multiple channel time series. In this approach, the global signal (i.e., average signal across channels) is removed from the time series of each channel by means of linear regression, potentially reducing shared variance due to global confounds. Yet, another approach proposed removing the average signal of only those channels located on the contralateral hemisphere to each specific channel (Pfeifer et al., 2018), which might reduce the risk of unintendedly removing functional signal of interest. External recordings of physiology (Scholkmann et al., 2013) have also been proposed in the literature for correcting contamination due to systemic physiology.

2.3. fNIRS in Infant Research

Developmental cognitive neuroscience is one of the research areas in which fNIRS technique has more relevance, and which is the focus of the current thesis. Several comprehensive reviews have summarized the main fNIRS-based findings to the study of early cognitive development, highlighting its potential to advance the current understanding about the functional organization of the infant brain (Minagawa Kawai et al., 2008; Lloyd-fox et al., 2010; Gervain et al., 2011; Aslin, 2012; Vanderwert et al., 2014; Aslin et al., 2015; Issard and Gervain, 2018). The study of language processing has been one of the research areas in which the application of fNIRS has been more beneficial (Gervain et al., 2011). Studies specific to this research area are reviewed in Chapter 5 of this thesis, as it provides

Functional Near-Infrared Spectroscopy - fNIRS

a more appropriate context. Similarly, resting-state fNIRS studies investigating spontaneous brain activity and functional connectivity in infant populations are reviewed in Chapter 3.

Beyond these research domains, fNIRS has become a significant neuroimaging tool that has helped answering numerous long-standing questions about infant cognition, and has yielded converging evidence for previous behavioural findings. The early fNIRS studies in healthy infants tried to demonstrate the ability of this technique to detect functional brain activation to simple visual (e.g., reverse checkerboards) (Meek et al., 1998; Hoshi et al., 2000) and auditory stimuli (e.g., music, tones) (Sakatani et al., 1999; Zaramella et al., 2001). In the object processing domain, a series of studies demonstrated that the features used to identify objects are age dependent, with infants below 9 months of age using shape information only, and older infants relying on color and shape information for object individuation (Wilcox et al., 2010; Wilcox et al., 2012; Wilcox et al., 2014). These studies also confirmed the main role of anterior temporal cortex in object identification, as this area responded selectively during events in which infants were able to notice a change in the featural properties of the object stimuli (e.g., shape, color), but did not activate for control conditions where the object remained unchanged. Alternatively, another fNIRS study showed that the ability for categorical color perception in the visual cortex might already be in place in younger infants at 5-7 months of age (Yang et al., 2016). Similarly, Hyde et al., (2010) employed fNIRS to investigate numerosity detection in infants at 6 months of age, before mental number representation capacity is fully established. At this age, the right inferior parietal sulcus demonstrated functional specialization for numerical cognition, which is consistent with the engagement of bilateral parietal regions observed in studies assessing number processing in adults and older children (Dehaene et al., 2003; Cantlon et al., 2006).

fNIRS has also revealed some of the neural strategies underlying the early stages of learning in the developing brain. A study on learning audio-visual associations provided evidence of expectation-based cross-modal responses in the occipital cortex of 6-month-old infants (Emberson et al., 2015). First, infants were familiarized with combinations of auditory and visual stimuli presented in a predictable temporal order. Then, authors used a stimulus omission paradigm to examine the occipital responses in trials where the presentation of the visual stimulus in the audio-visual pair was unexpectedly omitted. This unexpected visual omission caused a robust response over the occipital cortex of the participants, suggesting the existence of an expectation-based feedback mechanism across auditory and visual perceptual modalities. Studies assessing the trajectory of audio-visual associative learning over the course of a task suggest a non-linear learning trajectory in infants, which is characterized by an initial phase where stimuli repetition elicits an increase in neural activity (i.e., repetition enhancement), followed by a decrease in activation (i.e., repetition suppression) at later stages (Gervain et al., 2008; Kersey and Emberson, 2017). Other fNIRS works have revealed that the learning response trajectory might be modulated by different factors, such as the brain region under assessment (Emberson et al., 2017), the type and complexity of the stimuli (Nakano et al., 2009), or the infants' attending preference (Watanabe et al., 2008).

In the domain of social cognition (see McDonald et al., 2018 for a recent review), cortical specialization for face processing has been one of the most widely explored topics using fNIRS. Differential hemodynamic responses to faces vs. control visual stimuli (e.g., visual noise, houses) have been documented over occipital areas at 4 (Csibra et al., 2004; Blasi et al., 2007) and 5 months of age (Di Lorenzo et al., 2019). Moreover, different patterns of brain activation to happy vs. angry facial expressions have been reported in 7- (Nakato et al., 2011a) but not in 5-month-old infants (Di Lorenzo et al., 2019). Infants studied around 8 months of age show stronger hemodynamic responses to their mother's face as compared to unfamiliar faces (Nakato et al., 2011b). At this age, infants respond differently to upright and inverted faces (Otsuka et al., 2007), and they also start displaying similar hemodynamic responses to faces presented from different views (e.g., frontal, profile) (Nakato et al., 2009), which might indicate a developmental change in infants' face perception/recognition ability in contexts of increased complexity.

Other important aspects of infant social cognition have been further investigated using fNIRS. Starting at around 4 months of age, infants showed preferential responses to dynamic social stimuli (activation), as opposed to dynamic non-social stimuli (non-activation) (Lloyd-Fox et al., 2009; Lloyd-Fox et al., 2011), and to human vs. mechanical action execution at 7-9 months of age (Biondi et al., 2016). Significant patterns of brain activation over bilateral temporal and frontal/prefrontal regions have been obtained to dynamic faces displaying communicative intent (e.g., mutual eye gaze or emotion expression) compared to control faces not signaling communicative intent (Grossman et al., 2010; Grossman et al., 2013; Urakawa et al., 2014). Finally, 12 months-old infants demonstrated increased activation in anterior orbitofrontal areas for emotional processing to familiar (i.e., mother) but not to unfamiliar faces, which authors suggested as indicative of a developing social attachment system (Minagawa-Kawai et al., 2009).

Recent technological advances in fNIRS instrumentation and methodology have offered the opportunity to spread the use of this technique to novel and exciting applications in developmental cognitive neuroscience research that were difficult to study up to this point. fNIRS has been confirmed as a promising tool to study the hemodynamic correlates of diverse cognitive functions in infants at risk for atypical neurodevelopment (Vanderwert et al., 2014). In particular, numerous works explored the presence of functional markers of atypical development associated with premature birth or perinatal brain injury (Emberson et al., 2017; Watanabe et al., 2017; Linke et al., 2018), as well as in infants at risk for developing neurodevelopmental disorders such as autism (Keehn et al., 2013; Braukmann et al., 2018) or Down's syndrome (Imai et al., 2014). Similarly, much effort has been directed to consolidate the implementation of this neuroimaging technique in low-resource settings, with the aim of investigating the consequences that malnutrition and social and environmental difficulties may have on the earliest stages of brain maturation (Lloyd-Fox et al., 2017; Lloyd-Fox et al., 2019; Perdue et al., 2019). Finally, recent works have demonstrated the feasibility to record fNIRS measurements from two or more participants simultaneously, also known as hyperscanning, an approach that might potentially provide an ideal framework for the investigation of infant-to-caregiver interactions in naturalistic environments (Azhari et al., 2019; Piazza et al., 2019).

2.4. Advantages, Limitations and Challenges of fNIRS

Compared to the other two neuroimaging techniques more commonly used in infant research (i.e., EEG and fMRI), fNIRS offers various practical advantages (Figure 2.9). Temporal resolution in most CW-NIRS systems is around 10 Hz (or higher), which is adequate to accurately track the hemodynamic response to stimuli typically assessed. Importantly, high frequency signal confounds due to cardiac and respiratory components can be reduced by means of signal filtering methods because, as opposed to fMRI, the superior temporal resolution of fNIRS prevents aliasing of these systemic physiological signals with the hemodynamic signal of interest. The spatial resolution of standard CW-NIRS systems is largely dependent on the number of sources and detectors incorporated into the optode setup. Increasing the number of sources and detectors will increase scalp surface coverage (i.e., lateral resolution), but the effective spatial resolution will still be limited to a loosely defined tissue volume below the surface located between each SD pair (around 2-3 cm), with no depth information (Fukui et al., 2003; Strangman et al., 2013).

High-density diffuse optical tomography systems (HD-DOT), which are based on the same principles as NIRS, use dense arrays of sources and detectors at multiple separations and with overlapping measurements that allow reconstructing three-dimensional images with depth information (Arridge, 1999; Boas et al., 2001; Gibson et al., 2005). Although still not reaching subcortical structures, this technology offers comparable spatial resolution to conventional fMRI measurements (White and Culver, 2010; Eggebrecht et al., 2012). More capabilities for its application to naturalistic and clinical setups and in special populations will become available with the wearable systems currently under development (Chitnis et al., 2016; Zhao and Cooper, 2017).

Specific properties of the infant head (e.g., thinner scalp and skull, less hair) make NIRS technique particularly suitable to the study of cortical activity in this population. The shortest scalp-brain distance in infants (Beauchamp et al., 2011) improves signal to noise ratio and increases recording depth to around 3 cm, which results in a light penetration into the cortex of approximately (1-1.5 cm), compared with recordings in adults where light penetration is considerably reduced (0.3-0.5 cm), and limited to the surface of the cortex (Fukui et al., 2003; Gervain et al., 2011; Strangman et al., 2013). NIRS instrumentation also shares some of the advantages of EEG for infant experimental testing. Both imaging techniques are noiseless, making them particularly suitable for studies involving auditory stimuli. fNIRS and EEG studies can be conducted in awake infants, as these techniques are flexible enough to accommodate to different head positions, as opposed to fMRI, where a more rigid head stabilization is required. This characteristic also allows infants to be accompanied by the parents during the whole testing, usually in their lap, which, in turn, improves infants' and parents' compliance with the study. Finally, fNIRS has demonstrated test-retest reliability for detecting brain activation in infants (Blasi et al., 2014), and its potential to be combined with other behavioural (e.g., eye-tracking, Urakawa et al., 2015) and neuroimaging modalities, such as fMRI (Strangman et al., 2002b; Steinbrink et al., 2006; Sasai et al., 2012; Sato et al., 2013) and EEG (Cooper et al., 2009; Telkemeyer et al., 2009; Telkemeyer et al., 2011; Wallois et al., 2012; Lee et al., 2020).

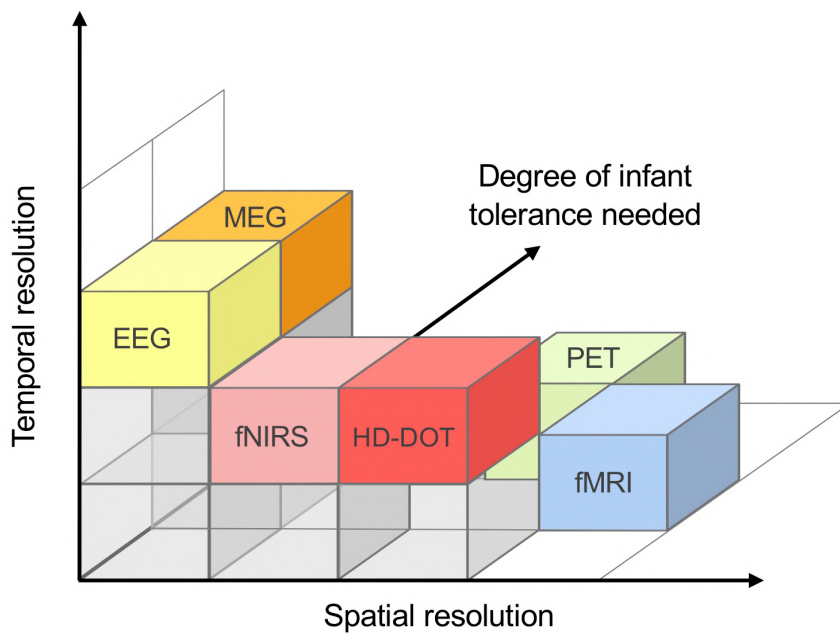


Figure 2.9 Comparison of different non-invasive neuroimaging techniques based on their spatial and temporal resolution, and the degree of infant tolerance needed for data acquisition (adapted from Lloyd-Fox et al., 2010).

A key limitation of fNIRS for testing infant subjects, which is inherent to other neuroimaging techniques as well, is that it requires the participant to remain still during data acquisition. Although it is assumed that fNIRS is relatively resilient to motion induced artifacts, and many reviews describe this attribute as one of its main advantages over other techniques (Minagawa Kawai et al., 2008; Lloyd-Fox et al., 2010; Gervain et al., 2011), this assertion is only true, and to a certain degree, if the optical probe is securely tight to the head, which is not always feasible when testing infant subjects. To prevent negative consequences on study outcomes and interpretation, it is therefore recommended to perform a thorough data quality assessment of individual datasets, and routinely implement (and understand) established signal processing procedures to deal with motion artifacts and physiological noise (Huppert et al., 2016; Pfeifer et al., 2018). Last but not least, it is essential that all this information is complete and properly described in publications (Cristia et al., 2013; Hocke et al., 2018; Pinti et al., 2019). In addition, it might be beneficial to build study-specific caps that fit properly to the infants' head, thus minimizing potential optode displacements due to head jerks (e.g., Emberson et al. 2015). It is also useful to reduce the weight of the apparatus to minimize the torque applied on the infants' head. These features will become more accessible with wireless and portable systems.

A related issue regarding signal interpretation has to do with the characteristics of the hemodynamic response measured in developmental populations. From the first fNIRS infant studies (e.g., Meek et al., 1998; Sakatani et al., 1999), there have been reports of hemodynamic response patterns that deviate from the canonical response direction typically associated with cortical activation (i.e., decrease in HbR and increase in HbO). Most early infant studies defined cortical activation solely based on HbO signal (for a discussion see Obrig and Villringer, 2003; Lloyd-Fox et al., 2010; Issard and Gervain, 2018) and disregarded HbR signal either before or after data analysis (e.g., Cristia et al., 2014;

Functional Near-Infrared Spectroscopy - fNIRS

Emberson et al., 2017). However, the fNIRS community has raised awareness on the importance of assessing HbO and HbR (and possibly HbT) to draw reliable scientific conclusions (de Roever et al., 2018), and most publications now report results from both parameters (e.g., Lloyd-Fox et al., 2014; Issard and Gervain, 2017).

The observed response variability might be explained by different factors such as technical differences (e.g., wavelength pair choice) between NIRS instruments (Boas et al., 2004), study-specific experimental aspects (Issard and Gervain, 2018), or physiological mechanisms related to perinatal neurovascular coupling development (Harris et al., 2011; Kozberg and Hillman, 2016). The canonical hemodynamic response to neural activity described in adults (i.e., localized functional hyperemia) has been shown to develop gradually during early infancy, in terms of its amplitude, and its spatiotemporal and spectral patterns (Arichi et al., 2012; Alcauter et al., 2015; Cusack et al., 2015; Nourhashemi et al., 2020). Concretely, infant hemodynamic responses display a smaller amplitude, a longer time to peak, and a higher variability in stimulus-evoked response direction (i.e., positive vs. negative). A better understanding of age and region-specific maturational changes in neurovascular response patterns could improve the precision of functional neuroimaging data analysis and interpretation, and also serve as a potential biomarker of typical and atypical brain development, making it an important area for future research.

fNIRS measurements are made from optodes (i.e., sources and detectors) placed on the surface of the scalp, providing no information about the underlying anatomy or the precise spatial origin of the recorded hemodynamic activity (Figure 2.10). The lack of structural information affects fNIRS data interpretation, restricting the localization of hemodynamic activity to macro-anatomical brain regions with position information (i.e., anterior-posterior, inferior-superior) in the best scenario. If no coregistration or positioning method is implemented, anatomical precision will be limited to larger cortical regions (i.e., frontal, temporal, parietal and occipital lobes). Moreover, when dealing with infant subjects it is generally difficult to ensure a consistent optode positioning across participants, which in turn reduces statistical power in group-level analysis (inter-subject variability). Inter-subject variability is further increased by individual differences in head size and shape, and in the location of internal brain structures with respect to the head surface (i.e., crano-cerebral relationship).

The localization of the optode setup across participants could be monitored using a 3D digitizer (e.g., PolhemusTM). However, in order to reliably track sensor positions this method requires participants to remain still during the localization process, which is challenging in awake infants. Brain activity localization accuracy can be improved by the coregistration of the fNIRS optode configuration with individual structural MRI data, but this multimodal approach would defeat the main purpose (i.e., portability and experimental flexibility) upon which the fNIRS technique is based. Alternatively, spatial registration of the fNIRS probe setup with underlying cortical regions can also be approximated using age-matched structural priors (e.g., 6-months - Akiyama et al., 2013; newborns - Brigadoi et al., 2014) without the need of individual structural MRI information. A full description of this approach as implemented in this thesis is included in Chapters 3 and 5.



Figure 2.10 Example of the NIRS cap arrangement employed in a study of this thesis (Chapter 5) showing the positioning of NIRS optodes (sources in red, detectors in green) on a baby doll. Optodes are positioned on an elastic cap (EasyCap, GmbH) in accordance with a subset of standard 10-20 positions. In order to maintain a good coupling between the optodes and the scalp, the cap is secured on the infant's head using a soft elastic chinstrap and a chest belt.

The common practice in most fNIRS studies is to configure the optode headgear relying on standardized positioning systems (e.g., international 10-20 system) that assume a consistent relationship between external anatomical landmarks and the underlying cortical structures. The international 10-20 system is a long-established approach that was originally developed for electrode placement in EEG studies (Jasper et al., 1958). In this system, four fiducial points (i.e., nasion, inion, left and right preauricular points) are used as reference to define the 10-20 standard positions of scalp sensors. These reference points define a perimeter in the transverse and median planes that is divided at intervals representing the 10% and 20% of the total distance. Three additional positions are positioned at each side of the head (F3, C3, P3 and F4, C4, P4), equidistant from the previously defined points. Recent works tried to determine the accuracy of this positioning system for the registration of fNIRS optodes relative to the underlying cortical regions in infants at different ages (1-4 months old - Kabdebon et al., 2014; 4-7 months old - Lloyd-Fox et al., 2014). These works demonstrated a marked stability in the registration of channel positions to underlying brain regions as determined by average or individual structural MRI data. They also provided a set of cortical projections of the standard 10-20 positions to different anatomical parcellations in these age ranges, which could serve as reference for cortical mapping of fNIRS channels for future infant studies if structural MRI data is not available.

Finally, after signal preprocessing, the majority of fNIRS studies apply statistical analysis methods to detect brain activation (e.g., stimulation vs. baseline) for an effect of interest, or to test activation differences between experimental groups or conditions (Ye et al., 2009; Hassanpour et al., 2014; Tak and Ye, 2014; Santosa et al., 2019). This step is crucial for drawing neuroscientific inferences, and for this reason recent publications have outlined various statistical challenges of task-based and resting-state fNIRS data analysis (Barker et al., 2013; Huppert, 2016; Santosa et al., 2017; Blanco et al., 2018). These challenges mainly pertain to how the characteristics of the fNIRS signal conflict with the mathematical assumptions of the statistical linear models usually employed in fNIRS studies.

Functional Near-Infrared Spectroscopy - fNIRS

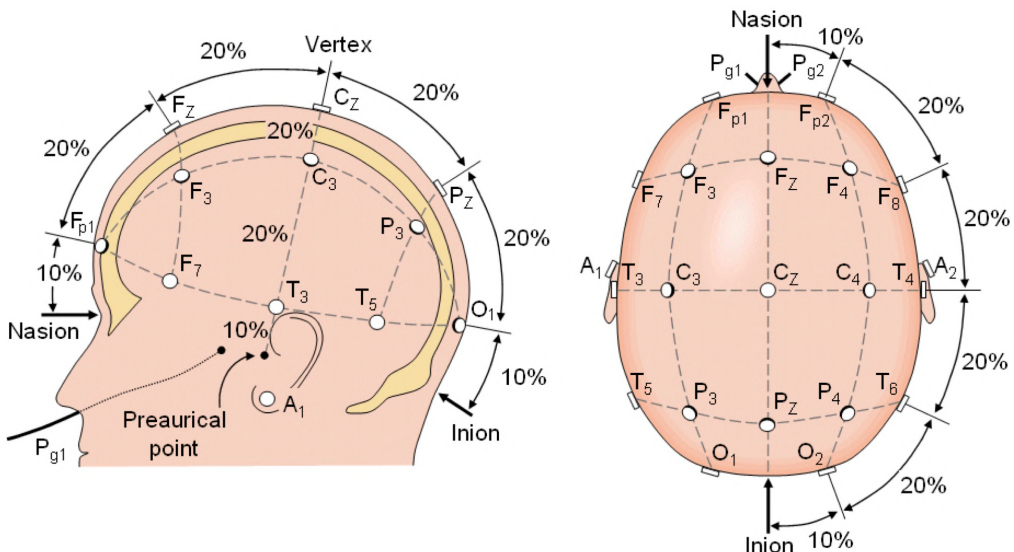


Figure 2.11 Sensor (i.e., optode or electrode) positioning defined by the international 10-20 system (Jasper, 1958) based on external anatomical landmarks (Figure adapted from www.BCI2000.org).

For example, the temporally autocorrelated structure of fNIRS signal disrupts the independency assumption between sample points, reducing the effective degrees of freedom of the statistical model, thus leading to uncontrolled false-discovery rates. Importantly, the issue of dealing with serial correlations in fNIRS data for the specific case of resting-state functional connectivity analyses is covered thoroughly in Chapter 4 (Blanco et al., 2018). Another potential violation of the statistical model arises from the different noise distributions present in the fNIRS signal due to motion artifacts. Concretely, noise is assumed to be normally distributed, but this is not the case in the presence of motion artifacts that frequently exist in the fNIRS signal, which will make these data points become outliers from the normal noise distribution (Huppert et al., 2016). These works demonstrated the importance of using correct statistical models that account for the limitations of standard statistical approaches and present methods for its implementation.

Chapter 3

Resting-State Functional Connectivity in 4-Month-Old Monolingual and Bilingual Infants

3.1. Theoretical Motivation

One way to understand the intrinsic functional organization of the human brain is through the measurement of resting-state functional connectivity (RSFC). RSFC reflects spontaneous but synchronized fluctuations in cerebral hemodynamic activity between brain regions that share a common role in supporting various, functionally relevant, sensory and cognitive processes (Biswal et al., 1995; Fox and Raichle, 2007; Damoiseaux et al., 2006). RSFC has been mostly investigated with functional magnetic resonance imaging (fMRI) techniques, mainly based on the blood oxygenation level dependent (BOLD) contrast, but also based on measurements of cerebral blood flow with arterial spin labelling (Zou et al., 2009), or cerebral blood volume with vascular space occupancy imaging (Miao et al., 2014; Huber et al., 2017). The existence of functional brain networks that coexist during resting-state has also been revealed in direct measurements of neuronal activity with electro- and magnetoelectroencephalography (EEG and MEG; Mantini et al., 2007; Brookes et al., 2011), suggesting that these signals cannot be attributed to physiological processes or artefactual components observed in vascular-related functional imaging techniques.

In adult subjects, temporally coherent resting-state hemodynamic fluctuations representing functional patterns of brain activity (i.e., brain networks) are observed among primary sensory cortices, such as the sensorimotor, visual and auditory regions, but also in regions supporting higher cognitive processes such as attention, executive control, memory and language (Damoiseaux et al., 2006; De Luca et al., 2006). It has been proposed that spontaneous neural activity encompassing functional brain networks might meet various functional roles, such as examining external and internal inputs on a recurrent basis (Fransson et al., 2005), providing balance between excitatory and inhibitory processes (Menon et al., 2011), or planning task performance (Tavor et al., 2016; Jiang et al., 2018; Fong et al., 2019). The relationship between spontaneous brain activity and task-related function has been confirmed by studies showing that brain areas activated during the performance of a particular cognitive task also display a correlated activity at rest (Smith et al., 2009), and that the response in individual functional areas is correspondingly modulated by the activity of functional resting-state networks (Fox et al., 2007). Furthermore, functional brain network configuration is highly consistent with the underlying structural connectivity (Honey et al., 2009; Uddin et al., 2011; Betzel et al., 2014).

RSFC can be measured using the same methodology in infants, children, and adults, thus providing a window into one aspect of neural development across the life span (e.g., Gao et al., 2017; Keunen et al., 2017; Zhang et al., 2019). Despite the challenges associated with neuroimaging research in developmental populations, a number of studies have characterized RSFC in infants and young children, mainly using fMRI (Fransson et al., 2007; Lin et al., 2008; Gao et al., 2009; Fransson et al., 2009; Perani et al., 2011; Damaraju et al., 2014; Gao et al., 2015; Gao et al., 2017; Keunen et al., 2017; Zhang et al., 2019). Some of these pioneering works focused on identifying the well-described adult resting-state networks in the developing infant brain, observing functional networks formed by anatomically and functionally coherent brain regions in infants' primary sensory regions such as the visual, auditory and sensorimotor cortices (Fransson et al., 2007; Lin et al.,

Resting-State Functional Connectivity in Infants

2008; Fransson et al., 2009; Damaraju et al., 2014; Gao et al., 2015). Resting-state networks representing higher-order cognitive functions such as the language network (Perani et al., 2011; Damaraju et al., 2014; Emerson et al., 2017), the dorsal attention network (Damaraju et al., 2014; Gao et al., 2015), or the default-mode network (Gao et al., 2009; Damaraju et al., 2014; Gao et al., 2015) have been observed during infancy as well, but showing a more protracted developmental trajectory. Concretely, the auditory/language network in infants involved the superior temporal gyrus and inferior frontal regions bilaterally, demonstrating a high resemblance with the adult spatial configuration (Perani et al., 2011; Damaraju et al., 2014). Interhemispheric connectivity between homologous regions in this network appeared well established early in development. Conversely, long-range intrahemispheric functional connectivity between inferior frontal and temporal regions characteristic of this network appeared weaker, possibly constrained by the extended maturational course of the underlying structural connectivity (Fransson et al., 2010; Perani et al., 2011).

RSFC has also proven to be a useful approach to investigate the influence of several prenatal and postnatal factors in functional brain development. As measured by fMRI studies, different trajectories of functional network development have been observed between premature and full-term infants (Damaraju et al., 2010; Doria et al., 2010; Smyser et al., 2010; Smyser et al., 2016). Furthermore, there is evidence showing that the configuration and maturational course of functional connectivity differs across neurotypical infants and toddlers in comparison to those at high-risk of neurodevelopmental disorders, such as autism spectrum disorder (Dinstein et al., 2011; Keehn et al., 2013; Emerson et al., 2017), Down's syndrome (Imai et al., 2014), or in newborns diagnosed with perinatal brain injury (Linke et al., 2018). Relevant to the current study, the development of functional network organization in the infant brain can also be modulated depending on various external or internal conditions that can be reliably investigated using RSFC (Zhang, H. et al., 2010), such as the caregivers' education level or socioeconomic status (Gao et al., 2015). As described in Chapter 1, a specific external factor (i.e., learning process) is growing up in a bilingual environment.

Previous evidence suggests that long-term exposure to two languages might alter the brain's functional (Parker Jones et al., 2011; Krizman et al., 2012; Berken et al., 2016) and structural organization (Mechelli et al., 2004; Luk et al., 2011; Mohades et al., 2012; García-Pentón et al., 2014; Mohades et al., 2015) as demonstrated by MRI studies in adults. Concretely, stronger functional connectivity in bilingual adults as compared to monolinguals has been observed in long-range bilateral and anterior-posterior connections on both hemispheres (Luk et al., 2011), and in brain networks associated with language and executive control processes (Grady et al., 2015; Berken et al., 2016; Sulpizio et al., 2020). More recently, Kousaei et al., (2017) found stronger internetwork connectivity between the default-mode network and the task-positive attention-network in simultaneous bilinguals (i.e., those exposed to two languages from birth) as compared to sequential bilinguals (i.e., those that learnt a second language at a later age). Similarly, Gullifer et al., (2018) showed that an earlier age of second language acquisition was related with a stronger functional connectivity between the left and right inferior frontal gyrus. Assessing whether such

differences between the monolingual and the bilingual brain can already be observed in infancy is of paramount relevance for research on brain development.

A number of studies showed that bilingualism induced brain adaptations might start already in early infancy (see Chapter 1), supporting the idea that the neural bases of bilingual language acquisition are established very early in life. Behavioural and brain differences across monolingual and bilingual infants have been conceptualized as different types of adaptation patterns to monolingual vs. bilingual environments. From the perspective of bilingual infants, this adaptation might facilitate the acquisition of two languages as opposed to one. Whether a bilingual environment has consequences when RSFC is considered is a relevant question, given that differences between monolingual and bilingual infants have been only observed in the presence of explicit cognitive and/or linguistic tasks (Conboy and Mills, 2006; García-Sierra et al., 2011; Petitto et al., 2012; Ferjan Ramírez et al., 2017; Nácar-García et al., 2018).

Measuring RSFC in monolingual and bilingual infants can reflect whether bilingual experience during the first months of life leads to specific adaptations in the intrinsic properties of functional brain organization that are observable in the absence of any task or stimuli (i.e., at rest). As RSFC provides a window to simultaneously study various functional systems, testing whether a functional adaptation to a bilingual context is evident at the earliest stages of human development is crucial for our understanding of how bilingualism interacts with general brain maturation patterns beyond task-specific language and cognitive processing.

The main aim of the work described in this chapter is to investigate whether early bilingual experience during the first months of life can lead to specific adaptations in the intrinsic properties of brain's function that are observable in the absence of any task or stimuli (i.e., at rest) using functional near-infrared spectroscopy (fNIRS). Due to its practical advantages fNIRS has emerged as an alternative to fMRI to characterize RSFC, especially in developmental populations. The feasibility of fNIRS to measure spontaneous cerebral hemodynamic activity was first demonstrated by Obrig et al., (2000). Since then, relevant work describing RSFC with fNIRS at different age ranges has been published, usually adapting functional connectivity analysis methods employed in fMRI research (Niu et al., 2013).

Using multichannel fNIRS systems, the visual (White et al., 2009; Mesquita et al., 2010), sensorimotor (Lu et al., 2010; Mesquita et al., 2010; Zhang H. et al., 2010) and auditory/language networks (Lu et al., 2010; Zhang Y.J. et al., 2010) have been identified. fNIRS has been also employed to investigate hemispheric asymmetry in functional networks, which showed a marked dominance of the right hemisphere in functional connectivity lateralization (Medvedev et al., 2014). Due to its higher sampling frequency, fNIRS allowed the investigation of temporal synchronization of spontaneous hemodynamic fluctuations over a range of frequency bands, revealing frequency-specific interactions between cortical regions (Sasai et al., 2011). More recently, the topological properties of functional network organization have been investigated applying graph metrics to fNIRS data (Niu et al., 2012; Novi et al., 2016; Geng et al., 2017; Wang et al., 2017; Cai et al.,

Resting-State Functional Connectivity in Infants

2018; de Souza et al., 2019), demonstrating high reproducibility and within-subject stability across network parameters. High-density diffuse optical tomography (HD-DOT) systems, which employ the same principles as fNIRS but with a much larger number of light sources and detectors, allow producing 3-dimensional images of functional brain activity at high spatial resolution. Using this technique functional connectivity has been mapped in adults and neonates, showing a strong within-subject agreement between the observed RSFC patterns and those obtained using fMRI (Eggebrecht et al., 2014; Ferradal et al., 2015).

Although fNIRS is particularly suitable to investigate functional brain development, studies that have employed this imaging technique to assess RSFC in infant populations are still scarce. Using a multichannel fNIRS setup covering the main cortical regions (i.e., frontal, temporal, parietal and occipital) Homae et al., (2010) described changes in cortical network organization from birth to 6 months of age. They observed that functional connectivity in frontal, temporal, parietal and occipital regions was constrained to spatially adjacent areas in neonates, with this pattern progressively evolving towards increased interhemispheric connectivity between homologous brain regions during the first months of life. These authors also demonstrated a modulation in RSFC patterns induced by task execution (Homae et al., 2011). They measured RSFC before and after presenting 3-month old infants with speech sounds, and showed an increase in fronto-temporal connectivity after stimuli presentation. Watanabe et al. (2017) and Taga et al. (2000; 2017) investigated the associative properties of resting-state oxyhemoglobin (HbO) and deoxyhemoglobin (HbR) time series as potential biomarkers for vascular and metabolic function in the infant brain. These studies shown that the phase relationship between HbO and HbR time series shifts from an in-phase state to an antiphase state during the first months of life (Taga et al., 2017), and that the developmental trajectory of this shift might be delayed in infants born preterm (Watanabe et al., 2017). Other works have further demonstrated the potential of fNIRS-RSFC to investigate typical and atypical functional brain development. Besides assessing the effect of premature birth in functional connectivity development (White et al., 2012; Fuchino et al., 2013; Watanabe et al., 2017), functional connectivity studies using fNIRS have also revealed alterations in the strength and synchronization of spontaneous HbO and HbR fluctuations in infants with Down's syndrome (Imai et al., 2014). Moreover, a recent work observed RSFC differences associated with the ability of self-recognition at 18 months of age (Bulgarelli et al., 2019). A few studies using HD-DOT in neonatal populations have also been able to characterize functional networks in the occipital (White et al., 2012; Ferradal et al., 2015), auditory, and middle temporal regions (Ferradal et al., 2015) with enhanced spatial accuracy. Other works assessed functional connectivity in infants using fNIRS, but their measurements were acquired during stimuli presentation and for this reason they are not discussed in detail in this chapter (Keehn et al., 2013; Molavi et al., 2014; Taga et al., 2018).

Most previous functional connectivity studies with fNIRS identified resting state networks at the single-subject level by means of a seed-based correlation analysis, which measures the temporal synchronization between time-series across multiple channels (White et al., 2009; Lu et al., 2010; Mesquita et al., 2010; Zhang Y.J. et al., 2010; White et al., 2012; Fuchino et al., 2013; Novi et al., 2016). Alternatively, independent component

analysis (ICA) has also been used to define maximally spatially or temporally independent components from individual datasets (Zhang H. et al., 2010; Zhang H. et al., 2011; White et al., 2012; Ferradal et al., 2015), which represent subject-specific independent patterns of functional connectivity.

These methods present some limitations when attempting to describe RSFC at the group-level, and to quantitatively compare RSFC patterns across experimental conditions or groups. For example, fNIRS spatial resolution is low and a method for channel localization is usually not available. Thus, the brain regions under investigation, as determined by seed channel selection, may vary across individuals, reducing statistical power. On the other hand, group-level functional connectivity studies based on ICA have often been computed by averaging those subject-specific components that match an a priori defined spatial configuration (e.g., bilateral and covering sensorimotor regions). However, individual data are usually affected by noise components of different levels and characteristics, which might result in an ICA separation that differs across subjects. Similarly, the accuracy and robustness of ICA method is determined by the number of sample points available for the estimation, which are considerably larger in group-level analysis as compared to an analysis at the single-subject level. The ultimate consequence of these limitations is that most previous fNIRS RSFC studies have evaluated group differences at the single channel level (e.g., Fuchino et al., 2013; Bulgarelli et al., 2019), using qualitative comparisons (e.g., Homae et al., 2010; White et al., 2012), or performing statistical analysis on specific connectivity indexes only (e.g., Homae et al., 2010; Imai et al., 2014; Watanabe et al., 2017).

To overcome the limitations of current group-level RSFC analysis methods with fNIRS (i.e., accurately describing RSFC at the group level and quantitatively comparing RSFC between experimental conditions and/or groups), three data-driven methodologies which are well established in resting-state fMRI research were implemented. These methods were employed to extract group-level large-scale functional connectivity patterns from the population of infants under investigation. Importantly, they enabled to quantitatively compare the prominence of functional networks across experimental groups. First, temporal group ICA (tGICA) with dual regression was implemented to extract group-level temporally independent patterns of spontaneous hemodynamic activity. By concatenating the fNIRS channel time courses of multiple subjects, tGICA generates a set of group-level maximally independent temporal time courses and its common aggregated spatial maps (i.e., functional networks, FN), which quantify the presence of each particular independent component on each specific channel. Group-level spatial maps, which spatially represent the FN of interest, can be regressed out to the subject level using spatio-temporal or dual regression (Beckmann et al., 2009; Smith et al., 2012), obtaining the subject-specific spatial maps. Between group differences are then assessed by performing statistical analyses across subject-specific maps on a channel by channel basis. The second method applied in this work was connICA (Amico et al., 2017), a connectome-based ICA approach in which a set of individual functional connectivity matrices or connectomes are used to obtain latent group-level independent functional connectome components (FCC) and its associated weights, quantifying the relative prominence of each FCC on each subject.

Resting-State Functional Connectivity in Infants

As a third method, between-group statistical comparisons of functional connectivity matrices were performed using an additional connectome-based approach, Network Based Statistics (NBS), which has been widely employed in MRI studies to perform group-level comparisons in structural and functional brain network organization (Zalesky et al., 2010; Zalesky et al., 2012). In this approach a statistical test of group differences (i.e. a t-test) is computed on the subjects' functional connectivity matrices for each channel pair, and clusters of interconnected edges above a preselected statistical threshold are identified. These values represent the thresholds for which the null hypothesis will be rejected at each channel pair, a similar approach as a massive univariate analysis. Then, the significance of the identified networks is tested using nonparametric permutation testing, controlling the familywise error rate at the network level based on the network size.

In this work, spontaneous hemodynamic brain activity was measured using fNIRS in a large cohort of 4-months old infants, to study the effect of bilingual language acquisition simultaneously on different functional brain systems, while avoiding potential confounds due to task interference. Assessing RSFC with fNIRS in developmental populations involves several challenges such as high attrition rate (i.e., low sample size), the difficulty to perform long recordings and data quality. In order to reduce the impact of these issues, spontaneous hemodynamic brain activity was measured during natural sleep, and quality assurance methods were implemented during data preprocessing. With this procedure a sample of almost one-hundred infants ($n = 99$) with good data quality and 9 minutes of continuous recordings was collected. The configuration of group-level RSFC patterns was examined using two ICA based methods: a temporal group ICA (tGICA) and a connectome-based ICA (connICA). A Network Based Statistics (NBS) approach was also implemented to compare large-scale network properties across experimental groups. The presence of the identified functional networks and functional connectome components was quantified in each participant, and results were compared across two monolingual (Spanish and Basque) and one bilingual group of 4-month-old infants (Spanish-Basque), in order to determine if simultaneously acquiring two languages from birth modulates functional network development at this early age.

3.2. Methods

Ethics Statement

This study was carried out at the Basque Center on Cognition, Brain and Language and received approval from its local ethical committee. The study involved the participation of infant subjects. Prior to participation, parents were informed about the aims of the study, the experimental procedures, and their legal rights, including the right to withdraw from the study at any moment without providing a reason and with no negative consequences. Written informed consent was obtained from the parents prior to data acquisition.

Study Population

123 healthy full-term infants participated in this study. In sixteen of these participants testing was not conducted because infants were not able to fall sleep. One participant was discarded for receiving a regular exposure to English. Two infants were

excluded before data preprocessing because their datasets were shorter than 600 seconds. Five infants ($n = 2$ Basque-Spanish bilingual infants, $n = 1$ Spanish monolingual infant and $n = 2$ Basque monolingual infants) were excluded during data preprocessing due to insufficient data quality. In the final sample, for which data was analysed and results are presented, 99 participants were included: 36 Basque-Spanish bilingual (BIL) infants (21 girls; mean age = 125 ± 4 days), 30 Spanish (SP) monolingual infants (13 girls; mean age = 123 ± 3 days) and 33 Basque (BQ) monolingual infants (17 girls; mean age = 122 ± 4 days). Participants' language background was assessed with a questionnaire filled by the parents, in which infants' percentage of exposure to each language (SP and BQ) during the first months of life was measured. Participants exposed to a single language (SP or BQ), or less than 10% of the time to a second language (SP or BQ), were included in each of the monolingual groups. Infants raised in a Spanish-Basque bilingual environment, those that were exposed to their two native languages from birth, formed the bilingual group. Participants' were recruited from the same region of the Basque Country (Gipuzkoa); a socioeconomic status questionnaire was completed to ensure that families showed similar levels of education, parental occupation and household income across groups.

Data Acquisition

Functional near-infrared spectroscopy (fNIRS) measurements were performed with a NIRScout system (NIRx Medical Technologies, CA, USA) at wavelengths 760 and 850 nm with a sampling rate of 8.93 Hz. Sixteen light emitters and 24 detectors were positioned on a stretchy fabric cap (Easycap GmbH, Germany) over frontal, temporal, parietal and occipital regions of both hemispheres according to the international 10-20 system. Each pair of an adjacent light emitter and a detector formed a single measurement channel, which generated 52 channels for each hemoglobin oxygenation state (i.e., oxyhemoglobin, HbO and deoxyhemoglobin, HbR). This configuration yielded source-detector separation distances ranging from approximately 20 mm to approximately 45 mm (Table 3.1). Nasion, inion and preauricular points were used as external head landmarks, and caps of two different sizes (i.e., 40 and 42) were employed to adapt to individual head perimeter/size. This approach ensured a consistent cap and optode positioning across infants (i.e., without additional MR images or external coordinate tracking system), so that channels corresponded to the same anatomical locations. Occipital channels were discarded in all participants for being particularly prone to contain signal artifacts, since during data acquisition the back part of the infants' head was leaning against the parent's body, and any minor movement resulted in the misplacement of these particular optodes. Thus, only data from the remaining 14 sources and 19 detectors (i.e., 46 channels) was analysed.

Infants' spontaneous hemodynamic activity was measured during natural sleep while leaning on their parents' lap in a sound attenuated room. The only source of illumination in the room was the screen of the recording computer, which was attenuated to low brightness levels. Recordings started when infants were relaxed, accustomed to the fNIRS cap and clear signs of sleep were noticeable. Over the duration of the recordings, parents were asked to remain silent and to minimize movements in order to avoid involuntary cap or optode displacement. Recordings lasted between 10 and 25 minutes

Resting-State Functional Connectivity in Infants

unless the infant woke up during the experiment. Recordings were interrupted if infants showed continued and excessive movement or signs of discomfort at any point.

The sensitivity profile of the fNIRS probe setup was computed to provide information of the brain areas under investigation, and for results visualization purposes. The probe setup (i.e., sources and detectors) was registered to an average 6-month-old infant template (Richards et al., 2016) to compute the sensitivity matrix of the source-detector configuration using *Toast++* (Schweiger and Arridge, 2014). The aggregated sensitivity profile of the fNIRS probe was obtained by adding the normalized cortical sensitivity profiles of each individual channel (Figure 3.1). Channel positions were defined as the grey matter node which coordinates were closest to the central point of the maximum sensitivity path along each source-detector pair. A 6-month-old average atlas (Akiyama et al., 2013) was used to compute a probabilistic spatial registration of the cortical structures underlying each channel. Channel coordinates were first transformed to the Akiyama et al., (2013) average T1 template space using Advanced Normalization Tools (ANTs) (Avants et al., 2009), and then registered into the Akiyama et al., (2013) anatomic atlas, defined by 116 cortical regions based on Automated Anatomical Labeling (AAL) (Tzourio-Mazoyer et al., 2002). For each channel, anatomical labels within a distance of 20 mm were defined by calculating the percentage of overlap with each AAL region (Figure 3.2 and Table 3.1).

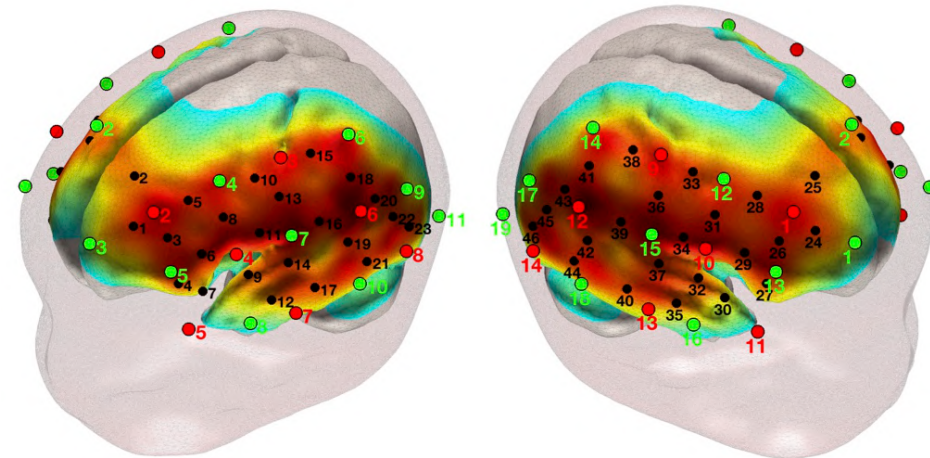


Figure 3.1 fNIRS optode (sources in red, detectors in green) and channel (black) localization in the current experimental setup. The normalized sensitivity profile of the current optode configuration is displayed in a 6-month-old infant head model.

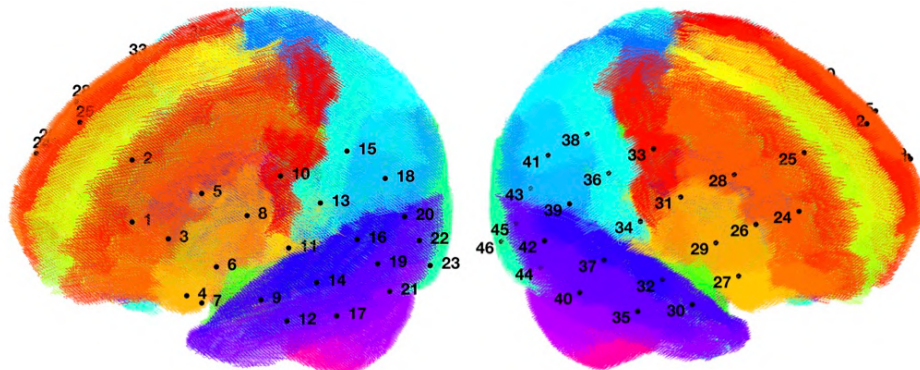


Figure 3.2 fNIRS channel localization registered to a 6-month-old infant AAL template.

Ch	S-D	S-D distance (mm)	AAL overlap (%)	Ch	S-D	S-D distance (mm)	AAL overlap (%)
1	F3 - AF3	30	Frontal_Mid_L (94) Frontal_Sup_L (6)	24	F4 - AF4	30	Frontal_Mid_R (100)
2	F3 - Fz	45	Frontal_Sup_L (79) Frontal_Mid_L (21)	25	F4 - Fz	45	Frontal_Sup_R (100)
3	F3 - F5	25	Frontal_Mid_L (100)	26	F4 - F6	25	Frontal_Mid_R (71) Frontal_Inf_Tri_R (29)
4	F7 - F5	20	Frontal_Inf_Orb_L (100)	27	F8 - F6	20	Frontal_Inf_Orb_R (69) Frontal_Inf_Tri_R (31)
5	F3 - FC3	25	Frontal_Mid_L (94) Frontal_Inf_Tri_L (6)	28	F4 - FC4	25	Frontal_Mid_R (100)
6	FC5 - F5	25	Frontal_Inf_Tri_L (100)	29	FC6 - F6	25	Frontal_Inf_Tri_R (100)
7	F7 - FT7	25	Frontal_Inf_Orb_L (100)	30	F8 - FT8	25	TempI_Pole_Sup_R (100)
8	FC5 - FC3	25	Frontal_Inf_Tri_L (83) Frontal_Inf_Oper_L (17)	31	FC6 - FC4	25	Frontal_Inf_Tri_R (93) Frontal_Inf_Oper_R (7)
9	FC5 - FT7	25	TempI_Pole_Sup_L (100)	32	FC6 - FT8	25	Temporal_Sup_R (79) TempI_Pole_Sup_R (21)
10	C3 - FC3	25	Precentral_L (100)	33	C4 - FC4	25	Precentral_R (100)
11	FC5 - C5	25	Rolandic_Oper_L (100)	34	FC6 - C6	25	Postcentral_R (69) Precentral_R (31)
12	T7 - FT7	25	Temporal_Mid_L (100)	35	T8 - FT8	25	Temporal_Mid_R (100)
13	C3 - C5	25	Postcentral_L (100)	36	C4 - C6	25	Postcentral_R (100)
14	T7 - C5	25	Temporal_Sup_L (100)	37	T8 - C6	25	Temporal_Sup_R (100)
15	C3 - CP3	25	Postcentral_L (100)	38	C4 - CP4	25	Postcentral_R (80) Parietal_Inf_R (20)
16	CP5 - C5	25	Temporal_Sup_L (100)	39	CP6 - C6	25	Supramarginal_R (100)
17	T7 - TP7	25	Temporal_Mid_L (94) Temporal_Inf_L (6)	40	T8 - TP8	25	Temporal_Mid_R (100)
18	CP5 - CP3	30	Supramarginal_L (100)	41	CP6 - CP4	30	Parietal_Inf_R (100)
19	CP5 - TP7	25	Temporal_Mid_L (100)	42	CP6 - TP8	25	Temporal_Mid_R (55) Temporal_Sup_R (45)
20	CP5 - P5	25	Temporal_Sup_L (76) Supramarginal_L (24)	43	CP6 - P6	25	Supramarginal_R (100)
21	P7 - TP7	25	Temporal_Inf_L (95) Temporal_Mid_L (5)	44	P8 - TP8	25	Temporal_Inf_R (64) Temporal_Mid_R (36)
22	P7 - P5	20	Temporal_Mid_L (100)	45	P8 - P6	20	Temporal_Mid_R (100)
23	P7 - PO7	20	Temporal_Inf_L (94) Temporal_Mid_L (6)	46	P8 - PO8	20	Occipital_Mid_R (100)

Table 3.1 Table depicting the brain labels of the fNIRS channels in the current setup based on the probabilistic spatial registration of the fNIRS channels to a 6-month-old infant AAL template.
Ch = Channel; S-D = Source-Detector pair.

Data Preprocessing

All data preprocessing and analyses were implemented in MATLAB (R2012b, R2014b, Mathworks, Massachusetts) using in-house scripts as well as third-party toolboxes and functions. Quality assurance figures were generated for all participants after each preprocessing step. An example of these figures is presented in Appendix A.

MATLAB Toolboxes employed in the current study:

- Homer2 software package (Huppert et al., 2009; <https://homer-fnirs.org>).
- BrainWavelet Toolbox (Patel et al., 2014; <http://www.brainwavelet.org/about>).
- ICASSO Toolbox (Himberg et al., 2004; <https://research.ics.aalto.fi/ica/icasso/>).

Resting-State Functional Connectivity in Infants

- Automatic Choice of Dimensionality for PCA (Minka, 2000; <https://tminka.github.io/papers/pca/>).
- Network Based Statistics (Zalesky et al., 2010; <https://www.nitrc.org/projects/nbs/>).

The preprocessing pipeline for each individual is presented below:

1. Light intensity data (i.e., raw data measured at the instrument) were converted into optical density changes. \Rightarrow hmrIntensity2OD function in Homer2.
2. Noisy segments typically occurring at the beginning and/or at the end of each dataset, corresponding to awake activity of the infants (i.e., before the infant fell asleep and/or after the infant woke up), were visually identified based on MATLAB plots and manually rejected. \Rightarrow Plot function in MATLAB.
3. Motion induced spikes and signal drifts were corrected using the wavelet-based despiking method (Patel et al., 2014), which has been described in chapter 2. \Rightarrow WaveletDespike function in Brain Wavelet Toolbox. Input parameters: wavelet = d4; threshold = 0.02; boundary = reflection; chsearch = moderate; nscale = extreme.
4. Optical density data were converted into HbO and HbR concentration changes. Differential path length factors of 5.3 (760 nm) and 4.2 (850 nm) were considered based on the general equation presented in Scholkmann et al., (2013). \Rightarrow hmrOD2Conc in Homer2.
5. Datasets were limited to 5000 samples (\sim 560 seconds) to ensure a homogenous contribution across participants, in terms of number of observations, for the first and second-level statistical analyses. This step was performed by visually inspecting the data in order to select the segment displaying the best data quality. \Rightarrow Plot function in MATLAB.
6. Temporal filtering and global signal regression were performed simultaneously in a unique nuisance regression step (Lindquist et al., 2019). Contribution of high-frequency physiological noise sources (e.g., respiration and cardiac pulsation) was accounted for by including sine and cosines functions for frequencies above 0.09 Hz in the model for nuisance regression. Very slow frequency fluctuations and signal drifts were modelled by adding the first 4 order Legendre polynomials to the design matrix. The average fNIRS signal was included in the regression model to remove globally occurring hemodynamic processes in cerebral and extracerebral tissues assumed to largely reflect systemic hemodynamic changes. As HbO and HbR are differently affected by global systemic processes, data of each hemoglobin chromophore were filtered independently by including in the model either the global HbO or HbR signal. \Rightarrow see MATLAB Box 3.1.

MATLAB Box 3.1

Implementation of filtering and global signal regression in a single linear regression model

```
% The following variables should be defined in advance
% data = data (HbO or HbR) in the format time x channels
% sf = sampling frequency of the fNIRS system
% global_signal = mean signal calculated on filtered data
% Note that global signal will be different on each participant and for HbO and HbR
% lpf = Low-pass filter

% 1 - Create Legendre Polynomials (high-pass filter)
% Compute length of the dataset (samples)
n_data = size(data,1);
% Compute length of the dataset (seconds)
s_data = n_data/sf;
% Calculate order of Legendre polynomials
k = 1 + floor(s_data/150);
% Create a basis set of Legendre polynomials (L)
n = linspace(-1,1,n_data)';
L = zeros(n_data,k+1);
for i = 1:k+1
    tmp = legendre(i-1,n);
    tmp = tmp(1,:);
    L(:,i) = tmp/max(abs(tmp));
end

% 2 - Create matrix of sines and cosines for all frequencies in the sf range
dft_matrix = dftmtx(n_data);
% Find index of the low-pass filter = frequency of interest
idx = floor((lpf/sf)*n_data);
% Select regressors of interest
dft_matrix_lpf = dft_matrix(idx:n_data-idx+1,:);
% Select sines and cosines
sin_lpf_mtx = imag(dft_matrix_lpf);
cos_lpf_mtx = real(dft_matrix_lpf);
% Matrix (time x frequency) of sines and cosines of frequencies above lpf
lpf_mtx = [cos_lpf_mtx' sin_lpf_mtx'];

% 3 - Compute nuisance regression (filter and global signal)
% Remember that the global signal for each participant should be calculated on
% filtered data to avoid reintroducing frequencies of non-interest
% Create matrix with regressors for filtering
reg_mat = [L lpf_mtx global_signal];
beta_data = pinv(reg_mat)*data;
data_filtered = data - reg_mat*beta_data
```

Data Analysis

Functional Connectivity Analyses

Temporal Group ICA

Group-level functional networks (FN) were computed by means of a tGICA (Beckmann et al., 2009; see Figure 3.8 below), by temporally concatenating all participants' datasets after time-series normalization to zero mean and unit variance, producing a single group dataset with dimensions [*channels* (46) x *Hb chromophores* (2) x *time points* (5000) x *participants* (99)]. The *FastICA* algorithm (Hyvärinen, 1999) was applied to the group dataset to extract 15 independent components (ICs), which corresponds to the number of principal components explaining 60% of group data variance. The choice of this parameter is explained in Appendix B. The subject-specific spatial maps associated with each independent FN were obtained using a dual-regression approach. This two-step method involves an initial spatial regression of the tGICA spatial maps of interest to the subject-specific fNIRS dataset, to obtain the subject-specific time courses associated with each group-level ICs. Then, a linear model fit is computed between the estimated subject-specific time courses and the subject-specific fNIRS datasets, to estimate the subject-specific spatial

Resting-State Functional Connectivity in Infants

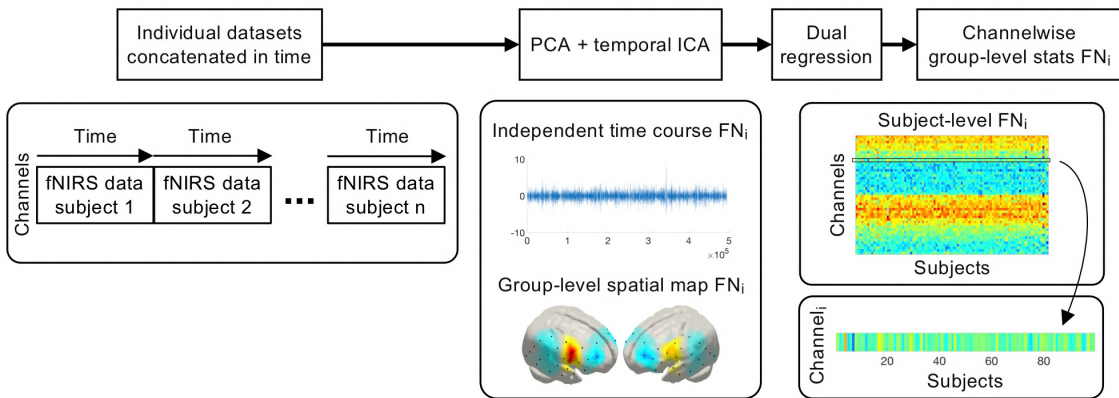


Figure 3.3 Processing pipeline for the temporal group ICA (tGICA) method.

maps. Statistically significant differences between groups were tested channelwise for each FN by performing a one-way random effects ANOVA with language background as a factor (i.e., BIL, SP and BQ), resulting in 15 spatial maps describing between group differences (i.e., channelwise F-test). Statistical tests were corrected for multiple comparisons at the channel level using the false discovery rate (FDR; $q < 0.05$) method (Benjamini and Hochberg, 1995).

Connectome Based Analyses

Two connectome-based analyses (Amico et al., 2017) were performed based on the individual functional connectivity matrices (i.e., connectomes) computed in all infants: 1) a connectome-based ICA (connICA, Amico et al., 2017), and 2) Network Based Statistics approach (NBS, Zalesky et al., 2010). The input of these methods are the functional connectivity matrices obtained for each participant, which were computed based on a robust Pearson's correlation approach as recommended in Santosa et al., (2017).

For each individual, the temporal synchronization between channels was evaluated by computing a pairwise robust Pearson's correlation between the time courses of the HbO and HbR signals separately at every channel for each infant. This robust correlation approach reduces the contribution of possible outlier time points (e.g. due to residual motion artefacts after preprocessing and wavelet denoising) in the correlation estimation (Santosa et al., 2017). Briefly, for each i, j element representing the preprocessed time series of channels i and j , a joint weighting matrix is calculated as

$$r\{t\} = \sqrt{{i_{\{t\}}}^2 + {j_{\{t\}}}^2}$$

A weighting function (S) defined as

$$S\left(\frac{r}{\sigma}\right) = \begin{cases} 1 - \left(\frac{r}{\sigma - k}\right)^2, & \left|\frac{r}{\sigma}\right| < k \\ 0, & \left|\frac{r}{\sigma}\right| \geq k \end{cases}$$

is applied to each i, j element such that $i_W = Si$ and $j_W = Sj$. The correlation for each entry of the functional connectivity matrix is computed between the preprocessed weighted

signals i_W , j_W . In this study, $k = 4.685$ was defined as this is the value usually employed in the literature, and σ was calculated from the median absolute deviation (MAD) of the signal r as $\sigma = 1.4826 \text{ MAD}(r)$ (Santosa et al., 2017). Individual robust functional connectivity matrices representing the temporal association between all channel pairs were defined for HbO and HbR, where the i_W , j_W element reflects the robust Pearson's correlation between channels i_W and j_W . For the sake of simplicity, hereinafter the robust functional connectivity matrices will be referred to as functional connectivity matrices. Individual functional connectivity matrices were then converted from r values to z -scores by Fisher's r-to-z transform (*atanh* function in MATLAB), and averaged across subjects within each experimental group. For illustration, the functional connectivity matrix of a representative infant and the average functional connectivity matrix for each group of infants (Spanish monolingual, Basque monolingual and Spanish-Basque bilingual) are presented in Figure 3.6.

connICA

Individual functional connectivity matrices of HbO and HbR were input to a hybrid connectome-based ICA (connICA) (Amico et al., 2017; Amico and Goñi, 2018). First, the upper triangular part of the symmetric functional connectivity matrices of HbO and HbR were vectorized and concatenated for each individual (see Figure 3.4). These vectors were concatenated in rows to form a group-level functional connectivity matrix of dimensions [99 participants] x [1035 connectivity pairs x 2 Hb chromophores]. The integration of the information on functional connectivity provided by HbO and HbR was done under the premise that similar RSFC patterns should be observed across Hb chromophores (Mesquita et al., 2010; Homae et al., 2011; Ferradal et al., 2015). Next, the *FastICA* algorithm (Hyvärinen, 1999) was applied to this group-level matrix to obtain a set of latent group-level independent functional connectome components (FCCs), and their corresponding weights in each participant. From this analysis 11 ICs were extracted, a number that is equal to the number of principal components necessary to explain 60% of the group data variance. The criteria for ICA model order selection are explained in detail in Appendix B. Finally, the individual IC weights were evaluated as random effects, and ANOVA was performed with language background as a factor (i.e., BIL, SP and BQ) to examine differences across experimental groups in the prominence of the extracted independent FCCs. Statistical tests were corrected for multiple comparisons at the component level using the false discovery rate (FDR; $q < 0.05$) method (Benjamini and Hochberg, 1995).

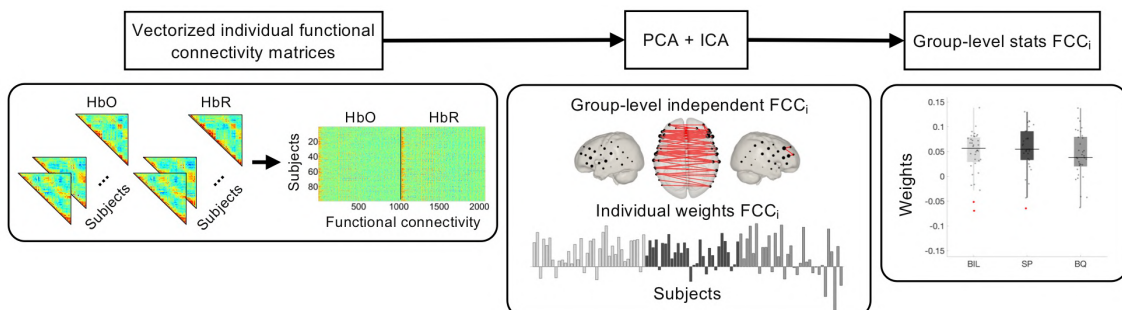


Figure 3.4 Processing pipeline for the connICA method.

Network Based Statistics

Between-group statistical comparisons of the functional connectivity matrices were also performed using a Network Based Statistic (NBS) approach (Zalesky et al., 2010). The first step of this method is to compute a statistical test (e.g., F-test) on the subjects' FC matrices at each channel pair, obtaining a matrix of the same size (i.e., 46 channels x 46 channels) with each entry filled with the values of the statistical test of interest. This step is equivalent to conducting a mass univariate testing approach at each entry of the FC matrices. In this study, a range of predefined statistical thresholds were applied to this matrix, and channel pairs exceeding the threshold were selected as possible connections for which the null hypothesis can be rejected at the network level. Then, clusters of connections (i.e., networks) are identified among the connections exceeding the threshold, being a network defined as a group of interconnected edges. The significance of the identified networks is tested using nonparametric permutation testing. Participants are randomly exchanged between experimental groups and the previous processing steps are repeated for each permutation ($N = 10,000$ permutations). A measure of the size (i.e., total number of connections) of each network is computed in each permutation and a null distribution is created with the maximal component sizes. Finally, the statistical significance of the network (i.e., the p-value) is calculated as the number of networks generated by permutations that had the same size or greater than the relevant network, divided by the total number of permutations. With this method the familywise error rate is controlled at the cluster level based on the network size. The NBS analysis approach was applied in HbO and HbR derived FC matrices separately, and results for both Hb chromophores are reported.

3.3. Results

Among the 123 infants who were recruited to participate in this study, 99 fNIRS recordings with good data quality in both oxyhemoglobin (HbO) and deoxyhemoglobin (HbR) chromophores were included after data preprocessing and detailed data quality assessment. The final sample included 36 Basque-Spanish bilingual (BIL) infants, 30 Spanish (SP) monolingual infants and 33 Basque (BQ) monolingual infants. For each infant, the data comprised 46 channels covering frontal, temporal and parietal regions of both hemispheres as displayed in Figure 3.1, which depicts the optode and channel location, and the sensitivity profile of the current setup. All infants showed clear peaks in the power spectrum related to the main frequency and harmonics of the respiratory and cardiac fluctuations. An antiphase relationship between HbO and HbR was also considered as data quality indicator (Watanabe et al., 2017) (see Appendix A and B). All of these subjects had recordings with a duration of 9 minutes, which were input for data analysis with temporal group ICA (tGICA), connICA and NBS.

Temporal Group ICA

The functional networks (FNs) obtained in the tGICA analysis (i.e., the ICA spatial maps) are displayed in Figure 3.5. For visualization purposes, relevant FN were selected based on their spatial configuration. FNs with a bilateral and symmetric configuration are

presented and discussed here. The full set of FNs is presented in Appendix B. FNs are depicted as statistical t-stat maps, which were computed from one-sample t-tests on the subject-specific reconstructed spatial maps at the channel level. The observed components were robust across multiple realizations of the ICA algorithm based on the ICASSO method (Himberg et al., 2004) showing consistency values (Iq) ranging from 0.49 to 0.91. All of these networks also exhibited high consistency across HbO and HbR, displaying correlation r values between -0.97 and -0.99 (Appendix B, Table 3.1), as expected due to hemodynamic physiology.

The first three FNs labelled as sensorimotor networks, revealed a symmetric pattern over bilateral areas in the precentral and postcentral gyrus. FN 4 and FN 5 covered mainly areas located in the inferior frontal gyrus and the superior temporal gyrus that could be associated with the auditory and the language networks, respectively. Two FNs were observed over frontal regions: FN 6 was confined to regions in the middle and superior frontal gyrus, and FN 7 comprised middle frontal areas and areas in the inferior parietal gyrus which could be related to the outer brain regions of the default-mode network that have been typically observed in RSFC studies with fMRI. Similar to previous evidence with fMRI data, the observed FNs also exhibited significant patterns of anticorrelated spontaneous activity. In FN 1-5 the spatial distribution of the anticorrelated patterns involved superior and middle frontal areas, in conjunction with posterior areas in the inferior and middle temporal gyrus and with inferior parietal regions. FN 6 showed anticorrelated activity with posterior temporal and inferior parietal regions. In FN 7 the negative spatial pattern was less prominent than the positive part, and included inferior frontal and superior temporal regions. The obtained group-level FNs for HbO and HbR were reconstructed to the subject space using a dual-regression approach (Beckmann et al., 2009) to yield the subject-specific FNs. Between group statistical analyses were conducted to assess the effect of early bilingual exposure on each channel and FN (one-way ANOVA at the channel level, FDR corrected among 46 channels, $q < 0.05$). Significant differences between experimental groups were not observed in any of the FNs under assessment in HbO and HbR.

Functional Network (FN)	Iq	r	ssd (%) total = 100	ssd (%) total = 60
FN 1 Sensorimotor	0.84	-0.99	8.8	4.1
FN 2 Sensorimotor	0.76	-0.98	4.3	3.9
FN 3 Sensorimotor	0.72	-0.99	5.5	3.9
FN 4 Auditory	0.49	-0.98	5.6	3.9
FN 5 Language	0.89	-0.99	7.4	4.0
FN 6 Frontal	0.91	-0.99	10.5	4.2
FN 7 Default-Mode	0.80	-0.97	6.2	4.0

Table 3.1 tGICA model order evaluation metrics for the PCA threshold selected in this study (i.e., 60%). ICASSO cluster robustness index (Iq) and HbO-HbR correlation (r) values are displayed. Sum of squared differences (ssd) are computed with respect to the data after PCA (total = 100%) and with respect to the original data without PCA (total = 60%).

Resting-State Functional Connectivity in Infants

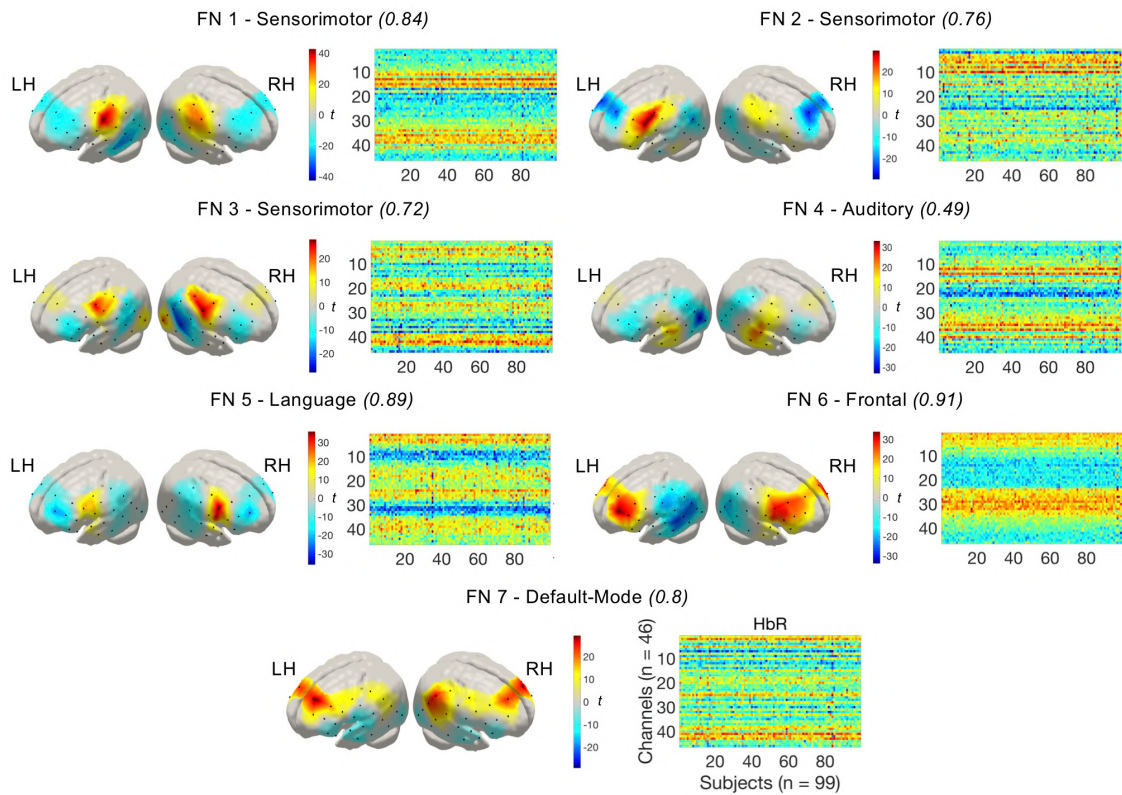


Figure 3.5 Functional networks (FNs) representing the spatial maps derived from the tGICA method. Colorbar shows the t-value of the channel level one-sample t-test computed for each spatial map. Individual spatial maps (i.e., dual-regression maps) of these FNs are displayed in matrix form with rows showing the weights of the FNs on each channel and columns representing participants.

connICA

The input of the connICA method are the functional connectivity matrices obtained for each participant, which were computed based on a robust Pearson's correlation approach as recommended in Santosa et al., (2017). A high degree of similarity can be observed at the individual and at the group level in the configuration of the functional connectivity matrices (Figure 3.6). A marked negative correlation between HbO and HbR and a stronger correlation between homotopic regions is also evident on these matrices. These features were considered indicative of the quality and reliability of the current datasets.

The group-level functional connectome components (FCCs) extracted from the connICA analysis are depicted in Figure 3.7. In this approach, relevant FCCs were also selected based on their spatial configuration. The full set of FCCs is presented in Appendix B. For the sake of representation, each plot only displayed the 10% largest positive connections between nodes (i.e., fNIRS channels), and the size of the node represented the number of connections linked to it. Similar to the tGICA results, FCCs showed a high level of robustness based on the ICASSO algorithm, with consistency values (I_q) between 0.5 and 0.96, and a large degree of similarity between the HbO and HbR derived components, with correlation r values between 0.7 and 0.95 (Table 3.2). The first FCC is characterized by local, short-range, connections between adjacent nodes. It involved

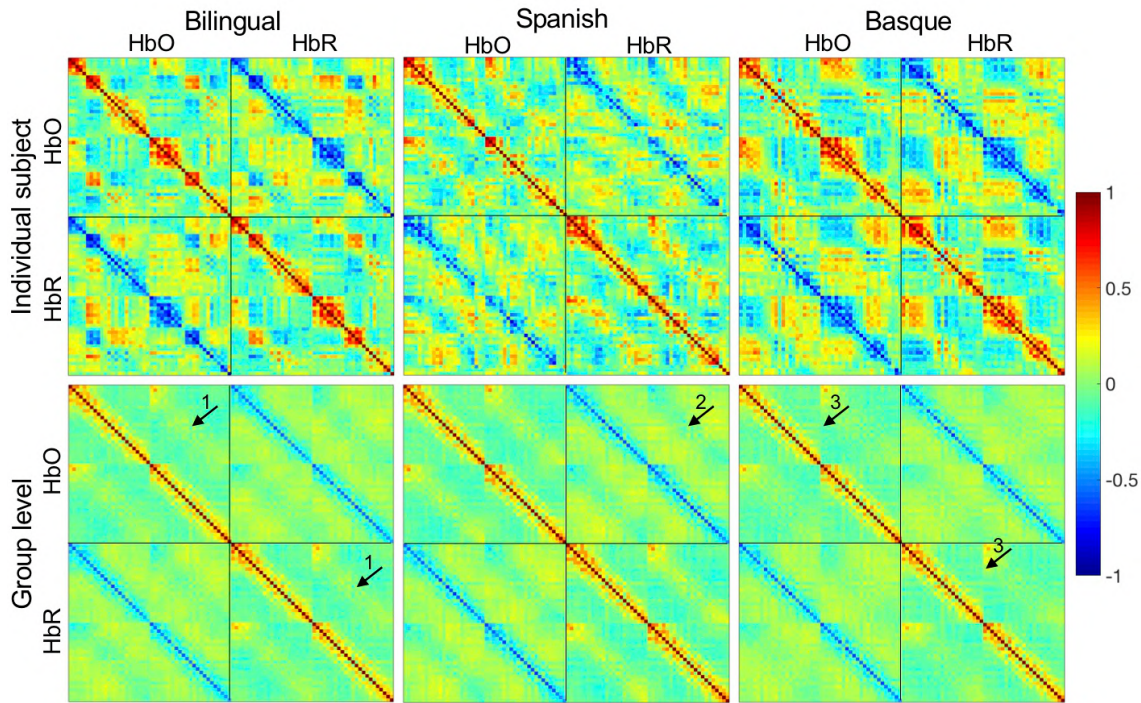


Figure 3.6 Robust functional connectivity matrices of representative individual subjects (first row) and at the group level (second row) for each of the three experimental groups. In each plot, the robust functional connectivity matrix for HbO and HbR is shown in the top-left part and bottom-right part, respectively. The robust functional connectivity matrix representing the correlation between HbO and HbR is shown in the top-right part. Note that plots are symmetric with respect to the main diagonal. In these plots, channels are ordered from anterior to posterior and from left to right. This allows visualizing an increased correlation between homotopic channels in HbO and HbR (see arrow 1), an increased negative correlation between homotopic channels between HbO and HbR (see arrow 2) and a clear delimitation of left and right hemispheres (see arrow 3).

within hemisphere connections between nodes over the whole fNIRS setup, with interhemispheric connections constrained to the most anterior nodes. FCC 2 reflected functional connectivity between homotopic channels across hemispheres. FCC 3 and FCC 4 showed a high degree of symmetry, displaying mainly short and long-range within hemisphere connections. FCC 5 and FCC 6 also showed a highly symmetric pattern, revealing that nodes located over superior temporal gyrus were functional hubs with a large number of intrahemispheric connections between temporal and frontal regions, and interhemispheric connections with frontal and posterior temporo-parietal regions. Finally, FCC 7 and FCC 8 were also highly symmetric, with their main functional hubs in precentral and inferior frontal regions showing intrahemispheric connections across frontal and precentral regions and interhemispheric connections between frontal, superior temporal and precentral regions. Appendix B includes the figures with the complete positive and negative parts of the component for all the functional components calculated with connICA approach and for HbO and HbR. Statistical analyses assessing significant differences across experimental groups were computed on the individual weights that quantify the prominence of each independent FCC in each individual. A one-way ANOVA at the FCC level (FDR corrected among 11 FCC, $q < 0.05$) indicated no significant differences between monolingual and bilingual infants in any of the FCCs.

Resting-State Functional Connectivity in Infants

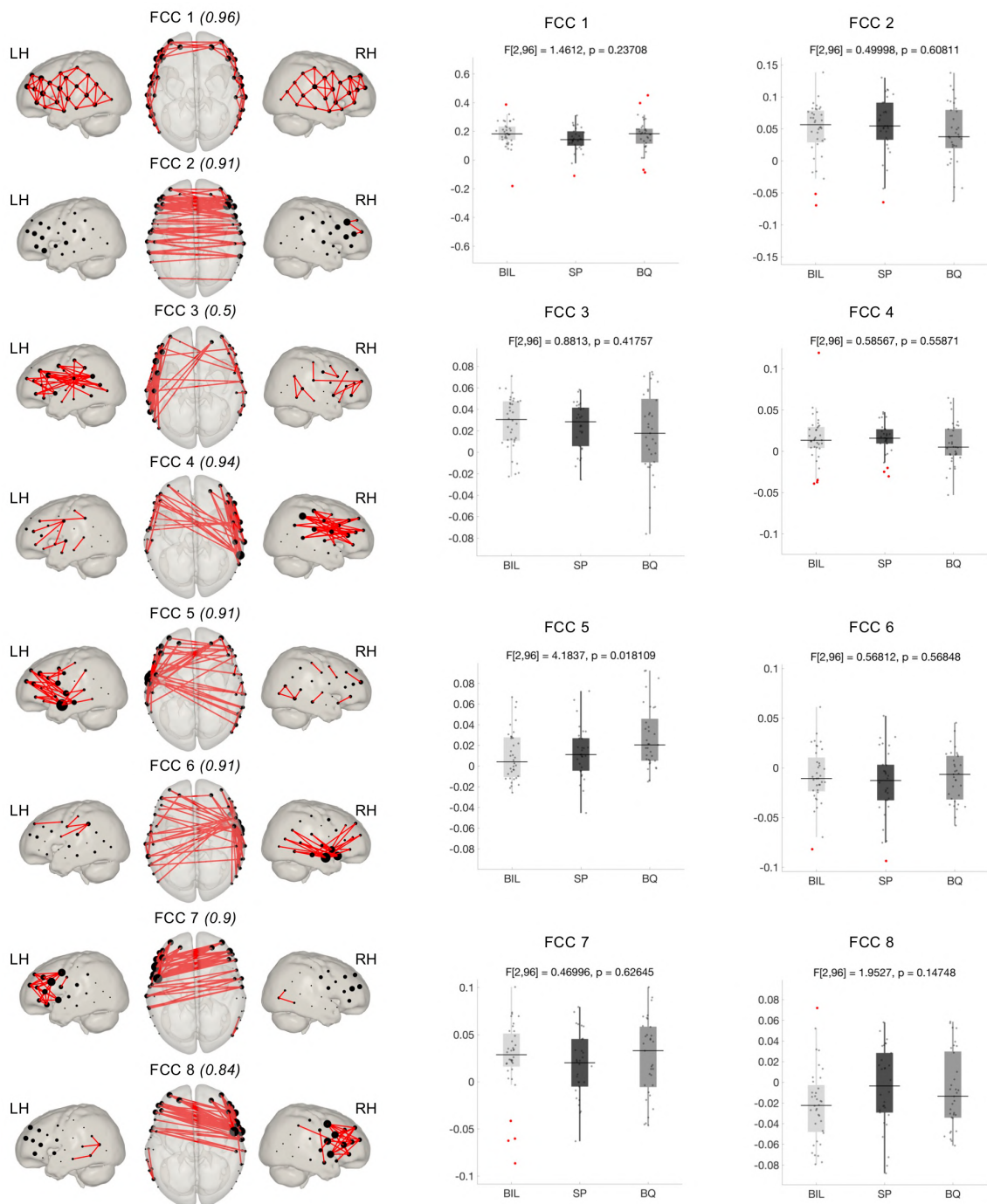


Figure 3.7 Functional connectivity components (FCC) extracted using the connICA method. Components have been thresholded to show only the top 10% of connections (absolute value). Node size was adjusted based on the number of connections reaching each node. Due to the high similarity between HbO and HbR components, FCCs are shown for HbR only.

Functional Connectome Component (FCC)	<i>Iq</i>	<i>r</i> (HbO-HbR)	<i>ssd</i> (100 %)	<i>ssd</i> (60 %)
FCC 1	0.96	0.95	24	5.5
FCC 2	0.91	0.88	7.2	5.5
FCC 3	0.50	0.70	7.4	5.4
FCC 4	0.94	0.72	7.8	5.4
FCC 5	0.91	0.80	7.3	5.5
FCC 6	0.91	0.83	7.3	5.4
FCC 7	0.90	0.90	8.8	5.6
FCC 8	0.84	0.84	7.3	5.4

Table 3.2 Model order evaluation metrics for the PCA threshold selected (i.e., 60%) in the connICA approach. ICASSO cluster robustness index (*Iq*) and HbO-HbR correlation (*r*) values are displayed. Sum of squared differences (*ssd*) are computed with respect to the data after PCA (total = 100%) and with respect to the original data without PCA (total = 60%).

NBS

Statistical differences between experimental groups were computed on the individual functional connectivity matrices using a Network Based Statistics (NBS) approach (Figure 3.8). Several NBS thresholds (F-values) were assessed to detect potential effects with different characteristics (e.g., weak effects involving a large number of connections or strong effects involving a small number of connections). Statistically significant differences between groups were not observed at any of the statistical thresholds considered either in HbO or HbR. Results showed that the size of the observed networks decreased for larger statistical thresholds (F-values). The curves of p-values were closer to significance for HbR group comparisons than for HbO at the lower statistical thresholds, where network size was also larger in HbR than in HbO. For higher thresholds (i.e., $F > 3$) HbO and HbR showed similar network size and p-values.

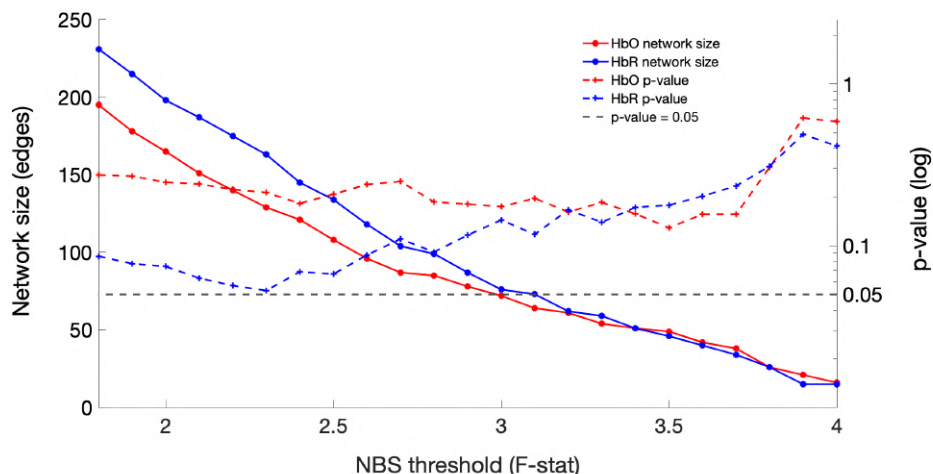


Figure 3.8 Statistical significance of the functional network differences assessed using NBS for a range of statistical thresholds. Between-group differences were not observed in any of the statistical thresholds under consideration.

3.4. Discussion

This work described resting-state functional connectivity (RSFC) based on long, high quality fNIRS data acquired on a large cohort of 4-month-old monolingual and bilingual infants to evaluate the effect of bilingualism in functional brain connectivity at this early stage of language acquisition. This sample of 99 valid participants is the largest sample of infants ever acquired with long fNIRS recordings (9 min per infant). While no significant group differences emerged to the main neuroscientific question of the study (i.e. differences between monolingual and bilingual infants), large-scale group-level RSFC patterns in the infant brain are reported, resembling those previously observed in the fMRI literature and in fNIRS studies with adults.

RSFC patterns were extracted using two data analyses approaches based on independent component analysis (ICA). The implemented ICA based group-level methods search for independence either between the time-courses of spontaneous hemodynamic activity measured with fNIRS (i.e., temporal group ICA - tGICA) (Beckmann et al., 2009; Smith et al., 2012) or between connectivity patterns across multiple functional connectivity matrices (connICA) (Amico et al., 2017). A Network Based Statistics (NBS) approach was also implemented to study between group-differences in functional network organization.

The main goal of this study was to assess whether an early and continued exposure to a bilingual environment during the first months of life might impact the configuration of the emerging functional connectivity. The human brain's ability to adapt to long-term environmental factors manifests prominently during the first stages of development and it is particularly relevant during early language experience. For this reason, how long-term exposure to two languages affects cognitive and functional brain development has drawn great attention in recent years (Petitto et al., 2012; Costa and Sebastián-Gallés, 2014; Byalistok, 2015; Kovacs et al., 2015). In the current work an effect of bilingualism in RSFC was not observed in any of the three independent functional connectivity analysis methods implemented. This is despite the fact that evidence of differences between monolingual and bilingual infants in previous studies manifested during language task performance (Conboy and Mills, 2006; García-Sierra et al., 2011; Petitto et al., 2012; Ferjan Ramírez et al., 2017; Nácar-García et al., 2018).

While no differences in RSFC emerged between monolingual and bilingual infants, large-scale RSFC patterns reported in the current study resemble those previously observed in prior studies. The functional networks (FNs) extracted with tGICA in the group of infants under assessment yielded evidence for the presence of a marked bilateral functional correlation between homotopic brain regions, which was observed in both HbO and HbR fluctuations. The spatial configuration of the observed FNs indicates that, at this age, RSFC predominantly consists on correlated activity between anatomically and functionally similar regions across hemispheres, as already described in previous works (Fransson et al., 2007; Homae et al., 2010; Perani et al., 2011; Damaraju et al., 2014). FNs located in primary sensorimotor (FN 1-3) and auditory regions (FN) were observed. These networks have been repeatedly reported in infant studies with fMRI (Fransson et al., 2007; Damaraju et

al., 2014; Gao et al., 2015), but evidence from infant studies using optical methods is still limited (Ferradal et al., 2015). A FN overlapping language related regions spreading over the inferior frontal gyrus and superior temporal gyrus (FN 5) was observed. Qualitative assessment of FNs implied a stronger involvement of the right hemisphere in the auditory (FN 5) and language (FN 4) networks (Figure 3.5). This shared feature between language-relevant FN could be linked with previous observations showing increased activity in the right hemisphere for speech input, which has been explained by the fact that infants in the first months of life mainly rely on prosodic information during language processing (Homae et al., 2006; Telkemeyer et al., 2009; Perani et al., 2011).

Homotopic areas over frontal regions also demonstrated a high degree of functional synchronization. One functional network (FN 6) was formed by multiple channels within frontal regions and across the midline. The spatial organization of this network supports existing evidence showing that frontal regions become functionally connected during the first year of life (Homae et al., 2010; Homae et al., 2011; Damaraju et al., 2014; Gao et al., 2015). The second functional network (FN 7) showed a symmetric functional connectivity pattern involving channels in middle frontal and inferior parietal regions, which is consistent with the spatial topology of the default-mode network. Evidence of a developing default-mode network has been observed in infants (Gao et al., 2009; Damaraju et al., 2014; Gao et al., 2015), even though these results should be interpreted with caution due to the limited spatial resolution of the current experimental setup and the inability of fNIRS to measure deep medial and subcortical regions, such as posterior cingulate cortex and precuneus that are usually reported in fMRI studies.

The connICA approach was applied to identify macroscale properties of functional network organization at the group level based on the individual functional connectivity matrices (Amico et al., 2017). The functional relations between fNIRS channels formed coherent interregional ensembles with distinct topological properties of large-scale functional connectivity. The first functional connectome component (FCC 1) showed short-range functional connectivity between adjacent channels, spanning the whole fNIRS optode setup. This functional connectivity pattern has been shown to progressively decrease over the course of development, whereas long distance connections tend to increase towards a more distributed functional brain organization (Homae et al., 2010; Ouyang et al., 2017). The second component (FCC 2) displayed interhemispheric correlations between homotopic regions. This type of functional connectivity is prevalent in most of the studies that have assessed RSFC in infant subjects and has been linked with the interaction between functional and structural brain maturation (Fransson et al., 2007; Homae et al., 2010; Perani et al., 2011; Gao et al., 2015). Due to the marked spatial symmetry observed in components FCC 3 to FCC 8, they are presented in pairs in Figure 3.7. FCC 3 and FCC 4 displayed mostly within hemispheric connectivity between anterior and posterior brain regions in the left and right hemispheres respectively. Functional networks extracted with the tGICA approach also showed patterns of long-range within hemisphere connectivity, but evidence from previous studies suggests that, at this age, this type of connectivity is still immature (Homae et al., 2010; Perani et al., 2011; Gao et al., 2015). FCC 5 and FCC 6 showed a functional hub in the left and right auditory cortices, which are densely

Resting-State Functional Connectivity in Infants

interconnected with frontal and posterior temporal regions within and across hemispheres. In FCC 7 and FCC 8 connections converged over channels located in precentral and inferior frontal gyrus, which showed intra and interhemispheric connections with channels localized in frontal regions. Due to their spatial characteristics, these components might well represent the activity of sensorimotor, auditory or language regions, in which functional brain networks have been consistently identified in infant populations (Fransson et al., 2007; Perani et al., 2011; Damaraju et al., 2014; Ferradal et al., 2015). Results for the NBS analysis revealed no significant differences between experimental groups. In contrast to connICA, this approach investigates global network differences based on the whole functional connectivity matrix, and not on specific components. Considering that differences were not observed in any subcomponent extracted using the connICA method, it might be reasonable that differences did not emerge either at the global level.

Results for both ICA methods showed reliable patterns of correlated and anticorrelated activity within the observed FNs and FCCs. A question that might arise from these findings is whether the observed patterns of negative functional connectivity are the result of the preprocessing pipeline including global signal regression, or if they reflect intrinsic, functionally meaningful properties of network organization (Murphy and Fox, 2017). To address this dichotomy, data analyses were repeated on the same datasets without applying global signal regression. Results demonstrated that anticorrelated patterns of functional connectivity were still present but FNs and FCCs were less spatially interpretable. Considering these outcomes, and in order to account for the effects of systemic physiological confounds that are commonly described in fNIRS recordings (Tachtsidis and Scholkmann, 2016), results with a preprocessing pipeline including global signal regression were described here.

Most previous optical imaging studies assessing RSFC reported only positive correlations, or presented both positive and negative correlations in the results but only discussed the former (Zhang H. et al., 2010; White et al., 2012). This has been in part due to the limited field of view of the fNIRS setups employed in these studies, but also due to the lack of a straightforward interpretation of the observed anticorrelated activity in the literature (Murphy and Fox, 2017). An interesting finding is that the regions involved in the anticorrelated networks observed in most of the primary FNs considerably overlap with the spatial configuration of the FN labelled as the default-mode network (FN 7). It is therefore a possibility that this activity might reflect higher-level functional interaction between task-positive and task-negative brain regions (Fox et al., 2005; Hampson et al., 2010; Murphy and Fox, 2017).

As the effect bilingualism on functional brain development may not be manifested as a differential configuration of intrinsic functional connectivity, the study presented in Chapter 5 aims to examine potential differences on language processing as a consequence of bilingualism in infants at the same age as in the current study. Furthermore, an effect of bilingualism on RSFC has only been demonstrated on adult participants (Luk et al., 2011; Grady et al., 2015; Berken et al., 2016; Kousaie et al., 2017; Gullifer et al., 2018; Sulpizio et al., 2020). Therefore, further research with monolingual and bilingual infants at different

ages should help clarify whether differences in intrinsic functional connectivity due to the complexity of growing exposed to two linguistic systems might emerge a later point in development.

It is also possible that testing asleep infants prevented from detecting subtle differences in RSFC properties across experimental groups (Watanabe et al., 2014; Lee et al., 2020). However, all previous studies assessing RSFC in infants of a similar age as here have been conducted during sleep, irrespective of the imaging modality (i.e., fMRI or fNIRS). Several studies have identified RSFC differences induced by the effect of different factors such as premature birth (Smyser et al., 2010) or socioeconomic status (Gao et al., 2015). These imaging techniques are extremely sensitive to motion induced artifacts that are commonly observed in acquisitions on awake participants. This considerably degrades the reliability of the inferred temporal correlations between voxel or channel time courses (Santosa et al., 2017). Since the priority for this study was to collect RSFC data of good quality, participants were tested during natural sleep only, which consequently also allowed performing longer recordings. In addition, by testing all infants under similar conditions (i.e., immediately after they fall sleep), a homogenous sleep state is ensured across participants (Gao et al., 2017), restricting any possible bias owing to differences in cognitive state across infants.

3.5. Summary

RSFC can be reliably measured in young infants using fNIRS. In this work, relying on datasets with high data quality and applying appropriate analyses techniques for group-level statistical comparisons, no differences emerged between monolingual and bilingual infants. In light of previous research that demonstrated neural adaptation in bilingual infants in linguistic tasks at 4 months of age, these results suggest that intrinsic functional networks of the brain are not affected by bilingual experience at 4 months of age. Further, considering previously reported differences in adult monolingual vs. bilingual RSFC patterns, the current results suggest that RSFC do not necessarily reflect differences as a function of bilingual vs. monolingual learning environment by 4 months of age. At what stage of development RSFC begin to show changes depending on language environment is open for future research

Chapter 4

Statistical Challenges in Resting-State Functional Near-Infrared Spectroscopy Data Analysis

4.1. Theoretical Motivation

As described in Chapter 2, the hemodynamic changes elicited by neuronal activity recorded in the functional near-infrared spectroscopy (fNIRS) signal contain multiple non-neuronal fluctuations, such as instrumental noise and trends, subject-specific components (e.g., motion-related effects), and hemodynamic fluctuations originated in the cerebral and extracerebral compartments (Tachtsidis and Scholkmann, 2016; Pfeifer et al., 2018). These systemic physiological fluctuations are mainly related to changes in blood pressure (0.1 Hz), respiration (0.3 to 0.6 Hz), and cardiac pulsation (1 to 2 Hz) and are consistently present at specific frequencies and across measurement channels. Consequently, the RS-fNIRS signal shows a colored frequency spectrum (i.e., it is not a white process with equal energy across all its frequencies), and it exhibits non-zero temporal autocorrelation.

This fact is relevant when resting-state (RS) functional connectivity is examined based on pairwise correlation measures. Physiological components in RS-fNIRS data introduce spurious common variance across time-series, artificially increasing correlation between the signals of different channels. RS-fNIRS time-series are also affected by the filtering effect of the actual hemodynamic response function (HRF) that acts as a low-pass filter with cut-off frequency approximately around 0.1 to 0.2 Hz. As first noted by Granger and Newbold (1974) the correlation between two random signals will artificially increase if these signals exhibit nonzero temporal autocorrelation. Thus, the intrinsic autocorrelation present in the RS-fNIRS time-series may artificially inflate correlation values, increase the false-positive rate under the null hypothesis of no correlation between channels, and potentially compromise the validity of data analyses outcomes (Huppert et al., 2016; Santosa et al., 2017).

The impact of temporal autocorrelation in the validity of statistical estimation has been widely discussed in the analysis of task-related activity in functional magnetic resonance imaging (fMRI) data (Bullmore et al., 1996; Friston et al., 2000; Woolrich et al., 2001), but only recently in the fNIRS literature (Barker et al., 2013; Hassanpour et al., 2014; Barker et al., 2016; Huppert, 2016). The most common way to account for signal autocorrelation is to prewhiten the signal, so that the residuals of a linear regression model, describing the hypothesized task-related activity, become uncorrelated (i.e., white). The use of prewhitening in the analysis of RS data is less common, and only few studies have suggested prewhitening of the signal itself, either in fMRI (Christova et al., 2011; Arbabshirani et al., 2014) or fNIRS data (Santosa et al., 2017). By prewhitening RS data, it is expected that the signals become white, removing temporal autocorrelation, thus reducing false-positive rates.

Yet, this approach also presents some caveats. It can be assumed that the colored frequency spectrum of the RS-fNIRS signal is partially originated by physiological noise or induced by the blurring effect of the HRF. However, spontaneous neural oscillations as measured with electrophysiological techniques also exhibit a colored frequency profile, typically characterized as a $1/f$ spectrum (Pritchard et al., 1992; Lombardi et al., 2017). In this scenario, convolving a neural signal with $1/f$ frequency profile with the HRF and adding physiological noise, as is the case in RS-fNIRS signals, would still leave a signal that

has a $1/f$ profile in the limited band of the HRF. Therefore, it might not be a reasonable null hypothesis to expect RS-fNIRS signals to be white, as this would imply that the information related to the HRF might have been partially or completely removed, which would complicate the neurophysiological interpretation of the signal that is left after applying prewhitening. A careful examination of the effect of prewhitening on the physiological and functional properties of the RS-fNIRS signal for functional connectivity analyses is necessary before routinely implementing this step in the RS-fNIRS preprocessing pipeline.

The current chapter evaluated the effect of prewhitening during the analysis of experimental RS-fNIRS data. For this purpose, two previous fNIRS studies that assessed RS activity in infants (Homae et al., 2010; Watanabe et al., 2017) were replicated on a dataset collected in 4-month-old sleeping infants, by following similar data acquisition, preprocessing, and analysis procedures as in the original studies. Results obtained following a standard preprocessing pipeline (i.e., as done in the previous studies) were compared with the results after incorporating two common prewhitening approaches in the preprocessing pipeline. The two prewhitening approaches included a non-parametric approach (i.e., assuming no model for the autocorrelation) widely used for fMRI data analyses (Woolrich et al., 2001), and a parametric approach assuming a stochastic autoregressive (AR) process as described in Barker et al., (2013). The comparison of the two algorithms allowed evaluating the consistency of the results across different prewhitening methods.

4.2. Methods

Ethics Statement

This study was carried out at the Basque Center on Cognition, Brain and Language and received approval from its local ethical committee. This study involved the participation of infant subjects. Prior to participation, parents were informed about the aim of the study, the experimental procedures, and their legal rights, including the right to withdraw from the study at any moment without providing a reason and with no negative consequences. Written informed consent was obtained from the parents prior to data acquisition.

Study Population and Data Acquisition

Data from 24 healthy infants were included in this study (age: 124 ± 3 days, 12 female). These data came from a subsample of the set of participants described in Chapter 3, concretely from the bilingual group. Data acquisition procedures were the same as those described in Chapter 3.

Data Preprocessing

All data preprocessing and analysis were implemented in MATLAB (R2012b, R2014b, Mathworks, Massachusetts) using in-house scripts as well as third-party toolboxes and functions.

The following MATLAB Toolboxes were employed in the current study:

- Homer2 Software Package (Huppert et al., 2009; <https://homer-fnirs.org>).
- BrainWavelet Toolbox (Patel et al., 2014; <http://www.brainwavelet.org/about>).
- Circular Statistics Toolbox (Berens, 2009; www.jstatsoft.org/article/view/v031i10).

The preprocessing pipeline for each individual included the following steps:

1. Light intensity data (i.e., raw data measured at the instrument) were converted into optical density changes. $\Rightarrow hmrIntensity2OD$ function in Homer2.
2. Noisy segments typically occurring at the beginning and/or at the end of each dataset, corresponding to awake activity of the infants (i.e., before the infant fell asleep and/or after the infant woke up), were visually identified based on MATLAB plots and manually rejected. $\Rightarrow Plot$ function in MATLAB.
3. Motion induced spikes and signal drifts were corrected using the wavelet-based despiking method (Patel et al., 2014; see Chapter 2) $\Rightarrow WaveletDespike$ function in Brain Wavelet Toolbox. Input parameters: wavelet = d4; threshold = 0.02; boundary = reflection; chsearch = moderate; nscale = extreme.
4. Optical density data were converted into HbO and HbR concentration changes. Differential path length factors of 5.8 (760 nm) and 4.2 (850 nm) were considered based on the general equation presented in Scholkmann et al., (2013). $\Rightarrow hmrOD2Conc$ in Homer2.
5. HbO and HbR signals were bandpass filtered between 0.005 and 1 Hz. This filter was selected in order to match one of the previous studies aimed to be replicated (Homae et al., 2010). $\Rightarrow hmrBandpassFilt$ in Homer2.
6. Datasets were limited to 5100 samples (~571 seconds) to ensure a homogenous contribution across participants, in terms of number of observations, for the first and second-level statistical analyses. This step was performed by visually inspecting the data in order to select the segment displaying the best data quality. $\Rightarrow Plot$ function in MATLAB.
7. Two prewhitening methods were implemented, creating three datasets for comparison in data analysis: 1) bandpass filter (standard data preprocessing), 2) non-parametric prewhitening, and 3) AR prewhitening.
8. The two prewhitening approaches created beginning and end effects in the signal that must be removed prior to data analyses. Hence, the first 150 samples and the last 5 samples of the selected segments were removed. The same approach was followed for the standard preprocessing dataset without prewhitening to match its duration with the recording duration of the two prewhitening approaches. After this step, the total duration of the individual time-series employed in data analyses was 4945 samples (~554 seconds).

Accounting for Temporal Autocorrelation with Prewitthing

Let us consider that the time-series of a specific channel \mathbf{y} follows a normal distribution with zero mean and covariance $\sigma^2\mathbf{V}$ (i.e., $\mathbf{y} \sim N(0; \sigma^2\mathbf{V})$), where \mathbf{V} is the autocorrelation matrix of \mathbf{y} describing the temporal correlation between each time point in the time-series and the rest of the time points. In order to remove temporal autocorrelation between sequential sample points, the aim of prewhitening is to find a matrix \mathbf{S} that filters \mathbf{y} such that $\mathbf{Sy} \sim N(0; \sigma^2\mathbf{SVS}^T)$ and enforces that $\mathbf{SVS}^T = \mathbf{I}$ (Figure 4.1 and footnote¹).

On each participant, each prewhitening method was applied independently on a channel-by-channel basis, for HbO and HbR (46 channels \times 2 hemoglobin parameters). In this work two common prewhitening procedures were implemented:

- 1) A non-parametric approach based on the estimates of the autocorrelation coefficients of the data (MATLAB Box 4.1).
- 2) A parametric approach based on an autoregressive (AR) model of the data.

Non-parametric Prewitthing Approach

In the non-parametric prewhitening approach, the matrix \mathbf{S} was defined based on the raw autocorrelation coefficients of the signal \mathbf{y} . First, the raw autocorrelation coefficients of \mathbf{y} were estimated (*xcorr* function in MATLAB) and used to define the sample autocorrelation matrix \mathbf{V} , which is a symmetric Toeplitz matrix (*toeplitz* function in MATLAB). Then, the Cholesky decomposition [Golub and Van Loan, (2012); *chol* function in MATLAB] of \mathbf{V} was computed to find \mathbf{K} such that $\mathbf{V} = \mathbf{KK}^T$. By defining $\mathbf{S} = \mathbf{K}^{-1}$, it can be shown that the prewhitened signal $\mathbf{y}_{pw} = \mathbf{Sy}$ followed $\mathbf{y}_{pw} \sim N(0; \sigma^2\mathbf{SVS}^T) = N[0; \sigma^2\mathbf{K}^{-1}\mathbf{KK}^T(\mathbf{K}^{-1})^T] = N(0; \sigma^2\mathbf{I})$.

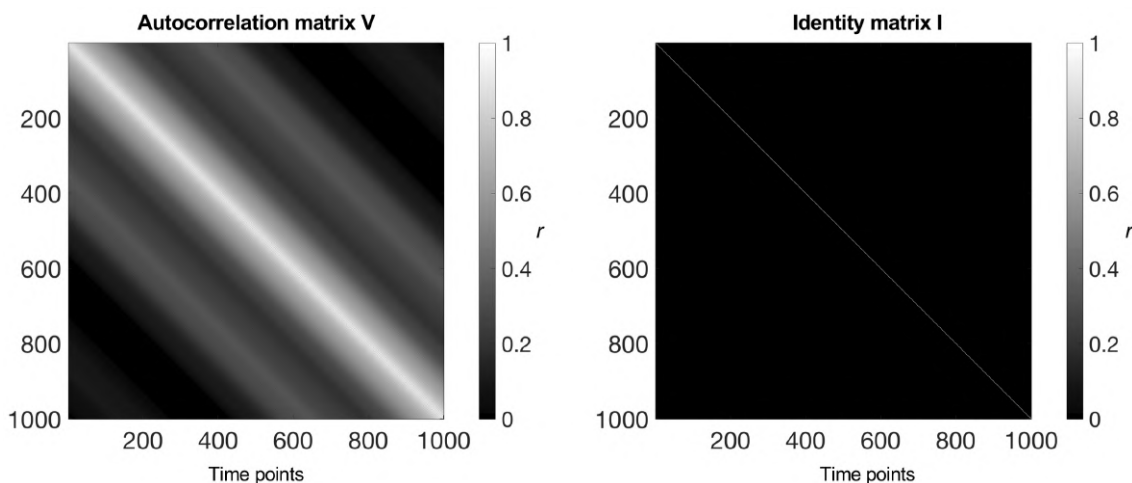


Figure 4.1 Autocorrelation matrix \mathbf{V} obtained from real fNIRS data (1000 time points, left), is presented with an identity matrix (right) of the same size for comparison purposes. In \mathbf{V} high correlation values at several time lags are observed, indicating high levels of correlation between sample points (i.e., temporal autocorrelation). By prewhitening, \mathbf{V} is enforced to become an identity matrix (i.e., zero autocorrelation).

¹Let $E[\mathbf{yy}^T] = \sigma^2 \mathbf{V}$. If $\mathbf{x} = \mathbf{Sy}$, then $E[\mathbf{xx}^T] = E[(\mathbf{Sy})(\mathbf{Sy})^T] = E[\mathbf{S}\mathbf{yy}^T\mathbf{S}^T] = SE[\mathbf{yy}^T]\mathbf{S}^T = \sigma^2\mathbf{SVS}^T$

MATLAB Box 4.1

Implementation of the non-parametric prewhitening approach on a single channel

```
% The following variables must be defined in advance:
% data = single channel signal

% Calculate autocorrelation of data
data_autocorr = xcorr(data, 'coeff');

% Keep only one side of the autocorrelation (they are symmetric)
data_autocorr = autocorr(length(data_autocorr):end);

% Create toeplitz matrix (V) of the autocorrelation sequence
% Keep upper triangular only (it is symmetric)
V = triu(toeplitz(data_autocorr));

% Apply cholesky decomposition → find K such that V = K*K'
K = chol(V).' ; % (.)' to make it lower triangular
S = inv(K);

% Apply prewhitening
data_pw = S*data;
```

Parametric AR Model Fitting Prewhitening Approach

The second prewhitening approach employed in this study attempted to model the signal autocorrelation in terms of an autoregressive (AR) process (Stoica and Moses, 2005; Madsen, 2007). In an AR model, the data at a specific time point y_t is modelled based on the data from previous time points and a random white component $\varepsilon_t \sim N(0; \sigma^2 I)$, which is usually referred to as the innovation term of the signal. Mathematically, an AR model of order P of the signal \mathbf{y} can be defined as $y_t - a_1 y_{t-1} - a_2 y_{t-2} - \cdots - a_p y_{t-p} = \varepsilon_t$, where a_t , ($t = 1, \dots, P$) are the AR coefficients of the model. In this work, the AR coefficients were estimated following the forward-backward least-squares approach described in Barker et al., (2013) which is available in Homer2 (Homer2 - Utilities - iWLS). In this procedure, AR coefficients were calculated for increasing model orders to find the order that minimized a given model order selection criterion. In this study, the AR coefficients up to an order of $P = 150$ coefficients were computed, and the model order that minimized the Bayesian Information Criterion (BIC) in this range was selected.

The BIC is an index based on the likelihood function to aid model selection among a set of two or more alternative models. It is defined as:

$$BIC = -2 \log(L) + k \log(n),$$

where k represents the model order P , n the number of observations (i.e., the length of the autoregressive model for each P) and L denotes the likelihood function of the model tested. It was observed that the optimal model order varied across channels and datasets with a range between $P = 60$ and $P = 110$. Subsequently, the channel time-series \mathbf{y} was filtered (*filter* function in MATLAB) with the linear filter defined by the AR coefficients of the selected model order, which resulted in the corresponding estimate of the innovation signal $\boldsymbol{\varepsilon}$ that was used for subsequent analyses.

Data Analysis

Study 1: Experimental Resting-State fNIRS Data

Functional Connectivity Analysis

Functional connectivity (FC) analysis methods described in the following section were applied independently to data that were preprocessed with a standard approach without prewhitening, as well as to data prewhitened with the non-parametric and AR procedures, and for both HbO and HbR. First, as a measure of the FC between channels, pairwise Pearson's correlation coefficients were computed between the time courses of the HbO, as well as HbR signals, between each channel pair for each subject (*corr* function in MATLAB, see also MATLAB Box A.3 in Appendix A). The correlation coefficients across all the channels can be represented as a FC matrix, where the i, j element of the matrix reflects the Pearson's correlation coefficient between channels i and j . Individual FC matrices were converted from r values to z values by Fisher's r-to-z transformation (*atanh* function in MATLAB) and averaged across subjects ($n = 24$) to obtain group HbO-FC and HbR-FC matrices. Average FC matrices were converted back to r values (*tanh* function in MATLAB) for the sake of presentation.

Hierarchical Clustering Analysis

A hierarchical clustering was performed at the group level (Homae et al., 2010, see MATLAB Box 4.2). First, HbO and HbR time-series of each participant were standardized to have zero mean and unit variance, and concatenated in time resulting in two datasets (HbO and HbR) with 46 channels \times (4945 samples \times 24 participants). Next, agglomerative hierarchical clustering was carried out on each of these datasets (*linkage* function in MATLAB) using correlation as distance metric ($1 - r$) and the Ward method to group channels and clusters based on their degree of similarity. The dendrogram plot of the hierarchical cluster tree (*dendrogram* function in MATLAB) was generated for two thresholds representing different levels of similarity. In order to display the same number of clusters (i.e., three or six clusters), different thresholds were considered across preprocessing methods (i.e., standard preprocessing or after prewhitening) and conditions (i.e., HbO, HbR).

MATLAB Box 4.2

Implementation of the group-level hierarchical clustering analysis

```
% The following variables must be defined in advance:
% data_HC = Group level matrix in the form time x channels obtained after
% standardizing (zero mean and unit variance) and concatenating in time the
% individual HbO or HbR time-series of all participants.
% cluster_threshold = Threshold to define clusters and determine unique colors for
% each cluster in the dendrogram plot.

% Calculate distance between channels (e.g., correlation or Euclidean)
data_dist = pdist(data_HC', 'correlation');

% Create the agglomerative hierarchical cluster tree (method: Ward)
data_link = linkage(data_dist, 'Ward');

% Dendrogram plot
dendrogram(data_link, 0, 'ColorThreshold', cluster_threshold);
```

Phase Difference Analysis

For each subject dataset the average phase difference between HbO and HbR signals was calculated on each individual channel to obtain the hemoglobin phase of oxygenation and deoxygenation (hPod) as explained in Watanabe et al., (2017). Briefly, for each channel Hilbert transformation was applied to HbO and HbR signals to calculate their corresponding instantaneous phase signals. These signals were then subtracted to obtain a phase difference signal between HbO and HbR. Next, the temporal average of the phase difference signal was computed for each HbO and HbR channel pair, resulting in a phase difference value (i.e., hPod) per channel. Standard and polar histograms were computed for each subject as well as for the entire group, where each subject contributed 46 values (i.e., number of channels). Statistical differences in average hPod values between the methods were investigated by using a Watson-Williams test (Berens, 2009), a circular analogue to a one-factor ANOVA. The same test was also employed in post-hoc pairwise comparisons. The MATLAB script to compute the phase difference analysis as implemented here is detailed in Appendix A - fNIRS Data Quality Assessment (MATLAB Box A.3).

Study 2: Simulations

Assessing False Positive Rate in Randomly Generated Time-series

To investigate the effect of prewhitening on the Pearson's correlation coefficient, two sets of randomly generated time-series of length 5000 sample points were simulated, and the distribution of the obtained Pearson's correlation coefficients between time-series pairs was evaluated over 3000 repetitions (e.g., Bright et al., 2016; Santosa et al., 2017). One set of simulated time-series was generated by filtering two random normally distributed signals with a $1/f$ shape filter, in order to make these signals match the frequency spectrum of spontaneous neural oscillations observed in electrophysiological recordings (Pritchard et al., 1992; Lombardi et al., 2017). The second set of simulated time-series pairs was generated with a white frequency spectrum. In addition, two different conditions of correlation were assessed for each set: 1) no correlation induced (i.e., the distribution of the correlation coefficients is expected to be centred in zero), and 2) an induced correlation of $r = 0.5$, which was generated by multiplying the time-series by an upper triangular matrix obtained by the Cholesky decomposition of the desired correlation matrix (i.e., $[1 \ 0.5; \ 0.5 \ 1]$).

Subsequently, the following processing steps were independently applied in each of the four simulated datasets (see Figure 4.2):

1. Signals were convolved with a hemodynamic response function (HRF) generated using a gamma function $\Gamma(t; n, \lambda)$ with parameters $n = 4$ and $\lambda = 2$.
2. Signals were added components simulating physiological noise that were generated as narrow-band filtered noise (0.25 - 0.35 Hz for respiration, 1.95 - 2.05 Hz and 3.95 - 4.05 Hz for cardiac pulse), as well as a white-noise component that simulated hardware-related random noise. This step yielded signals with similar power spectral density as our real fNIRS experimental data.

Statistical Challenges in Resting-State fNIRS Data Analysis

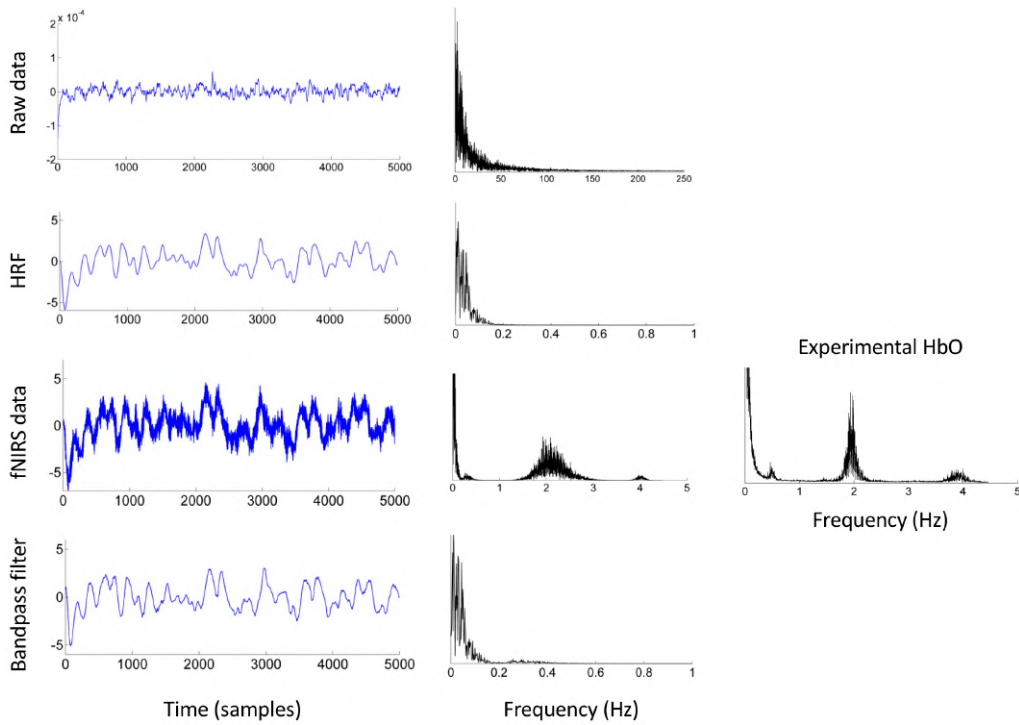


Figure 4.2 Example of a simulated signal and its power spectral density at each processing step. The power spectrum of an example of real experimental HbO data is presented for comparison.

3. Signals were bandpass filtered between 0.005 and 1 Hz, following the same preprocessing pipeline as the one employed for experimental data.
4. Prewitthing was applied independently to each signal using two different procedures (i.e., non-parametric approach and parametric AR fitting approach).
5. In each repetition ($n = 3000$) and after every preprocessing step, Pearson's correlation coefficient was computed between pairs of randomly generated signals to evaluate the effect of each step in the distribution of correlation coefficients.

Effect of Prewitthing on Simulated Resting-State Functional Connectivity Patterns

To further investigate the effect of prewhitening on the analysis of resting-state functional connectivity (RSFC), 20 datasets with similar RSFC patterns as those observed in real experimental data were simulated. Each dataset included 40 time-series of 5000 sample points, thus each of the datasets simulated RS data of a participant. The original time-series were random uncorrelated signals with a $1/f$ frequency spectrum. Different levels of correlation between the simulated signals were induced, producing adjacency matrices showing specific and known correlation patterns. The same correlation structure was imposed in the 20 simulated participants. The correlation structure was induced to approximately match the shape of the adjacency matrices observed in our experimental RS-fNIRS data. A correlation of $r = 0.8$ was induced between neighbouring channels, whereas a correlation of $r = 0.6$ was induced between homotopic channels. Correlations of $r = 0.1$ or $r = 0.2$ were simulated between the remaining pairs of channels. Similar to previous simulations, these signals were convolved with the HRF and corrupted with physiological noise to create simulated fNIRS datasets, and then bandpass filtered. The two prewhitening procedures were then applied to these datasets. Changes in the spatial patterns of

correlation were investigated by assessing the group level adjacency matrices of the simulated fNIRS data after bandpass filtering (standard preprocessing) and after the two types of prewhitening. The same hierarchical clustering approach as described above was also performed to investigate whether the induced spatial clustering structure was preserved after each processing step.

4.3. Results

Study 1: Experimental Resting-State fNIRS Data

Functional Connectivity Analysis

The effect of the different preprocessing steps and prewhitening methods on the HbO and HbR signals is illustrated in Figure 4.3, for an exemplar subject. Without bandpass filtering, the HbR signal showed a high autocorrelation value even after 300 temporal lags (~30 s), whereas the autocorrelation coefficients of the HbO signal became approximately zero after ~200 temporal lags (~20 s). After bandpass filtering (0.005 to 1 Hz), the HbO and HbR signals showed similar autocorrelation values that decreased to zero after ~200 temporal lags. As shown in the bottom plots of Figure 4.3, the non-parametric and AR prewhitening procedures reduced the autocorrelation of the data, as expected for its purpose. Autocorrelation coefficients shrink to values closer to zero at shorter lags using the AR approach than the non-parametric approach. The range of the optimal AR model in this study varied from $P = 60$ up to $P = 110$ at a sampling rate of 8.93 Hz (i.e., a range from 6.7 to 12.3 s), which was similar to those observed in Santosa et al., (2017) which reported model orders up to $P = 40$ at a sampling rate of 4 Hz (i.e., also ~10 s). Apart from the sampling rate, the optimal AR model order is also related to signal quality and might vary across measurement channels.

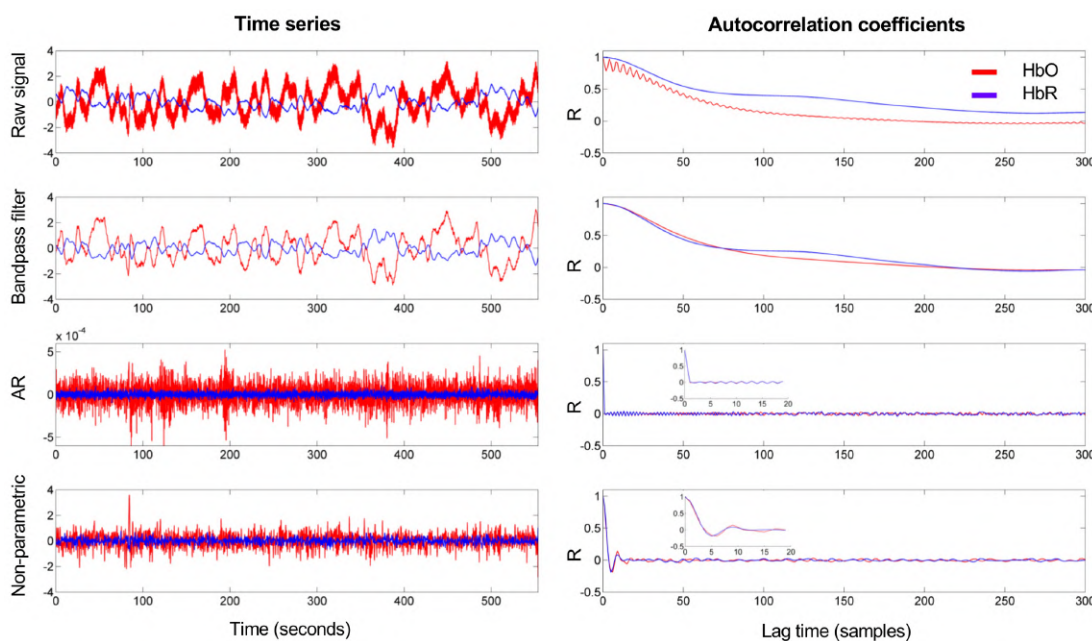


Figure 4.3 Left column represents the times-series of a single channel for HbO (red) and HbR (blue) at different steps of the preprocessing. The right column represents the first 300 autocorrelation coefficients obtained at each preprocessing step.

The FC matrices for the three preprocessing approaches, for an individual subject (first row) and at the group level (second row), are displayed in Figure 4.4. It is generally assumed that HbO and HbR signals in fNIRS data should be negatively correlated (see Appendix A). This assumption was fulfilled both at the individual and at the group level when data was only preprocessed using bandpass filtering. Moreover, homologous regions of both hemispheres showed high correlation values in HbO and HbR, forming clusters and a clear spatial distribution around the main diagonals. In contrast, by incorporating any of the two prewhitening procedures as part of the preprocessing pipeline the negative correlation between HbO and HbR disappeared, and the correlation between homologous regions was only evident in HbO, with a different spatial distribution in each method.

The effect of prewhitening was also investigated by looking at the distribution of correlation values across HbO, HbR, and between HbO and HbR (Figure 4.5). For that, correlation coefficients were transformed to z-scores by Fisher's z-transformation. For each condition (i.e., HbO, HbR, and HbO-HbR), individual z-scores were evaluated as random effects and ANOVA was performed with preprocessing method as a factor (3 groups of 24 infants in total). Pairwise multiple comparison tests were performed following the Tukey's honestly significant difference criterion, a multiple comparisons test on the group means based on a studentized range distribution. For HbO, a significant difference between the three methods ($F[2,69] = 8.62$, $p = 0.0004$) was observed. Post-hoc tests showed that z-scores in HbO for the AR method were larger than those of the non-parametric approach ($p = 0.0002$). For HbR, a significant difference between the methods ($F[2,69] = 146.13$, $p < 0.00001$) was also found. Post-hoc tests revealed that z-scores in the bandpass filter method were larger than those of the non-parametric ($p < 0.00001$) and the AR approaches ($p < 0.00001$). For the HbO-HbR condition, a significant difference between the methods

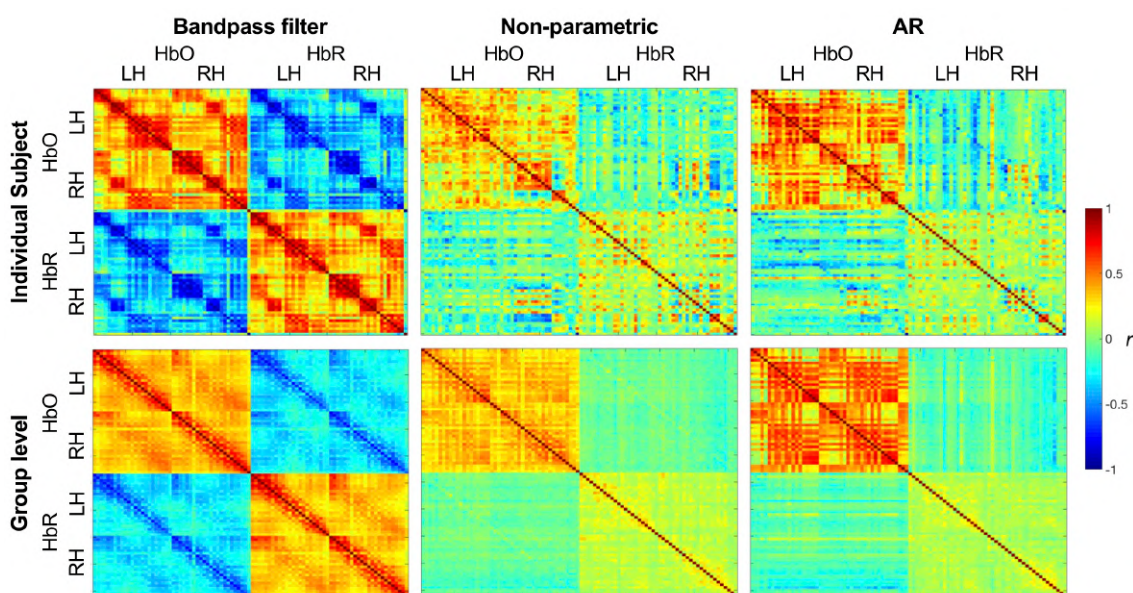


Figure 4.4 Adjacency matrices for an individual subject (first row) and at the group level (second row) for the three types of preprocessing. In each plot, the matrix for HbO and HbR is shown in the top-left part and bottom-right part, respectively (RH: channels in right hemisphere, LH: channels in left hemisphere). The matrix representing the correlation between HbO and HbR is shown in the top-right side. Note that the plots are symmetric with respect to the main diagonal.

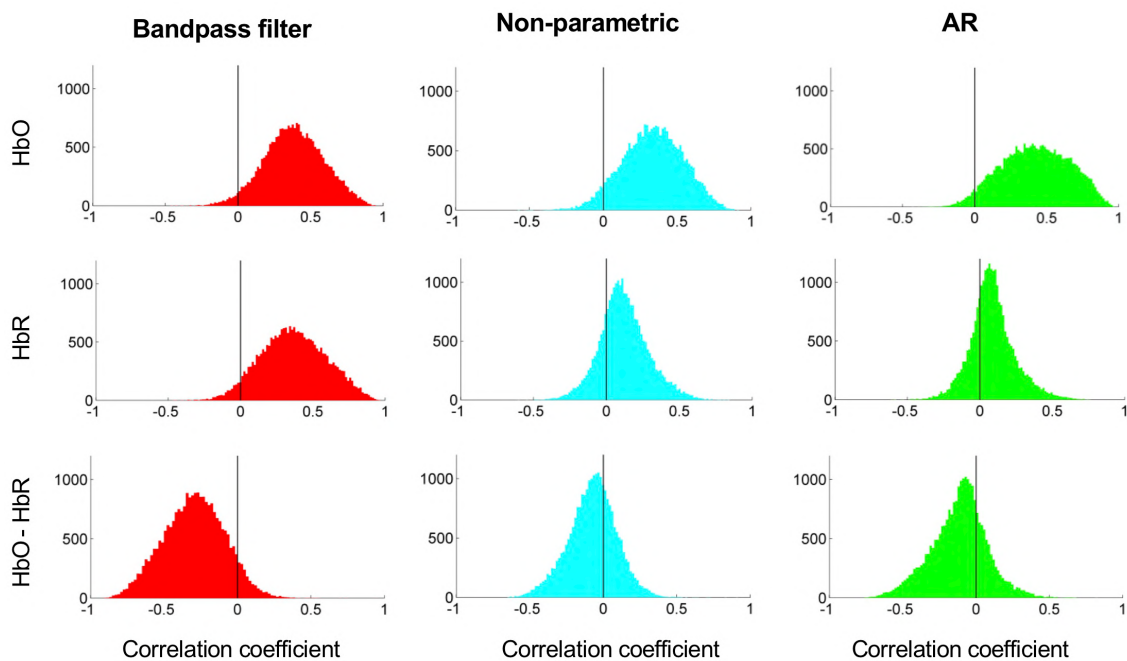


Figure 4.5 Histograms of the group level correlation r values for the different preprocessing methods. Each column shows the comparison between preprocessing methods for the different conditions (i.e., HbO, HbR, and HbO – HbR). Each infant contributed with $46 \times 45/2 = 1035$ correlation r values (upper triangular connectivity matrix) to each histogram.

was also observed ($F[2,69] = 91.9$, $p < 0.0001$). Pairwise post-hoc tests demonstrated that z-scores in the bandpass filter condition were smaller (i.e., larger negative correlation values) than in the non-parametric ($p < 0.00001$) and AR approaches ($p < 0.00001$).

Hierarchical Clustering Analysis

As illustrated in Figure 4.6, the results of the hierarchical clustering analysis obtained with the standard preprocessing were consistent with the results previously reported in Homae et al., (2010). A large degree of reproducibility was observed between studies despite differences in data acquisition (46 channels as opposed to 94 channels) and dataset recording duration for each infant (9 minutes in our study instead of 3 minutes in Homae et al., 2010). Also, 4-month-old infants were assessed in the current study, which corresponds to an intermediate age between the infants at 3 and 6 months of age which were tested in the previous study. For HbO, clusters were formed between homologous regions of both hemispheres if only bandpass filtering was applied. These cluster split into individual frontal, temporal, and parietal regions on each hemisphere at a lower threshold (i.e., larger degree of similarity). In the non-parametric and AR prewhitening approaches clustering between homologous regions was preserved, but with different spatial patterns in each method. In the non-parametric approach, the most posterior parietal channels in both hemispheres clustered along with the most frontal channels. The AR prewhitening approach showed a similar distribution as the non-parametric approach, except the anterior-posterior cluster was formed between channels located in the frontotemporal region and the posterior parietal region. For the lower threshold, AR prewhitening resulted into a larger number of interhemispheric clusters than the non-parametric approach, being

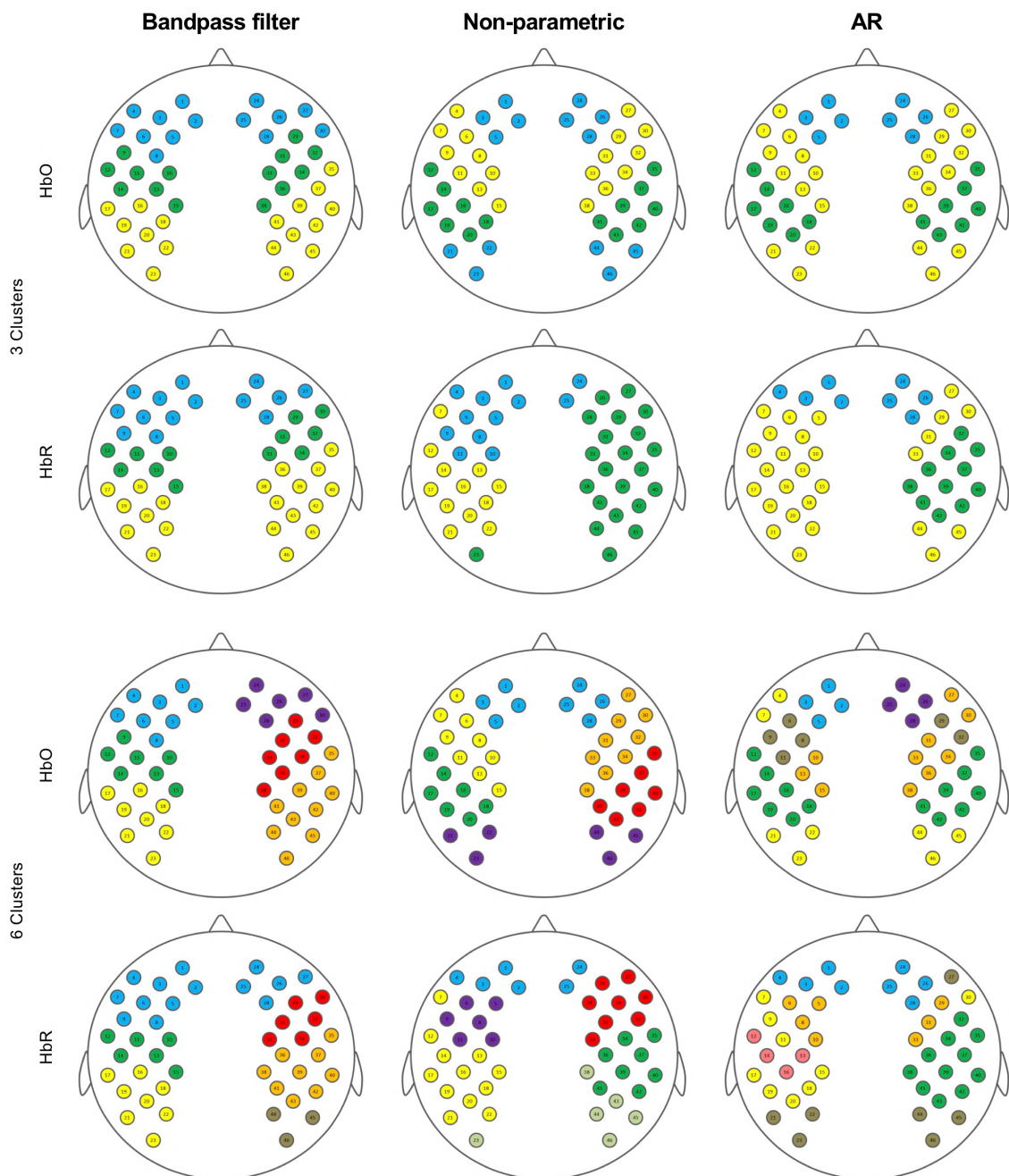


Figure 4.6 Hierarchical clustering analysis of HbO and HbR data. Top two rows show results for the higher threshold corresponding to three clusters. The two rows at the bottom of the figure show results for the lower threshold corresponding to six clusters.

the clustering in the later condition more similar to that obtained with the standard preprocessing. As for HbR data, the spatial distribution of clusters with only bandpass filtering was comparable to that obtained in HbO and to previously reported results (Homae et al. 2011). Results with the two prewhitening procedures exhibited a less bilateral spatial distribution, which was restricted to a few channels. A frontal cluster involving both hemispheres was formed in the two prewhitening approaches, regardless of the threshold, but channels over the main temporal and parietal clusters appeared scattered across and within hemispheres, with no clear spatial configuration.

Hemoglobin Phase Difference Analysis

The distribution of phase difference (hPod) values across channels in a representative subject as well as at the group level for the three preprocessing methods is shown in Figure 4.7. The distribution of hPod values after bandpass filtering followed a similar pattern as in previous observations (Watanabe et al., 2017). In the standard and polar histograms with only bandpass filtering most hPod values were close to π radians (i.e., 180 degrees), which corresponds to an antiphase pattern between HbO and HbR signals. Prewhitening disrupted this pattern, making the overall distribution of hPod values more widespread. The distribution of hPod values for the AR approach showed a mode closer to π (i.e., antiphase) than the non-parametric approach. A Watson–Williams test in average hPod values revealed a statistically significant difference between the methods ($F[2, 69] = 63.4342$, $p < 0.0001$). Post-hoc pairwise comparison tests revealed that mean hPod values in the bandpass filter method were larger than those of the non-parametric ($F[1, 46] = 144.8$, $p < 0.0001$) and AR approaches ($F[1, 46] = 64.7$, $p < 0.0001$). Significant differences were also observed between the two prewhitening methods, the AR approach showing larger hPod values than the non-parametric approach ($F[1, 46] = 14.1$, $p = 0.0004$).

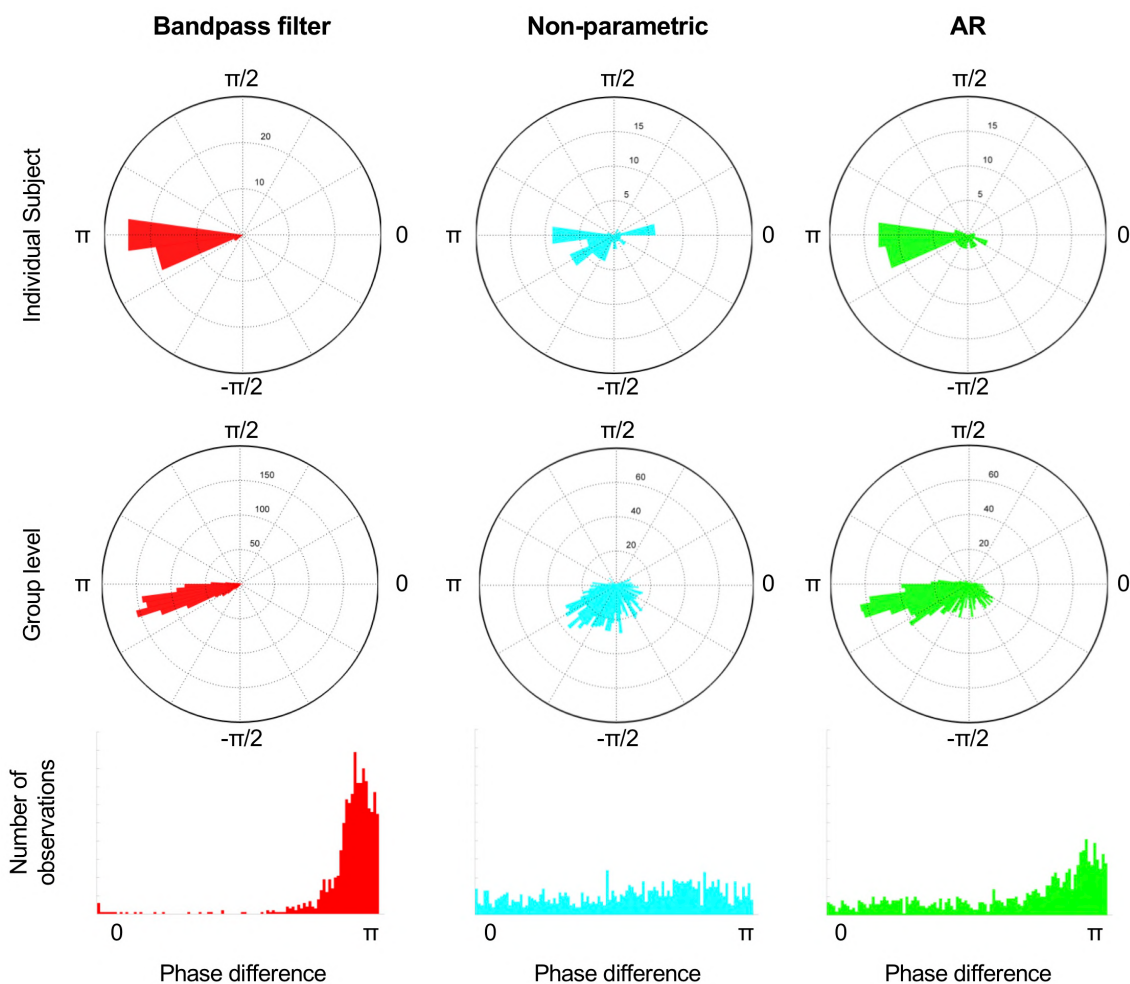


Figure 4.7 Polar histograms showing phase difference (hPod) values for an individual subject (top row) and at the group level (middle row) for the three preprocessing methods. Histograms in bottom row show the distribution of absolute hPod values at the group level.

Study 2: Simulations

The histograms of the Pearson's correlation coefficients after each preprocessing step, and for each simulated dataset are displayed in Figure 4.8. Signals showing a $1/f$ spectrum and a white spectrum are shown on the top and bottom part of the figure, respectively. For the two sets of simulated data without correlation ($r = 0$), the distribution of correlation coefficients became wider after convolution with the HRF and bandpass filtering, suggesting that both steps artificially increased correlation values and consequently increased false-positive rates. After prewhitening, correlation coefficients became centred in zero again. The distribution of the coefficients with the non-parametric prewhitening approach was similar as in the distribution obtained with the original signal, whereas it became narrower after AR-based prewhitening. For an induced correlation of $r = 0.5$ the distribution of correlation coefficients was wider for the signals with a $1/f$ power spectrum than for the signals with a white spectrum, due to their intrinsic autocorrelation. Similar to the scenarios observed with a correlation of $r = 0$, convolving the signals with the HRF widened the distribution of correlations, and bandpass filtering reduced the confounding effects due to physiological noise. Decisively, both prewhitening approaches substantially reduced the correlation between the time-series towards zero. Notably, the non-parametric prewhitening resulted in distributions centred in zero for datasets with $1/f$ spectrum in the two correlation conditions. Similar results were obtained for the dataset with a white spectrum and $r = 0$. The dataset with a white spectrum and $r = 0.5$ showed a distribution slightly shifted toward positive correlation values. The AR approach showed a similar distribution across datasets and conditions, characterized by a narrow shape and centred above zero.

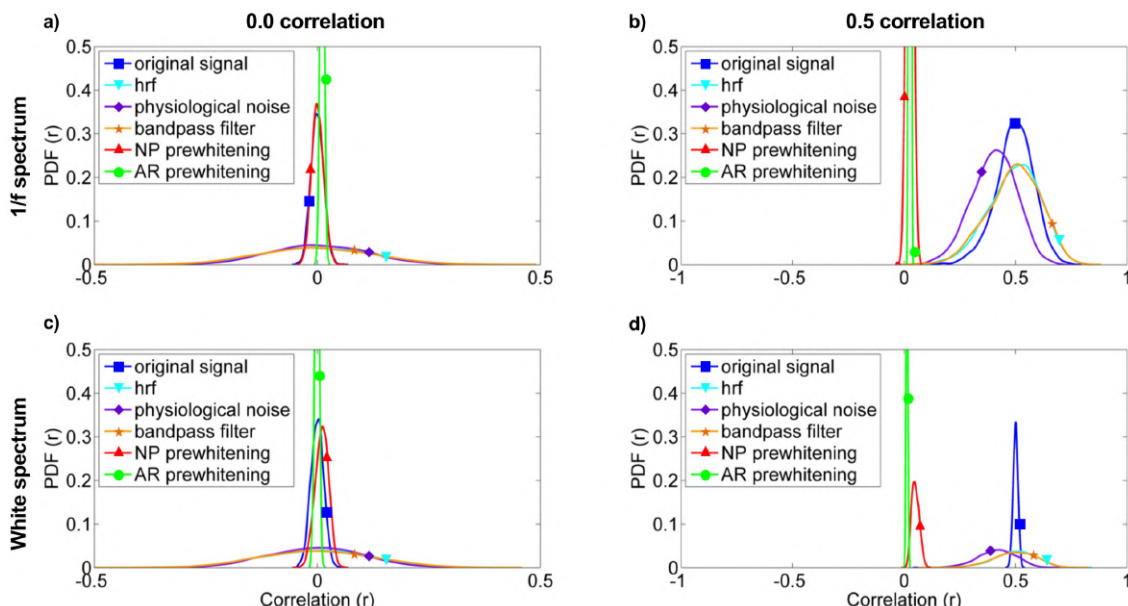


Figure 4.8 Distribution of Pearson's correlation coefficients (3000 repetitions) for two sets of simulated time-series under different levels of correlation. The distribution of correlation coefficients is plotted after each preprocessing step. Each plot represents (a) uncorrelated signals with $1/f$ power spectrum. (b) signals with $1/f$ power spectrum and an induced correlation of $r = 0.5$. (c) Uncorrelated signals with a white power spectrum. (d) signals with a white power spectrum and an induced correlation of $r = 0.5$. NP = non-parametric.

Group level adjacency matrices for the four conditions assessed in the second set of simulations are presented in Figure 4.9. Adjacency matrices for the simulated (raw) neural data and for the fNIRS data showed the expected induced correlation patterns. By contrast, the two prewhitening procedures reduced the correlation between channels toward values close to zero, in agreement with the patterns of the distributions shown in Figure 4.8. Prewhitening also altered the spatial configuration of the adjacency matrices, although part of the induced correlation structure is preserved (note differences in the scale of the plots in the second and third rows).

Finally, the hierarchical clustering analysis for the simulated raw and fNIRS data (Figure 4.10) showed the expected spatial clustering configuration, with “anterior” and “posterior” channels clustering together and splitting by “hemisphere” when the threshold was set to display larger degrees of similarity (i.e., dark and light for blue and red colours). After prewhitening, the “anterior” and “posterior” clusters were preserved at the higher threshold, but the clustering configuration was disrupted when clusters between more similar channels were displayed. With the non-parametric prewhitening the spatial configuration changed and clusters that do not belong to the original structure were formed. The AR prewhitening approach also resulted in different clusters from those of the original configuration.

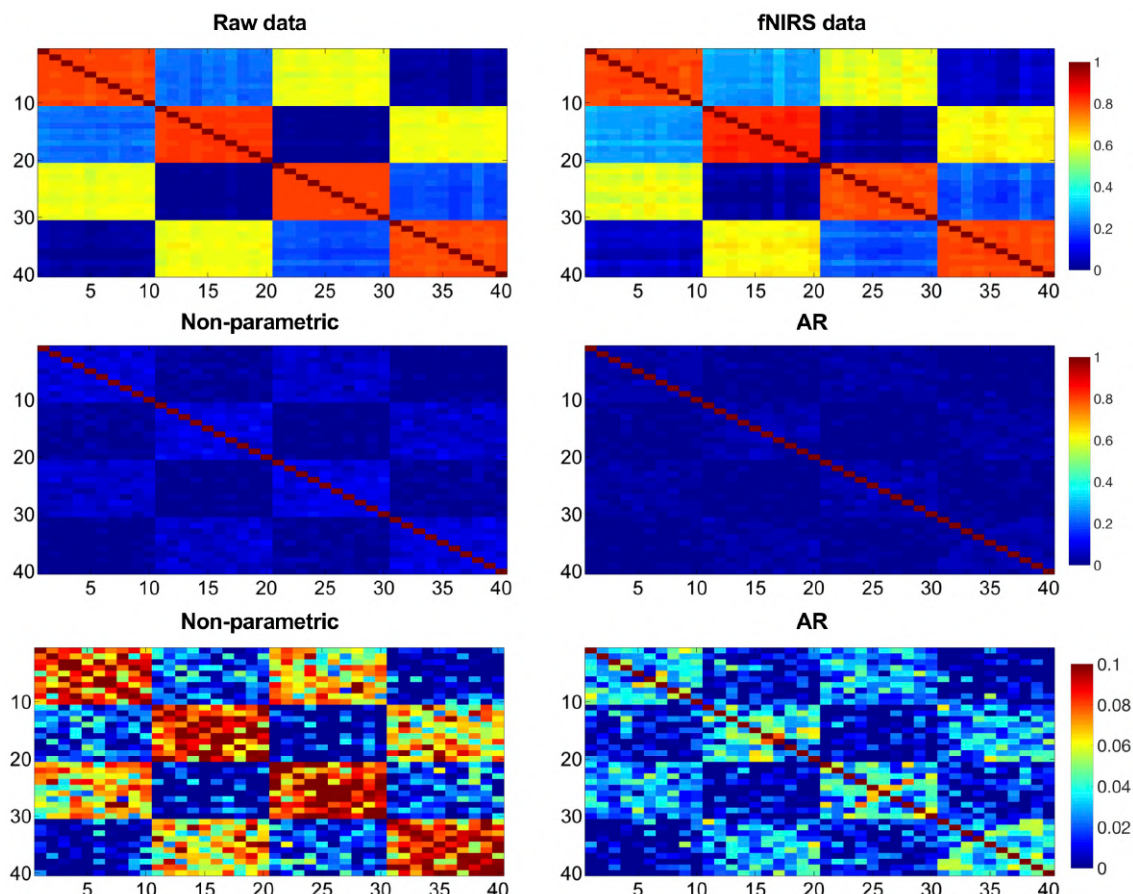


Figure 4.9 Group-level adjacency matrices from simulated data generated to show RSFC patterns resembling real data. First row displays the results for the simulated raw (neural) and fNIRS data. The second row shows the adjacency matrices after applying the two prewhitening procedures. The third row shows the same matrices after adjusting the scale.

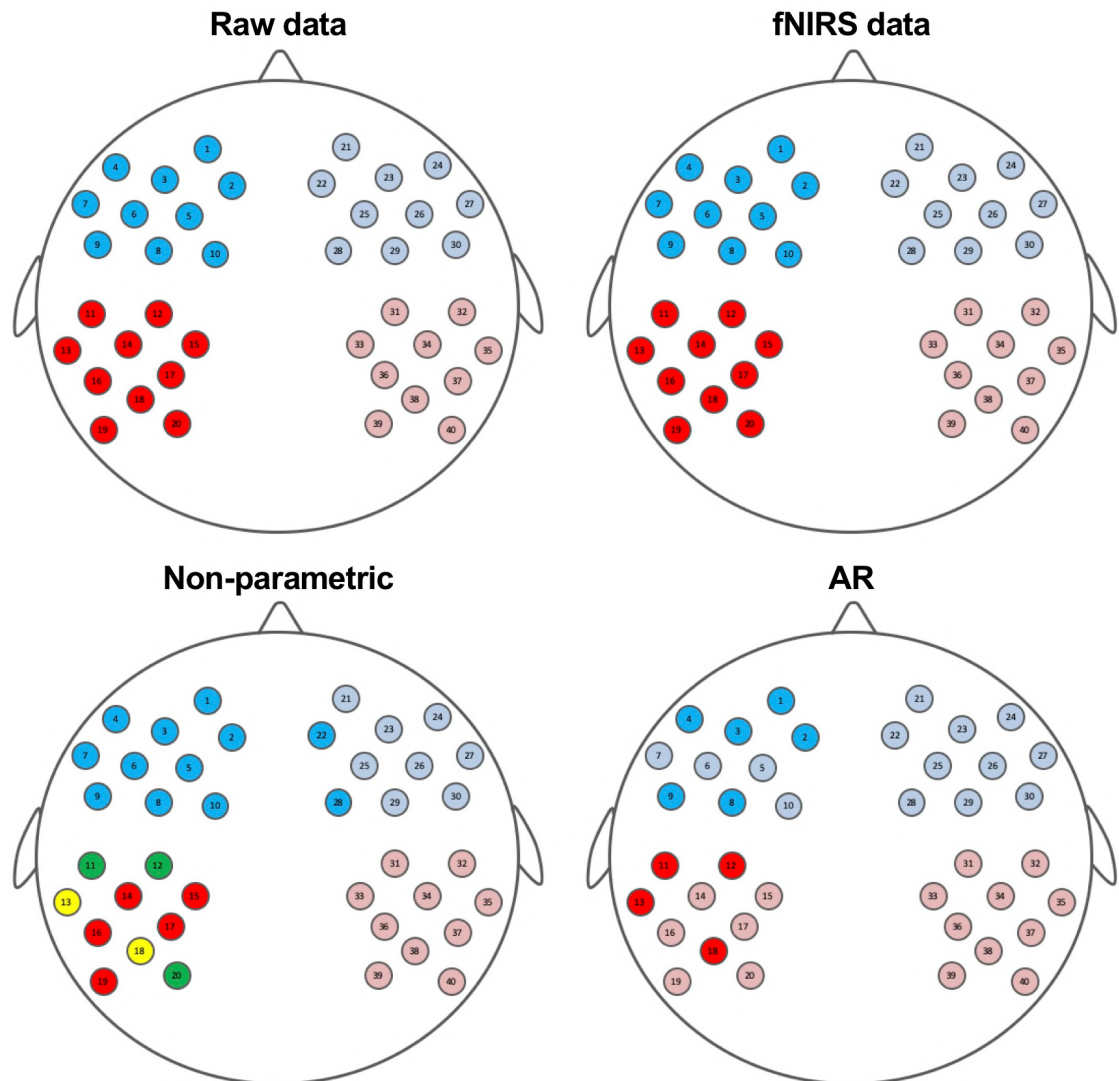


Figure 4.10 Results of the hierarchical clustering analysis corresponding to simulated “participants”. First row shows the results for the simulated raw (neural) and fNIRS data. Second row displays the results after applying each prewhitening procedure. Each color represents channels that are grouped together forming clusters based on similarity. For the blue and red clusters, dark and light colors indicate that these channels belong to the same cluster if a higher threshold is considered, but split into two clusters at lower thresholds (i.e., larger degree of similarity). In the non-parametric method, green and yellow colors indicate that a new cluster is formed between those channels.

4.4. Discussion

The validity of the standard RS-fNIRS data analysis approach is compromised by the presence of physiological and artefactual fluctuations that increase the level of autocorrelation in the data, as well as introduce shared variance across different channels, leading to uncontrolled false-positive rates (Santosa et al., 2017). One of the main causes of this issue is the presence of temporal autocorrelation in the RS-fNIRS data due to the slow nature of hemodynamic fluctuations in the extracerebral and cerebral compartments. To overcome this problem, it has been suggested that temporal autocorrelation should be removed in RS-fNIRS data via prewhitening procedures before performing RSFC analyses.

The rationale presented in Santosa et al., (2017) to recommend the use of prewhitening in RS-fNIRS data, which has also been proposed for RS-fMRI studies (e.g., Christova et al., 2011), is based on the fact that temporal autocorrelation inflates relatedness measures, such as Pearson's correlation coefficient. In Santosa et al. (2017), two random uncorrelated signals were convolved with a canonical hemodynamic response function (HRF) and added physiological noise (i.e., cardiac pulse and respiration) to show the properties of real RS-fNIRS signals. They demonstrated that this step made signals self-correlated, consequently increasing correlation between them and producing false-positive rates around 80%. In their work, prewhitening indeed removed temporal autocorrelations, and false-positive rates returned to the expected true value of 5%. Nevertheless, it is also true that the neuronal signals underlying the hemodynamic fluctuations observed in fNIRS, and also fMRI, are not expected to show a white frequency spectrum. Prewhitening the fNIRS signal, and consequently altering the expected power law behaviour of RS-fNIRS data in the frequency band of the HRF, may compromise the interpretation of RSFC results (and its link with previous literature assessing RSFC), as the prewhitened signals will no longer hold the specific properties of spontaneous hemodynamic fluctuations as measured with fMRI and fNIRS (i.e., BOLD or HbO and HbR).

Here, using experimental RS-fNIRS data obtained from 4-month-old infants, the effect of two prewhitening methods (prewhitening based on a non-parametric approach, and prewhitening based on an AR fitting approach) on different functional connectivity measures was assessed, and compared with a standard preprocessing pipeline not including prewhitening. Furthermore, results were also compared with previous studies measuring RS activity in infants using fNIRS. This study yielded three relevant findings. First, the results of two previous infant RS-fNIRS studies (Homae et al., 2010; Watanabe et al., 2017) were replicated using the standard preprocessing pipeline including bandpass filtering but not prewhitening. Second, results after data prewhitening were different from those presented in the original studies. Third, each prewhitening method produced different results.

One of the most relevant observations of this work is that the negative correlation and antiphase state between HbO and HbR signals was no longer visible after prewhitening (Figures 4.4, 4.5, and 4.7), although there was a slight tendency towards an antiphase relationship with the AR approach. This result contradicts previous observations of the intrinsic physiological relationship between HbO and HbR signals (Wolf et al., 2002; Obrig and Villringer, 2003; Watanabe et al., 2017), raising an important discussion point. The autocorrelation of the signal originates from all its sources, including not only artifactual and non-neurobiological physiological confounds, but also brain-related hemodynamic activity, as the HRF acts as a low-pass filter. Removing temporal autocorrelation from RS-fNIRS signals might imply that the hemodynamic signal of interest is also partially or completely removed, causing that the expected negative correlation between HbO and HbR signals disappears. This fact raises concerns about the effects of using prewhitening in RS-fNIRS studies. Furthermore, it questions the neurobiological significance of the remaining signal after applying prewhitening.

It could be assumed that the signals after prewhitening (i.e., innovations) do not represent HbO and HbR fluctuations, but they reflect the activity-inducing signals underlying them. From that perspective, prewhitening could be understood as a hemodynamic deconvolution procedure, as it has been proposed for fMRI data analysis (Gitelman et al., 2003; Caballero et al., 2013; Karahanoğlu et al., 2013). However, this is not the primary goal of prewhitening as it is understood in this work (i.e., removing the signal autocorrelation). Results of the current work indicate that further investigation on the neurobiological relevance of the prewhitened signal in RS-fNIRS data is still required before directly adopting this procedure.

Results with simulated data for both prewhitening approaches indicated a significant reduction in the correlation values obtained in HbR adjacency matrices, but not in HbO (Figures 4.4 and 4.5). It is important to note that motion induced artifacts, although sparse, might still be present in experimental RS-fNIRS data, and potentially modulating correlation between channels. Here a standard Pearson's correlation approach was followed in order to match previous literature, but FC matrices can also be calculated based on robust correlation methods which downweight the effect of motion artifacts (e.g., Santosa et al., 2017; see also Chapter 3). Prewhitened data was visually inspected and time-points presumably showing motion related artifacts co-occurred across HbO and HbR. Therefore, differences across HbO and HbR on the distribution of correlation values after prewhitening cannot be attributed to different motion-related effects across components.

Alternatively, these results could be explained by the fact that HbO is more sensitive to physiological fluctuations than HbR. Thus, HbO might be more prone to non-stationary low-frequency physiological fluctuations related to modulations in cardiac rate (Kirilina et al., 2013), breathing (Holper et al., 2015), and systemic blood pressure (Boas et al., 2004; Kirilina et al., 2012). It is difficult to explain these physiological processes by means of stationary models of correlations such as those explored here. Nonetheless, these processes could potentially modulate non-stationary dynamics of hemodynamic fluctuations during resting-state, and account for a substantial part of the correlation between channels in experimental HbO data after prewhitening.

Finally, simulations demonstrated that convolving two uncorrelated time-series with the HRF artificially increased the correlation between them, resulting in larger false-positive rates. These results were already noted by Santosa et al., (2017) in similar simulations, and they are also in line with the simulations of fMRI-like data reported in Bright et al., (2016). Figure 2 in Bright et al., (2016) demonstrated that false-positive rate increased due to the effect of bandpass filtering. Specifically, narrower bandpass filters and faster sampling rates showed the highest false-positive rates (the effect of bandpass filtering the data can be considered equivalent to convolution with the HRF). In all the simulated conditions (i.e., $r = 0$ and $r = 0.5$), AR prewhitening removed correlation between the signals and centred the distribution of the measured correlation r values in zero. Non-parametric prewhitening also removed the correlation and centred the correlation r values in zero, except for the signals with a white spectrum and $r = 0.5$, where the distribution of correlation coefficients was slightly shifted toward positive values.

In the second set of simulations, modulations in RSFC spatial correlation patterns due to the effect of prewhitening were investigated. Similar correlation patterns were observed between the “original data” (i.e., simulated neural activity where the correlation structure was induced) and the simulated “fNIRS data”. For both prewhitening approach investigated here, correlation between channels was reduced to close to zero levels, and the shape of the adjacency matrices disrupted. It is important to note that all the “participants” were simulated with the same original correlation structure. This is a very unlikely scenario in the case of real RS-fNIRS data where results are likely to differ considerably after applying prewhitening.

4.5. Summary

The RS-fNIRS signal requires specific considerations during data preprocessing and analysis. In particular, the RS-fNIRS signal shows a colored frequency spectrum, which can be observed as temporal autocorrelation, thereby introducing spurious correlations. Prewhitening of the RS-fNIRS signal has been proposed as a necessary step to remove the signal temporal autocorrelation and therefore reduce false-discovery rates. However, the impact of this step on the analysis of experimental RS-fNIRS data has not been thoroughly assessed prior to the present study. This chapter investigated the implications of including prewhitening as part of the RS-fNIRS data preprocessing pipeline. More specifically, the effect of prewhitening was assessed by replicating the results of two previous infant RS-fNIRS studies, and comparing the outcome of a standard preprocessing pipeline with the outcome after incorporating prewhitening. Results from previous studies were replicated with the standard preprocessing pipeline but not with the ones including prewhitening. Importantly, the expected anticorrelation and antiphase state between HbO and HbR disappeared after data prewhitening. Also, different prewhitening procedures yielded different results, both compared to the standard RS-fNIRS preprocessing method and across prewhitening procedures. Undoubtedly, the statistical challenges that have been recently described by Huppert et al., (2016) and Santosa et al., (2017) for both functional task-based and resting-state fNIRS data should be taken into consideration. However, based on these results, a better understanding of the effect of prewhitening in RS-fNIRS data, and of the neurophysiological significance of the prewhitened signal, is still required to determine if prewhitening should be applied and, if so, which prewhitening procedure is more appropriate.

Chapter 5

Hemodynamic Correlates of Speech Processing in Bilingual and Monolingual Infants

5.1. Theoretical Motivation

The main goals of this Chapter are to investigate the functional neural correlates of speech processing in 4-month-old infants, and evaluate potential differences between monolingual and bilingual infants. While Chapter 3 illustrated a comparable functional brain network organization across bilingual and monolingual 4-month-olds during a resting-state condition, it is still unclear whether neural adaptations across these two populations are observable during speech processing.

Previous studies showed great variability on the reported brain activation patterns supporting speech processing in 4-month-old infants. This variability might be partly explained by various methodological limitations present in these works such as a small sample size or a reduced data quality. To overcome these limitations, another goal of this Chapter is to implement a methodology that can be used to reliably identify the brain areas responsible for speech processing in infants using functional near-infrared spectroscopy (fNIRS) (see Chapter 2 for a review). First, a large number of participants with high data quality are considered. The effect of global systemic physiology in the estimated brain responses is investigated, as previous works suggested that functional neuroimaging studies using fNIRS should correct for the possible task-evoked physiological noise (Pfeifer et al., 2018). Following the recommendations outlined in the fNIRS literature HbO and HbR data are analysed and reported in the results (Obrig and Villringer, 2003). Finally, efficient procedures for stimuli presentation that simultaneously allow the detection of brain activation and the accurate estimation of the shape of the hemodynamic response are implemented (Kao et al., 2009). The group-level data analyses approach and the methods for performing statistical comparisons between experimental groups include procedures for multiple comparison correction.

In the first part of this Chapter the brain areas that have been identified as part of the language processing network in infants are described. Then, literature is linked with the main theoretical question of interest for this work, which aims to examine differences in brain activation patterns during speech processing across monolingual and bilingual infants (see also Chapter 1, where the main developmental milestones of bilingual language acquisition and cognition are described).

Neural Correlates of Speech Processing in Infants

The brain regions involved in speech processing are similar across infants and adults (e.g., Friederici, 2002; Meyer et al., 2002; Perani et al., 2011). In infants, the temporal and frontal perisylvian brain regions seem to play a central role in processing speech sounds. Specifically, the primary and secondary auditory cortices in the superior temporal gyrus and the inferior frontal gyrus have been consistently reported as showing activation in studies assessing brain responses to speech in newborns (Peña et al., 2003; Kotilahti et al., 2010; Perani et al., 2011; Sato et al., 2012; Vannasing et al., 2016; May et al., 2017) and older preverbal infants (Dehaene-Lambertz et al., 2002; Dehaene-Lambertz et al., 2006; Homae et al., 2006; Bortfeld et al., 2009; Dehaene-Lambertz et al., 2010; Fava et al., 2014; Shultz et al., 2014; Homae et al., 2011; Minagawa-Kawai et al., 2011; Altvater-Mackensen

Hemodynamic Correlates of Speech Processing in Infants

and Grossman, 2016). Some of these studies also addressed the longstanding question of whether infants are born with innate mechanisms that are preferentially attuned to process speech in the left hemisphere (LH), or whether the observed LH dominance is common to all acoustic signals, and this hemisphere only becomes functionally specialized for speech after certain amount of experience with linguistic inputs. In order to answer this question, the studies compared prelinguistic infants' brain responses to speech stimuli and a diverse range of non-speech stimuli with similar structured acoustic properties.

Backward speech has been one of the most commonly employed non-linguistic acoustic control condition for forward speech. Backward speech preserves fast transitions present in forward speech, and it also shows similar pitch and intensity characteristics. However, several segmental and suprasegmental information is altered in backward sentences, and this condition is distinctly non-linguistic, since most of its sounds cannot be produced by the human vocal tract. Studies in newborns demonstrated enhanced activation to forward vs. backward speech stimuli mainly over temporal brain regions in the LH (Peña et al., 2003; Sato et al., 2012; Vannasing et al., 2016), and in the left angular gyrus and precuneus in 2-3-month-old infants (Dehaene-Lambertz et al., 2002).

It has been proposed that speech processing requires integrating linguistic information over multiple time-scales (Hickock and Poeppel 2007). One scale refers to fast, segmental, information conveyed by separable sound units in speech, such as phonemes. Another scale denotes slow, suprasegmental, information carried by larger speech chunks (i.e., syllables, words or phrases), and which incorporates various aspects of spoken language such as intonation patterns or rhythm; also known as prosody. According to this hypothesis, the sensitivity to specific spectrotemporal properties of speech differs between hemispheres, with fast/segmental phonetic level information recruiting the auditory cortex bilaterally, and slow/prosodic information being predominantly processed over the right auditory cortex (Hickock and Poeppel 2007). Based on this premise, and given the importance of linguistic rhythm for language discrimination during the first stages of language acquisition (Gervain et al., 2010, see also Chapter 1), various works have investigated the early sensitivity to segmental and suprasegmental aspects of speech in infants' left and right auditory cortices.

Using non-speech acoustic stimuli with varying temporal structures (fast vs. slow) resembling the temporal structure of different speech formants (e.g., phonemes, syllables), Telkemeyer et al. (2009) demonstrated that newborns preferentially process fast acoustic modulations, such as those present in phonemes, over bilateral temporo-parietal regions; whereas a right hemispheric (RH) dominance was observed for slow acoustic modulations with prosodic like temporal properties. This hypothesis was further supported by Homae et al. (2006) which showed similar bilateral activation patterns to both normal and artificially flattened speech stimuli in 3-month-old infants. Flattened speech conveys the same segmental information as normal speech, but in this condition the prosodic information of the original sentence has been removed. Indeed, direct comparisons between normal and flattened conditions in this study revealed enhanced activation over RH temporo-parietal regions for normal speech (Homae et al., 2006). Perani et al., (2011) observed similar brain

activation patterns in newborns presented with normal and hummed speech stimuli, primarily involving the superior temporal gyrus, the inferior frontal gyrus and the inferior parietal lobule bilaterally. Instead, flattened speech elicited deactivation responses over inferior frontal cortex, hippocampus and posterior cingulate cortex in both hemispheres, and in the left inferior parietal lobule. A comparison between stimulus conditions revealed a stronger activation for normal speech as compared to flattened speech over the right auditory cortex. As opposed to flattened speech, hummed speech is an acoustic control condition where fast transitions mainly reflecting phonemic information have been removed, but prosodic information remains unchanged. The lack of hemispheric specialization between normal and hummed speech observed in this study might reflect the essential role of sentential prosody during the early stages of language acquisition.

Most of the above reviewed neuroimaging studies assessing speech processing in infancy reported functional activation in classic LH language areas in response to forward speech sounds only; or alternatively, a superiority in these areas to process speech stimuli as compared to non-speech stimuli (Peña et al., 2003; Kotilahti et al., 2010; Sato et al., 2012; Vannasing et al., 2016; May et al., 2017). Studies assessing infants between 2-4 months of age also reported evidence supporting a LH advantage for speech processing (Dehaene-Lambertz et al., 2002; Dehaene-Lambertz et al., 2010; Minagawa-Kawai et al., 2011). However, several works have also provided evidence against the postulated LH superiority for speech processing. For example, Dehaene-Lambertz, et al., (2002) observed significant differences in lateralization between forward and backward speech stimuli over parietal (e.g., angular gyrus and precuneus), but not temporal regions. May et al., (2017) reported greater activation to forward vs. backward speech over bilateral anterior temporal regions for participants' native language, but not when these conditions were contrasted using non-native speech sounds. Perani et al., (2011) showed comparable levels of activation over left and right auditory cortices in response to normal speech, and Fava et al., (2014) reported no differences between speech and music processing in preverbal infants.

Language Discrimination in Infants

Language acquisition begins as soon as infants are able to hear spoken language, about 3 months prior to birth (e.g., Werker, 2018). Exposure to their native language while still in the womb modulates infants' language preference at birth, which is reflected by the infants' behavioural preference for a familiar language by the time they are born (Mehler et al., 1988; Moon et al., 1993). Research examining the neural foundations of infants' early native language preference usually reported increased sensitivity to native speech stimuli. Nonetheless, the interpretation of the outcomes derived from these studies is not always straightforward, since direct statistical comparisons between conditions are usually not performed.

In newborns, May et al., (2011) reported an overall increase in activation in various fNIRS channels distributed across both hemispheres when listening to a familiar language (English), and a deactivation response when listening to an unfamiliar language (Tagalog). However, direct comparisons between the two conditions yielded no significant differences.

Hemodynamic Correlates of Speech Processing in Infants

Sato et al., (2012) observed a selective activity to the maternal language (Japanese vs. English) in one fNIRS channel located in left temporo-parietal areas. In this age group, Vannasing et al., (2016) also provided evidence for a hemispheric functional asymmetry in language processing, characterized by an early LH dominance for native speech stimuli (French), and a RH dominance for non-native speech stimuli (Arabic); but direct statistical comparisons between native and non-native speech stimuli were either not significant or not presented in the results. On the other hand, May et al., 2017 showed no differences in brain activation patterns between native (English) and rhythmically distinct non-native language (Spanish) conditions. However, their results indicated a difference over bilateral anterior temporal regions between FW and BW speech for native language only, which was interpreted as an effect of language familiarity.

Specialized brain responses for native language processing have been also observed later in development. In 4-months-old infants, familiar (Japanese) and unfamiliar (English) conditions comparably activated left temporal regions, but the magnitude of the response in a fNIRS channel located in the left superior temporal area was significantly higher during maternal language processing (Minagawa-Kawai et al., 2011). In full-term (3 and 6-month-old) and preterm (6 and 9-month-old) infants, patterns of brain oscillatory activity measured using electroencephalography (EEG) showed enhanced gamma-band responses to native (Italian) and non-native, but rhythmically similar (Spanish), languages as compared to a non-native and rhythmically different condition (Japanese) (Peña et al., 2010). However, the distinction of languages belonging to the same rhythmic class (i.e., Italian and Spanish) was only observed in the older age groups (i.e., 6-month-old full term and 9-month-old preterm), but not in younger full-term and preterm infants that were tested at 3 and 6 months after birth, respectively. Besides the impact of experience, this study also pointed out the role of neural maturation for the early development of language discrimination abilities, particularly those needed to distinguish rhythmically similar languages.

Bilingual Language Discrimination

As discussed in Chapter 1, the effect of language familiarity on early speech processing can also be examined from a different perspective. In a bilingual learning environment, infants are exposed to the linguistic regularities of not one, but two inputs simultaneously. While bilingual infants' overall language exposure should be comparable to that of monolinguals, bilingual infants likely receive less exposure to each of their languages, compared to their monolingual peers, because their exposure time is split between two inputs. A bilingual environment has been shown to have consequences on infants' behavioural and brain responses when spoken language processing is considered.

Behavioural Evidence

At the behavioural level, bilingualism has an impact on attention allocation to languages. Byers-Heinlein et al., (2010) demonstrated that, at birth, English monolingual infants showed a strong preference for their native language over a rhythmically distant language (Tagalog), thus replicating earlier studies (Mehler et al., 1988; Moon et al., 1993). On the other hand, English-Tagalog bilingual infants, showed similar preferential responses to their both native languages, indicative of both speech inputs being recognized as familiar.

At 4 months of age, Spanish or Catalan monolingual and Spanish - Catalan bilingual infants showed comparable auditory language discrimination capacities (Bosch and Sebastián-Gallés, 2001). However, as in newborns, an early bilingual environment has been shown to induce specific learning adaptations related to attention allocation towards familiar and unfamiliar languages. Molnar et al., (2014) showed that Spanish - Basque bilingual infants exhibited longer sustained attention periods than monolinguals when processing their native spoken languages, and they were able to perceptually discriminate them, even when they belonged to the same rhythmic class. Similarly, monolingual infants displayed faster orientation patterns towards their native language (Spanish or Catalan - Bosch and Sebastián-Gallés 1997; French or American - Dehaene-Lambertz et al., 1998), whereas Spanish - Catalan bilingual infants showed the opposite pattern, orienting faster to the presentation of an unknown language (Bosch and Sebastián-Gallés 1997).

Neuroimaging Evidence

Neuroimaging evidence assessing the impact of early language experience in spoken language processing is scarce in the age group of interest for the current study (i.e., 4-month-old infants). Using EEG during a language discrimination/recognition task, Nácar-García et al., (2018) examined Spanish or Catalan monolingual and Spanish-Catalan bilingual 4.5-month-old infants brain responses to speech utterances in their native and non-native languages. In monolingual infants, authors found shorter latencies in the P200 component (indicative of early discrimination) for the native language (Spanish or Catalan), as compared to a non-native and rhythmically different language (i.e., German), but not when this condition was contrasted with a non-native and rhythmically similar language (i.e., Italian). Bilinguals showed similar latencies in the P200 for the three language conditions, thus indicating a similar processing for familiar and unfamiliar languages. Conversely, bilinguals showed enhanced theta band (4-7 Hz) oscillatory activity towards their native language. This frequency band is assumed to largely track suprasegmental properties of speech, and thus, the increased activity displayed by bilingual infants on this frequency band might reflect an additional reliance on this type of linguistic information during native language processing (Nácar-García et al., 2018).

In a recent study, Mercure et al., (2020) evaluated brain responses to spoken and signed-language in English monolingual, unimodal bilingual (English + another spoken language) and bimodal bilingual (English + British Signed Language) infants between 4 and 8 months of age using fNIRS. At the group level, considering all the participants in the three experimental groups, results showed a bilateral activation over inferior frontal and posterior temporal regions for spoken language. On the other hand, signed language primarily activated right temporoparietal regions. When assessing the effect of language modality (spoken vs. signed language), the comparison between experimental groups revealed an unexpected effect. While activation responses to spoken and signed language showed no lateralization effects in monolingual and bimodal bilingual infants, unimodal bilingual infants' brain responses were right lateralized over posterior temporal regions for spoken and signed language conditions. These findings suggest that the experience with two spoken languages might require a more effortful cognitive processing, as compared to being

Hemodynamic Correlates of Speech Processing in Infants

exposed to one spoken and one signed language, as is the case of bimodal bilingual infants in which the perceptual discrimination between the two language modalities might be more easily accomplished. Results of this work can also be linked with previous evidence that demonstrated enhanced visual speech processing abilities in unimodal bilingual infants (Weikum et al., 2007; Sebastián-Gallés et al., 2012). This fact could also explain the increased RH activation during speech processing observed in this study.

In summary, bilingual and monolingual infants showed similar language discrimination capacities at 4 months of age, but the cognitive and functional mechanisms employed to perform this distinction might differ across language groups. While monolingual infants displayed a behavioural and functional preference for their native language, bilingual infants seem to allocate more attention to unfamiliar linguistic stimuli and to recruit different neural mechanisms in order to track specific properties of speech. This differential processing might be also reflected in their functional responses towards speech stimuli which involved the recruitment of additional brain regions in the RH.

Study Aims

In this work, brain responses to Spanish forward and backward speech stimuli were recorded in 4-month-old Spanish-Basque bilingual and Spanish monolingual infants using fNIRS. The main goal of this study was to assess the effect of early linguistic experience on functional brain activation patterns during native language processing. As a second goal, this study aimed to provide an accurate description of the brain areas showing functional activation to forward and backward speech stimuli in a relatively large sample of participants ($n = 58$), with a high number of trials, and optimal data quality.

Previous fNIRS studies presented a reduced statistical power in terms of the number of subjects and valid trials analyzed (Peña et al., 2003; Kotilahti et al., 2010; May et al., 2011; Minagawa-Kawai et al., 2011; Sato et al., 2012; May et al., 2017), reported results of one fNIRS hemoglobin parameter only (i.e., oxyhemoglobin HbO, deoxyhemoglobin HbR or total hemoglobin HbT) (Peña et al., 2003; May et al., 2011; Minagawa-Kawai et al., 2011; Sato et al., 2012; Vannasing et al., 2016; May et al., 2017; Mercure et al., 2020), based their conclusions on uncorrected multiple hypothesis testing results (Peña et al., 2003; Altvater-Mackensen and Grossman, 2016; May et al., 2017), or did not perform direct statistical comparisons between experimental conditions (Peña et al., 2003; Kotilahti et al., 2010; Sato et al., 2012; Vannasing et al., 2016; May et al., 2017). In order to reduce the attrition rate and maximize data quality, acquisition of fNIRS measurements were performed during natural sleep, the same as in the study presented in Chapter 3 and similar to other fNIRS studies performed in young infants (Dehaene-Lambertz et al., 2002; Peña et al., 2003; Homae et al., 2011). A methodology for stimuli randomization that simultaneously optimized the experimental design for the detection of brain activation and for the estimation of the shape of the hemodynamic response was implemented (Kao et al., 2009). This methodology also facilitated the acquisition of a large number of trials by reducing testing time. Two data analyses methods based on a general linear model framework were performed to target each of these goals.

5.2. Methods

Ethics Statement

This study was carried out at the Basque Center on Cognition, Brain and Language and received approval from its local ethical committee. The study involved the participation of infant subjects. Prior to participation, parents were informed about the aim of the study, the experimental procedures, and their right to withdraw from the study at any moment without providing a reason and with no negative consequences. Written informed consent was obtained from the parents prior to data acquisition.

Study Population

Eighty-one healthy 4-month-old infants participated in this study. Participants were recruited from the same region of the Basque Country (Gipuzkoa), a predominantly bilingual region in which Spanish and Basque are learnt at home or/and at school from a very young age. A socioeconomic status questionnaire was completed to ensure that families showed similar levels of education, parental occupation and household income. Participants' language background was assessed with a questionnaire filled by the parents, in which infants' percentage of exposure to each language, Spanish (SP) and Basque (BQ), during the first months of life was assessed. In this study two language groups were considered: Spanish-Basque bilingual (BIL) infants and Spanish monolingual (SP) infants. Infants raised in a Spanish-Basque bilingual environment, those that were exposed to their two native languages from birth, formed the bilingual group. Only infants with a percentage of exposure to SP between 20% and 80% were included in this group. Participants exposed to SP only (i.e., >90% of the time) were included in the monolingual group. Participants with a percentage of exposure between 80% and 90%, were classified as undetermined language background (Table 5.1). These participants were included in the whole-group analyses, but were excluded for the between-group statistical comparisons.

In nine of the 81 infants no recording took place as they were unable to fall sleep. In addition, 14 infants ($n = 7$ BIL, $n = 6$ SP and $n = 1$ undetermined language background) were excluded during data preprocessing due to insufficient data quality or recording duration. Concretely, infants that were not able to complete the entire experiment or those that presented low quality data, as determined by the data quality assessment routine during preprocessing (see Appendix A), were not included for data analysis. In the final sample, for which data was analysed and results are presented 58 participants were included (Table 5.1): 26 BIL infants (15 girls; mean age = 125 ± 4 days; mean exposure to SP = $52\% \pm 16\%$, range = [20.4 % - 78.6 %]), 21 SP monolingual infants (10 girls; mean age = 123 ± 5 days;

Language Background	n	Age (days)	Exposure to Spanish (%)	Range [max - min] (%)
Spanish-Basque Bilingual	26	125 ± 4	52 ± 16	[20.4 - 78.6]
Spanish Monolingual	21	123 ± 5	98 ± 2	[93.8 - 100]
Undetermined	11	124 ± 3	85 ± 3	[80.5 - 89.2]

Table 5.1 Summary information of the participants included in the study of this chapter.

Hemodynamic Correlates of Speech Processing in Infants

mean exposure to SP = $98\% \pm 2\%$, range = [93.8 % - 100 %]) and 11 infants with an undetermined language background (6 girls; mean age = 124 ± 3 days; mean exposure to SP = $85\% \pm 3\%$, range = [80.5 % - 89.2 %]).

Stimuli

Three Spanish native female speakers were recorded reading aloud sentences from *The Little Prince* book (Saint-Exupéry et al., 1943). Each speaker recorded the same 120 utterances which ranged in number of syllables between 15 and 18 (30 utterances of each length). From this set, 24 utterances were selected for each speaker, with no repetition between them (i.e., in total 72 different sentences were selected). Sentences were manually segmented to the precise onset and offset time, and next normalized in intensity (70dB) and peak amplitude across speakers using Praat (Boersma and Weenik, 1990). The final set comprised 72 utterances with a mean duration of 3.2 ± 0.2 seconds, range [3 - 3.7]. Backward (BW) sentences were generated from the set of forward (FW) sentences using Praat. It is important to note here that the experimental paradigm employed in this study was originally designed for a simultaneous fNIRS-EEG study, but due to the complexity of the setup and (thesis) time constraints it was finally limited to fNIRS only. The paradigm was designed as follows (Figure 5.1A): for each condition (i.e., FW and BW speech stimuli) 24 blocks were created. Each block was formed by three sentences of the same speaker, with an inter-sentence interval of 0.5 seconds. Mean block duration = 10.6 ± 0.2 seconds, range [10.1 - 11.4]. The initial goal of this design was to provide 24 blocks for fNIRS data analysis and 72 trials for EEG data analysis for each condition.

In order to counterbalance stimuli presentation order between conditions, four stimuli randomizations were created using the procedure described in Kao et al., (2009). Briefly, the main statistical goals in studies measuring the hemodynamic response to stimuli are: 1) detect brain regions that show activation to the presented stimuli, and/or 2) provide an accurate estimation of the shape of the hemodynamic response. As reference, the first of these goals will be better achieved with a block design, whereas an event-related design will be more optimal for the second goal. However, pursuing both goals (i.e., detection power and estimation efficiency) simultaneously in one study is also possible if an optimal multi-objective randomized experimental design is implemented (Kao et al., 2009). Although this approach was originally designed for fMRI studies, it can be extended to fNIRS studies since both imaging techniques measure the same underlying neurophysiological hemodynamic mechanism.

First, this method requires the user to specify a weight for four design objectives: i) detection power, ii) estimation efficiency, iii) desired fraction of trials per condition (i.e., stimulus frequency), and iv) predictability (i.e., controlling psychological confounds induced by subject's prediction of the successive events). With this information the algorithm searches an optimal design sequence via a multi-objective optimization problem that is solved using a genetic algorithm. The initial search pool is formed by a set of fMRI designs that are known to be optimal for each of the goals independently and a set of random experimental designs. Then, the algorithm proceeds iteratively and generates new design sequences using three different methods [*crossover* - interchange portions of

different sequences; *mutation* – randomly replace specific events (i.e., stimulus, rest); *immigration* – add new designs sequences], and the fitness of each design for each experimental goal is assessed. In each repetition the best designs are stored, as they will form the initial pool of the next repetition until a stopping rule is met (e.g., optimal multi-objective design efficiency or number of repetitions) (Kao et al., 2009).

In this study, the two design sequences were generated with this approach (Figure 5.1B), and two additional design sequences were generated by swapping the order of experimental conditions (i.e., FW and BW speech stimuli). Participants were randomly assigned to one of these four randomizations for stimuli presentation, all of them with the same number of blocks per condition (i.e., 24 blocks) and a similar duration of approximately 17 minutes. As it can be observed in Figure 5.1B, these optimal designs rarely include rest blocks (i.e. where no stimulus is presented) between two experimental blocks. This is a common feature in multi-objective designs in the search for an optimal trade-off between detection and efficiency.

Data Acquisition Procedure

FNIRS measurements were performed with a NIRScout system (NIRx Medical Technologies, CA, USA) at wavelengths 760 and 850 nm with a sampling frequency of 15.625 Hz. Eight light emitters and 12 detectors were positioned on a stretchy fabric cap (Easycap GmbH, Germany) over frontal, temporal and parietal regions of both hemispheres according to the international 10-20 system. Nasion, inion and preauricular points were used as external head landmarks in order to ensure that optode and cap positioning with respect to these anatomical landmarks was equivalent across infants. Each pair of an adjacent light emitter and a detector formed a single measurement channel, which generated 24 channels for each hemoglobin oxygenation state (i.e., oxyhemoglobin, HbO and deoxyhemoglobin, HbR) consisting of source-detector separation distances ranging from 20 to 32 mm (Table 5.2).

The sensitivity profile of the fNIRS probe setup was computed to provide information of the brain areas under investigation, and for results visualization. The probe setup (i.e., sources and detectors) was registered to an average 6-month-old infant template (Richards et al., 2016) to compute the sensitivity matrix of the source-detector configuration using *Toast++* (Schweiger and Arridge, 2014). The aggregated sensitivity profile of the fNIRS probe was obtained by adding the normalized cortical sensitivity profiles of each individual channel (Figure 5.2). Channel positions were defined as the grey matter node which coordinates were closest to the central point of the maximum sensitivity path along each source-detector pair. A 6-month-old average atlas (Akiyama et al., 2013) was used to compute a probabilistic spatial registration of the cortical structures underlying each channel (Figure 5.3). Channel coordinates were first transformed to the Akiyama et al., (2013) average T1 template space using Advanced Normalization Tools (ANTs) (Avants et al., 2009), and then registered into the Akiyama et al., (2013) anatomic atlas, defined by 116 cortical regions based on Automated Anatomical Labeling (AAL) (Tzourio-Mazoyer et al., 2002). For each channel, the AAL anatomical labels within a distance of 20 mm were defined, and the percentage of overlap with each AAL region was calculated (Table 5.2).

Hemodynamic Correlates of Speech Processing in Infants

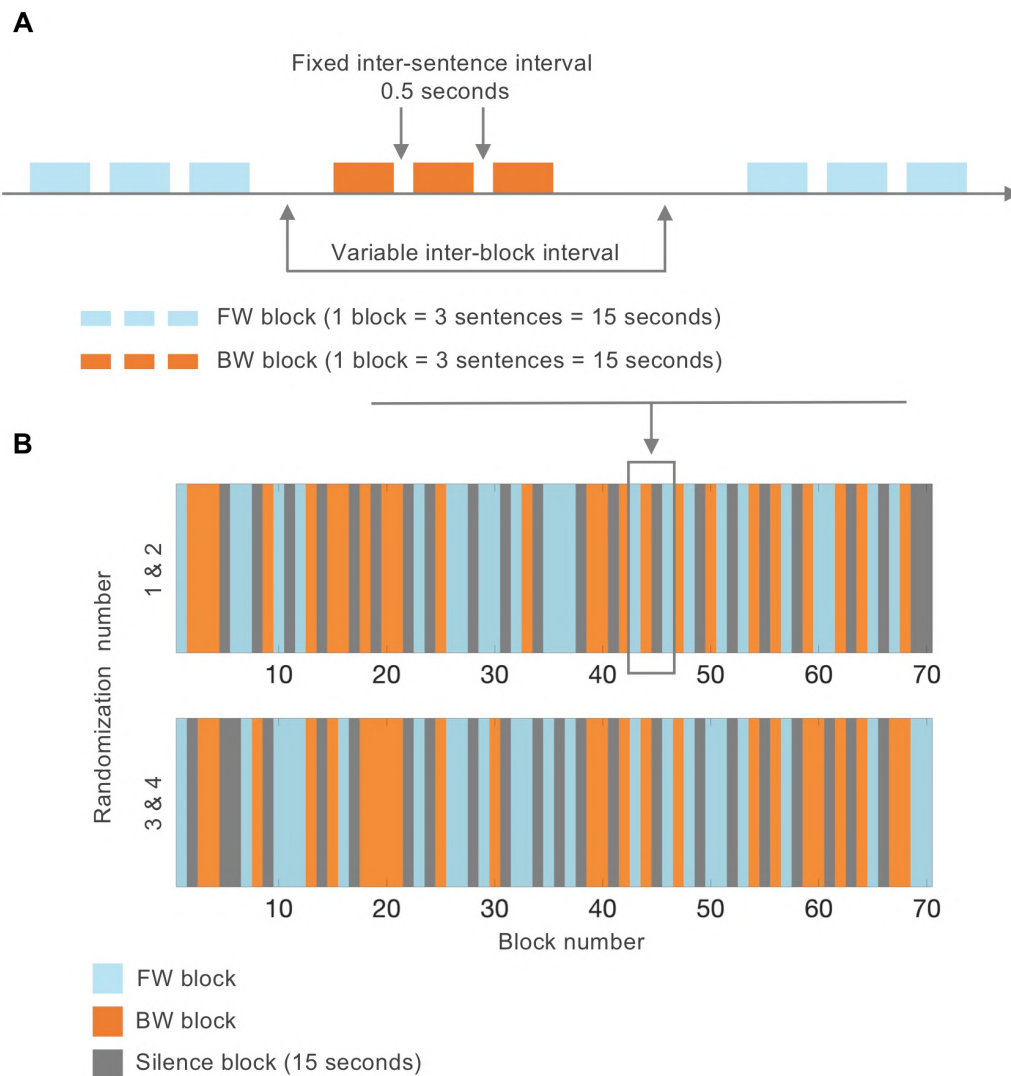


Figure 5.1 **A)** Blocks for FW and BW conditions were formed by three individual sentences and an inter-sentence interval of 0.5 seconds. A silence period was also added at the end of each block to match them all in duration (15 seconds). **B)** Four stimuli randomization paradigms optimized for detection power and estimation efficiency (Kao et al., 2009) were employed in the current study.

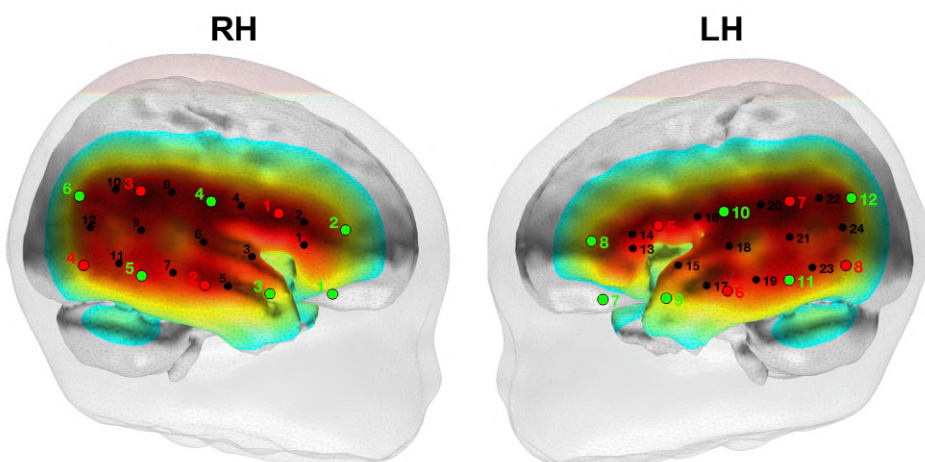


Figure 5.2 fNIRS optode (sources in red, detectors in green) and channel (black) localization in the current experimental setup. The normalized sensitivity profile of the current optode configuration is displayed in a 6-month-old infant head model.

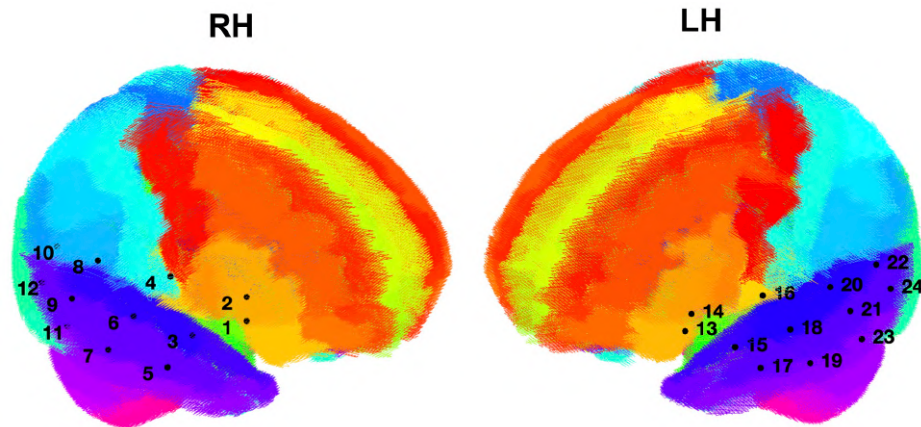


Figure 5.3 fNIRS channel localization registered to a 6-month-old infant AAL template (Akiyama et al., 2013).

Ch	S-D	S-D distance (mm)	AAL overlap (%)	Ch	S-D	S-D distance (mm)	AAL overlap (%)
1	FC6 - F8	30	Frontal_Inf_Tri_R (100)	13	FC5 - F7	30	Front_Inf_Orb_L (95) Frontal_Inf_Tri_L (5)
2	FC6 - F6	25	Frontal_Inf_Tri_R (100)	14	FC5 - F5	25	Frontal_Inf_Tri_L (100)
3	FC6 - FT8	25	Temporal_Sup_R (79) Temp_Pole_Sup_R (21)	15	FC5 - FT7	25	Temp_Pole_Sup_L (100)
4	FC6 - C6	25	Postcentral_R (69) Precentral_R (31)	16	FC5 - C5	25	Rolandic_Oper_L (100)
5	T8 - FT8	25	Temporal_Mid_R (100)	17	T7 - FT7	25	Temporal_Mid_L (100)
6	T8 - C6	25	Temporal_Sup_R (100)	18	T7 - C5	25	Temporal_Sup_L (100)
7	T8 - TP8	25	Temporal_Mid_R (100)	19	T7 - TP7	25	Temporal_Mid_L (94) Temporal_Inf_L (6)
8	CP6 - C6	25	Supramarginal_R (100)	20	CP5 - C5	25	Temporal_Sup_L (100)
9	CP6 - TP8	25	Temporal_Sup_R (45) Temporal_Mid_R (55)	21	CP5 - TP7	25	Temporal_Mid_L (100)
10	CP6 - P6	25	Supramarginal_R (100)	22	CP5 - P5	25	Temporal_Sup_L (76) SupraMarginal_L (24)
11	P8 - TP8	25	Temporal_Inf_R (64) Temporal_Mid_R (36)	23	P7 - TP7	25	Temporal_Inf_L (95) Temporal_Mid_L (5)
12	P8 - P6	20	Temporal_Mid_R (100)	24	P7 - P5	20	Temporal_Mid_L (100)

Table 5.2 Brain labels of the fNIRS channels in the current setup based on the probabilistic spatial registration of the fNIRS channels to a 6-month-old infant AAL template. Ch = Channel; S-D = Source-Detector pair.

During the study infants rested on their parents' lap facing the speakers presenting the stimuli. First, the fNIRS cap was placed on the infants' head. Then a feed and wrap approach was used to promote sleep and the experiment began when clear signs of sleep were noticeable on the infant. During the first participants it was observed that the sudden change from a room in complete silence to high-volume stimuli presentation was making the infants a wake. Therefore, for the next sessions it was decided to progressively increase volume during the first 30 seconds manually by one of the experimenters in order to avoid this effect. This portion of the data was excluded for the analyses during data preprocessing.

Data Preprocessing

All data preprocessing and analyses were implemented in MATLAB (R2012b, R2014b, Mathworks, Massachusetts) using in-house scripts as well as third-party toolboxes and functions.

Hemodynamic Correlates of Speech Processing in Infants

The MATLAB toolboxes employed in the current study are:

- Multi-Objective Optimal Experimental Designs for ER-fMRI Using MATLAB (Kao et al., 2009; <https://www.jstatsoft.org/article/view/v030i11>).
- Homer2 software package (Huppert et al., 2009; <https://homer-fnirs.org>).
- BrainWavelet Toolbox (Patel et al., 2014; <http://www.brainwavelet.org/about>).

The preprocessing pipeline for each individual is presented below:

1. Light intensity data (i.e., raw data measured at the instrument) were converted into optical density changes. \Rightarrow *hmriIntensity2OD* function in Homer2.
2. The first 30 seconds of experimental data were masked due to volume issues. Motion artifacts were identified and masked for subsequent analyses. \Rightarrow *hmriMotionArtifact* function in Homer2. Input parameters: tMask = 5; tMotion = 0.1; STDEVthresh = 20; AMPthresh = 0.2. These parameters were manually tuned to identify the largest and longest artifact corrupted periods. Note that a tMask of 5 seconds implies that five seconds of data before the start and end of each segment marked as motion artifact were excluded.
3. Motion induced spikes and signal drifts were corrected using the wavelet-based despiking method (Patel et al., 2014) described in chapter 2. \Rightarrow *WaveletDespike* function in Brain Wavelet Toolbox. Input parameters: same parameters as in Chapter 3. The algorithm was applied to the complete dataset in order to improve its performance and correct those artifacts not detected in step 2.
4. Optical density data were converted into HbO and HbR concentration changes. Differential path length factors of 5.3 (760 nm) and 4.2 (850 nm) were considered (see Chapter 3) \Rightarrow *hmriOD2Conc* in Homer2.
5. Very slow frequency fluctuations and signal drifts were modelled by up to 8 order Legendre polynomials, which were regressed out in a nuisance regression step. Contribution of high-frequency physiological noise sources (e.g., respiration and cardiac pulsation) were low-pass filtered using a zero-phase digital filter with cut-off frequency 0.3 Hz. \Rightarrow *hmriBandpassFilt* function in Homer2. This cut-off frequency was selected based on the power spectral density of the global signal (Figure 5.4).
6. Globally occurring hemodynamic processes in cerebral and extracerebral tissues assumed to largely reflect systemic hemodynamic changes were removed using linear regression. Prior to this step the average signal was filtered with the same parameters as the data to avoid reintroducing frequencies of non-interest. As HbO and HbR are differently affected by global systemic processes, data of each hemoglobin chromophore were filtered independently by including in the model either the global HbO or HbR signal.

As in the study presented in Chapter 3, quality assessment figures were generated for all participants after each preprocessing step (see Appendix A).

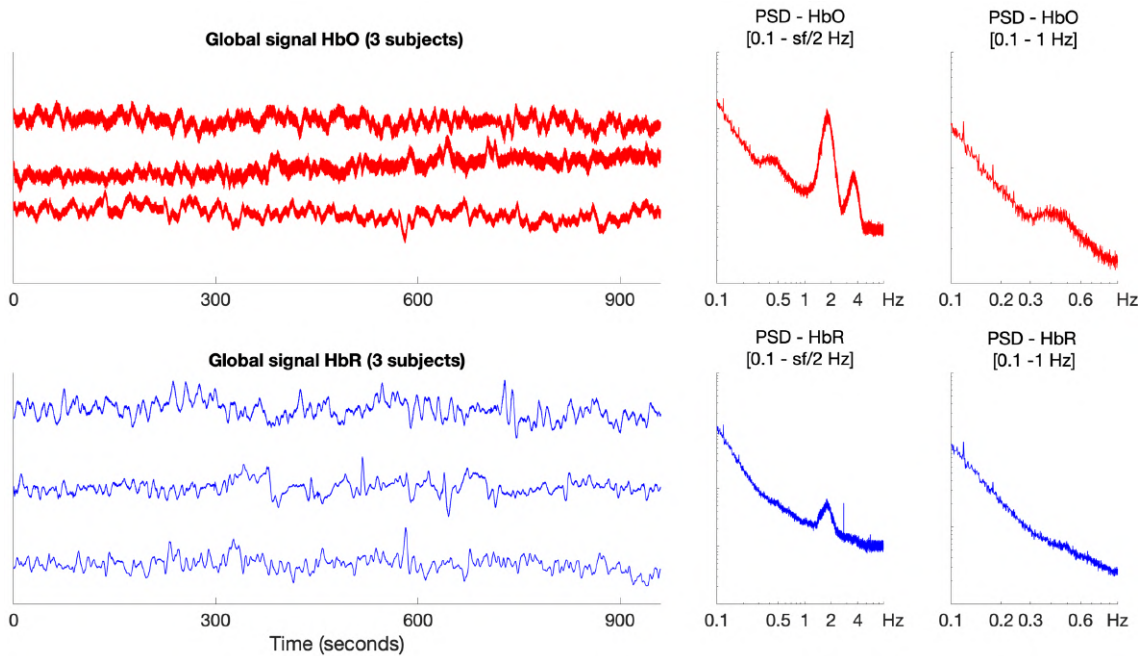


Figure 5.4 Global average signal for HbO and HbR computed across all participants in the study. Three examples of these signals are presented. The mean power spectral density (PSD) of the signals was calculated and it is presented for two different frequency ranges. In HbO, clear peaks can be observed at 2 and 4 Hz representing the cardiac pulse and its harmonics. A smaller peak is observed at 0.3 Hz potentially indicating a respiration component. Sampling freq. (sf) 15.625 Hz.

Data Analysis

For each participant, and for each experimental condition, the percentage of block-related data included for data analysis after censoring motion affected time points was calculated (Figure 5.5). In this step, it was also assessed that every time point inside each block (5 seconds baseline plus stimulus block duration, around 16 seconds in total) retained a similar number of data points after data censoring due to motion. The aim was to ensure that for both experimental conditions, time points during the entire block duration were similarly represented, in order to provide an accurate estimation of the whole shape of the hemodynamic response in subsequent analyses.

Two general linear model (GLM) analyses were performed to study the brain's response to FW and BW speech (Figure 5.6). The GLM assumes that the hemodynamic changes induced by individual components present in the signal add linearly to give the observed hemodynamic time course. The contribution of each of these components to the measured signal can be described as $\mathbf{y} = \mathbf{X}\boldsymbol{\beta} + \mathbf{e}$, where the term \mathbf{y} represents the measured HbO and/or HbR time series of a channel. This time series is modelled as a function of a set of explanatory variables (i.e., regressors) that comprise the design matrix \mathbf{X} . The term $\boldsymbol{\beta}$ represents the individual contribution of each regressor to the observed data, and the term \mathbf{e} denotes the error between the observed data and the specified model. Depending on the aim of the model, the design matrix can include regressors of interest (e.g., task-related regressors), regressors of non-interest (e.g., noise terms), or both.

Hemodynamic Correlates of Speech Processing in Infants

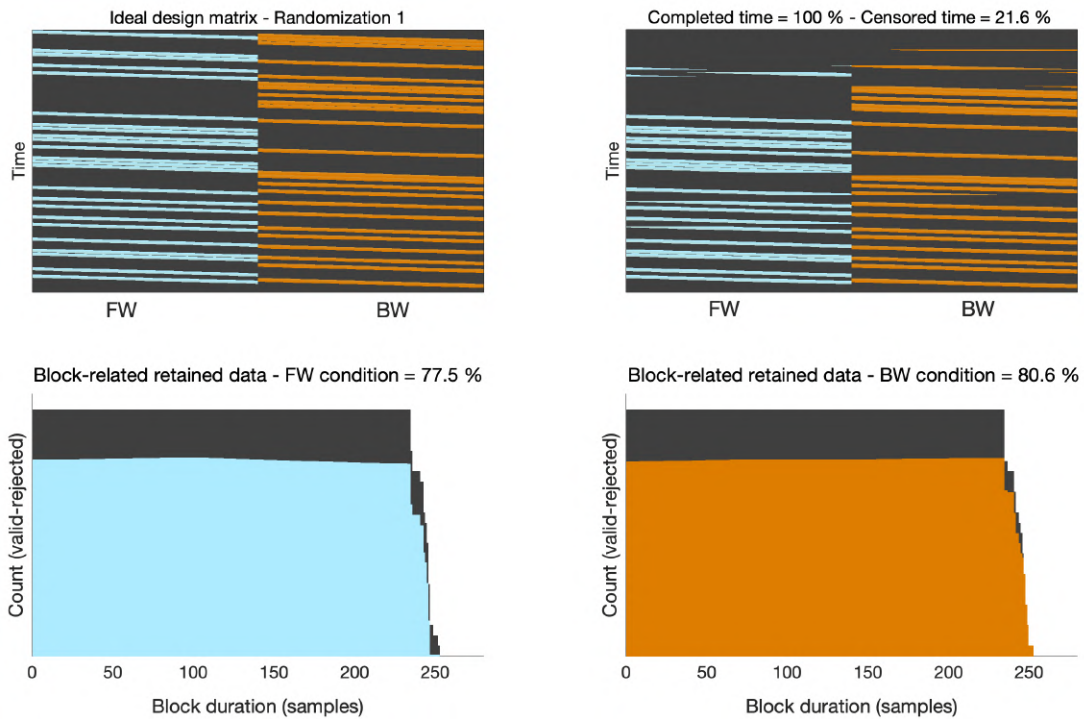


Figure 5.5 Motion affected time points were excluded for data analysis. The impact of motion censoring was evaluated on each participant by calculating the percentage of block-related time censored on each experimental condition. It was also ensured that specific time-points inside each block contributed with a similar amount of data to statistical analyses (bottom row).

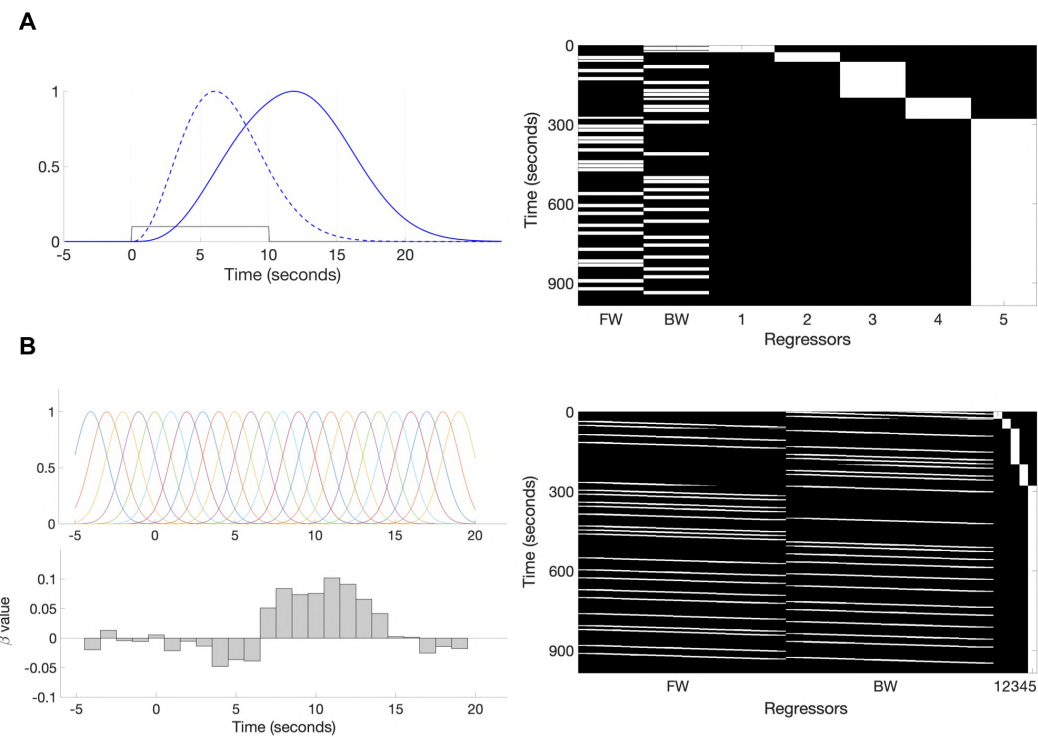


Figure 5.6 A) GLM modelling of the HbO and HbR signals for each condition using regressors time-locked to stimuli which were obtained by convolving a gamma function with peak at 6 seconds (dashed blue) and a square-wave of 10 seconds (grey). **B)** Deconvolution model using a set of gaussian basis functions as FIR components.

Assuming that the error follows a Normal distribution, the best linear unbiased estimate of β is obtained by the minimum least-squares solution: $\hat{\beta} = (\mathbf{X}^T \mathbf{X})^{-1} \mathbf{X}^T \mathbf{y}$, where \mathbf{X}^T and \mathbf{X}^{-1} are the transpose and inverse matrix of \mathbf{X} . The regressors of the design matrix \mathbf{X} are adapted according to the specific goals of the analysis, either estimating the amplitude of the functional response to stimulation (i.e. detection) or estimating the temporal shape of the hemodynamic response (i.e. efficiency). The optimized stimuli presentation approach employed in this study provided an experimental paradigm that allowed efficiently targeting both experimental goals simultaneously.

Detection-based analysis

The first experimental goal of this study aimed to detect areas/channels showing functional activation to the presentation of FW and BW speech stimuli (Figure 5.6A). Here the operational definition of functional activation for fNIRS based studies (i.e., increase in HbO, decrease in HbR) was considered (Obrig and Villringer, 2003). Based on this premise, regressors were generated for each experimental condition by convolving boxcar functions of 10 seconds duration with a model of the expected hemodynamic response function, a gamma function with peak at 6 seconds (Dehaene-Lambertz et al. 2002; Homae et al., 2006; Arichi et al., 2012). Boxcar regressors were also included in the model for each separate data segment formed after removing censored time periods (5 segments in Figure 5.6A) in order to model potential baseline differences between each of these periods. This analysis yields the β -values representing the mean effect of individual functional responses to each experimental condition FW and BW for HbO and HbR per participant.

Two group-level statistical analyses were performed based on these estimates. First, for a whole-sample analysis of activations, a one-sample t-test was performed on the individual β -values in order to detect the brain regions that were sensitive to the speech stimuli of each experimental condition. Second, for the statistical comparisons between groups, differences in mean β -values between bilingual and monolingual infants were modelled in a two-way mixed effects ANOVA for each channel, and for HbO and HbR separately. The mixed design was determined by the two independent variables that were manipulated in this experiment, one repeated-measures independent variable with two levels (i.e., FW and BW conditions), and one between-group independent variable with two levels (i.e., language background BIL vs. MON). Statistical tests were corrected for multiple comparisons at the channel level using the false discovery rate (FDR) method ($q < 0.05$, Benjamini and Hochberg, 1995).

FIR-based analysis

The second experimental goal of this study aimed at estimating the shape of the HRF evoked by each stimulus condition, which can be accomplished by using a finite impulse response (FIR) or deconvolution model. For each infant, HbO and HbR channel time courses were modelled using a Gaussian basis set consisting of 24 overlapping one-second gaussian functions (Figure 5.6B), spanning -5 seconds to 20 seconds around each stimulus onset. The hemodynamic response for each experimental condition, and each channel, is generated from the deconvolution of the 24 β -values extracted and the Gaussian

Hemodynamic Correlates of Speech Processing in Infants

basis set. As in the previous approach, potential baseline differences between each of the individual periods generated by motion censoring were modelled using boxcar regressors (5 segments in Figure 5.6B). At the group level, the average HRFs evoked by each condition at each individual channel are presented in the Results section. Between-group statistical analysis comparing the HRFs across experimental groups were conducted using a threshold free cluster enhancement method (Smith and Nichols, 2009).

Threshold-Free Cluster Enhancement

Potential differences on the HRF time-courses were investigated using a threshold-free cluster enhancement (TFCE) method (Smith and Nichols, 2009). This cluster-based correction for multiple comparison method follows a similar rationale as standard cluster-based inference methods employed in previous EEG (Maris and Oostenveld, 2007; Mensen and Khatami, 2013) and fNIRS studies (e.g., Mahmoudzadeh et al., 2013; Abboub et al., 2016; Ferry et al., 2016). Briefly, statistical comparisons between HRF time courses involve performing multiple statistical tests (i.e., one for each HRF time point), usually across multiple channels. Performing such a large number of tests increases the likelihood of observing significant effects (type 1 error rate), making it necessary to incorporate methods to control the enhanced false-positive rate. Cluster-based methods provide a way to control the family-wise error rate (FWER) for the statistical analysis of data in which spatial and/or temporal dependencies are expected between tests, as in the case of EEG event-related potentials (ERP), or fMRI and fNIRS HRF time courses.

The first step (1) in standard cluster-based methods is to perform a statistical test (e.g., two sample t-test) at each element of the time-series (i.e., HRF) under assessment, obtaining a series of values (e.g., t-values) which represent the difference between the amplitude responses of groups A and B at each time-point. In the next step (2), a predefined statistical threshold is used to create clusters of connected variables based on their temporal proximity (i.e., neighbouring/adjacent time points) amongst those time-points exceeding the threshold. Identified clusters can then be characterized on the basis of their size/extent (i.e., number of time-points), height (i.e., maximal statistical value) or by a combined metric considering both parameters (Pernet et al., 2015). The statistical significance of the extracted clusters is computed by means of non-parametric permutation testing (3). In this particular example, the individual HRFs of each participant are randomly permuted across experimental groups A and B, and for a number of permutations (e.g., 1000) steps (1) and (2) are repeated. Amongst the observed clusters in each permutation the maximum value of the selected cluster attribute (e.g., extent or height) is stored. These values create the null distribution from which the statistical significance of the selected attribute of the original cluster is estimated. This is accomplished by dividing the number of values in the empirical distribution of maxima that are higher than the original value, by the total number of permutations performed.

The main issue of this approach is the need of a priori defining an arbitrary statistical threshold that determines how clusters are formed. As effects in the signal might manifest in different shapes (e.g., broad effects with lower statistic values, sharp/short effects with high statistic value), the choice of the cluster-forming threshold is not trivial, and it may have

a large impact on the results (Smith and Nichols, 2009). TFCE provides a solution for this issue by including a range of all possible cluster-forming thresholds, and integrating the information obtained for each of them according to the following formula:

$$TFCE(t) = \int_{h=h_0}^{h(t)} extent(h)^E height(h)^H dh$$

At each time point t the *extent* (i.e., number of time points) and *height* (i.e., t-value) of the formed clusters are calculated and scaled by two weighting parameters E and H that determine whether to give more weight to spatially large clusters, or to those clusters showing large t-values, respectively. The range of all possible cluster forming statistical thresholds is determined by the initial value \mathbf{h}_0 , the maximum value \mathbf{h} , and the differential value between consecutive thresholds $d\mathbf{h}$. Thus, the TFCE integral represents the area of the cluster delimited by these parameters. This area is calculated for each statistical threshold in the range, and its value assigned to all the time points in the particular threshold under assessment that meet $height(t) > h(t)$. Given $d\mathbf{h}$, the integral above can be approximated as a discrete sum of all the areas/values under each time point, generating a TFCE value for each sample (Figure 5.7). Similarly, a p-value for each of these values can be calculated using permutation. In the current study, the default parameters $E = 0.5$ and $H = 2$, which have been validated for fMRI (Smith and Nichols, 2009) and EEG data (Mensen and Khatami, 2013; Pernet et al., 2015), were employed. The resolution $d\mathbf{h}$ for TFCE calculation was set at 0.01, the initial TFCE value \mathbf{h}_0 was set at 0.1 and \mathbf{h} was set as the maximum F-value in each test. For this analysis data (individual HRF time courses) were downsampled to approximately 4 Hz to reduce computational time. The TFCE approach implemented in the current study was performed at the channel level, thus ignoring potential spatial dependencies between channels.

Following the previous analysis, a two-way mixed effects ANOVA was performed at each time point in a subset of channels where a possible effect may be present, which was decided based on visual inspection of original F-values time courses (Appendix C). This selection was performed to reduce the computational time of the TFCE procedure. In HbO, channels 9, 16, 19 and 21 were selected for showing a possible main effect of language, and channels 13, 14 and 15 were selected to assess the presence of a potential interaction effect. The same channels were selected in HbR, although observed effects were smaller in this hemodynamic parameter. Channel 7 was also selected because of a possible interaction effect in HbR. Non-parametric permutation testing with 1000 iterations and unrestricted randomization of observations (i.e., language BIL and MON, condition FW and BW) was performed to assess the significance of the observed TFCE values forming clusters. The maximum TFCE value obtained at each iteration and for each curve (i.e., main effect of language and interaction) was stored to create the two null distributions against which the statistical significance of the original TFCE values was computed. In post-hoc pairwise comparisons the same approach was followed but using instead the t-value curves obtained from two-sample t-tests (Appendix C).

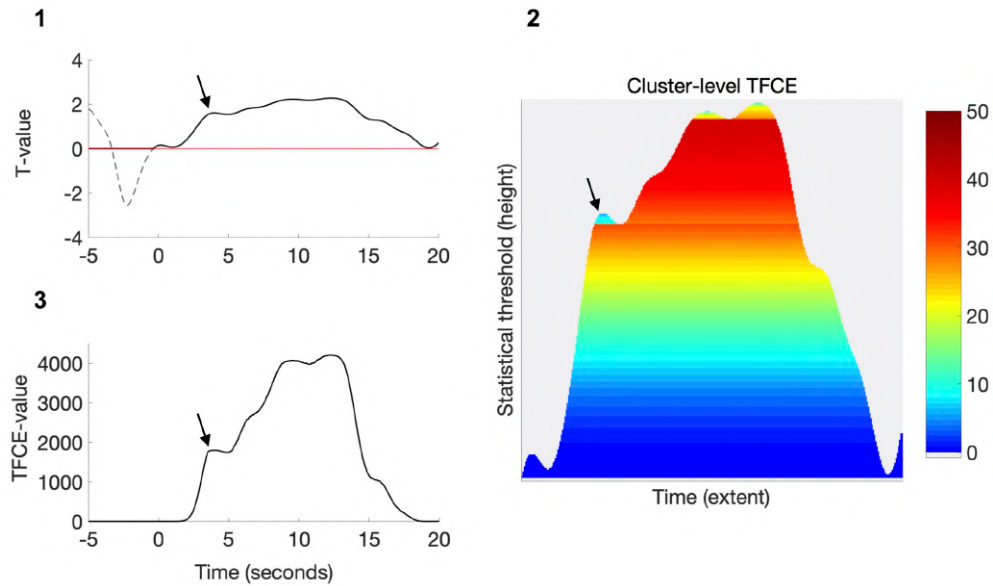


Figure 5.7 Example describing the processing pipeline of the TFCE method. 1) A statistical test is conducted at each time point, and all values in the curve higher than an initial threshold h_0 are selected as potential cluster-forming candidates. 2) For each statistical threshold the area delimited by **extent** and **height**values is computed and assigned to those time-points exceeding the threshold. 3) By adding the obtained values at each time point a TFCE value is generated for each sample. The arrow points to the same peak in the three steps and illustrates TFCE enhancement.

5.3. Results

Most of the infants that were able to fall sleep completed the entire experiment with no interruptions. At the group level, considering the 58 infants that were included for data analysis, the percentage of block-related data completed by these infants was computed (see Figure 5.5 for an individual example). Silence periods and segments at the beginning/end of the experiment were not included. Considering the whole sample, the mean percentage of block-related time completed for forward (FW) condition was $93\% \pm 6\%$, range = [72 % - 100 %], and for backward (BW) condition this percentage was $93\% \pm 4\%$, range = [80 % - 100 %]. In bilinguals, the mean percentage of block-related time completed for FW condition was $94\% \pm 4\%$, range = [82 % - 100 %], and for BW condition this percentage was $94\% \pm 3\%$, range = [88 % - 99 %]. In the monolingual group, for FW condition the percentage of block-related data included was $91\% \pm 6\%$, range = [75 % - 99 %], and for BW condition this percentage was $92\% \pm 5\%$, range = [80 % - 99 %]. According to the minimum of these values (72 %), at least 17 out of 24 blocks were completed by each infant and for each condition, although in general the number of completed blocks was higher. Furthermore, this analysis also confirmed that all time points inside each block, and for FW and BW conditions, were similarly represented and no data segment was particularly affected by the censoring procedure.

For the sake of clarity, the results for the group-level analysis ($n=58$) are presented first, and then results of the comparisons between groups ($n = 26$ bilingual infants, $n=21$ monolingual infants). Participants with an undetermined language background ($n=11$) were excluded for the between-group comparisons.

Whole Group Results

Detection-based analysis

The results of the one sample t-test analysis are shown in Figure 5.8A. To highlight, a large agreement between HbO and HbR results was observed in most of the channels, matching the operational definition of cortical activation for fNIRS data, i.e., an increase in HbO and a decrease in HbR, or the opposite (Obrig and Villringer, 2003). These results were considered more reliable than those in which only one of the chromophores showed a significant effect. Channel 7 (right middle temporal area) and channels 17, 18, 19 and 21 (left temporal areas) showed a significant activation response (i.e. increase in HbO and decrease in HbR) in response to FW and BW speech stimuli. On the other hand, channels 1, 2, 13 and 14 (bilateral inferior frontal areas) and channels 16 and 4 (around precentral/postcentral regions) showed a deactivation response (i.e., decrease in HbO and increase in HbR) to FW and BW speech stimuli. In channel 8 (right supramarginal gyrus) a deactivation response was observed for BW speech only. In FW condition deactivation was only significant for HbO. Finally, channel 15 showed a significant increase in HbR for BW speech, but this effect was not observed in HbO. Paired t-tests at the channel level assessing differences between experimental conditions revealed no significant differences in activation to FW and BW speech stimuli neither in HbO nor in HbR. In order to examine the effect of global signal regression the same results were produced without applying this preprocessing step (Appendix C, Figure C.1A).

FIR-based analysis

In addition, group-averaged HRFs for HbR and HbO and each experimental condition are presented in Figure 5.8B. Similar to the previous results, channels 17, 18, 19 and 7 (bilateral temporal regions) demonstrated a clear hemodynamic response characterized by an increase in HbO and a decrease in HbR. A trend towards a positive response can be also observed in channels 21 and 9, but with reduced amplitude. Conversely, channels 1, 2, 3, 4, 13 and 14 showed a negative hemodynamic response pattern (i.e., decrease in HbO and increase in HbR). A similar trend but with smaller amplitude is observed in channels 8 and 16. The equivalent results computed using a preprocessing pipeline not including global signal regression are presented in Appendix C (Figure C.1B). In order to compare the HRF time courses of FW and BW conditions, Figure C.2 in Appendix C separately shows the hemodynamic responses for HbO and HbR data, along with the corresponding standard deviation of the averaged hemodynamic response time courses. As it can be observed in this figure, there is a large resemblance between the responses to FW and BW speech stimuli.

The mean hemodynamic response time courses of channels demonstrating brain activation were averaged together across conditions, including positive and negative responses, to provide information of the HRF dynamics in this sample of 4-month-old infants, and for comparison with the HRF model employed in the activation-based analysis (Figure 5.9). In HbO, the hemodynamic response peaked around 8-9 seconds after stimulus onset, reached a plateau that lasted around 4-5 seconds, and then progressively

Hemodynamic Correlates of Speech Processing in Infants

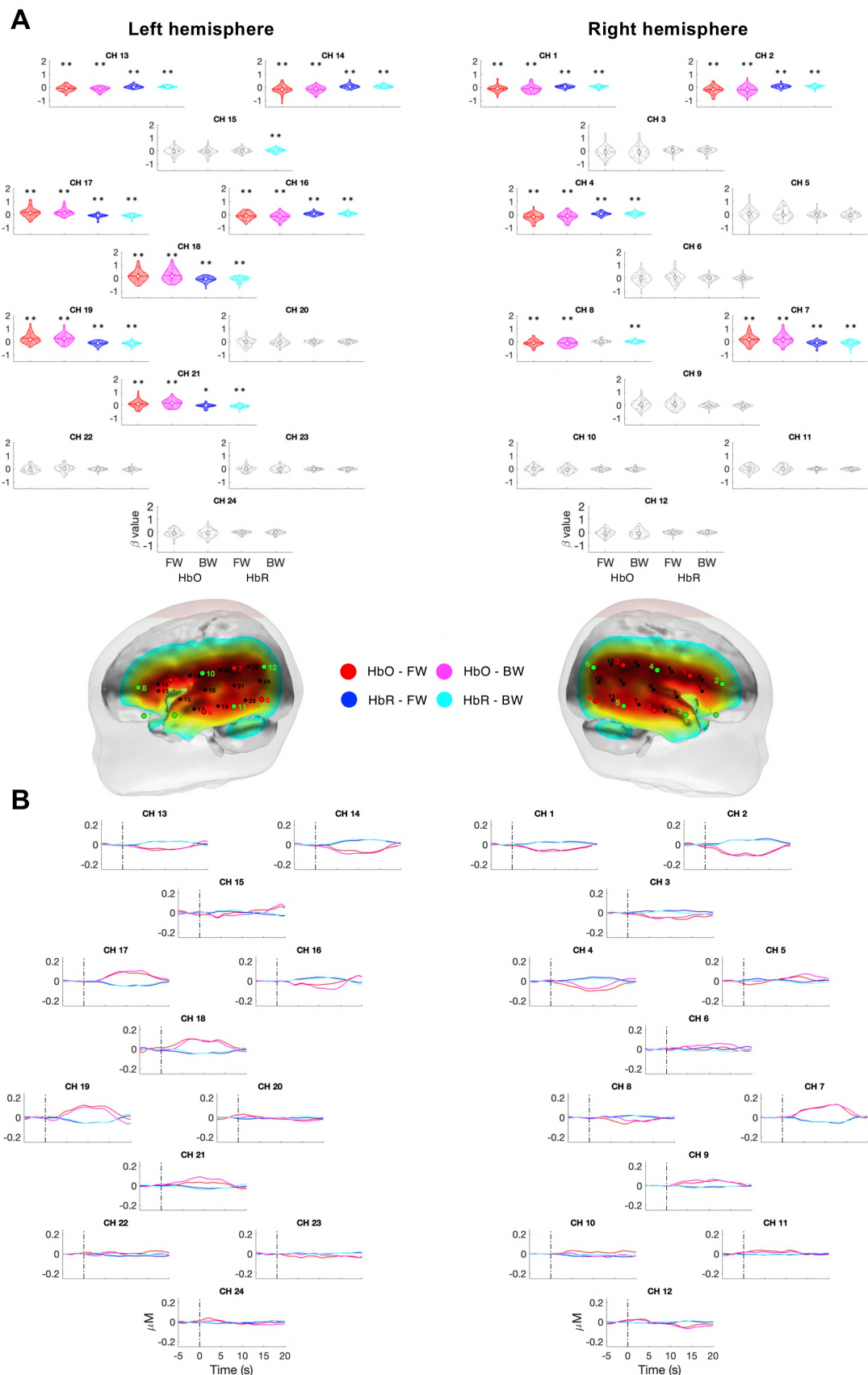


Figure 5.8 A) Channels showing a significant activation/deactivation as determined by one-sample t-tests for each of the experimental conditions (FW, BW). * $p < 0.05$, ** $p < 0.05$ (FDR corrected). **B)** Group-averaged HRFs at each channel location and for each experimental condition estimated by the FIR-based analysis. Time zero indicates stimulus onset.

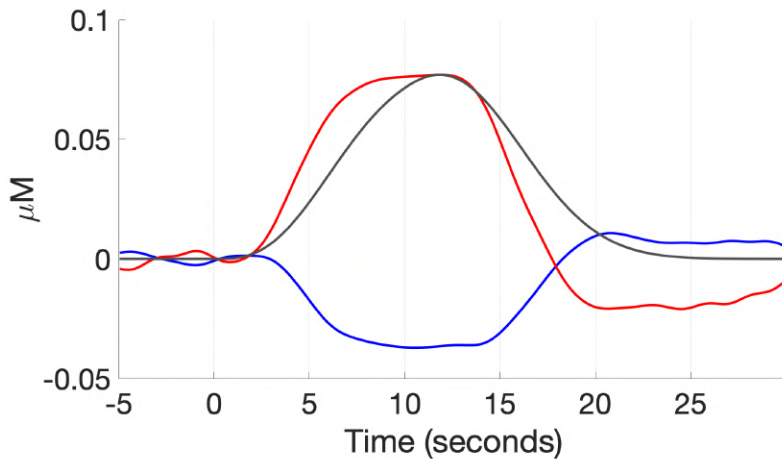


Figure 5.9 Average HRF response at the group level (HbO-red, HbR-blue), computed from channels showing activation or deactivation responses in Figure 5.8B (i.e., channels 1, 2, 3, 4, 7, 9, 13, 14, 16, 17, 18, 19, 21). In grey, the model employed for the estimation of the β -values is displayed.

decreased. A post-stimulus undershot starting approximately 17-18 seconds after stimulus onset and peaking at 20 seconds can also be distinguished. Then, the signal progressively returned to baseline values. The temporal properties of the HbR response pattern parallel those observed in HbO. However, the magnitude of the response in HbO was on average around 2.5 times larger than in HbR. The HRF model employed in the activation-based analysis and the HRF estimated in the second analysis showed a high resemblance. Nonetheless, this comparison enables to conjecture that differences between both types of analysis (i.e. activation-based vs. FIR-based) could be associated with the fact that the HRF model hypothesized in the activation-based analysis does not include an undershoot period and the slight temporal delay observed between the two-time courses.

Between-Group Comparisons

Detection-based analysis

A two-way mixed effects ANOVA with Condition (repeated measures, FW-BW) and Language (between-group factor, BIL-MON) as factors was performed on the estimated β -values at each channel, and for HbO and HbR. Results of the observed significant effects are summarized in Table 5.3.

In HbO, significant main effects were observed for Language in channel 9 (right superior/middle temporal, $F_{1,45} = 4.29, p = 0.044, \eta_p^2 = 0.087$, BIL > MON), and for Condition in channels 13 (left inferior frontal, $F_{1,45} = 4.52, p = 0.039, \eta_p^2 = 0.091$, BW > FW, larger negative response) and 16 (left rolandic operculum, $F_{1,45} = 4.29, p = 0.044, \eta_p^2 = 0.087$, BW > FW, larger negative response). Further, a significant interaction of Language * Condition was observed in channel 14 (left inferior frontal, $F_{1,45} = 5.23, p = 0.027, \eta_p^2 = 0.104$) and 18 (left superior temporal, $F_{1,45} = 5.79, p = 0.020, \eta_p^2 = 0.113$). In channel 14, bilinguals showed a larger negative response to FW speech stimuli, whereas monolinguals showed a larger negative response to BW speech. Significant differences were not observed in pairwise post-hoc contrasts. The interaction effect in channel 18 is

Hemodynamic Correlates of Speech Processing in Infants

	Independent variable (IV)	CH	Hb	F-value	p-value	η_p^2	Levels of the IV [marginal means]
Main effects	Language	9	HbO	4.28	0.044	0.087	BIL, MON [0.136, -0.044]
	Condition	13	HbO	4.52	0.039	0.091	FW, BW [-0.062, -0.122]
	Condition	16	HbO	4.29	0.044	0.087	FW, BW [-0.043, -0.128]
	Language	23	HbR	6.60	0.013	0.128	BIL, MON [0.005, 0.053]
Interactions	Language * Condition	14	HbO	5.23	0.027	0.104	BIL [FW, BW] [-0.163, -0.105] MON [FW, BW] [-0.084, -0.191]
	Language * Condition	18	HbO	5.79	0.020	0.113	BIL [FW, BW] [0.105, 0.238] MON [FW, BW] [0.225, 0.153]
	Language * Condition	18	HbR	9.76	0.003	0.178	BIL [FW, BW] [-0.031, -0.092] MON [FW, BW] [-0.130, -0.055]

Table 5.3 Summary of significant results obtained in the two-way mixed ANOVA analysis. None of these results was significant after multiple comparisons correction (FDR method).

displayed in Figure 5.10. As can be seen in the figure, this effect is driven by bilinguals showing a larger response (i.e., increase in HbO) to BW speech, and monolinguals showing a larger response to FW speech. Significant differences were not observed in pairwise post-hoc contrasts.

In HbR, a significant main effect for Language was observed in channel 23 (left middle/inferior temporal, $F_{1,45} = 6.6, p = 0.013, \eta_p^2 = 0.128, \text{MON} > \text{BIL}$), and a significant Language * Condition interaction was observed in channel 18 (left superior temporal, $F_{1,45} = 9.76, p = 0.003, \eta_p^2 = 0.178$). This latter interaction is displayed in Figure 5.10. Analogous to the observations in the same channel for HbO, bilinguals showed a larger response (i.e., decrease in HbR) to BW speech, whereas monolinguals showed a larger response to FW speech. Significant differences were not observed in pairwise post-hoc contrasts. None of the observed effects in HbO and HbR was significant when corrected for multiple comparisons across channels using the False Discovery Rate approach (FDR, $q < 0.05$, Benjamini and Hochberg, 1995).

FIR-based analysis

Second, differences between bilinguals and monolinguals in the HRF time courses obtained to each experimental condition (FW, BW speech) were investigated. In channels 7, 9, 13, 14, 15, 16, 19 and 21, a two-way mixed effects ANOVA was performed at each time point for the HbO and HbR time courses. The resulting time courses of F-statistics (Appendix C, Figure C.3) were corrected using the threshold-free cluster enhancement (TFCE) method (Smith and Nichols, 2009). In channel 14 (left inferior frontal) a significant interaction effect was observed (TFCE correction for multiple comparisons) for HbO data only. This difference was driven by an effect from 10.8 seconds to 13.9 seconds. In this cluster, bilinguals showed a more negative response to FW speech than monolinguals.

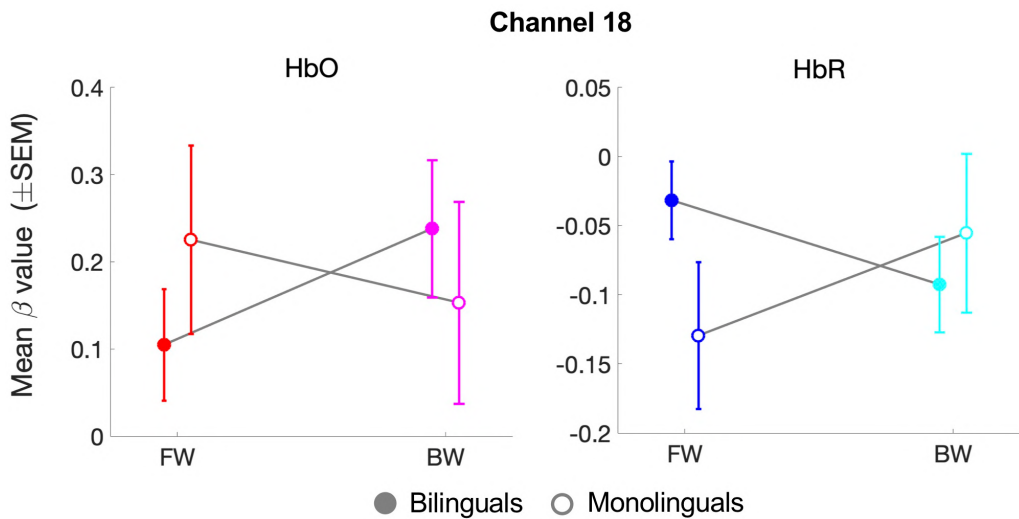


Figure 5.10 An interaction effect which was consistent across HbO and HbR was observed in channel 18 (left superior temporal). In both Hb parameters bilinguals showed higher activation to BW speech and monolinguals showed higher activation to FW speech stimuli. Post-hoc pairwise comparisons revealed no differences in any of the pairwise contrasts.

In contrast, monolinguals showed a more negative response than bilinguals for BW speech. Pairwise post-hoc contrasts in the t-values time courses (Appendix C Figures C.4 and C.5) revealed that these effects were not significant. In channel 15 a significant interaction effect was observed (TFCE correction for multiple comparisons) for HbO data only. This difference was driven by an effect from 10.1 seconds to 11.1 seconds. Pairwise post-hoc contrasts in the t-values time courses (Appendix C Figures C.4 and C.5) revealed a significant difference between groups for FW speech (TFCE correction for multiple comparisons), driven by bilinguals showing a negative response to FW speech and monolinguals showing a positive response to FW speech. A significant cluster was observed, most compatible with an effect from 9.2 seconds to 12.4 seconds with a mean effect of $0.158\mu\text{M}$ [$0.155, 0.162\mu\text{M}$]. Significant main or interaction effects were not observed in any of the other channels under assessment.

Analysis of the HRF time courses based on F-values, and using a TFCE method for multiple comparisons correction, was found relatively strict. In order to assess the presence of other potential weak effects, additional exploratory pairwise contrasts on t-values time courses of all channels were performed, for FW and BW conditions, and in HbO and HbR data (Appendix C Figures C.4 and C.5). This analysis was also corrected for multiple comparisons using the TFCE method. In the description of these results a distinction has been made to differentiate activation (HbO increase, HbR decrease) and deactivation (HbO decrease, HbR increase) effects. Table 5.4 summarizes all of these results.

Channel 1 (right inferior frontal) showed a significant difference for FW condition in HbO (BIL > MON, deactivation) compatible with an effect from 15.0 seconds to 17.0 seconds with a mean effect of $0.087\mu\text{M}$ [$0.085, 0.089\mu\text{M}$] was observed. Channel 9 (right superior/middle temporal) exhibited a significant difference for FW condition in HbO (BIL > MON, activation) compatible with an effect from 8.1 seconds to 13.3 seconds with a mean effect of $0.164\mu\text{M}$ [$0.160, 0.167\mu\text{M}$] was observed. In this channel, a similar effect

Hemodynamic Correlates of Speech Processing in Infants

CH	Hb	Condition	Effect (activation/deactivation)	Timepoints (s)	Mean effect (μM)	95% CI
1	HbO	FW	BIL > MON, deactivation	15.0 – 17.0	0.087	[0.085, 0.089]
9	HbO	FW	BIL > MON, activation	8.1 – 13.3	0.164	[0.160, 0.167]
13	HbO	FW	BIL > MON, deactivation	15.5 – 18.6	0.090	[0.088, 0.091]
15	HbO	FW	MON activation BIL deactivation	9.2 – 12.4	0.158	[0.155, 0.162]
16	HbO	FW	BIL > MON, deactivation	8.9 – 13.3	0.140	[0.136, 0.143]
7	HbR	FW	BIL > MON, activation	7.1 – 12.7	0.070	[0.069, 0.072]
9	HbR	FW	BIL > MON, activation	9.6 – 12.6	0.072	[0.071, 0.073]
21	HbR	FW	BIL > MON, activation	17.2 – 18.7	0.054	[0.054, 0.055]
24	HbR	BW	MON > BIL, activation	18.7 – 20	0.067	[0.065, 0.068]

Table 5.4 Summary of significant results obtained from pairwise comparisons (t-tests) between groups on the HRFs across experimental conditions (TFCE correction for multiple comparisons).

was observed for FW condition in HbR (BIL > MON, activation) from 9.6 seconds to 12.6 seconds with a mean effect of $0.072\mu\text{M}$ [0.071, $0.073\mu\text{M}$]. Channel 13 (left inferior frontal) showed a significant difference for FW condition in HbO (BIL > MON, deactivation) driven by an effect from 15.5 seconds to 18.6 seconds with a mean effect of $0.090\mu\text{M}$ [0.088, $0.091\mu\text{M}$]. Channel 16 (left Rolandic operculum) displayed a significant difference for FW condition in HbO (BIL > MON, deactivation) driven by a cluster starting at 8.9 seconds to 13.3 seconds with a mean effect of $0.140\mu\text{M}$ [0.136, $0.143\mu\text{M}$]. Channel 7 (right middle temporal) showed a significant difference for FW condition in HbR (BIL > MON, activation) driven by an effect from 7.1 seconds to 12.7 seconds with a mean effect of $0.070\mu\text{M}$ [0.069, $0.072\mu\text{M}$]. Channel 21 (left middle temporal) showed a significant difference for FW condition in HbR (BIL > MON, activation) compatible with an effect from 17.2 seconds to 18.7 seconds with a mean effect of $0.054\mu\text{M}$ [0.054, $0.055\mu\text{M}$]. Channel 24 (left middle temporal) showed a significant difference for BW condition in HbR (MON > BIL, activation) driven by a cluster starting at 18.7 seconds to 20 seconds with a mean effect of $0.067\mu\text{M}$ [0.065, $0.068\mu\text{M}$] was observed. No significant effects were found in the rest of the channels under assessment for either HbO or HbR.

5.4. Discussion

This work examined how early linguistic experience in a bilingual environment modulates 4-month-old infants' brain responses to speech (forward, FW) and non-speech (backward, BW) sounds using fNIRS, based on a large sample of participants and a large number of trials. Stimuli presentation was optimized for two general linear model (GLM) based analyses (Kao et al., 2009). The first analysis method (i.e., detection-based analysis) was employed to efficiently detect the brain regions activated by the presentation of FW and BW speech stimuli. With the second analysis method (i.e., FIR-based analysis), the shape of the hemodynamic response function (HRF) in infants at 4 months of age in response to FW and BW speech stimuli was estimated. At the whole group level a high resemblance between the results of the two data analysis methods was observed. The

agreement in the results could be further improved by using a better model of the HRF in infants at this age, which is still not available. Minagawa-Kawai et al., (2011) followed a different approach. First, they estimated the shape of the HRF in a group of infants in a similar way as it was done in the current work. Then, they used this information to design the HRF model for the estimation of the β coefficients in a subsequent analysis. Although this approach might seem more precise, it also presents a circularity risk, and for this reason it was not implemented here.

Whole Group Level

The detection-based analysis revealed significant brain activation responses (i.e., increase in HbO, decrease in HbR) in four channels located in left superior and middle temporal regions, and in one channel located in right middle temporal region. Allowing some uncertainty in channel localization, these results are in close agreement with the organization of the infant language system around perisylvian areas reported in previous infant literature (Dehaene-Lambertz et al., 2002; Dehaene-Lambertz et al., 2006; Perani et al., 2011). The patterns of HRF obtained with the FIR-based analysis revealed activation responses in channels located over the same bilateral temporal areas. The FIR analysis showed a high resemblance between the shape of the estimated HRF and the adult canonical HRF, in terms of latency and amplitude difference between peak and undershoot periods (Arichi et al., 2012). Although some infant studies have showed a slightly slower time-to-peak latency (Minagawa-Kawai et al., 2011), overall the shape of the estimated response (i.e., HbO and HbR) also matches previous infant literature (Bortfeld et al., 2007; Mahmoudzadeh et al., 2011; Arichi et al., 2012; Sato et al., 2012; Issard and Gervain, 2018). Both analysis methods also showed significant deactivation responses (i.e., decrease in HbO, increase in HbR) to FW and BW speech stimuli in bilateral inferior frontal regions, extending to more posterior regions around the central sulcus.

At the group level, no differences were observed on the brain responses to FW and BW speech conditions, in any of the analysis methods, unlike previously reported (Dehaene-Lambertz et al., 2002; Peña et al., 2003; Sato et al., 2012; May et al., 2017). A potential explanation for the lack of differences observed between the conditions might be because infants were tested during sleep in the current study. Nevertheless, the infant brain is able process information during sleep (Tarullo, 2011). For instance, infants showed the ability to distinguish their mother vs. a stranger's voice (deRegnier et al., 2000), or to detect a deviant tone amongst a set of previously habituated standard tones (Cheour et al., 2002). Most previous works that observed differences between speech and non-speech conditions, using various imaging modalities, were conducted in infants during natural sleep (Peña et al., 2003; Kotilahti et al., 2010; Perani et al., 2011; Sato et al., 2012; Abboub and Gervain, 2016; Vannasing et al., 2016; May et al., 2017); although some activation differences in dorsolateral prefrontal cortex between FW and BW conditions were only detected in awake infants (Dehaene-Lambertz et al., 2002). Furthermore, neonates showed comparable brain responses during active and quiet sleep states when processing acoustic stimuli consisting of speech and music samples (Kotilahti et al., 2010).

Hemodynamic Correlates of Speech Processing in Infants

It still might be the case that testing asleep infants might have potentially masked differences in brain activation between conditions. Although all of the infants were scanned shortly after falling sleep, and thus it is assumed that all of them were in the same sleep stage during the recordings, it is well known that changes in autonomic physiology and arousal occur during sleep (Gaultier et al., 1995; Duyn et al., 2020). A recent study with awake infants, observed focal brain activation patterns in occipital and temporal regions in response to visual and auditory stimuli, respectively (Taga et al., 2018). However, auditory responses became more global when infants were tested during natural sleep, thus disrupting the expected spatial response pattern over temporal regions. These global activation patterns were tentatively explained as infants' perception being more synesthetic during sleep. It is also nevertheless possible that the global effects were a consequence of their fNIRS data preprocessing pipeline, which not included any specific step for the removal of global systemic physiological effects.

Several authors have claimed that the removal of global systemic physiology is an essential (Tachtsidis and Scholkmann, 2016; Pfeiffer et al., 2018; Pinti et al., 2019; see also Chapter 2 of this thesis), yet not widely adopted, preprocessing step in fNIRS research. To understand the effect of removing global systemic effects in the current study, activation responses and HRFs were estimated using a data preprocessing pipeline applying standard bandpass filtering only (Appendix C Figure C.1). Significant activation responses were observed across most fNIRS channels in the setup. Moreover, the HRFs without global signal regression revealed a global component (i.e. present across all channels). These HRFs were shorter in duration, with HbO responses showing a clear bump at around 5 seconds. The presence of this global component of undetermined nature across all channels in the setup raised doubts in the interpretation of these results. Thus, in the present work it was decided to reduce the impact of global components by using a global signal regression approach (Pfeiffer et al., 2018), as short-separation channels were not available in the fNIRS setup. Similar global trends were also apparent in other previous fNIRS works assessing brain responses to auditory stimuli in infants, and that not included any specific preprocessing step to remove global fluctuations (e.g., Watanabe et al., 2010; Homae et al., 2011; May et al., 2011). The origin and underlying physiological mechanisms contributing to this component constitute a relevant topic for future work.

Another potential explanation for the dissimilar outcomes across studies is the number of participants and valid trials included in data analysis. In this work, high quality data from 58 participants is presented. Each participant has on average 21 trials per condition. This number exceeds those presented in previous works [e.g., Peña et al., (2003) 12 infants, a maximum of 10 trials; Kotilahti et al., (2010) 13 infants, unknown number of trials; May et al., (2011) 20 infants, 4 valid trials on average; Minagawa-Kawai et al., (2011) 12 infants, 8-12 trials; Sato et al., (2012) 12 participants, 5 valid trials on average; Vannasing et al., (2016) 27 participants, 14 valid segments on average; May et al., (2017) 24 infants, a maximum of 8 trials; Mercure et al., (2020) 60 participants, 5 valid trials per condition on average]. Despite the large number of participants and valid trials per condition available in the current study, which might have been adequate for group-level analyses, these numbers might still be insufficient for between-group statistical comparisons.

Importantly, for both analysis approaches, the two experimental conditions (i.e., FW and BW speech), and for activation and deactivation effects, the extracted brain activation patterns and hemodynamic responses matched the expected relationship between HbO and HbR responses as measured with fNIRS (i.e., HbO increase and HbR decrease, or the opposite for deactivation responses; Obrig and Villringer, 2003; see also Chapter 2). The temporally anticorrelated dynamics of HbO and HbR responses were observed even in those channels not showing statistically significant activation, or clear HRF responses. Most of the previous infant studies using fNIRS have focused their results in HbO parameter only, based on the premise that it is a better marker of brain activity and has a higher signal-to-noise than HbR (e.g., Sato et al., 2012). In these studies, statistically significant results in HbR are often not observed, or the outcomes of this parameter are directly not discussed (May et al., 2011; Minagawa-Kawai et al., 2011; Sato et al., 2012; Vannasing et al., 2016; May et al., 2017; Mercure et al., 2020). Our results demonstrated that reliable, robust and consistent responses are feasible in both Hb parameters providing a large number of participants and trials is collected.

A relevant finding of the current study are the deactivation responses observed bilaterally over inferior frontal regions. As is can be inferred from Figure C.1B (Appendix C), this effect was not due to the global signal regression step applied during preprocessing, as similar deactivation responses were also present when hemodynamic responses were estimated without including this step. Furthermore, deactivation responses cannot be attributed to a generalized altered hemodynamic response pattern during sleep, as typical HRF patterns were observed in bilateral temporal regions during the presentation of speech and non-speech stimuli (Figure 5.8).

A series of studies assessing the brain responses to auditory stimulation suggested that during sleep, information processing in a particular brain region might be achieved by suppressing the activity of alternative brain regions (Czisch et al., 2002; Czisch et al., 2004). Similar to the current study, Wilf et al. (2016) presented awake and asleep participants (adult subjects) with acoustic stimuli including different levels of linguistic information (i.e., scrambled speech, pseudowords and sentences). Here, activation responses over the auditory cortex were present during sleep, but responses in the inferior frontal regions responsible for language processing were completely suppressed. These results indicate that sensory processing is relatively preserved during sleep, but activity in higher order cognitive processes might be significantly reduced.

Another plausible explanation is that this response inhibition mechanism might modulate cortical reactivity to certain external stimuli during sleep, thus operating as a sleep protecting mechanism (Zou et al., 2020). As in previous works (Portas et al., 2000; Czisch et al., 2004; Wilf et al., 2016), negative responses in the current study were mainly observed in channels located over left and right prefrontal regions. This region represents one of the functional hubs of the default-mode network, a functional brain network assumed to reflect the baseline or default-mode state of the brain, and which also demonstrates a functional deactivation during goal-oriented behaviours (Raichle et al., 2001). Interestingly, a similar deactivation pattern was observed in 3-month-old infants during the presentation of speech

Hemodynamic Correlates of Speech Processing in Infants

stimuli (Dehaene-Lambertz et al., 2006). Considering the spatial resolution of fNIRS and channel localization precision, the possibility that the observed negative responses in the current work reflect the activity of this network cannot be completely ruled out.

Yet, another potential explanation for the functional deactivation responses observed in the current study, and one that has been recurrently proposed in previous infant fNIRS studies (Wilcox et al., 2009; Kotilahti et al., 2010; Quaresima et al., 2012; de Roeck et al., 2018) is the blood stealing effect from spatially adjacent brain regions. According to this view, the increased blood flow over activated brain regions is compensated by a deactivation, or blood flow reduction, in adjacent brain regions (Shmuel et al., 2001). This effect might be more strongly observed in areas that are served by the same vascular system, as is the case in the current work in which regions showing activation and deactivation responses are supplied by the middle cerebral artery. However, this hypothesis still remains to be tested as other works have reported deactivation responses in the absence of concurrent positive responses, thus discarding the possibility of a blood stealing effect (Czisch et al., 2004; Shekhar et al., 2019).

Between-Group Comparisons

Activation differences between monolingual and bilingual infants' responses were observed in various fNIRS channels. These effects were statistically weak, and only the strongest effects derived from these two analysis methods are discussed hereinafter. Concretely, differences that were either 1) present across HbO and HbR, 2) significant after multiple comparisons correction or/and 3) consistent across data analysis methods, are discussed.

The strongest effect was observed in channel 18 located in the superior temporal gyrus. Here, a significant interaction effect in HbO and HbR indicated that bilingual infants showed higher activation to BW speech, whereas monolinguals' brain activation was higher for FW speech. Few studies have compared speech processing in bilingual and monolingual infants at this early age. Nonetheless, this result could be linked with previous evidence that showed a behavioural preference in 4-month-old monolingual infants for their native language, and a stronger preference for the unfamiliar input displayed by their bilingual peers (Bosch and Sebastián-Gallés, 1997; Molnar et al., 2014). In addition, neuroimaging research assessing the role of familiarity on infants' brain responses to spoken language has consistently observed increased left lateralized activation in temporal regions to familiar vs. unfamiliar languages (Minagawa-Kawai et al., 2011; Sato et al., 2012; Vannasing et al., 2016), a result that somehow parallels the pattern observed in the current work. Monolingual infants, who are assumed to have more experience with their native language than bilinguals, showed the expected left hemispheric dominance towards their familiar language condition (i.e., Spanish-FW). On the other hand, bilingual infants displayed a relatively lower activation to FW condition as compared to monolinguals, which might reflect the reduced experience with this input. Alternatively, the higher activation in bilingual infants towards BW condition might also indicate their increased interest in unfamiliar, novel auditory stimuli. This mechanism (i.e., flexibility of attention) has been proposed as a specific cognitive adaptation that might allow bilingual infants to cope with

the increased complexity of a dual language environment (Costa and Sebastián-Gallés, 2014; Bialystok, 2015).

Similarly, in channel 15, located in the anterior part of the superior temporal gyrus, bilingual and monolingual infants showed HRFs of opposite sign only in HbO. In this channel, monolinguals displayed a positive activation response to FW stimuli, whereas bilinguals demonstrated a low amplitude deactivation response. This effect denoting a stronger left lateralized activation for speech in monolingual infants is similar to the one discussed above for channel 18, which is also located in the superior temporal gyrus but more posteriorly.

An interaction effect (HbO only) in channel 14, localized in the left inferior frontal region, revealed that this channel was differentially sensitive to the stimulus condition across groups. In monolinguals, this channel showed enhanced deactivation responses to BW speech. Conversely, bilingual infants showed similar deactivation responses to FW and BW speech stimuli in this channel. Previous evidence has confirmed the role of left inferior frontal region for the detection of mismatching audio-visual information in 6-month-old infants, with matching trials showing higher positive (activation) responses and mismatching trials showing higher negative (deactivation) responses (Altvater-Mackensen and Grossman, 2016). Although the link is rather speculative, deactivation responses in this region observed in the current work might be indicative of a similar processing, with monolinguals showing higher deactivation responses to the unfamiliar/mismatch condition, while this distinction being less salient in the case of bilingual infants. Importantly, the same interaction effect (HbO only) was confirmed as significant in the FIR-based analysis.

Lastly, bilingual infants showed an increased activation in right superior/middle temporal gyrus (i.e., channel 9), as demonstrated by the two data analyses. The activation-based analysis showed that, considering both experimental conditions (i.e., FW and BW speech), bilinguals' activity in this region was higher than in monolinguals, although only observed for HbO. The FIR-based analysis of the HRFs revealed a similar outcome, but only for the FW speech condition in both HbO and HbR. By looking at the HRF curves (Figures C4 and C.5 in Appendix C), it can be noticed that the magnitude of the response in the right temporal region (channels 7 and 9) is higher in bilingual infants. A more bilateral language representation in bilinguals has been proposed (Hull and Vaid, 2007; Archila-Suerte et al., 2013), which might be explained by the recruitment of additional brain regions due to the increased cognitive demands of the bilingual input (Costa and Sebastián-Gallés, 2014), but further evidence for this lateralization difference in infancy is still required.

As discussed in Chapter 1, another potential explanation for the observed differences might be related with a less left-hemispheric dominance in bilinguals due to a reduced, or delayed, functional specialization to their native language. Several works have demonstrated that monolingual infants became specialized earlier in the properties of their native language (Bosch and Sebastián-Gallés, 1997; Weikum et al., 2007; Sebastián-Gallés et al., 2012; Nácar-García et al., 2018). Although native language performance is fundamentally equivalent between monolingual and bilingual infants, bilingual infants showed sustained sensitivity to the properties of unfamiliar languages when monolingual

Hemodynamic Correlates of Speech Processing in Infants

infants are no longer able to do so (Weikum et al., 2007; Petitto et al., 2012; Sebastián-Gallés et al., 2012). These findings might suggest a different developmental transition in the perceptual sensitive periods during speech processing between bilingual and monolingual infants (Kuhl, 2010; Petitto et al., 2012; Kovacs et al., 2015; Werker and Hensch, 2015), which can complement the attentional adaptation hypothesis (Costa and Sebastián-Gallés, 2014; Byalistok, 2015; Comishen et al., 2019). The delayed functional specialization observed in bilingual infants at the behavioural level might be present at the neural level as well. Considering speech processing, as in the current work, these adaptations might manifest as an additional involvement of right hemispheric regions, or analogously, as a decreased left-hemispheric specialization.

In the rest of the channels showing differences between groups, higher activation/deactivation responses were observed in bilingual as compared to monolingual infants for FW speech; except for an effect in the posterior part of the left middle-inferior temporal gyrus suggesting a higher activation in this region in monolingual infants. Overall, the effects observed in between-group comparisons were small, which might indicate a lack of statistical power. Therefore, any activation differences between bilingual and monolingual infants observed in the current work should be cautiously interpreted.

5.5. Summary

The study presented in this chapter described the brain activation responses to speech and non-speech stimuli in 4-month-old bilingual and monolingual infants using fNIRS. At the group level, functional brain activation to the auditory stimuli was observed bilaterally in classical language and auditory regions in the superior and middle temporal gyrus, with activation patterns showing a higher lateralization towards the left hemisphere. No differences were observed between forward and backward speech conditions after multiple comparison corrections suggesting that, under the current experimental conditions, the infant brain did not signal a distinction between the two acoustic inputs. Deactivation responses were observed bilaterally in the inferior frontal gyrus, but the functional mechanisms underlying this process require more evaluations.

Potential tendencies emerged when comparing bilingual and monolingual infants. Monolinguals showed a more left-lateralized pattern of brain activation for speech stimuli of their native language, whereas bilinguals showed more bilateral activity over temporal regions and less marked preference towards speech vs. non-speech condition. These results fit previous observations showing dissimilar developmental pathways between bilingual and monolingual infants during the earliest stages of language acquisition (e.g., Bosch and Sebastián-Gallés, 1997; Nácar-García et al., 2018). However, the ability of the current work to robustly detect these differences might have been hindered by a limited statistical power.

This work also produced several methodological advancements of relevance for future fNIRS research. An optimized stimulus presentation procedure was implemented, which can be adapted for different statistical goals such as detecting brain activation, estimating the shape of the hemodynamic response function, or both, depending on the research question under investigation. An efficient experimental design for stimuli

presentation can be particularly meaningful for infant fNIRS studies in which data quality is more heavily dependent on time constraints. This approach allowed us to collect an unprecedented number of trials for each experimental condition. Second, a method to perform statistical comparison on the hemodynamic response time courses without the need of selecting a particular response feature (e.g., mean or peak amplitude) was implemented. Following the outcomes of Chapter 3, this work further highlighted the importance of data quality for obtaining robust and reliable fNIRS measurements. In addition, this work explored how different methodological approaches for fNIRS signal processing, for example not accounting for global systemic physiology, might impact study outcomes and lead to inaccurate interpretations.

Conclusions and Future Work

This thesis investigated potential differences in functional brain activity between 4-month-old monolingual and bilingual infants (Chapter 1) using functional near-infrared spectroscopy (fNIRS, Chapter 2). Examining resting-state functional connectivity (Chapter 3) allowed to simultaneously describe and compare the intrinsic configuration of numerous functional systems supporting different cognitive processes. Chapter 4 described specific methodological issues to consider when analysing resting-state fNIRS measurements. Chapter 5 examined whether the reported behavioural differences between 4-month-old monolingual and bilingual infants during speech processing could also be manifested as dissimilar patterns of brain activation towards speech stimuli. Due to the limited amount of studies that have compared early language acquisition in monolingual and bilingual setups using neurophysiological measures, findings derived from this thesis could help to better understand established behavioural evidence, and provide insights for future lines of research in the (bilingual) language acquisition field.

Functional Imaging in 4-Month-Old Infants

One of the main goals of this thesis was to provide robust and replicable outcomes based on fNIRS resting-state and task-based measurements in 4-month-old infants that could serve as reference for future research works in this population. In the last years, a growing number of brain imaging studies have conducted fNIRS in developmental populations. Some of these works yielded unexpected outcomes, which are challenging to explain and link to established literature, and which often contradict the inherent properties of the neurophysiological signal that is measured with fNIRS.

In this work, at the whole-group level, the observed resting-state functional connectivity patterns and the brain activation responses towards speech stimuli involved regions that were spatially consistent with prior literature. As an example, classic functional networks overlapping primary auditory and sensorimotor regions were identified. Speech stimuli elicited brain responses in bilateral middle and superior temporal regions and in the inferior frontal gyrus, which correspond to brain areas that are known to support auditory and language processes. Besides the spatial characteristics of the reported functional networks and responses, the presence of relevant features of the fNIRS signal corroborated the reliability of the measurements obtained in the current work. Concretely, the outcomes presented in the studies of this thesis showed: i) the assumed statistical relationship between oxy- and deoxyhemoglobin (HbO and HbR) signals (i.e., negative correlation or antiphase state), ii) the direction of activation responses always showing opposite sign across HbO and HbR, indicative of activation or deactivation hemodynamic responses, and iii) the shape of the estimated hemodynamic response resembling the canonical model.

Nonetheless, it is acknowledged that not all research can be conducted under the conditions that were available in the current work (e.g., testing a large number of participants, and during natural sleep). Taking into account the importance of conducting research in this population, a major advancement for the field would be a commitment to

data sharing in a way that is easily accessible by other researchers. This would be a simple, yet relevant step that could help explaining potential inconsistencies of the results and avoiding over interpretation of research findings. It is planned that the data of the studies presented in this thesis will be made available in an open access repository at the time of publication.

Functional Adaptations due to an Early Bilingual Environment

So far only a few studies have investigated the consequences of an early bilingual environment on functional brain development. These studies have been mainly supported by behavioural evidence showing that both linguistic capacities and learning trajectories are essentially comparable across monolingual and bilingual infants, but the latter present various behavioural and functional adaptations when processing linguistic inputs, presumably induced by the added complexity of growing up in bilingual learning environment.

Despite acquiring resting-state fNIRS measurements showing a large agreement with the fundamental properties of the fNIRS signal, and observing functional networks spatially consistent with established literature, the study described in Chapter 3 comparing resting-state functional connectivity patterns across monolingual and bilingual infants revealed no differences between experimental groups. Functional connectivity differences as a result of a dissimilar language background have only been observed in adult subjects (Luk et al., 2011; Grady et al., 2015; Berken et al., 2016; Kousaie et al., 2017; Gullifer et al., 2018; Sulpizio et al., 2020). Hence, future work should aim to disentangle whether potential differences might manifest later in development; for example by conducting a longitudinal study considering a big sample of infants with different levels of linguistic experience. Such a study would also benefit of a denser fNIRS array (e.g., high-density diffuse optical tomography) with enhanced spatial sensitivity, and a more precise optode localization method.

Similarly, reliable fNIRS measurements and spatially meaningful brain activation patterns towards auditory speech stimuli were obtained in the study presented in Chapter 5. A limitation of this study, including speech stimuli of a shared native language (i.e., Spanish), is that the experimental design did not allow to discern the role of experience from the role of bilingualism in the comparison of functional activation patterns extracted during language processing. Concretely, the observed (weak) effects could not be incontestably attributed to a reduced exposure to a particular language only, as they could also be associated to the very fact of being bilingual. In a future study, the effect of bilingualism could be ruled out, for example by including two groups of bilingual infants tested on one common familiar and on one unfamiliar language for each of them, respectively. A more comprehensive, but challenging, setup could also include electroencephalography (EEG) measurements to simultaneously examine how each of these groups tracks relevant temporal and spectral properties of speech such as rhythm.

The studies presented in Chapters 3 and 5 yield either non-significant, or only weak evidence for the effect of early bilingualism in functional brain activation or connectivity patterns. Discerning whether these results are merely not informative or they indicate

support for the null hypothesis (i.e., absence of evidence vs. evidence of absence) would provide a more accurate and complete interpretation of the observed effects. An ongoing work is to complement the traditional frequentist null-hypothesis testing approach employed in these studies with a Bayesian hypothesis testing method, which would permit establishing quantitative predictions on the absence or the presence of the investigated effect (Keysers et al., 2020).

Methodological Outputs

This thesis also describes various methodological outputs from a signal processing and data analysis point of view, which might be particularly relevant for studies using fNIRS in developmental populations. First, a data quality assessment routine was implemented in all the studies of this thesis. The quality indicators that were used (e.g., power spectral density assessment, phase difference between HbO and HbR and signals) were established according to recommendations by fNIRS experts gathered from reviews (Tatchsidis and Scholkmann, 2016; Pinti et al., 2019), seminal papers (Obrig et al., 2003), training workshops and recommendations at the fNIRS Society meetings. Although carrying out a quality assessment routine for every single participant and sharing this information with the community might seem a trivial step for more experienced fNIRS researchers, this simple approach for understanding fNIRS data is essential for those researchers new to the field; particularly given that neuroscientific studies are performed by researchers from a broad range of backgrounds such as psychology, linguistics, statistics or engineering.

A fundamental difference between the fNIRS data preprocessing pipeline employed in the studies of this thesis with respect to previous fNIRS infant works is the addition of a step for removing global systemic physiology. Accounting for global, systemic hemodynamic changes, for example by regressing out the signal from short-distance channels is an established preprocessing step in fNIRS studies with adults where such channels are available (Saager and Berger, 2008; Gagnon et al., 2014). The feasibility of this approach is very limited in developmental populations due to the small head size of infants such that global signal regression becomes the most practical and feasible alternative (Tatchsidis and Scholkmann, 2016). Even though some works suggested that global hemodynamic effects might not severely impact fNIRS measurements with infants (Emberson et al., 2016), and avoid performing this global regression step, the patterns of brain activation tend to spread across all channels in the setup and not localized in the a priori expected region. Here, the presence of global effects in resting-state and task-based fNIRS paradigms with infants was also demonstrated when global signal regression was not performed. Trying to understand the benefits and downsides of this step, and its interaction with other steps of the standard infant fNIRS preprocessing pipeline deserves further investigation. This work can also include data analysis pipelines that incorporate advanced statistical methods such as prewhitening and robust regression (Huppert et al., 2016), which adapt the statistical model to account for the specific sources of noise present in the fNIRS signal. Similarly, the findings reported in Chapter 4 opened a discussion about the implications of incorporating prewhitening to the resting-state fNIRS data preprocessing pipeline and about the prewhitening method that would be more appropriate for those

fNIRS users interested in including this step. Future work should also explore alternative statistical methods to approach the issue of temporal autocorrelation on functional neuroimaging signals, such as those used to estimate the effective degrees of freedom or to correct the variance of Pearson's correlation coefficient (Patel and Bullmore, 2016; Afyouni et al., 2018; James et al., 2019).

This thesis also introduced several data analysis methods to investigate resting-state and task-based experimental paradigms that are novel for fNIRS data. In Chapter 3, two methods to extract group-level functional connectivity networks and components were adapted from the functional magnetic resonance imaging (fMRI) literature (Smith et al., 2012; Amico et al., 2017; Amico and Goñi, 2018). These approaches were implemented by incorporating specific characteristics of the fNIRS signal, such as the expected resemblance between the HbO and HbR functional connectivity patterns. Furthermore, these properties were exploited to develop a new approach for order selection that ensured the robustness of the obtained patterns. Future lines of research could also explore implementing novel advanced functional connectivity analyses such as complex network analyses, dynamic causal modelling and psycho-physiological interactions to the acquired datasets. By applying these methods, it would be possible to characterize individual functional connectivity profiles (de Souza et al., 2019) and investigate potential associations between specific network features and different cognitive or clinical outcomes of interest (Hassanpour et al., 2017).

In Chapter 5, a threshold-free cluster enhancement (TFCE) method was implemented to perform statistics in the entire time courses of the extracted hemodynamic responses. This is the first time TFCE is implemented for the analysis of fNIRS data, and the parameters were selected based on previous EEG and fMRI works (Smith and Nichols, 2009; Mensen and Khatami, 2013; Pernet et al., 2015). The parameters used in the current work downweight the effect of cluster extent, partially reducing the importance of broad but weak effects. On the other hand, the effect is enhanced in time points showing high statistical values, therefore assigning more relevance to strong and peaky clusters. Future research should investigate the best way to tune these parameters to efficiently detect both types of effects considering the type of responses commonly observed in fNIRS data.

Resumen

La adquisición del lenguaje es un proceso que ese encuentra determinado tanto por mecanismos de desarrollo cognitivo, como por la experiencia lingüística durante los primeros años de vida. Aunque se trata de un proceso relativamente complejo, los bebés muestran una gran habilidad para el aprendizaje del lenguaje. Un entorno de aprendizaje lingüístico bilingüe podría considerarse aun más complejo, ya que los bebés están expuestos a las características lingüísticas de dos lenguas simultáneamente. En primer lugar, los bebés que crecen en un entorno bilingüe tienen que ser capaces de darse cuenta de que están expuestos a dos lenguas diferentes, y posteriormente deben separar y aprender las características específicas de cada una de ellas; por ejemplo, los distintos fonemas, palabras o estructuras gramaticales. Aunque la exposición lingüística total de los bebés bilingües debería ser comparable a la de los bebés monolingües, es probable que la exposición a cada una de las lenguas de su entorno sea menor, ya que tienen que dividir su tiempo de exposición entre ambas. Si bien los bebés bilingües parecen no tener problemas para enfrentarse a un contexto de aprendizaje potencialmente más complejo, ya que alcanzan las distintas etapas de adquisición del lenguaje a un ritmo similar a los bebés monolingües, sí se han observado adaptaciones a nivel conductual y a nivel de funcionamiento cerebral que podrían producirse como consecuencia de este contexto.

En el primer capítulo de la tesis se realiza una revisión detallada de la literatura sobre la adquisición del lenguaje en entornos bilingües durante los primeros meses de vida, con especial énfasis en las posibles adaptaciones que tienen lugar en los bebés bilingües durante este proceso. Estudios previos han demostrado que la forma en la que los bebés monolingües y bilingües dirigen su atención a estímulos lingüísticos difiere entre ambos grupos. Los bebés bilingües parecen mostrar mayor interés hacia estímulos lingüísticos novedosos, mientras que los bebés monolingües se ven más atraídos por la información lingüística relacionada con su lengua materna. Por otra parte, algunas habilidades perceptivas, como la capacidad para diferenciar dos lenguas en base a información lingüística visual, pero no auditiva, parecen seguir una trayectoria diferente entre estos dos grupos. Si bien los bebés monolingües se especializan antes en las características de su lengua materna, reduciendo progresivamente su habilidad para discriminar otras lenguas no presentes en su entorno, los bebés bilingües parecen mantener sus capacidades de discriminación lingüística durante más tiempo, además de utilizar diferentes estrategias para conseguirlo, lo cual podría suponer un mecanismo de adaptación a su entorno lingüístico más complejo. Además, también se ha observado que crecer en un entorno lingüístico bilingüe podría influir en el desarrollo de otras funciones cognitivas más allá del ámbito del lenguaje, y más concretamente en las funciones ejecutivas. Algunas de estas diferencias también han sido confirmadas mediante estudios de neuroimagen, por ejemplo, al comparar las respuestas cerebrales de bebés monolingües y bilingües ante sonidos del habla de la lengua materna y una lengua desconocida. Sin embargo, debido a la dificultad que supone realizar este tipo de estudios en población infantil, algunos de estos estudios cuentan con importantes limitaciones metodológicas, las cuales también se describen a lo largo de la tesis, y que los estudios realizados pretenden superar.

El objetivo general de esta tesis doctoral ha sido estudiar la influencia del bilingüismo en el desarrollo funcional del cerebro durante los primeros meses de vida. Concretamente, el grupo experimental de interés para los estudios de esta tesis han sido los bebés de 4 meses de edad, por tratarse del primer momento del desarrollo donde se han observado diferencias tanto conductuales, como a nivel de funcionamiento cerebral entre bebés monolingües y bilingües. Los estudios principales de esta tesis se han centrado en investigar si una exposición temprana y continuada a un entorno bilingüe podrían producir cambios en la organización y el funcionamiento cerebral, especialmente en áreas asociadas al lenguaje, siendo estas diferencias observables mediante el empleo de técnicas de neuroimagen funcional adaptadas para su uso con población infantil. Concretamente, para la realización de los estudios presentados se ha utilizado la técnica de neuroimagen funcional espectroscopia del infrarrojo cercano (*functional near-infrared spectroscopy - fNIRS*), cuyos fundamentos se describen en detalle en el capítulo 2. Esta técnica utiliza las propiedades de la luz infrarroja para penetrar los tejidos del cuerpo humano, ya que la piel, el cráneo y los tejidos cerebrales no absorben este tipo de luz. Esta propiedad permite relacionar las variaciones de intensidad que se producen en la luz al atravesar los tejidos cerebrales con los cambios que se producen en la concentración de oxígeno en áreas específicas del cerebro, los cuales representan una medida indirecta de actividad cerebral.

Experimento 1. Conectividad Funcional en Estado de Reposo

El primer estudio experimental de la tesis (capítulo 3) estudia la actividad funcional del cerebro en estado de reposo en bebés de 4 meses utilizando fNIRS. Estudiar la actividad del cerebro en estado de reposo es una forma de entender la organización funcional del cerebro, evitando la interferencia debida a diferencias individuales que puede darse en estudios que requieren la ejecución de una tarea específica. Este tipo de paradigma experimental permite estudiar la conectividad funcional (*functional connectivity - FC*), es decir la activación sincronizada entre áreas del cerebro que comparten un rol común durante la ejecución de diferentes procesos cognitivos, por ejemplo la red visual, la red auditiva, la red motora o la red del lenguaje.

Este estudio incluyó datos de fNIRS de gran calidad recogidos en 99 niños de 4 meses de edad, con una duración de 9 minutos en cada uno de ellos, formando una muestra sin precedentes si se compara con estudios anteriores que han estudiado FC con fNIRS en población infantil. Los 99 participantes pertenecían a tres entornos lingüísticos diferentes: bilingües español-euskera, monolingües de español y monolingües de euskera. Además, se implementaron métodos para el estudio de la FC a nivel de grupo, sin necesidad de dividir a los participantes en base a condiciones experimentales. Esto permitió que los resultados de este estudio fueran calculados sobre una muestra de 99 participantes, y no a nivel de sub-grupo o individuo como se ha realizado en estudios anteriores de FC con fNIRS. Los resultados de este estudio revelaron mapas de FC a nivel de grupo que coinciden con estudios previos de neuroimagen realizados con resonancia magnética funcional, en los cuales la literatura es más extensa, tanto en adultos como en población infantil. Sin embargo, la comparación estadística entre los grupos experimentales (bilingües vs monolingües) no encontró diferencias en los patrones de estas redes entre los

grupos. Puesto que hasta ahora únicamente se han observado diferencias en FC debido a un entorno bilingüe en poblaciones adultas, futuras investigaciones con participantes en distintas etapas del desarrollo podrían ayudar a clarificar cuándo y bajo qué condiciones comienzan a manifestarse estas diferencias en la organización funcional del cerebro durante la infancia.

Experimento 2. Retos Estadísticos durante el Procesamiento de la Señal de fNIRS

En el capítulo 4 de la tesis se presenta un estudio metodológico, en el cual se discute el problema de la autocorrelación temporal en la señal fNIRS, una propiedad de la señal que puede inducir falsos resultados en estudios de conectividad funcional (FC). Esta característica en la señal de fNIRS se debe principalmente a la alta frecuencia de muestreo de la señal de este sistema de neuroimagen, y a la presencia de componentes fisiológicos (e.g., respiración o pulso cardiaco) que coexisten con la señal hemodinámica de interés, es decir con aquella que refleja de manera indirecta la actividad neuronal.

En este estudio se evalúan empíricamente los dos métodos principales que se habían propuesto para eliminar el efecto de la autocorrelación temporal presente en la señal de fNIRS. Los análisis realizados demuestran que estos métodos son eficaces en esta tarea, pero que también modifican ciertas propiedades intrínsecas de la señal neurofisiológica medida con fNIRS, y en las cuales están basados todos los estudios previos de la literatura sobre FC. Los análisis realizados demuestran que utilizando un análisis clásico de la señal fNIRS es posible replicar los resultados de dos estudios recientes de FC realizados en población infantil. Por el contrario, al eliminar la autocorrelación mediante los métodos propuestos en la literatura no es posible replicar los resultados de ninguno de los estudios. Por lo tanto, en base a los resultados, se concluye que para considerar la aplicación rutinaria de este paso durante el preprocesado de la señal fNIRS es necesario que su efecto se investigue más detalladamente, con el objetivo de entender la relevancia neurofisiológica de la señal fNIRS tras eliminar su autocorrelación intrínseca. Futuros estudios podrían determinar el procedimiento más apropiado para corregir el elevado número de falsos positivos en estudios de FC utilizando fNIRS, y proponer nuevos métodos que podrían aplicarse sin la necesidad de alterar las propiedades intrínsecas de la señal.

Experimento 3. Respuestas Cerebrales a Estímulos Lingüísticos

En el capítulo 5 se investigan las respuestas cerebrales de bebés monolingües y bilingües ante estímulos lingüísticos. Puesto que las diferencias entre estos grupos no se manifiestan en su actividad cerebral en estado de reposo, la hipótesis para este estudio plantea que los patrones de actividad cerebral podrían diferir en cuanto a las áreas encargadas del procesamiento del lenguaje, ya sea por el hecho de crecer en un entorno bilingüe, o por la reducida exposición que los bebés bilingües presentan hacia cada una de sus lenguas.

Al igual que en el estudio de FC, para este estudio se obtuvieron datos de gran calidad en 58 niños de 4 meses de edad, en este caso monolingües de español y bilingües de español y euskera. Los participantes fueron expuestos a frases en español mientras se

midio su actividad cerebral utilizando la técnica de fNIRS. Para el diseño experimental del estudio, se utilizó un procedimiento optimizado basado en algoritmos genéticos por primera vez en fNIRS que permite investigar tanto las áreas cerebrales activadas, como la forma de la respuesta hemodinámica de forma más eficiente (i.e. mayor número de eventos por unidad de tiempo) que con paradigmas más convencionales y ampliamente utilizados en estudios de fNIRS.

Los análisis a nivel de grupo, es decir considerando las respuestas de todos los participantes de manera conjunta, mostraron actividad funcional en áreas clásicamente asociadas a la audición y el lenguaje como el giro temporal superior y medio de ambos hemisferios, aunque con cierta tendencia hacia una mayor lateralización hacia el hemisferio izquierdo. Se observaron diferencias significativas entre los grupos experimentales, especialmente en áreas cerebrales relacionadas con el procesamiento de la información auditiva. Estos resultados podrían ser muy relevantes ya que demostrarían que un entorno bilingüe podría producir una adaptación funcional en el cerebro durante los primeros meses de vida, confirmando así las hipótesis desarrolladas en previos estudios conductuales. Sin embargo, estos resultados deben ser interpretados con cautela, ya que los efectos detectados fueron relativamente débiles, tal y como demostraron los procedimientos estadísticos aplicados para la corrección por comparaciones múltiples.

Discusión General

En resumen, esta tesis analiza el impacto que supone la exposición temprana a un entorno bilingüe para el desarrollo funcional del cerebro. Los estudios presentados en esta tesis podrían tener importantes implicaciones teóricas para futuras investigaciones centradas en entender las primeras etapas de la adquisición del lenguaje. Concretamente, los resultados sugieren que el contexto lingüístico durante los primeros meses de vida podría causar cambios en la organización funcional del cerebro los cuales son observables durante el procesamiento de estímulos lingüísticos, y que sin embargo no se manifiestan al examinar la organización funcional del cerebro en estado de reposo. En esta tesis también se proponen varios avances metodológicos de relevancia en cuanto al procesamiento y al análisis de la señal de fNIRS. Asimismo, se demuestra la utilidad de la técnica fNIRS para medir de forma fiable el funcionamiento cerebral en población infantil utilizando diferentes paradigmas experimentales. A lo largo de este trabajo también se incide en la importancia de aplicar una metodología transparente y replicable en futuras investigaciones en el campo de la neurociencia cognitiva del desarrollo.

List of Publications Derived from the Thesis

Borja Blanco, Monika Molnar and César Caballero-Gaudes, "Effect of prewhitening in resting-state functional near-infrared spectroscopy data" *Neurophotonics* 5(4), 040401 (2018). [doi: 10.1117/1.NPh.5.4.040401].

Borja Blanco, Monika Molnar, Manuel Carreiras, Liam H. Collins-Jones, Ernesto Vidal, Robert J. Cooper and César Caballero-Gaudes, "Monolingual and bilingual infants rely on the same brain networks: Evidence from resting-state functional connectivity ". *Under review*.

Borja Blanco et al. "Hemodynamic correlates of speech processing in 4-month-old bilingual and monolingual infants". *In preparation*.

Appendix A

fNIRS Data Quality Assessment

In this Appendix, various fNIRS data quality indicators are described. These indicators can be computed at different steps of data preprocessing in order to assess the quality of individual datasets. The MATLAB scripts to compute some of these parameters and to produce the data quality assessment figures for visual inspection are also provided. Three examples of real resting-state data with diverse quality levels (High = A, Mid = B, Low = C) are presented.

- As a first step in data quality assessment routine, channel time series (e.g., intensity, optical density, concentration) can be inspected to detect motion-induced artifacts and signal drifts.
- As a second indicator, the presence of physiological components, such as respiration (0.6 Hz) and cardiac pulsation (2 Hz), in the power spectral density of HbO and HbR prior to temporal filtering can be assessed.
- A negative correlation between HbO and HbR signals (i.e., an antiphase state) (Cui et al., 2010; Watanabe et al., 2017) is also considered as a valid indicator of good data quality. Finally, the statistical association between time series fluctuations of Hb chromophores (HbO and HbR) is expected to be characterized by a strong negative correlation (Malonek and Grinvald, 1996; Villringer and Chance, 1997; Obrig and Villringer, 2003; Montero-Hernandez et al., 2018) and an antiphase state (Taga et al., 2000; Taga et al., 2017; Watanabe et al., 2017). These properties, which describe the intrinsic relationship between HbO and HbR hemodynamic fluctuations, have been confirmed in previous task-based (Wolf et al., 2002; Boas et al., 2003) and resting-state fNIRS studies in infants and adults (Taga et al., 2000; Zimeo-Morais et al., 2017; Watanabe et al., 2017), and even algorithms that maximize the negative correlation between Hb chromophores have been proposed as signal improvement, noise reduction, methods (Cui et al., 2010).

A.1. Time-Series Visualization

In MATLAB Box A.1 the script to generate the figures of the raw intensity time series and the time series after conversion to optical density is described. These figures provide a general overview of dataset quality, primarily regarding the presence of motion artifacts, baseline shifts and corrupted/saturated channels (Figure A.1). Note that these scripts generate figures for a single participant. Also note that scale in these plots might vary for different populations or fNIRS systems and should be adjusted accordingly by the user.

MATLAB Box A.1

Script to visualize time series (e.g., intensity and OD) of an individual participant. Two methods for data visualization are described 1) 2D line plots and 2) greypLOTS.

```
% The following variables should be defined in advance:
% Intensity and OD data for each wavelength in the format (time x channels)
% data_raw_wl1 and data_raw_wl2; data_OD_wl1 and data_OD_wl2
% N = number of samples/length of the dataset (5500 in this example)
% sf = sampling frequency (8.93Hz in this example)

% Create time vector (to display seconds instead of samples)
t = (0:N-1)/sf;

% ----- Visualization method 1 - 2D line plots
% Plot raw intensity time series
subplot(3,2,1)
plot(t, data_raw_wl1)
% Add titles, axes limits and axes labels
set(gca, 'YScale', 'log')
xlim([0 t(end)]); xlabel('Time (seconds)')
ylim([0 2.5]); ylabel('Intensity (log)');
title ('wl1 - 760 nm');

% Same steps for wavelength 2
subplot(3,2,2)
plot(t, data_raw_wl2)
set(gca, 'YScale', 'log')
xlim([0 t(end)]); xlabel('Time (seconds)')
ylim([0 2.5]); ylabel('Intensity (log)');
title ('wl2 - 850 nm');

% Plot OD time series
subplot(3,2,3)
plot(t, data_OD_wl1)
xlim([0 t(end)]); xlabel('Time (seconds)')
ylim([-1.5 2]); ylabel('OD (A.U.)');

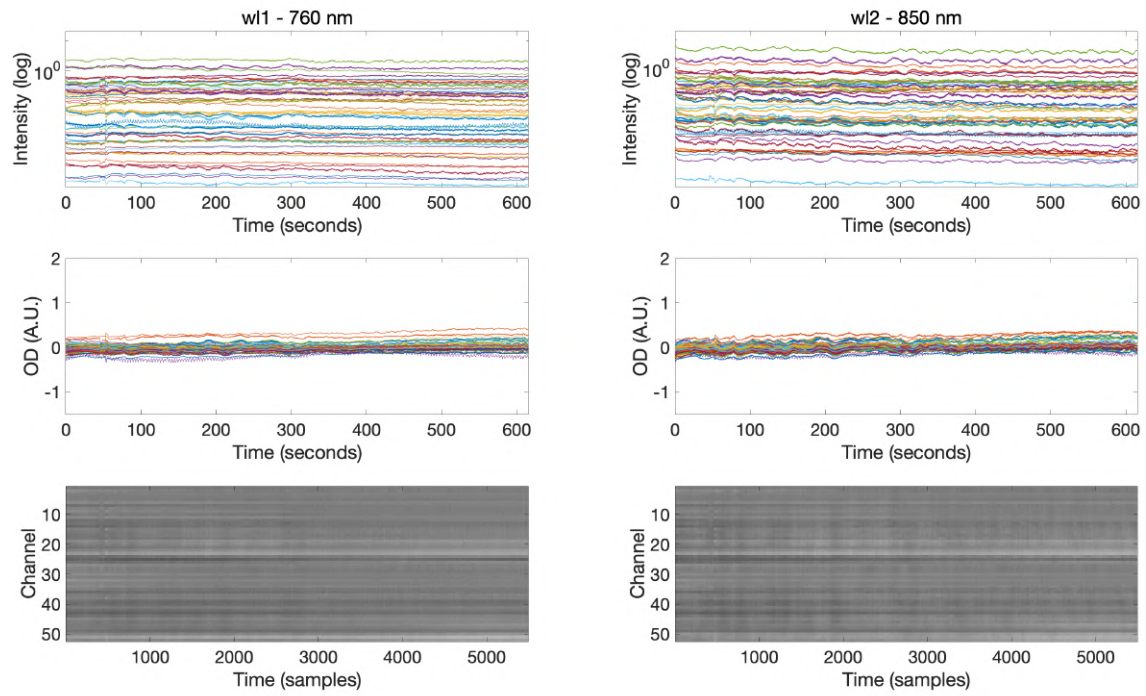
% Same steps for wavelength 2
subplot(3,2,4)
plot(t, data_OD_wl2)
xlim([0 t(end)]); xlabel('Time (seconds)')
ylim([-1.5 2]); ylabel('OD (A.U.)');

% ----- Visualization method 2 - GreypLOTS
subplot(3,2,5)
imagesc(data_OD_wl1', [-1 1])
xlabel('Time (samples)'); ylabel('Channel')

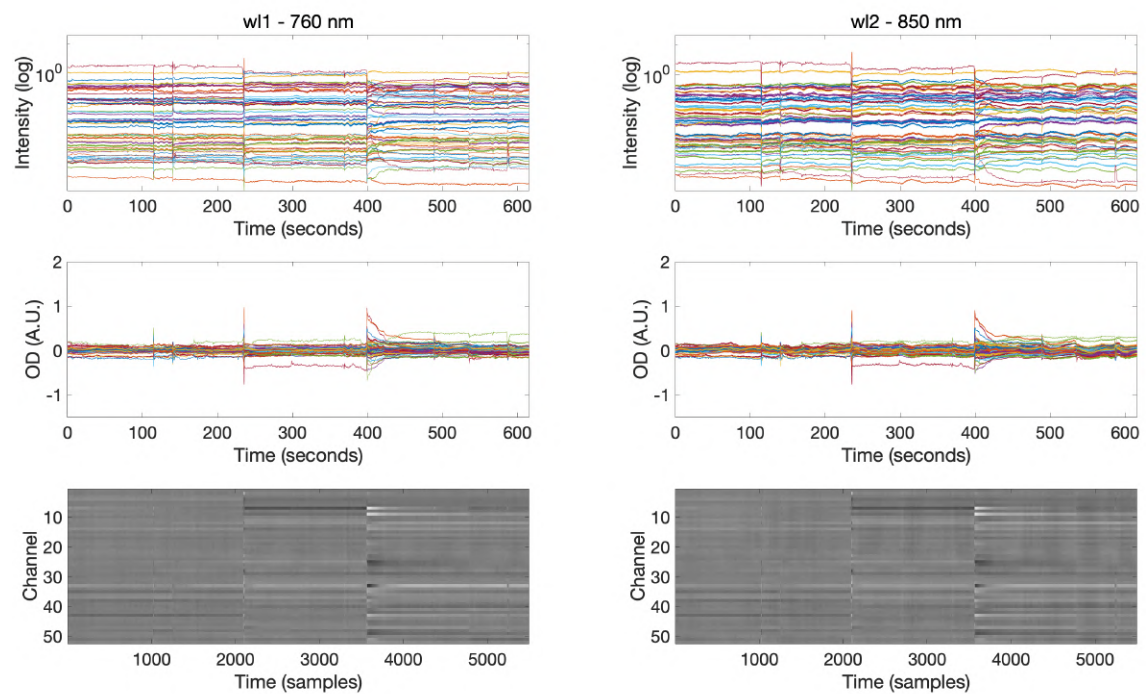
subplot(3,2,6)
imagesc(data_OD_wl2', [-1 1])
xlabel('Time (samples)'); ylabel('Channel')
colormap gray
```

fNIRS Data Quality Assessment

Example A



Example B



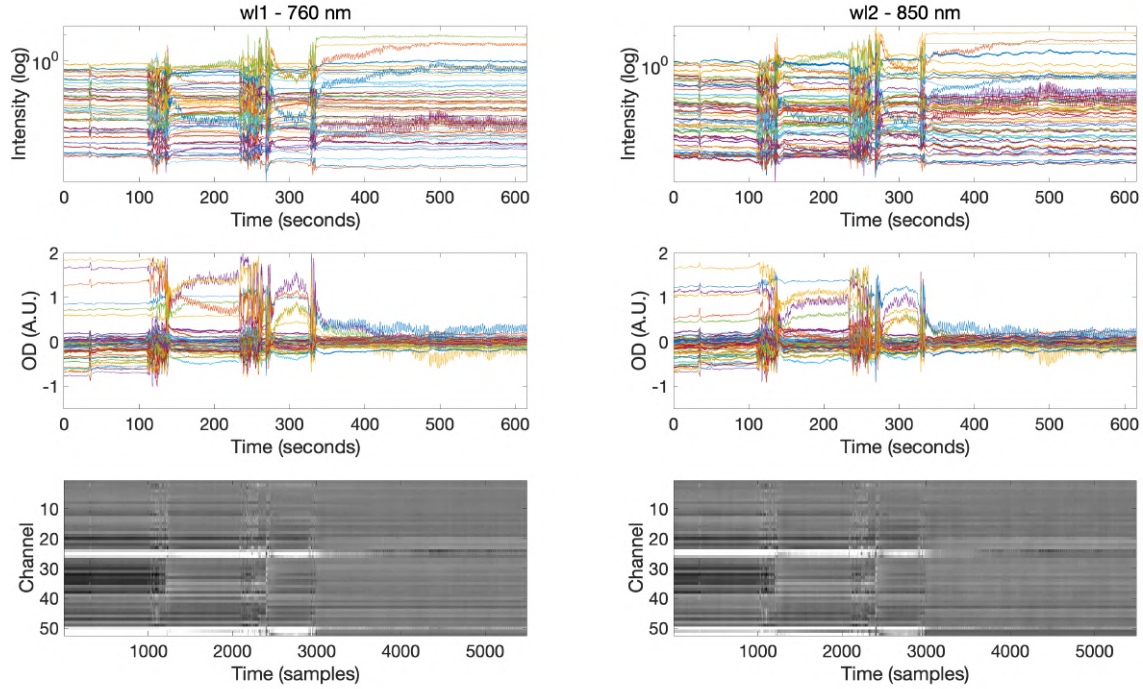
Example C

Figure A.1 The first row in this figure shows the signal intensity time courses for the recorded channels in each wavelength (i.e., 760nm and 850nm) in a logarithmic scale. The second row displays the OD time courses for all channels in each wavelength. The third row in this figure shows an image plot of the time courses of OD data (also referred to as greyplots). Each row in this figure (y axis) displays a single channel, columns (x axis) correspond to time points and signal intensity values are represented as different color intensity levels in a gray scale. In these plots it can be observed that signals in Example A are smooth, with no abrupt intensity changes. In contrast, in Examples B and C intensity changes associated with motion artifacts are noticeable in several time points. In Example B brief motion related signal intensity changes are observed at time points around 200 and 400 seconds (i.e., 2000 and 3500 samples). In Example C several periods affected by motion artifacts as well as baseline shifts are apparent.

A.2. Power Spectral Density Assessment

The presence of physiological components (e.g., respiration, cardiac pulse) in the power spectral density (PSD) of HbO and HbR time series is considered one of the main indicators of good optode-scalp coupling. In MATLAB Box A.2 the script to compute and plot the information provided by this metric is described. In infants the main physiological components are usually observed at ~0.6 Hz (respiration) and ~2 Hz (cardiac pulse) and its corresponding harmonics (see Figure A.2).

MATLAB Box A.2

Script to plot power spectral density of HbO and HbR. Three visualization methods are presented

```
% The following variables should be defined in advance:
% data_HbO and data_HbR (calculated from OD data using hmrOD2Conc)
% N = number of samples/length of the dataset
% sf = sampling frequency (8.93Hz in this example)
% Calculate frequency range
freq = linspace(0, sf/2, N/2+1);

% Compute Fourier Transform of HbO and HbR
fft_HbO = fft(data_HbO); % Fourier Transform HbO data
fft_HbO = 2*abs(fft_HbO(1:N/2+1, :)); % Keep only first half
fft_HbR = fft(data_HbR); % Fourier Transform HbR data
fft_HbR = 2*abs(fft_HbR(1:N/2+1, :)); % Keep only first half

% 1 - Plot mean HbO PSD across channels
subplot(2,3,1)
plot(freq, mean(fft_HbO,2), 'r', 'linewidth', 1); box off
xlim([0 sf/2]); xlabel('Frequency (Hertz)');
ylim([0 800]); title ('Mean PSD HbO')

% 2 - Plot mean HbO PSD across channels (log scale)
subplot(2,3,2)
plot(freq, mean(fft_HbO,2), 'r', 'linewidth', 1); box off
set(gca, 'XScale', 'log'); set(gca, 'YScale', 'log')
xlim([0 sf/2]); xlabel('Frequency (Hertz)')
title ('Mean PSD HbO (log scale)')

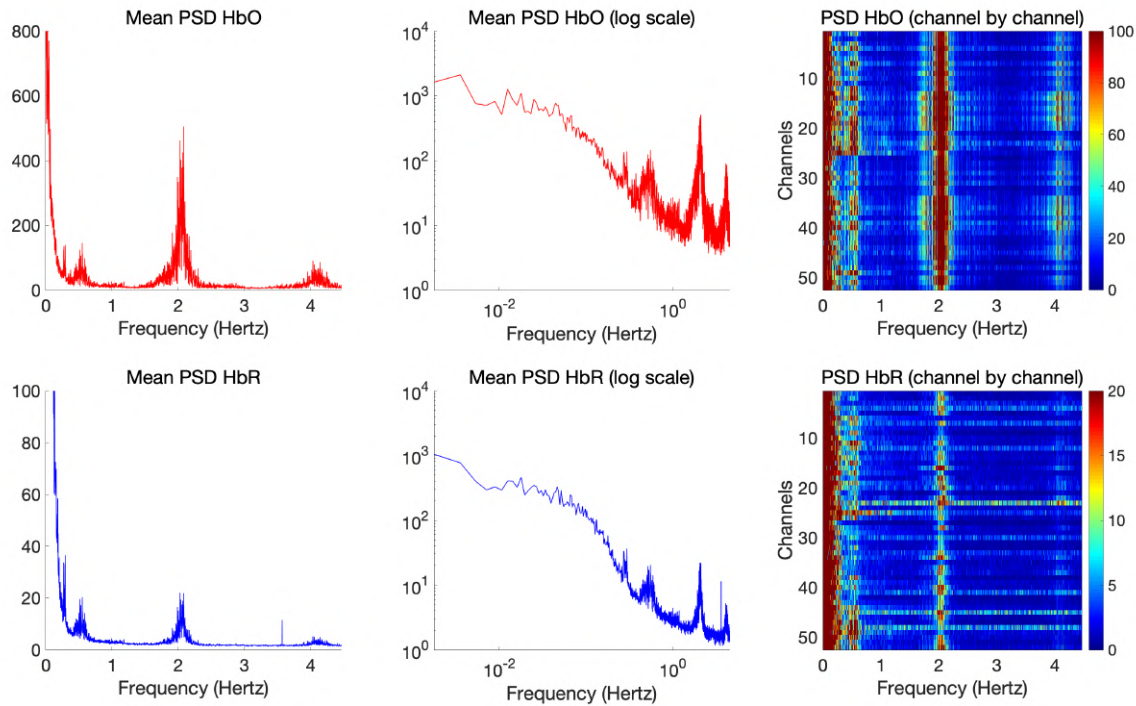
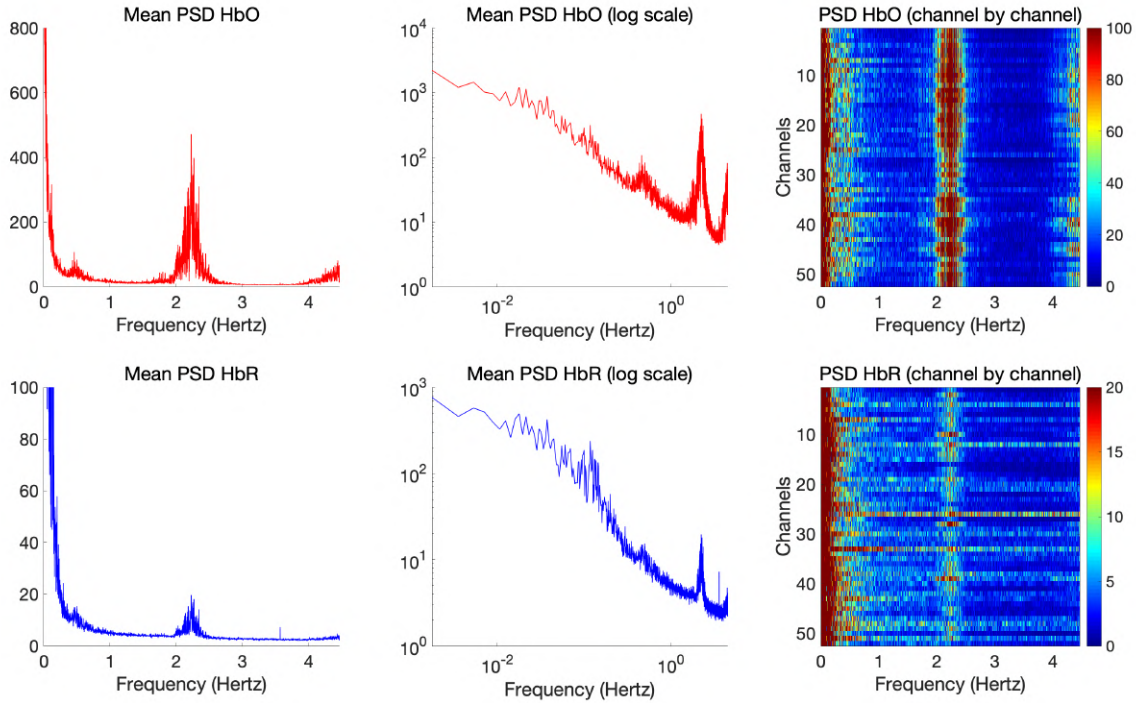
% Create XTickLabels for channel by channel plots
freq_list = [0 ,1 ,2, 3, 4];
idx = zeros(1, length(freq_list));
for i = 1:length(freq_list)
    dist = abs(freq - freq_list(i));
    minDist = min(dist);
    idx (i) = find(dist == minDist);
end
freq_labels = {'0', '1', '2', '3', '4'};

% 3 - Plot HbO PSD channel by channel
subplot(2,3,3)
imagesc(fft_HbO, [0 100])
set(gca, 'XTick', idx, 'XTickLabel', freq_labels)
xlabel('Frequency (Hertz)'); ylabel('Channels')
title ('PSD HbO (channel by channel)')
colormap jet; colorbar

% 1 - Plot mean HbR PSD across channels
subplot(2,3,4)
plot(freq, mean(fft_HbR,2), 'b', 'linewidth', 1); box off
xlim([0 sf/2]); xlabel('Frequency (Hertz)');
ylim([0 100]); title ('Mean PSD HbR')

% 2 - Plot mean HbR PSD across channels (log scale)
subplot(2,3,5)
plot(freq, mean(fft_HbR,2), 'b', 'linewidth', 1); box off
set(gca, 'XScale', 'log'); set(gca, 'YScale', 'log')
xlim([0 sf/2]); xlabel('Frequency (Hertz)')
title ('Mean PSD HbR (log scale)')

% 3 - Plot HbR PSD channel by channel
subplot(2,3,6)
imagesc(fft_HbR, [0 20])
xlabel('Frequency (Hertz)'); ylabel('Channels')
set(gca, 'XTick', idx, 'XTickLabel', freq_labels)
title ('PSD HbR (channel by channel)')
colormap jet; colorbar
```

Example A**Example B**

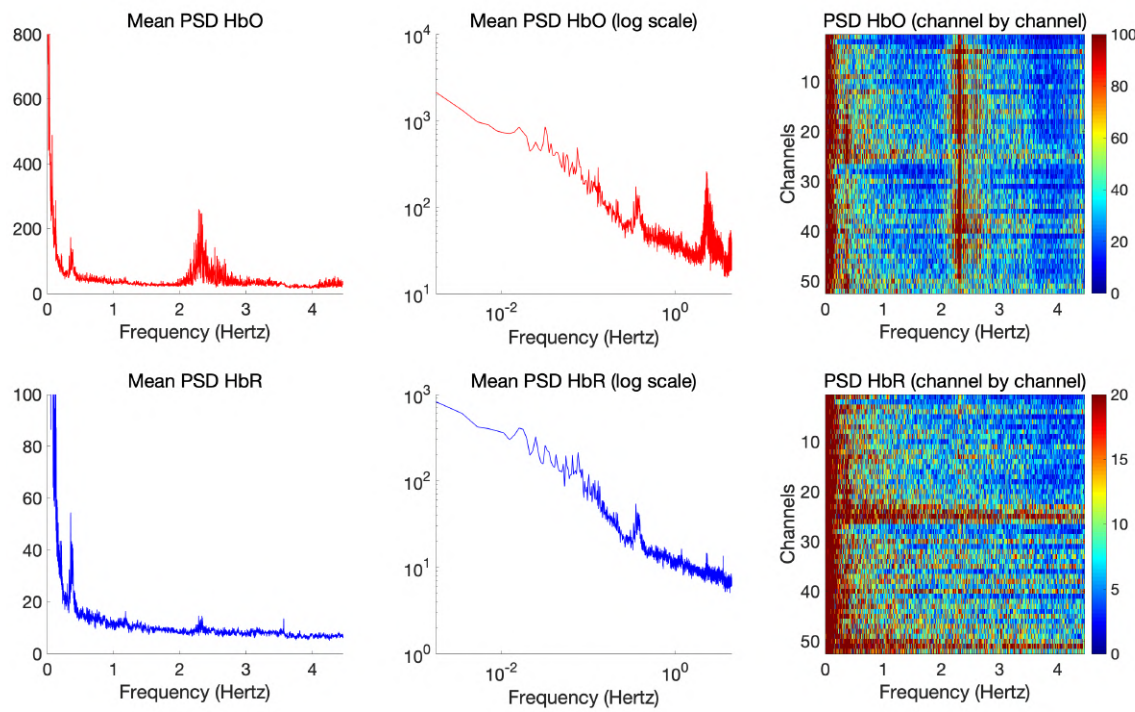
Example C

Figure A.2 Three different methods to visualize PSD of HbO (top row) and HbR signals (bottom row) are presented. First column depicts the average PSD across channels for each chromophore, showing clear peaks at ~ 0.6 Hz and ~ 2 Hz and its harmonics. Second column shows the average PSD across channels on a logarithmic scale, demonstrating a similar outcome. The third column in this figure shows an image of the PSD at the channel level for HbO and HbR signals. In the three examples presented, physiological components display larger power in the HbO signal (note differences in scale), but they are also present visible in the HbR signal. As expected for resting-state data power is maximal at low frequencies where spontaneous hemodynamic fluctuations reside. By looking at the channel by channel plots it is also evident that PSD in Examples A and B looks cleaner than in Example C, which exhibits the lowest data quality.

A.3. HbO – HbR Statistical Relationship

A negative correlation is expected between HbO and HbR time series, which can be evaluated by calculating the adjacency matrix based on the pairwise Pearson's correlation coefficients between HbO and HbR signals. Similarly, a phase difference close to an antiphase state (180°) should be evident between HbO and HbR chromophores (Watanabe et al., 2017). MATLAB Box A.3 provides the script to compute and visualize these indicators in an individual dataset (Figure A.3). The same plots for bandpass filtered HbO and HbR data are presented for the sake of comparison and to facilitate interpretation of phase difference plots, which are otherwise heavily influenced by high frequency physiological components.

MATLAB Box A.3

Script to plot HbO and HbR adjacency matrices (HbO, HbR, HbO-HbR) and 2) channelwise phase difference between HbO and HbR

```
% The following variables should be defined in advance:
% data_HbO and data_HbR (raw HbO and HbR concentration data)
% ch = number of channels of the dataset (52 in this example)

% Compute and plot adjacency matrices
subplot(1,4,1)
imagesc(corr(data_HbO), [-1 1]); colorbar
xlabel('Channels'); ylabel({'Raw data'; 'Channels'})
title('HbO'); axis square

subplot(1,4,2)
imagesc(corr(data_HbR), [-1 1]); colorbar
xlabel('Channels');
title('HbR'); axis square

subplot(1,4,3)
imagesc(corr(data_HbO, data_HbR), [-1 1]); colorbar
xlabel('Channels');
title('HbO-HbR'); axis square

% Compute hPod value (HbO-HbR phase difference as described in Watanabe et al., 2017)
hPod = zeros(1, ch);
for nch = 1:ch

    % Calculate the Hilbert transformation of the signals
    HbO_hilbert = hilbert(data_HbO(:, nch));
    HbR_hilbert = hilbert(data_HbR(:, nch));

    % Calculate instantaneous phase
    HbO_inst = unwrap(angle(HbO_hilbert));
    HbR_inst = unwrap(angle(HbR_hilbert));

    % Calculate phase difference
    ph_dif = HbO_inst - HbR_inst;

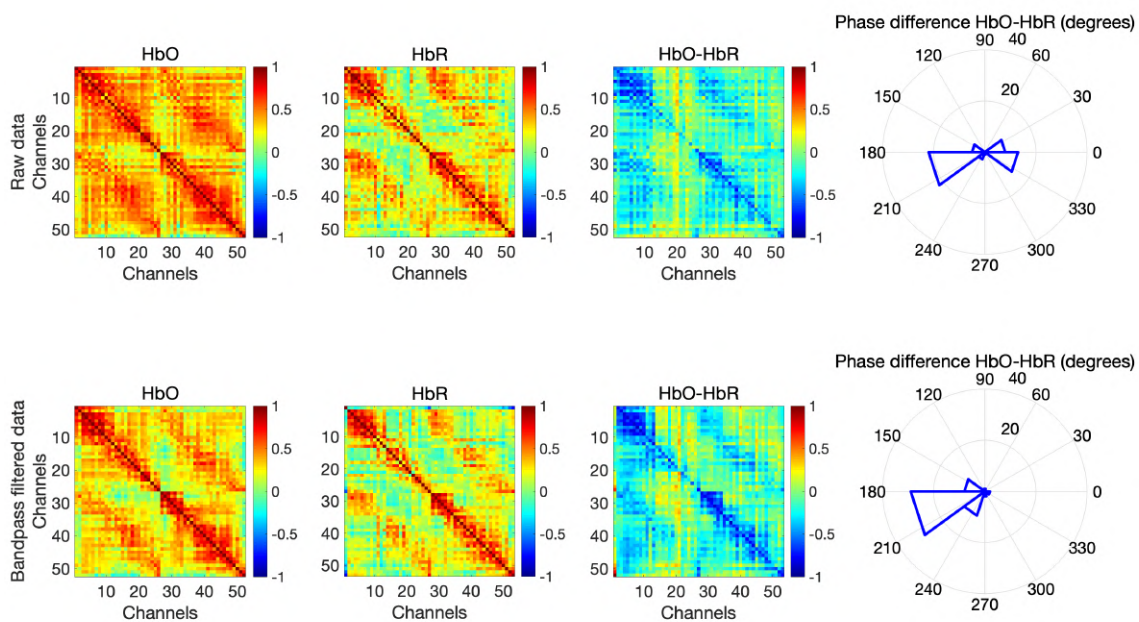
    % Compute and store hPod
    hPod (nch) = angle(mean(exp(sqrt(-1)*ph_dif)));

end

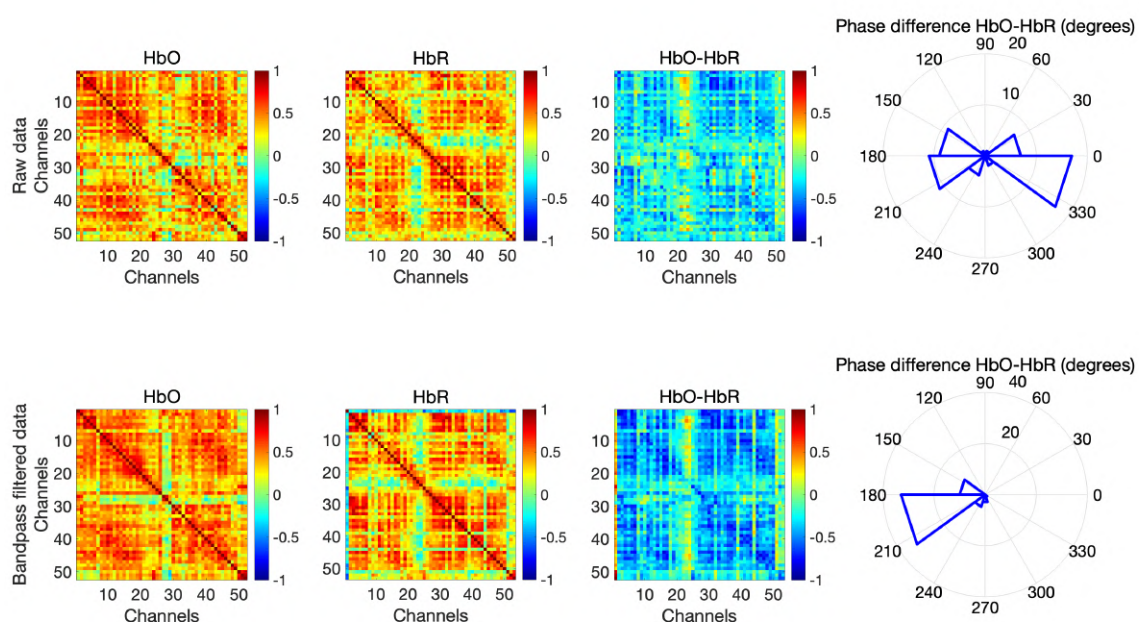
subplot(1,4,4)
h = rose (hPod, 10);
set(h, 'linewidth', 4, 'color', 'b')
title('Phase difference HbO-HbR (degrees)')
```

fNIRS Data Quality Assessment

Participant A



Participant B



Participant C

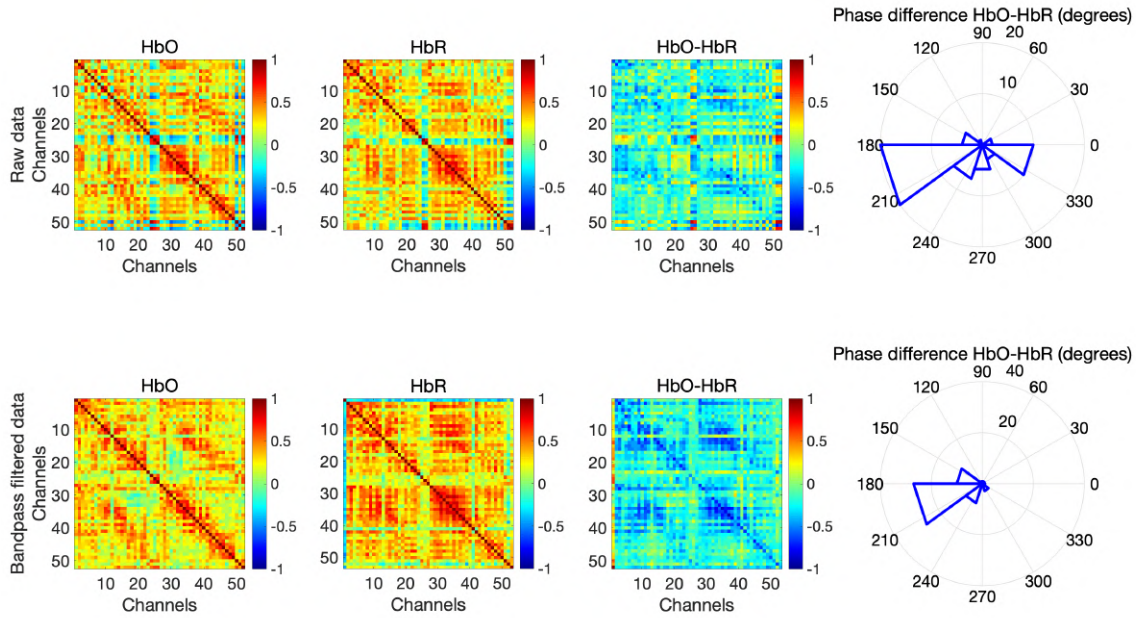


Figure A.3 Each row in this figure displays the adjacency matrices and the phase difference for raw and bandpass filtered concentration data respectively. The first column shows the HbO adjacency matrices of this dataset, which are mostly positive. The second column shows the HbR adjacency matrices, which exhibit a similar pattern. In these matrices the highest correlation values are observed between adjacent channels (i.e., main diagonal) and between homotopic channels. As channels are ordered from left to right (i.e., channels 1-26 are localized in the left hemisphere and channels 27-52 belong to the right hemisphere) homotopic connectivity can be inferred in a second diagonal in the middle of the upper (or lower) triangular part of these matrices. Note that adjacency matrices are symmetric with respect to the main diagonal. The third column in this figure represents the HbO-HbR adjacency matrices, which is the main parameter of interest for data quality assessment due to the expected statistical association (i.e., strong negative correlation) between HbO and HbR time series. The expected negative correlation is apparent in these matrices, and also a high similarity with the patterns observed in HbO and HbR adjacency matrices. The fourth column shows the angle histogram plots of the phase difference between HbO and HbR time series. In raw data most channels show a close to antiphase state, a pattern that is more prominent after bandpass filtering, probably due to the exclusion of high frequency components. The overall stronger correlation between HbO channels, which is probably induced by the larger presence of physiological components in the HbO signal, is another interesting feature that can be observed in these plots.

Appendix B

Supplementary Materials Chapter 3

This Appendix contains the Supplementary Materials of the study presented in Chapter 3. In particular, the procedure for model order selection in the independent component analysis (ICA) based resting-state functional connectivity (RSFC) approaches employed in this study is described. This data-driven procedure could serve as reference for future ICA based studies using fNIRS, or at least be informative for data quality evaluation. The second section of this Appendix includes the supplementary results of the study. Figures of group-level data quality evaluation are presented, in which two previous fNIRS studies assessing RSFC in infants are replicated in each of the investigated experimental groups. Finally, the complete set of components extracted from the ICA based approaches to investigate RSFC are displayed, including some components that have not been presented in the main text. Inclusion/exclusion criteria of the components was based on their spatial configuration and interpretability, as is standard in this type of studies.

B.1. ICA Model Order Selection

Independent component analysis (ICA) is a data analysis method routinely applied in resting-state functional connectivity (RSFC) studies to decompose the data into statistically independent components (ICs) associated with the measured spontaneous brain activity. The conceptual idea behind ICA is that the recorded signal (e.g., BOLD in functional magnetic resonance imaging - fMRI, or HbO and HbR in functional near-infrared spectroscopy - fNIRS) consists of a linear mixture of functionally relevant signals and noise, which could be explained by several statistically ICs stemming from various sources. In RSFC analyses, this approach should ideally allow separating ICs associated with spontaneous resting-state activity (i.e., functional networks) from those related to noise.

Based on the characteristics of the data and the experimental question of interest, ICA can decompose the data into a number of maximally ICs in different dimensions, such as space or time. However, as mentioned before, not all the estimated ICs are reliable, robust or neurophysiologically meaningful. A number of the extracted ICs might be associated with noise, or they might explain a very small portion of data variance. Currently there is no method to objectively and *a priori* determine the number of meaningful components (i.e., those describing functional networks) that should be expected in the observed signal (e.g., BOLD in fMRI or HbO and HbR in fNIRS). Thus, a recurrent issue in studies using ICA to investigate RSFC is how to determine the number of ICs to be estimated, or alternatively, the number of true underlying sources in the data.

The question of how to calculate the optimal number of ICs to be estimated has been mainly explored in the context of resting-state fMRI studies. One of the most widely adopted approaches to decide the number of ICs to be estimated is to perform a principal component analysis (PCA) prior to ICA (Majeed and Avison, 2014). This step will reduce the dimensionality of the data by removing noise-related components, which are usually identified as those accounting for the smallest percentage of data variance. Next, the number of components to be estimated by the ICA algorithm is matched with the number of components that are retained after applying PCA. This approach has the disadvantage that an arbitrary threshold selection is still needed (i.e., number of PCA components or percentage of explained variance to retain), an issue that is intended to be overcome with the method proposed below. Some works adopted a more subjective approach, considering a number of ICs based on their spatial interpretability given the inferred dimensionality of the data (e.g., Van de Ven et al., 2004; Smith et al., 2012). Other studies tried to determine the true dimensionality of the data by means of model order selection procedures (e.g., Calhoun et al., 2001; Damoiseaux et al., 2006; Filippini et al., 2009), such as the Laplace approximation based on Bayesian model selection proposed by Minka et al., (2000). However, none of these solutions for optimal model order estimation have been established as standard for ICA based studies. Yet, an accurate model order selection is relevant, as it can significantly impact the characteristics of the inferred ICs (Abou Elsoud et al., 2010), as demonstrated by studies investigating the effect of model order selection (e.g., low model order vs. high model order) on the characteristics of the extracted functional connectivity patterns (e.g., Abou Elseoud et al., 2010; Abou Elseoud et al., 2011;

Damaraju et al., 2014). These studies demonstrated that large-scale functional connectivity patterns are more precisely described using low model orders, and fine-grained components are usually distinguishable at higher model orders only. If dimensionality (i.e., model order) gets too small there is risk of merging several ICs and lose spatial specificity, whereas very large model orders result in spatially sparse components, and might require sub-dividing/splitting functionally related ICs.

Few studies have used ICA to assess functional connectivity in resting-state fNIRS data. These studies proposed explaining a percentage of data variance (e.g., 99%; Zhang H. et al., 2010; Zhang H. et al., 2011) or extracting a range of ICs for each participant (e.g., 10-20 ICs; White et al., 2012; Ferradal et al., 2015), but the rationale underlying these choices was not discussed. As stated above, one can arbitrarily (or based on previous works) select a number of PCA components (or percentage of explained variance) to be retained, and then use the same number of components for model order selection in the ICA. The option proposed in this Appendix, and which has been implemented in the study presented in Chapter 3, is to evaluate certain properties of the ICA decomposition across several PCA thresholds, and then select the optimal model order based on the outcome of the studied properties. A data-driven approach is proposed to determine the optimal number of ICs to be estimated by the ICA algorithm in RSFC studies using fNIRS data. This approach for ICA model order selection is based in two metrics that exploit specific defining properties of ICA estimation and fNIRS data:

- 1) The robustness of the estimated ICs across multiple realizations of the ICA algorithm.
- 2) The assumed statistical relationship between the HbO and HbR derived ICs.

Methods

All data preprocessing and analyses were implemented in MATLAB (R2012b, R2014b, MathWorks, Massachusetts) using in-house scripts as well as third-party toolboxes and functions (see MATLAB Box B.1).

MATLAB Toolboxes employed in this analysis:

- *ICASSO* Toolbox (Himberg et al., 2004; <https://research.ics.aalto.fi/ica/icasso/>).
- Automatic Choice of Dimensionality for PCA (Minka, 2000; <https://tminka.github.io/papers/pca/>).

The datasets employed in this Appendix are the ones presented in Chapter 3 - Resting-state Functional Connectivity in Infants using fNIRS. As a reminder, in this study two ICA based methods were implemented, which have been described in detail in Chapter 3. In the first method, the time-series of the participants are used to obtain temporally independent group-level components (temporal group ICA - tGICA, Beckman et al., 2009). In the second method, individual functional connectomes are employed to obtain group-level independent functional connectivity patterns (connICA - Amico et al., 2017).

These two methods rely on the *FastICA* algorithm for independent component extraction. In this algorithm, the first set of weights used to estimate the independent components (ICs) is randomly generated, and then updated by a learning rule (e.g., non-

gaussianity) across multiple iterations until convergence. This causes that, for a given particular input, the *FastICA* decomposition into components might vary depending on the initialization, making the algorithm intrinsically non-deterministic. A reliable interpretation of the results requires selecting only those ICs that are considered robust; being robustness defined by the identifiability/repeatability of each specific component across multiple realizations of the *FastICA* algorithm with different random initializations. Here, the robustness of the estimated ICs is evaluated across multiple PCA thresholds by using the *ICASSO* stabilization method (Himberg et al., 2004).

One of the goals of the data-driven exploratory method presented in this Appendix is to investigate the stability of the estimated components by running the *ICASSO* algorithm across a range of PCA thresholds. Then, *ICASSO* reliability estimates are employed to select the PCA threshold in which the number of robust components is larger, or alternatively, to analyze only those components that are deemed robust. For the two ICA functional connectivity methods employed in the current work (i.e., tGICA and connICA), *ICASSO* cluster quality/robustness index (I_q) values were obtained for each component, and at each PCA threshold. By clustering together the set of all estimated ICs based on a similarity metric (e.g., absolute value of mutual correlation coefficients), this index quantifies the robustness of the estimated components across several realizations of the ICA algorithm. Specifically, the calculation of this index takes into consideration the compactness of the cluster (i.e., similarity between ICs belonging to the cluster) and the isolation of the cluster (i.e., similarity between components that belong to the cluster and those belonging to other clusters). The ideal outcome is one in which clusters are compact (i.e., high intracluster similarity) and isolated (i.e., low intercluster similarity). Values for the I_q index range between 0 (low robustness) and 1 (high robustness). In this work, 100 realizations of the ICA algorithm (*FastICA*, Hyvärinen, 1999) were computed for each PCA threshold under assessment (i.e., 60, 65, 70, 75, 80, 85, 90, 95 and 99), representing the percentage of explained data variance to be retained.

The expected statistical association between HbO and HbR chromophores can be used as a second metric to evaluate the reliability of the ICs extracted from the ICA algorithm. As explained in Chapter 2 (see also Appendix A), the relationship between time series fluctuations of Hb chromophores is expected to be characterized by a strong negative correlation. A high correlation/similarity between the extracted HbO and HbR components will imply that these components are consistent across Hb chromophores, and therefore that they follow the expected physiological properties of fNIRS data, making them more reliable. In each of the ICA methods employed in the current study (i.e., tGICA and connICA) the expected statistical relationship between HbO and HbR derived ICs differs slightly, and therefore should be clarified first to aid the reader's understanding. In the tGICA approach, the ICs are estimated from the HbO and HbR time series (Amico and Goni, 2018), which are expected to show a negative correlation between them (see individual examples in Appendix A). In this approach, the first output from the ICA algorithm are the group-level temporally-independent time series, which are common to HbO and HbR data. The second output of the ICA algorithm, the weights, specify the contribution of each IC time series on each channel. fNIRS data comprises HbO and HbR

channels, each of them with a different weight. Since a strong negative correlation between HbO and HbR time series is assumed, these weights, which spatially represent the functional networks of interest, should show a highly similar spatial configuration in both chromophores (i.e., HbO and HbR), but with opposite sign (e.g., positive in HbO and negative in HbR). The predicted statistical relationship between HbO and HbR spatial patterns can be investigated by computing the Pearson's correlation coefficient between the HbO and HbR spatial maps (i.e., channel weights), which is expected to be high and negative. In the connICA approach, in contrast, a strong positive correlation between the estimated HbO and HbR independent functional components is expected, as the input to the ICA algorithm in this approach are the HbO and HbR functional connectivity matrices, which should show alike topology across chromophores (see Appendix A). Thus, for each ICA approach, and as a second reliability metric, Pearson's correlation coefficient was computed between the HbO and HbR components extracted at each PCA threshold.

Results and Discussion

The results of the robustness analysis for the two ICA methods are presented in descending order (i.e., components with larger I_q first) in Figure B.1. Rows in this figure represent the percentage of explained PCA variance, and columns index each of the estimated independent components (ICs). Color scale in this figure represents the I_q value returned by the *ICASSO* algorithm. In the tGICA approach, higher I_q values (i.e., more robustness) were obtained at the lower PCA thresholds (60% and 65% explained variance). For higher thresholds, the first 15-20 ICs also showed high I_q values. These values start decaying as the number of ICs increased, and were particularly low at the higher thresholds (above 80% explained variance). A similar trend can be observed in the connICA approach. The highest I_q values were obtained at the lower PCA thresholds (60% - 70% explained variance), whereas the I_q values for higher PCA thresholds were only high up to the first 15 ICs and then progressively decreased.

Figure B.2 shows the results of the analysis of the second reliability metric, which evaluates the statistical relationship between HbO and HbR components. In the tGICA approach HbO and HbR spatial maps (i.e., channel weights) displayed a strong negative correlation at the lower PCA thresholds, up to 75% of explained variance. At higher thresholds, correlation between HbO and HbR components remained negative, but it decreased considerably, and the number of components not showing this pattern increased. The analysis for the connICA method yielded similar results as the tGICA approach. Note that in this case the statistical relationship between HbO and HbR components is expected to be positive. At lower PCA thresholds (60%, 65% explained variance) the correlation between HbO and HbR components was notably high ($r \geq 0.7$). At higher PCA thresholds, correlation between components remained positive, but with low correlation values, indicating that the similarity between HbO and HbR components was lower at these thresholds.

Based on these two metrics (i.e., robustness of the estimated ICs, and correlation between HbO and HbR components) an appropriate choice for PCA model order, and in turn for the subsequent ICA method, corresponds to a PCA threshold of 60% or 65%

explained variance in both ICA approaches (i.e., tGICA and connICA). These values provide the ICs with higher robustness values, and those that meet the criteria assuring a reliable HbO-HbR statistical relationship. Independent components estimated at higher PCA thresholds (i.e., higher ICA model orders) are either not robust, or the relationship between HbO and HbR is altered leading to unexpected patterns.

One might argue that this choice (e.g., 60% explained variance) represents a very low percentage of explained data and that a more conservative approach, explaining more variance (e.g., 90% or 99%), would be more advisable in order to avoid the risk of throwing away meaningful signal. However, it is also true that due to the reduced spatial resolution of fNIRS and the number of channels available, which consequently also limit the cortical regions under assessment (i.e., field of view). Thus, the expected number of signals of interest, those referring to potentially meaningful functional networks, cannot possibly be very high.

In order to reinforce the outcome of this method for model order selection, and as a third metric, the variance explained by each IC was computed by calculating the sum of squared differences between the data at each PCA threshold, and the data after reconstructing it by removing one particular component at a time. In this way, the percentage of explained variance by each component can be calculated, either with respect to the original data (without PCA) or for the data employed in the ICA analysis (after applying PCA). This analysis showed that, for the two analyses approaches (i.e., tGICA and connICA), the ICs at the selected 60% PCA threshold explained the largest amount of data variance, while also obtaining the highest values in the robustness and consistency metrics (Figure B.3). At higher PCA thresholds, explaining the same amount of variance (i.e., 60%) would require including components that are not robust, or which do not show the expected statistical association between HbO and HbR.

Based on this information, for the tGICA approach 15 principal components were selected corresponding to 60% explained variance (see Table B.1 for a summary of the three metrics at this threshold). For the connICA method 11 principal components were considered which corresponds to 60% explained variance (see Table B.2 for a summary of the three metrics at this threshold). As a reference, the Laplace approximation based on Bayesian model order selection (Minka, 2000) yielded an optimal model order of 27 components (i.e., 73.5% explained variance) for the tGICA approach, and an optimal model order of 17 components for the connICA method (i.e., 66.34% explained variance).

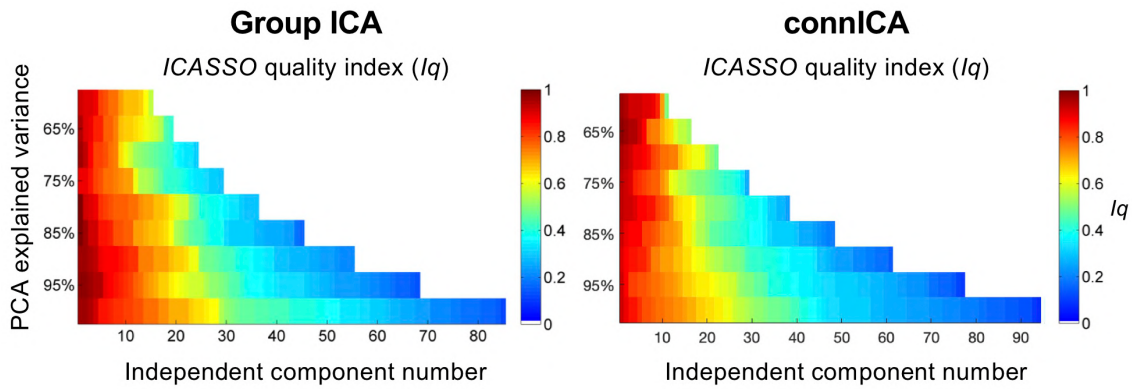


Figure B.1 Plot ranking the independent components obtained in the tGICA and connICA approaches based on the *ICASSO* cluster quality index (Iq) for a range of PCA thresholds.

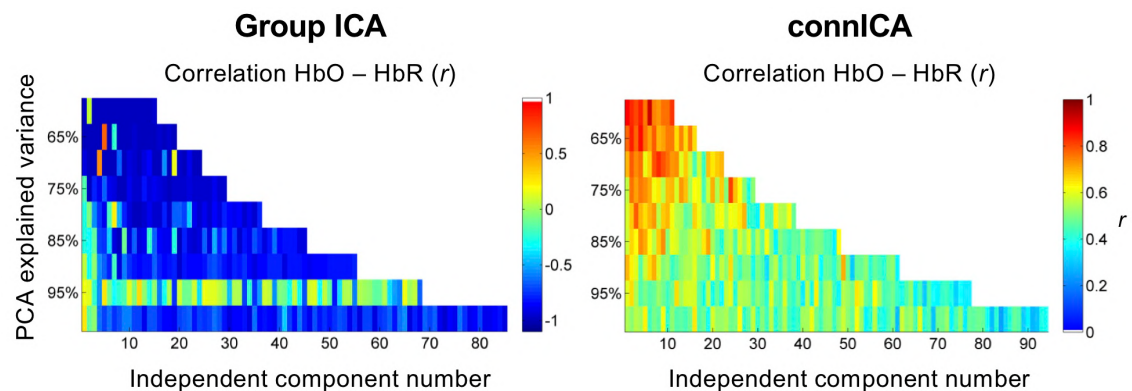


Figure B.2 Plot showing the correlation coefficient between HbO and HbR components. In the tGICA approach correlation is computed between the weights of HbO and HbR channels for each IC. In the connICA approach, correlation is computed between the first and the second half of the functional connectome component, which represent HbO and HbR respectively. ICs are ordered by Iq to maintain consistency across figures.

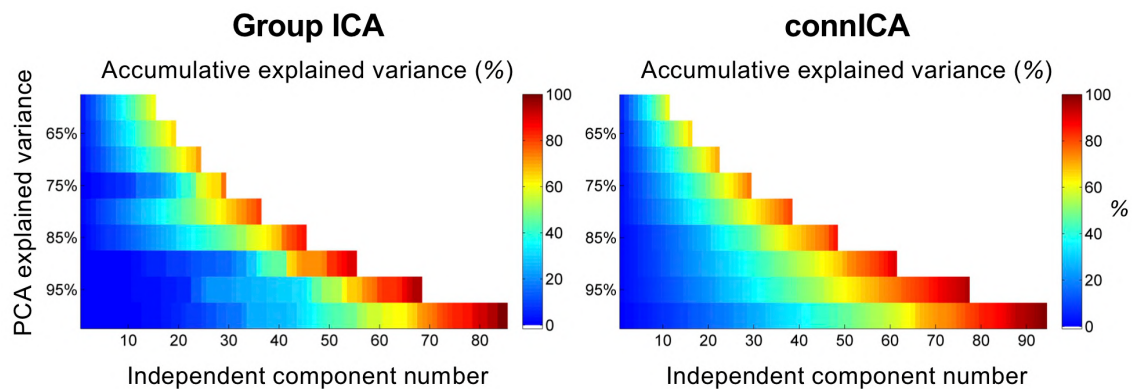


Figure B.3 Plot displaying the accumulative explained variance by the ICs obtained at each PCA threshold. It can be observed that as PCA threshold increases, a larger number of ICs are required to explain the same amount of variance (e.g., 11 ICs explain 60% of the variance for a PCA threshold of 60%, whereas around 65 components are necessary to explain 60% of the variance at a PCA threshold of 99%). ICs are ordered by Iq .

MATLAB Box B.1

Script for model order selection in group ICA based approaches considering various component quality metrics for a range of PCA thresholds (e.g., I_q , correlation HbO-HbR, explained variance)

```
% The following variable should be defined in advance:
% group_data = tGICA or connICA group data
% Compute accumulative explained variance across PCA components
[~, ~, latent, ~, ~] = pca(group_data);
exp_var = cumsum(latent)./sum(latent);

% Define PCA thresholds (percentage of explained variance)
PCA_th = [0.6 0.65 0.7 0.75 0.8 0.85 0.9 0.95 0.99];

% Compute number of components corresponding to different PCA thresholds
nComp = zeros(1, length(PCA_th));
for i = 1:length(PCA_th)
    nComp(i) = length(find(exp_var < PCA_th(i)))+1;
end

% Define number of ICASSO realizations (M) and initialize variables to store info
M = 100;
ICAinfo.Iq = zeros (length(nComp), max(nComp));
ICAinfo.ssd_PCA = zeros (length(nComp), max(nComp));
ICAinfo.ssd_orig = zeros (length(nComp), max(nComp));
ICAinfo.HbOHbR = zeros (length(nComp), max(nComp));

% For each PCA threshold
for i = 1: length(nComp)

    % Run PCA
    [coeffs, score, latent] = pca(group_data, 'NumComponents', nComp(i));
    PCA_matrix = score * coeffs';
    PCA_matrix = bsxfun(@plus, PCA_matrix, mean(group_data,2));
    group_ICA = PCA_matrix;

    % Run ICASSO (optional parameters are user selectable)
    sR = icassoEst('randinit', group_ICA', M,'numOfIC', nComp(i));
    sR = icassoExp(sR);
    icassoShow(sR, 'L', nComp(i), 'estimate', 'demixing');
    [iq, icaSM, w, icaTC] = icassoShow(sR,'L', nComp(i),'colorlimit', [.6 .7 .8 .9]);

    % Order components (icaSM and icaTC) by iq and store info
    [iq_order, idx_order] = sort(iq, 'descend');
    icaSM = icaSM(:, idx_order);
    icaTC = icaTC(idx_order, :);
    ICAinfo.Iq(i, 1:nComp(i)) = iq_order;

    % Compute and store explained variance by each IC (sum of squared differences)
    for j = 1: nComp(i)

        ica_temp = icaTC;
        ica_temp(j,:) = 0;
        data_rec = icaSM*ica_temp;

        diff_pca = group_ICA' - data_rec;
        diff_orig = group_data' - data_rec;

        PCA_temp(i,j) = sum(diff_pca(:).^2);
        orig_temp(i,j) = sum(diff_orig(:).^2);

    end

    ICAinfo.ssd_PCA(i, :) = PCA_temp(i,:)./sum(PCA_temp(i,:))*100;
    ICAinfo.ssd_orig(i,:) = orig_temp(i,:)./sum(orig_temp(i,:))*100*PCA_th(i)

    % Get ICA_HbO and ICA_HbR data to assess correlation between components
    % Separate HbO and HbR components (differs between tGICA and connICA)
    % In tGICA separate HbO and HbR spatial maps (number of channels/2)
    % In connICA separate the functional connectome components (number of edges/2)
    temp_cor = corr([ICA_HbO, ICA_HbR]);
    temp_mat = zeros(1, nComp(i));

    % Calculate correlation between HbO and HbR components and store
    for d = 1:nComp(i) % number of components extracted at each PCA threshold
        temp_mat(1,d) = temp_cor(d, nComp(i)+d);
    end

    ICAinfo.HbOHbR(i, 1:nComp(i)) = temp_mat;

end

% Produce images with the information for different PCA thresholds stored in ICAinfo
% For example: imagesc (ICAinfo.Iq, [0 1])
```

B.2. Supplementary Results

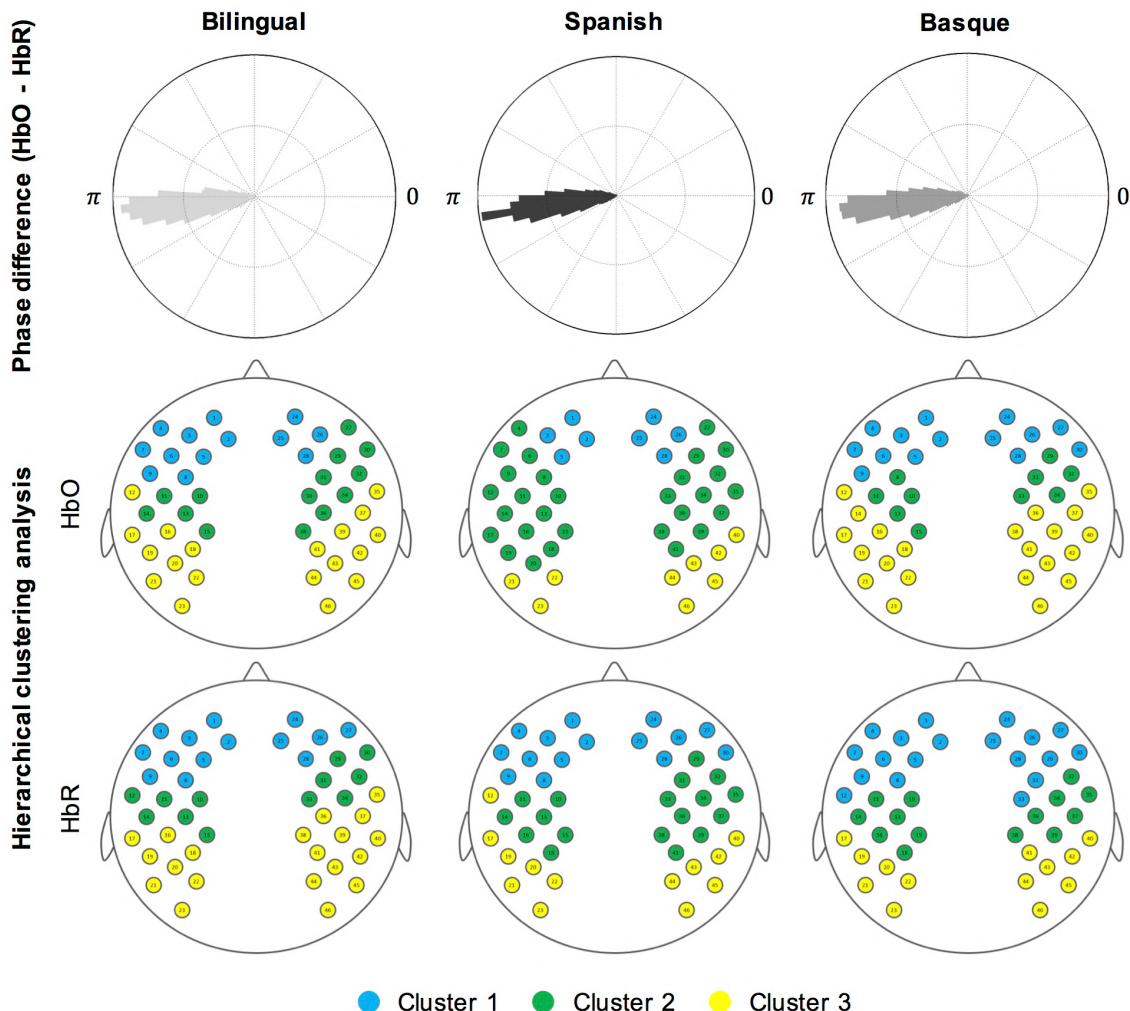


Figure B.4 Group-level data quality assurance figures replicating two previous infant studies assessing resting-state functional connectivity using fNIRS. First row shows the channelwise average phase difference (hPod value, Watanabe et al., 2017) between HbO and HbR in each experimental group. The three groups show a similar pattern characterized by an antiphase state between HbO and HbR, which replicates the outcome from the previous study. Second and third rows in this figure show the results of a hierarchical clustering approach (Homae et al., 2010) in which channels' time series are clustered based on similarity. A similar cluster configuration can be observed across groups in HbO and HbR. Cluster 1 is formed by channels located in the most anterior part of both hemispheres. Cluster 2 comprises channels located in middle brain regions, predominantly covering somatosensory regions. Channels located in the most posterior part of the setup are grouped together in cluster 3.

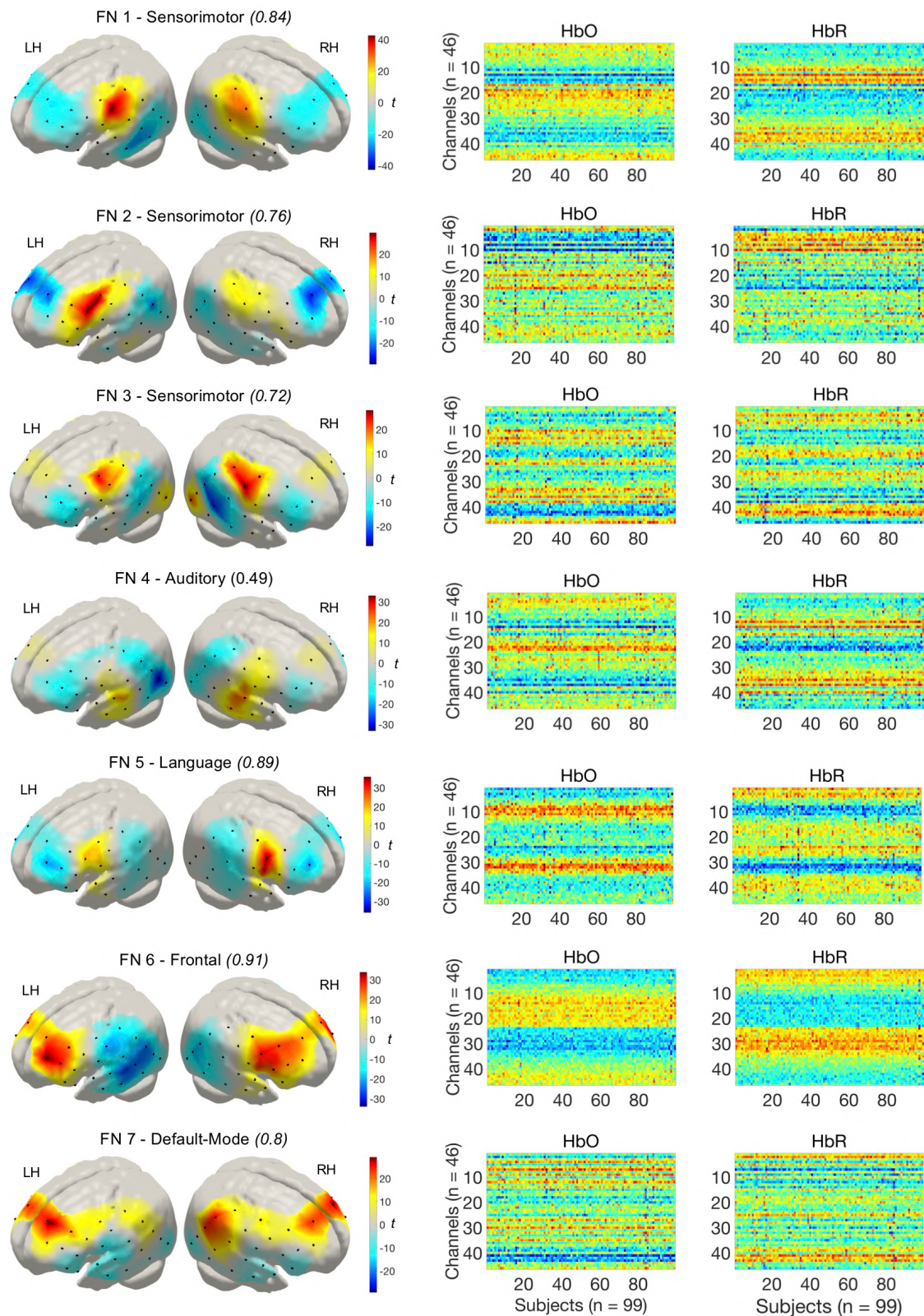


Figure continues in next page

Supplementary Materials Chapter 3

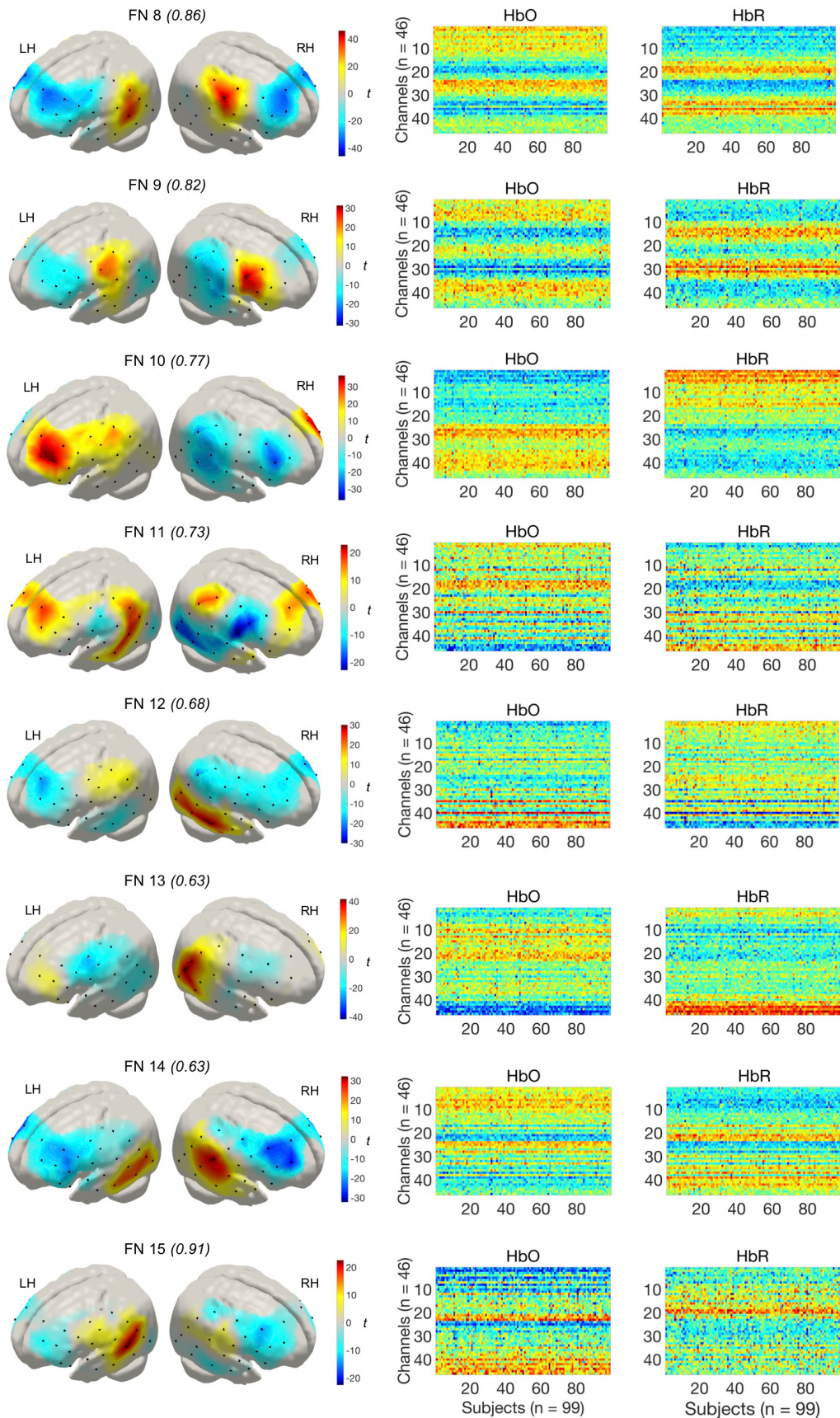


Figure B.5 Functional networks ($n = 15$) maps extracted with the tGICA approach. Each functional network map was reconstructed to the subject space using dual-regression. These subject-level maps for HbO and HbR are presented in the middle and rightmost columns. Due to the high similarity between HbO and HbR components, functional network maps are displayed for HbR only.

Functional Network (FN)	<i>Iq</i>	r (HbO-HbR)	ssd (100 %)	ssd (60 %)
FN 1 Sensorimotor	0.84	-0.99	8.8	4.1
FN 2 Sensorimotor	0.76	-0.98	4.3	3.9
FN 3 Sensorimotor	0.72	-0.99	5.5	3.9
FN 4 Auditory	0.49	-0.98	5.6	3.9
FN 5 Language	0.89	-0.99	7.4	4.0
FN 6 Frontal	0.91	-0.99	10.5	4.2
FN 7 Default-Mode	0.80	-0.97	6.2	4.0
FN 8	0.86	-0.99	8.9	4.1
FN 9	0.82	-0.99	7.2	4.0
FN 10	0.77	-0.98	7.3	4.0
FN 11	0.73	-0.98	4.5	3.9
FN 12	0.68	-0.98	5.7	3.9
FN 13	0.63	-0.98	5.1	3.9
FN 14	0.63	-0.99	9.0	4.1
FN 15	0.91	0.02	3.8	3.8

Table B.1 tGICA model order evaluation metrics for the PCA threshold selected (i.e., 60% - 15 ICs) in the study described in Chapter 3. *ICASSO* cluster robustness index (*Iq*) and HbO-HbR correlation (r) values are displayed. Sum of squared differences (ssd) are computed with respect to the data after PCA (total = 100%) and with respect to the original data without PCA (total = 60%). Components (FN) are ordered based on their spatial configuration and interpretability in the same order as they are presented in the figures of Chapter 3.

Supplementary Materials Chapter 3

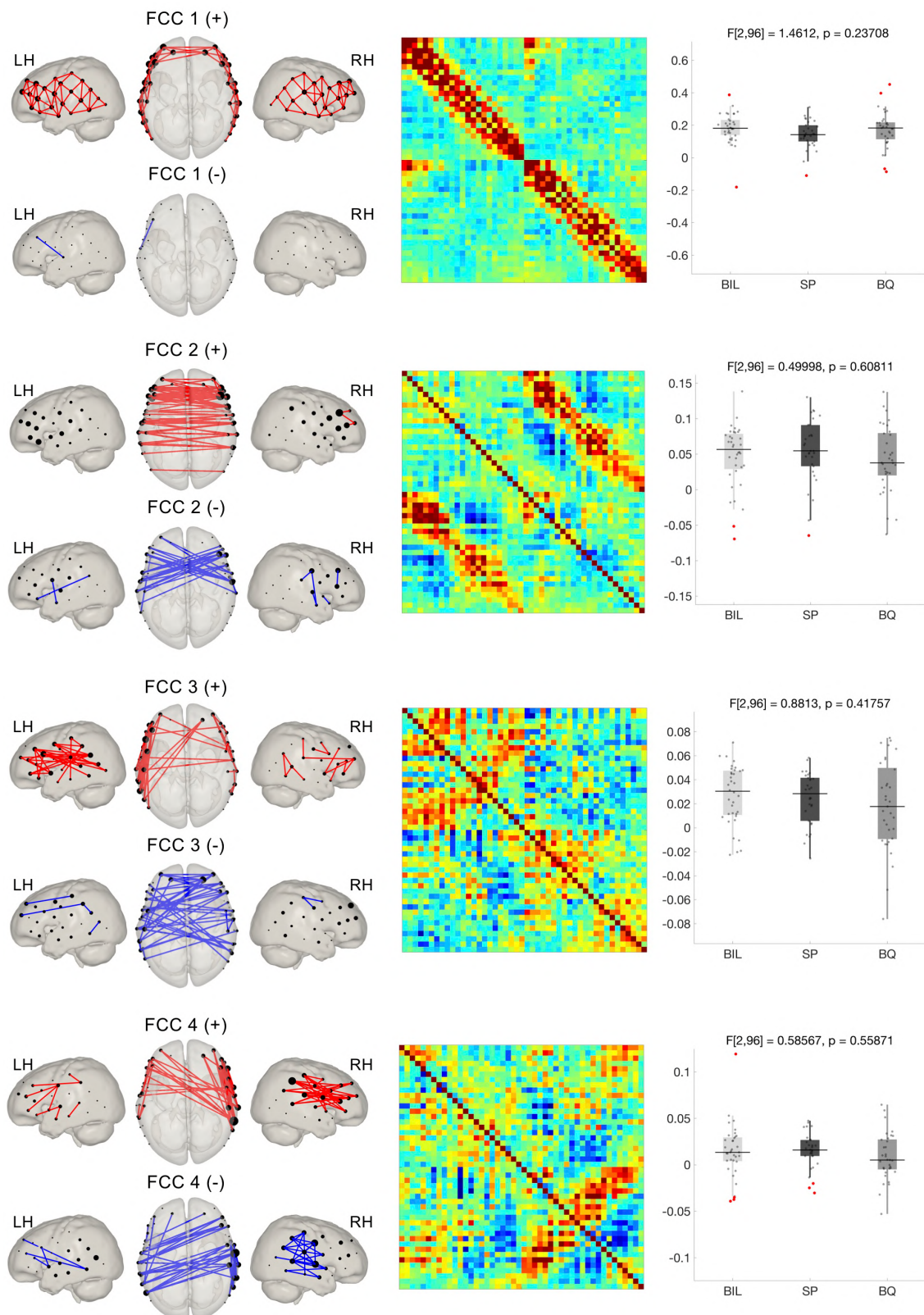


Figure continues in next page

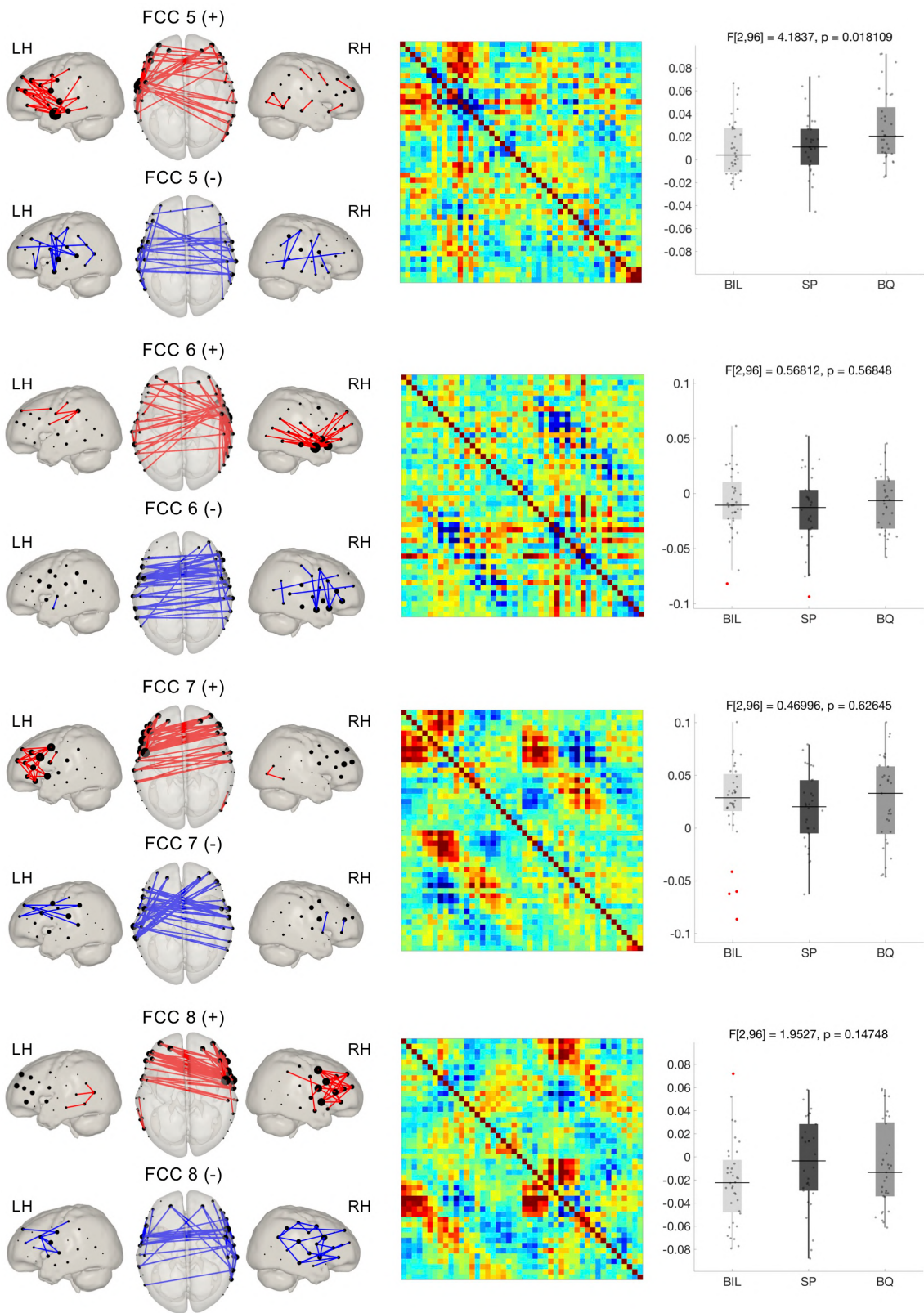


Figure continues in next page

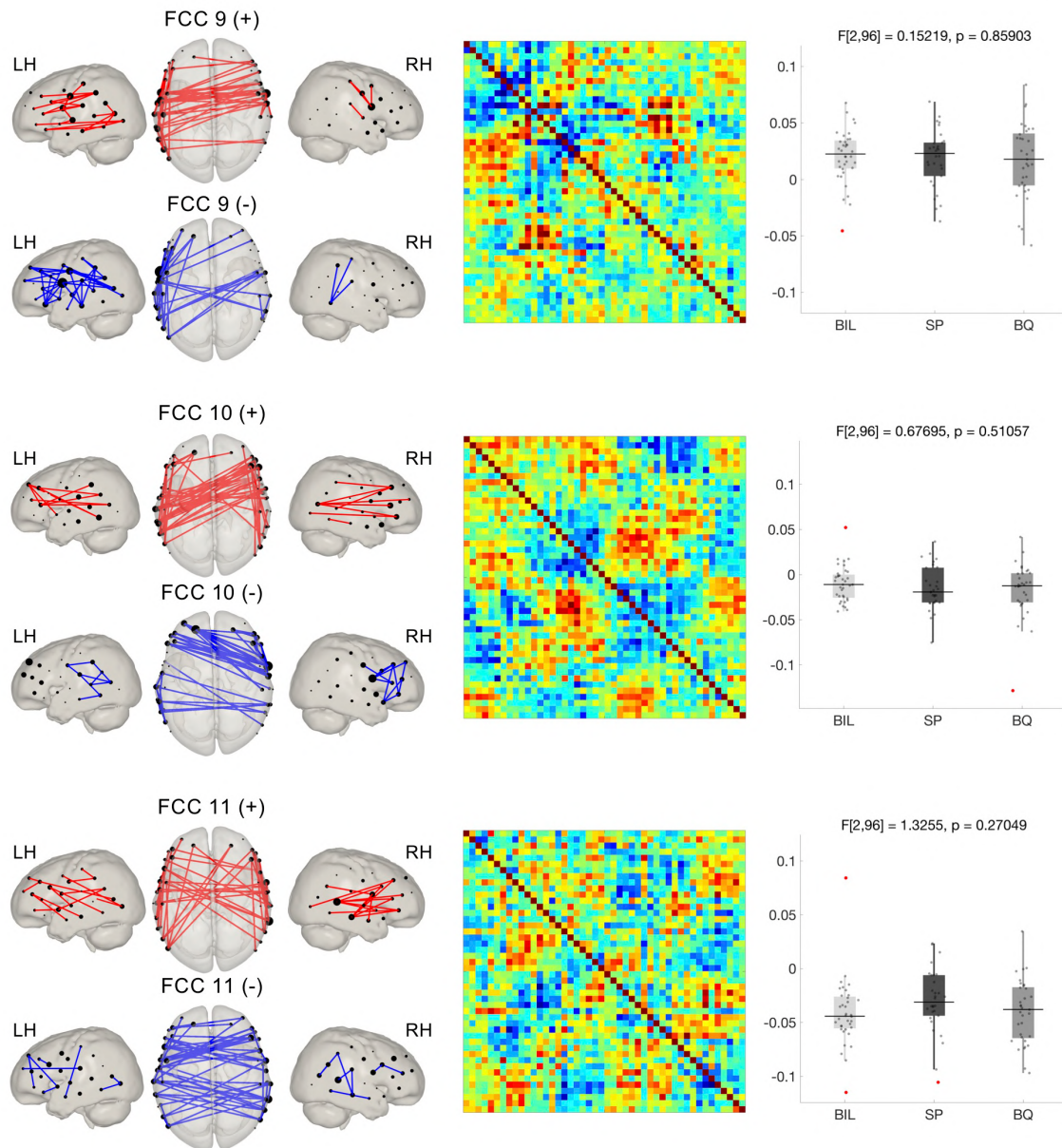


Figure B.6 Functional connectome components (FCC) obtained with the connICA method. Leftmost column shows the positive and negative parts of the components, represented as nodes and edges (top 10% connections) in a brain template. The middle column shows the components as reconstructed in their original form (i.e., adjacency matrices), with HbO and HbR displayed in the upper and lower triangular sections of the matrix respectively. Statistical comparisons on the weights for each component (right column) revealed no differences between groups. Due to the high similarity between HbO and HbR components FCCs are shown for HbR only.

Functional Connectome Component (FCC)	<i>Iq</i>	<i>r</i> (HbO-HbR)	ssd (100 %)	ssd (60 %)
FCC 1	0.96	0.95	24	5.5
FCC 2	0.91	0.88	7.2	5.5
FCC 3	0.50	0.70	7.4	5.4
FCC 4	0.94	0.72	7.8	5.4
FCC 5	0.91	0.80	7.3	5.5
FCC 6	0.91	0.83	7.3	5.4
FCC 7	0.90	0.90	8.8	5.6
FCC 8	0.84	0.84	7.3	5.4
FCC 9	0.88	0.72	7.6	5.5
FCC 10	0.90	0.74	8.0	5.4
FCC 11	0.71	0.67	7.6	5.4

Table B.2 Model order evaluation metrics for the PCA threshold selected (i.e., 60% - 11 ICs) in the connICA approach for the study described in Chapter 3. *ICASSO* cluster robustness index (*Iq*) and HbO-HbR correlation (*r*) values are displayed. Sum of squared differences (ssd) are computed with respect to the data after PCA (total = 100%) and with respect to the original data without PCA (total = 60%). Components (FCC) are ordered based on their spatial configuration and interpretability in the same order as they are presented in the figures of Chapter 3.

Appendix C

Supplementary Figures Chapter 5

This Appendix contains the Supplementary Figures for the study presented in Chapter 5 “Hemodynamic Correlates of Speech Processing in Bilingual and Monolingual Infants”.

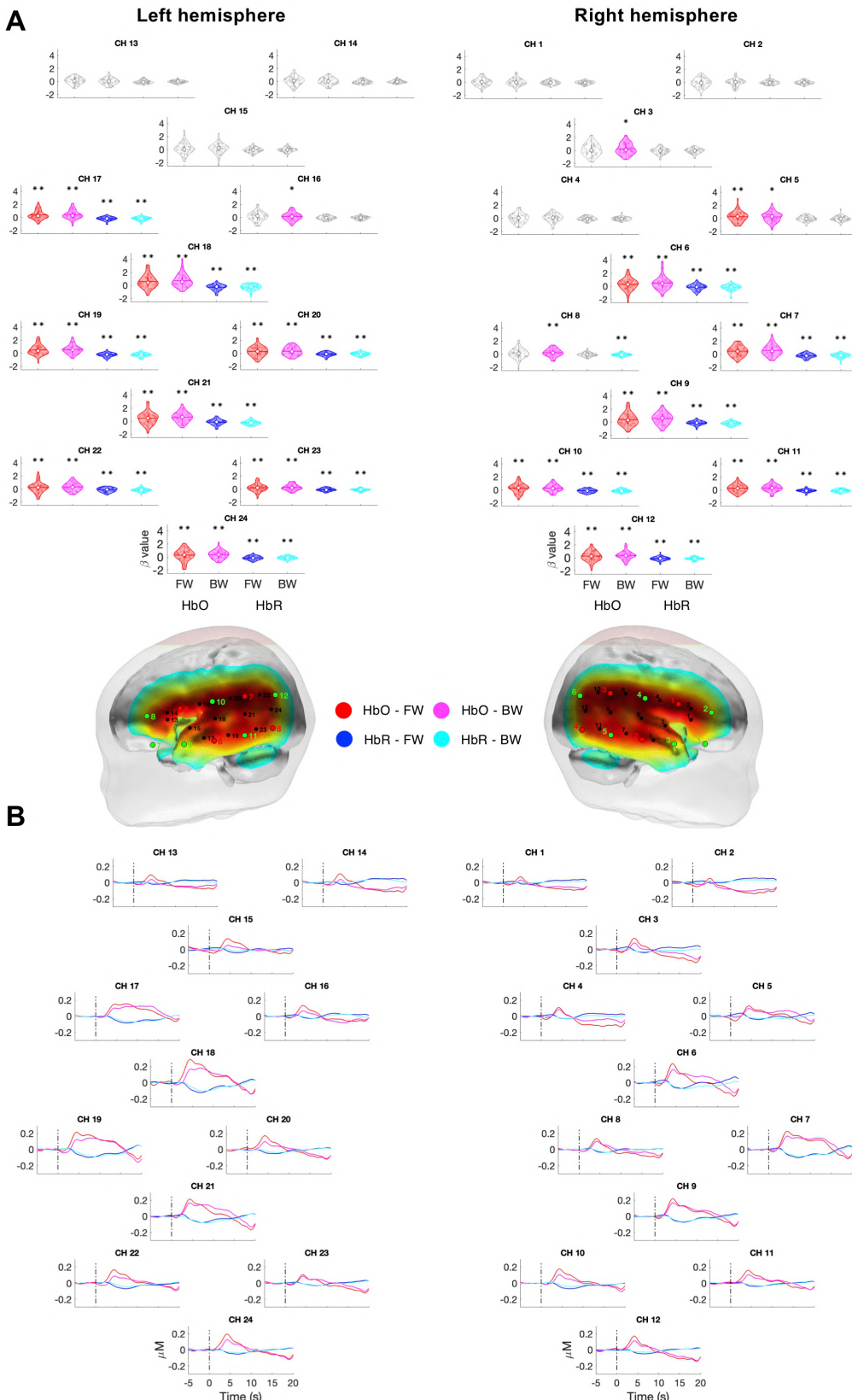


Figure C.1 Results presented in this figure are equivalent to those displayed in Figure 5.8, except here results were computed following a standard preprocessing pipeline, and not one including global signal regression. **A)** Channels showing a significant activation/deactivation as determined by one-sample t-tests in the β -values for each experimental condition (FW, BW). * $p < 0.05$, ** $p < 0.05$ (FDR corrected). **B)** Group-averaged HRFs at each channel location and for each experimental condition estimated by the FIR analysis. Zero-point in the time line marks stimulus onset.

Supplementary Figures Chapter 5

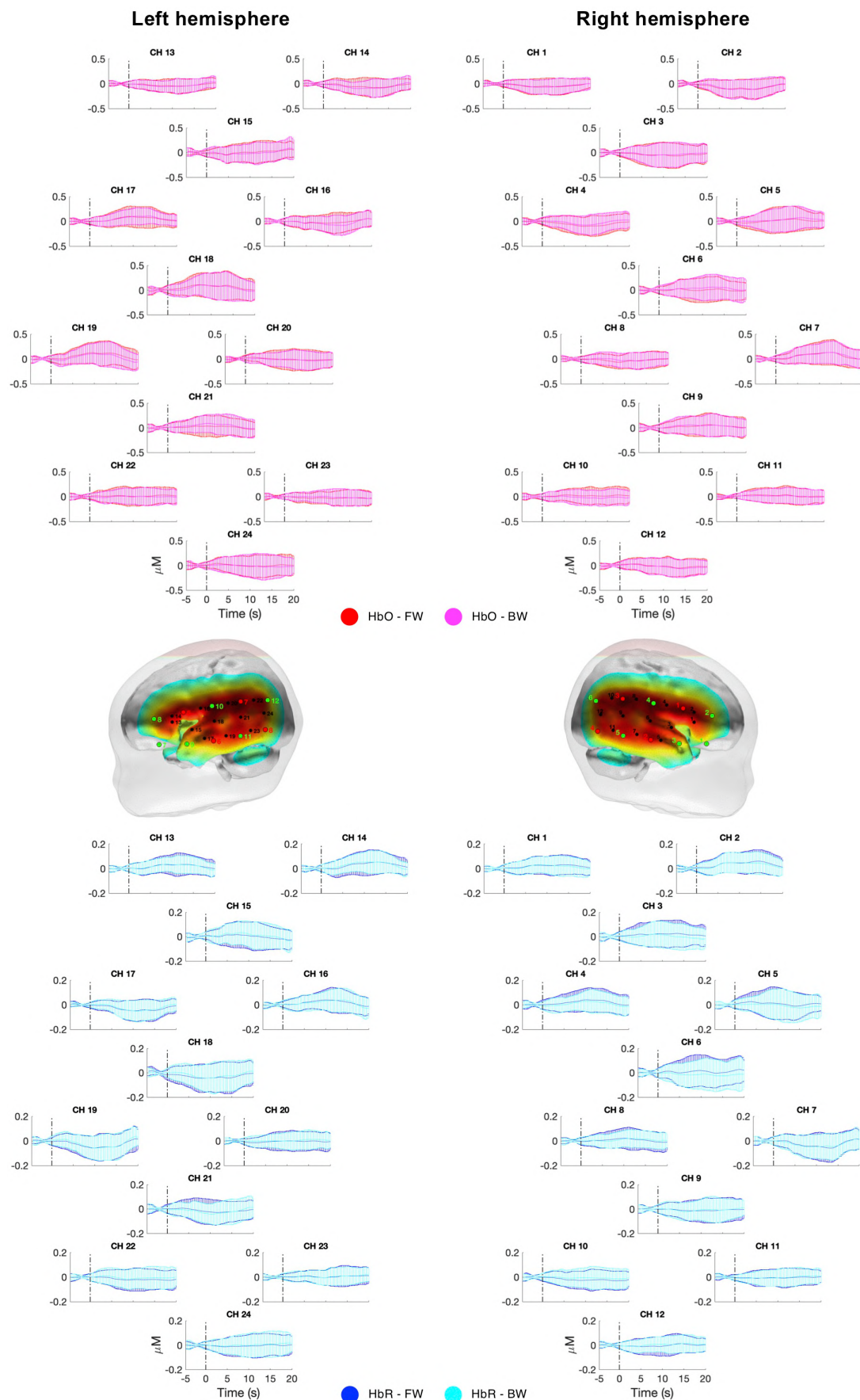


Figure C.2 Comparison of group-level hemodynamic response time courses (mean and standard deviation) between FW and BW speech conditions for HbO and HbR data.

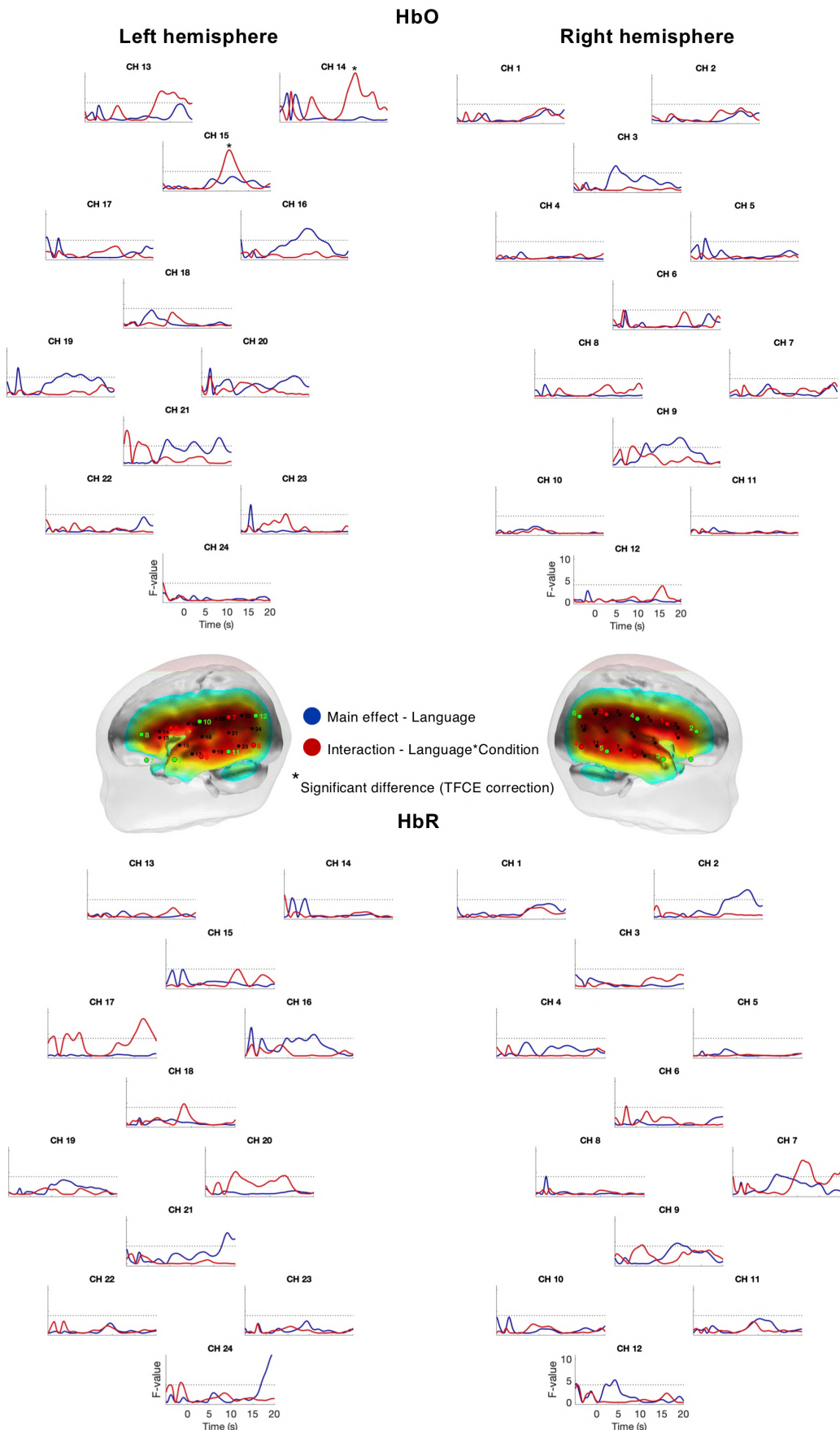


Figure C.3 Channelwise time courses of F-values computed at each time point to assess clusters showing significant main (blue) and interaction (red) effects using the TFCE method.

Supplementary Figures Chapter 5

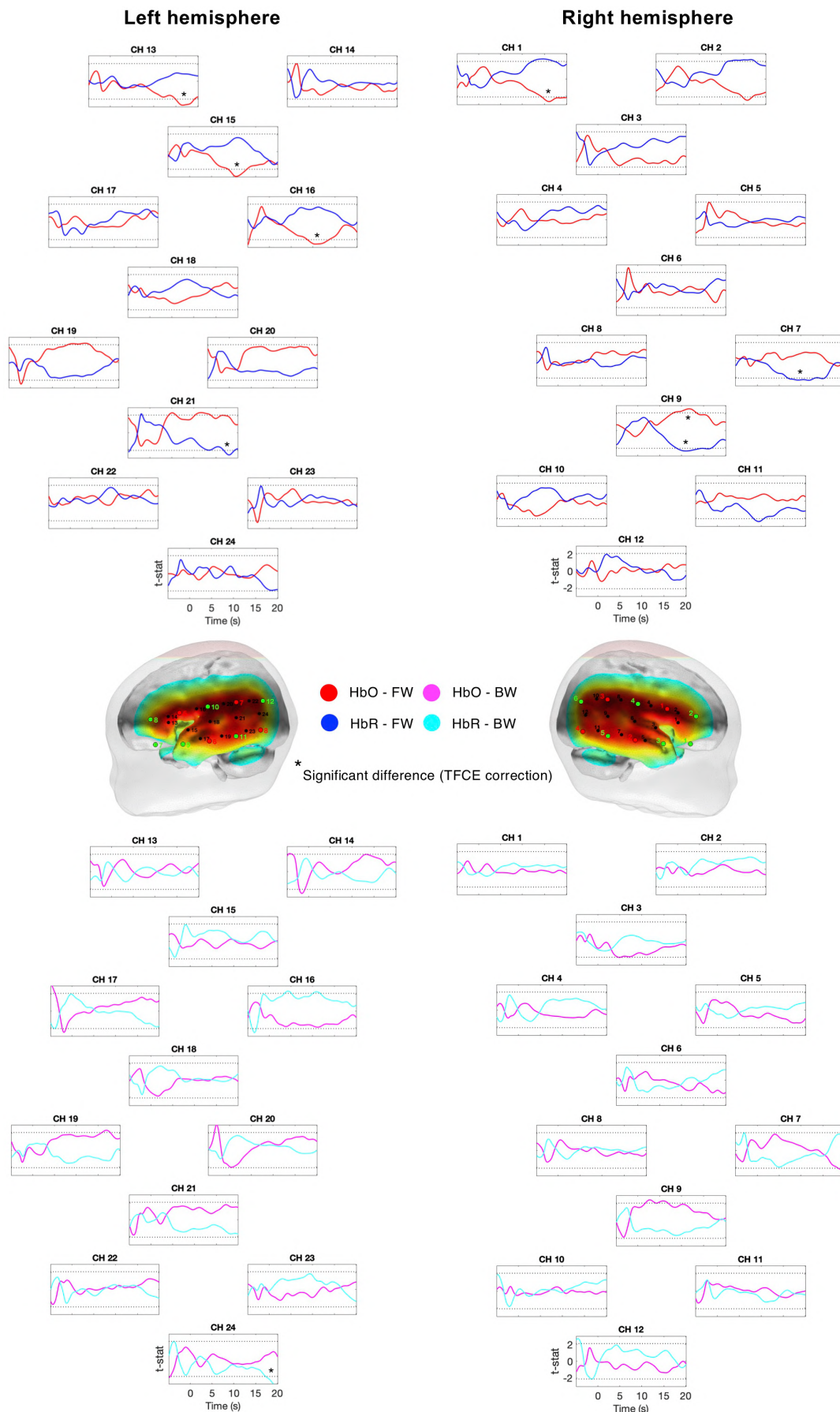


Figure C.4 Channelwise time courses of t-values computed at each time point for each experimental condition to evaluate clusters showing significant effects using the TFCE method.

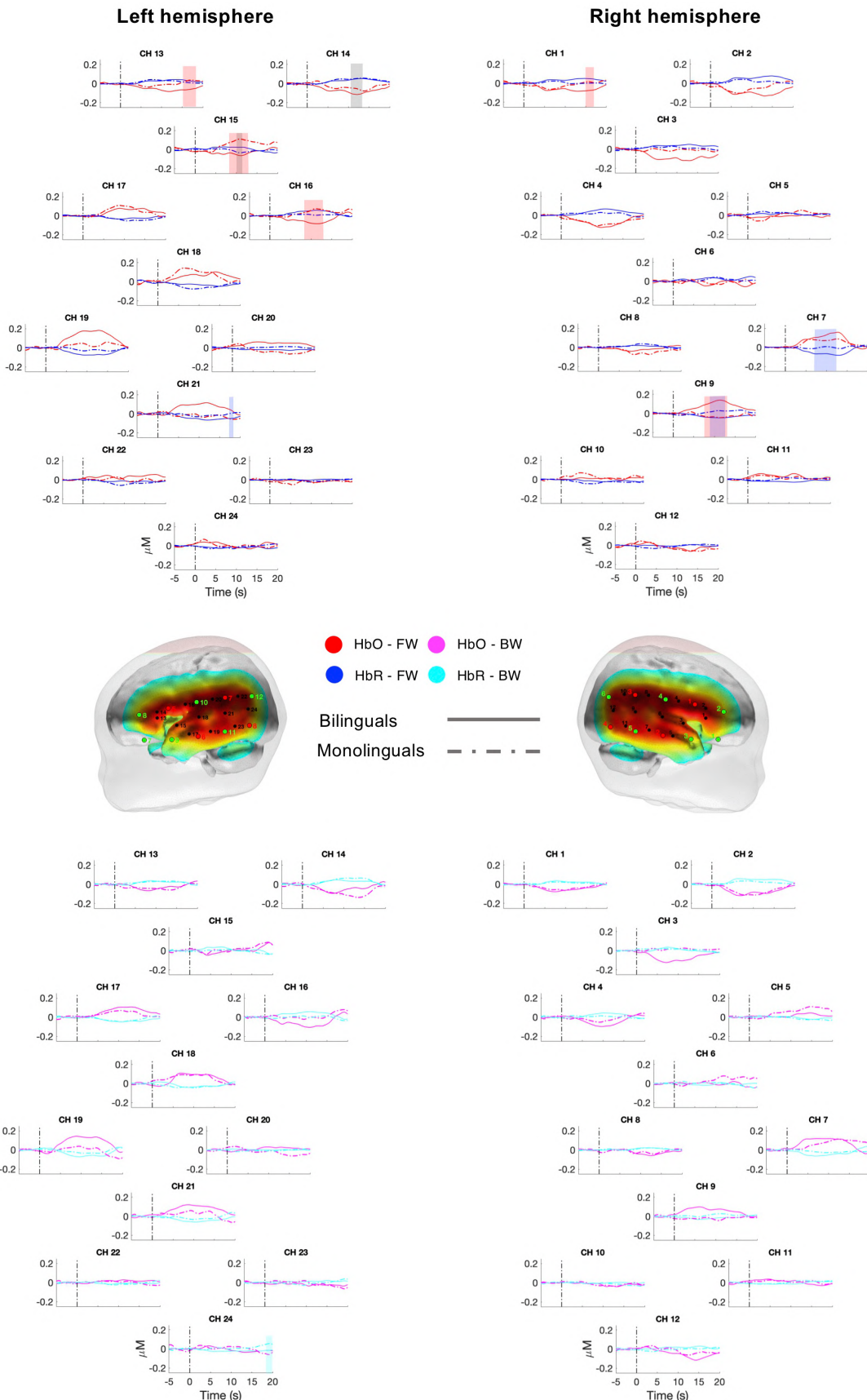


Figure C.5 Hemodynamic responses extracted in each experimental group (i.e., bilingual and monolingual infants), for FW and BW conditions and for HbO and HbR data. Shaded areas represent time windows where significant effects were observed after multiple comparisons correction using the TFCE method. F-tests (grey); post-hoc t-tests (color matching condition).

Bibliography

- Abboub, N., Nazzi, T., and Gervain, J. "Prosodic grouping at birth". *Brain Lang.* 162, 46-59 (2016). [doi: 10.1016/j.bandl.2016.08.002].
- Abou-Elseoud, A., Starck, T., Remes, J., Nikkinen, J., Tervonen, O., and Kiviniemi, V. "The effect of model order selection in group PICA". *Hum. Brain Map.* 31(8), 1207-1216 (2010). [doi: 10.1002/hbm.20929].
- Abou Elseoud, A., Littow, H., Remes, J., Starck, T., Nikkinen, J., Nissilä, J., Timonen, M., Tervonen, O., and Kiviniemi, V. J. "Group-ICA model order highlights patterns of functional brain connectivity". *Front. Syst. Neurosci.* 5, 37 (2011). [doi: 10.3389/fnsys.2011.00037].
- Afyouni, S., Smith, S. M., and Nichols, T. E. (2018). "Effective degrees of freedom of the Pearson's correlation coefficient under serial correlation". *bioRxiv*, 537-541 (2018). [doi: 10.1101/453795].
- Akiyama, L. F., Richards, T. R., Imada, T., Dager, S. R., Wroblewski, L., and Kuhl, P. K. "Age-specific average head template for typically developing 6-month-old infants". *PLOS one* 8(9), e73821 (2013). [doi: 10.1371/journal.pone.0073821].
- Albareda-Castellot, B., Pons, F., and Sebastián-Gallés, N. The acquisition of phonetic categories in bilingual infants: New data from an anticipatory eye movement paradigm. *Dev. Sci.* 14(2), 395-401 (2011). [doi: 10.1111/j.1467-7687.2010.00989.x].
- Alcauter, S., Lin, W., Smith, J. K., Goldman, B. D., Reznick, J. S., Gilmore, J. H., and Gao, W. "Frequency of spontaneous BOLD signal shifts during infancy and correlates with cognitive performance". *Dev. Cogn. Neurosci.* 12, 40-50 (2015). [doi: 10.1016/j.dcn.2014.10.004].
- Altvater-Mackensen, N., and Grossmann, T. "The role of left inferior frontal cortex during audiovisual speech perception in infants". *Neuroimage*, 133, 14-20 (2016). [doi: 10.1016/j.neuroimage.2016.02.061].
- Amico, E., Marinazzo, D., Di Perri, C., Heine, L., Annen, J., Martial, C., Dzemidzic, M., Kirsch, M., Bonhomme, V., Laureys, S., and Goñi, J. "Mapping the functional connectome traits of levels of consciousness". *Neuroimage* 148, 201-211 (2017). [doi: 10.1016/j.neuroimage.2017.01.020].
- Amico, E., and Goñi, J. "Mapping hybrid functional-structural connectivity traits in the human connectome". *Net. Neuro.* 2(3), 306-322 (2018). [doi: 10.1162/netn_a_00049].
- Arbabshirani, M. R., Damaraju, E., Phlypo, R., Plis, S., Allen, E., Ma, S., Mathalon, D., Preda, A., Vaidya, J. G., Adali, T. and Calhoun, V. D. "Impact of autocorrelation on functional connectivity". *Neuroimage* 102(Pt 2), 294-308 (2014). [doi: 10.1016/j.neuroimage.2014.07.045].
- Archila-Suerte, P., Zevin, J., Ramos, A. I., and Hernandez, A. E. "The neural basis of non-native speech perception in bilingual children". *Neuroimage*, 67, 51-63 (2013). [doi: 10.1016/j.neuroimage.2012.10.023].
- Arichi, T., Fagiolo, G., Varela, M., Melendez-Calderon, A., Allievi, A., Merchant, N., Tusor, N., Counsell, S.J., Burdet, E., Beckmann C., and Edwards, A. D. "Development of BOLD signal hemodynamic responses in the human brain". *Neuroimage*, 63(2), 663-673 (2012). [doi: 10.1016/j.neuroimage.2012.06.054].
- Arridge, S. R. "Optical tomography in medical imaging". *Inv. Problems* 15(2), R41 (1999). [doi: 10.1088/0266-5611/15/2/022].
- Aslin, R. N. "Questioning the questions that have been asked about the infant brain using near-infrared spectroscopy". *Cogn. Neuropsych.* 29(1-2), 7-33 (2012). [doi: 10.1080/02643294.2012.654778].
- Aslin, R. N., Shukla, M., and Emberson, L. L. "Hemodynamic correlates of cognition in human infants". *Ann. Rev. Psych.* 66, 349-379 (2015). [doi: 10.1146/annurev-psych-010213-115108].
- Avants, B. B., Tustison, N., and Song, G. "Advanced normalization tools (ANTS)". *Insight J.* 2, 1-35 (2009).
- Ayneto, A., and Sebastián-Gallés, N. "The influence of bilingualism on the preference for the mouth region of dynamic faces". *Dev. Sci.* 20(1), e12446 (2017). [doi: 10.1111/desc.12446].
- Azhari, A., Leck, W. Q., Gabrieli, G., Bizzego, A., Rigo, P., Setoh, P., Bornstein, H. and Esposito, G. "Parenting stress undermines mother-child brain-to-brain synchrony: A hyperscanning study". *Sci. Rep.* 9(1), 1-9 (2019). [doi: 10.1038/s41598-019-47810-4].
- Barker, J. W., Aarabi, A. and Huppert, T. J. "Autoregressive model-based algorithm for correcting motion and serially correlated errors in fNIRS". *Biomed. Opt. Express* 4(8), 1366-79 (2013). [doi: 10.1364/BOE.4.001366].

- Barker, J. W., Rosso, A. L., Sparto, P. J. and Huppert, T. J. "Correction of motion artifacts and serial correlations for real-time functional near-infrared spectroscopy". *Neurophotonics* 3(3), 31410 (2016). [doi: 10.1111/1.NPh.3.3.031410].
- Beauchamp, M. S., Beurlot, M. R., Fava, E., Nath, A. R., Parikh, N. A., Saad, Z. S., Bortfeld, H., and Oghalai, J. S. "The developmental trajectory of brain-scalp distance from birth through childhood: implications for functional neuroimaging". *PloS one*, 6(9) (2011). [doi: 10.1371/journal.pone.0024981].
- Beckmann, C. F., Mackay, C. E., Filippini, N., and Smith, S. M. "Group comparison of resting-state fMRI data using multi-subject ICA and dual regression". *Neuroimage* 47(Suppl 1), S148 (2009). [doi: 10.1016/S1053-8119(09)71511-3].
- Behrendt, H. F., Firk, C., Nelson, C. A., and Perdue, K. L. "Motion correction for infant functional near-infrared spectroscopy with an application to live interaction data". *Neurophotonics*, 5(1), 015004 (2018). [doi: 10.1111/1.NPh.5.1.015004].
- Benjamini, Y., and Hochberg, Y. "Controlling the false discovery rate: a practical and powerful approach to multiple testing". *J. R. STAT. SOC. B.* 57(1), 289-300 (1995). [doi: 10.1111/j.2517-6161.1995.tb02031.x].
- Berens, P. "CircStat: A MATLAB Toolbox for Circular Statistics". *J. Stat. Softw.* 31(10), (2009). [doi: 10.18637/jss.v031.i10].
- Berken, J. A., Chai, X., Chen, J. K., Gracco, V. L., and Klein, D. "Effects of early and late bilingualism on resting-state functional connectivity". *J. Neurosci.* 36(4), 1165-1172 (2016). [doi: 10.1523/JNEUROSCI.1960-15.2016].
- Betzel, R. F., Byrge, L., He, Y., Goñi, J., Zuo, X. N., and Sporns, O. "Changes in structural and functional connectivity among resting-state networks across the human lifespan". *Neuroimage*, 102, 345-357 (2014). [doi: 10.1016/j.neuroimage.2014.07.067].
- Bialystok, E. "Bilingualism and the development of executive function: The role of attention". *Child Dev. Perspect.* 9(2), 117-121 (2015). [doi: 10.1111/cdep.12116].
- Bialystok, E. "The bilingual adaptation: How minds accommodate experience". *Psychol. Bull.* 143(3), 233-262 (2017). [doi: 10.1037/bul0000099].
- Biondi, M., Boas, D. A., and Wilcox, T. "On the other hand: increased cortical activation to human versus mechanical hands in infants". *Neuroimage*, 141, 143-153 (2016). [doi: 10.1016/j.neuroimage.2016.07.021].
- Biswal, B., Yetkin, F. Z., Haughton, V. M. and Hyde, J. S. "Functional connectivity in the motor cortex of resting human brain using echo-planar MRI". *Magn. Reson. Med.* 34(4), 537-41 (1995). [doi: 10.1002/mrm.1910340409].
- Blanco, B., Molnar, M., and Caballero-Gaudes, C. "Effect of prewhitening in resting-state functional near-infrared spectroscopy data". *Neurophotonics*, 5(4), 040401 (2018). [doi: 10.1111/1.NPh.5.4.040401].
- Blasi, A., Fox, S., Everdell, N., Volein, A., Tucker, L., Csibra, G., Gibson A. P., Johnson M. H., and Elwell, C. E. "Investigation of depth dependent changes in cerebral haemodynamics during face perception in infants". *Phys. Med. Biol.* 52(23), 6849 (2007). [doi: 10.1088/0031-9155/52/23/005].
- Blasi, A., Lloyd-Fox, S., Johnson, M. H., and Elwell, C. "Test-retest reliability of functional near infrared spectroscopy in infants". *Neurophotonics*, 1(2), 025005 (2014). [doi: 10.1111/1.NPh.1.2.025005].
- Boas, D. A., Brooks, D. H., Miller, E. L., DiMarzio, C. A., Kilmer, M., Gaudette, R. J., and Zhang, Q. "Imaging the body with diffuse optical tomography". *IEEE Sign. Proc. Mag.* 18(6), 57-75 (2001). [doi: 10.1109/79.962278].
- Boas, D. A., Strangman, G., Culver, J. P., Hoge, R. D., Jasdzewski, G., Poldrack, R. A., Rosen, B. R., and Mandeville, J. B. "Can the cerebral metabolic rate of oxygen be estimated with near-infrared spectroscopy?". *Phys. Med. Biol.* 48(15), 2405 (2003). [doi: 10.1088/0031-9155/48/15/311].
- Boas, D. A., Dale, A. M., and Franceschini, M. A. "Diffuse optical imaging of brain activation: approaches to optimizing image sensitivity, resolution, and accuracy". *Neuroimage*, 23, S275-S288 (2004). [doi: 10.1016/j.neuroimage.2004.07.011].
- Boersma, P. and Weenik, P. "Praat: Doing Phonetics by Computer". *Ear Hearing*, 32(2), 266-268 (1990). [doi: 10.4278/0890-1171-5.2.91].
- Born, P., Rostrup, E., Leth, H., Peitersen, B., and Lou, H. C. "Change of visually induced cortical activation pattern during development". *Lancet* 347: 543 (1996). [doi: 10.1016/s0140-6736(96)91175-7].

- Born, P., Leth, H., Miranda, M., Rostrup, E., Stensgaard, A., Lars- son, H. B. W., Peitersen, B., and Lou, H. C. "Visual activation in infants and young children studied by functional magnetic resonance imaging". *Ped. Res.* 44: 578-583 (1998). [doi: 10.1203/00006450-199810000-00018].
- Born, A. P., Law, I., Lund, T. E., Rostrup, E., Hanson, L. G., Wildschiodtz, G., Lou, H. C., and Paulson, O. B. "Cortical deactivation induced by visual stimulation in human slow-wave sleep". *Neuroimage*, 17(3), 1325-1335 (2002). [doi: 10.1006/nimg.2002.1249].
- Bortfeld, H., Wruck, E., and Boas, D. A. "Assessing infants' cortical response to speech using near-infrared spectroscopy". *Neuroimage*, 34(1), 407-415 (2007). [doi: 10.1016/j.neuroimage.2006.08.010].
- Bortfeld, H., Fava, E., and Boas, D. A. "Identifying cortical lateralization of speech processing in infants using near-infrared spectroscopy". *Dev. Neuropsych.* 34(1), 52-65 (2009). [doi: 10.1080/87565640802564481].
- Bosch, L., and Sebastián-Gallés, N. "Native-language recognition abilities in 4-month-old infants from monolingual and bilingual environments". *Cognition* 65(1), 33-69 (1997). [doi: 10.1016/S0010-0277(97)00040-1].
- Bosch, L., and Sebastián-Gallés, N. "Evidence of early language discrimination abilities in infants from bilingual environments". *Infancy*, 2(1), 29-49 (2001). [doi: 10.1207/S15327078IN0201_3].
- Bosch, L., and Sebastián-Gallés, N. "Simultaneous bilingualism and the perception of a language-specific vowel contrast in the first year of life". *Lang. Speech*, 46(2-3), 217-243 (2003). [doi: 10.1177/00238309030460020801].
- Braukmann, R., Lloyd-Fox, S., Blasi, A., Johnson, M. H., Bekkering, H., Buitelaar, J. K., and Hunnius, S. "Diminished socially selective neural processing in 5-month-old infants at high familial risk of autism". *Eur. J. Neurosci.* 47(6), 720-728 (2018). [doi: 10.1111/ejn.13751].
- Brigadoi, S., Aljabar, P., Kuklisova-Murgasova, M., Arridge, S. R. and Cooper, R. J., "A 4D neonatal head model for diffuse optical imaging of pre-term to term infants". *Neuroimage*, 100, 385-394 (2014). [doi: 10.1016/j.neuroimage.2014.06.028].
- Brigadoi, S., Ceccherini, L., Cutini, S., Scarpa, F., Scatturin, P., Selb, J., Gagnon, L., Boas, D. and Cooper, R. J. (2014). "Motion artifacts in functional near-infrared spectroscopy: a comparison of motion correction techniques applied to real cognitive data". *Neuroimage*, 85, 181-191 (2014). [doi: 10.1016/j.neuroimage.2013.04.082].
- Brigadoi, S. and Cooper, R. J., "How short is short? Optimum source-detector distance for short-separation channels in functional near-infrared spectroscopy". *Neurophotonics*, 2(2), 025005 (2015). [doi: 10.1117/1.NPh.2.2.025005].
- Brigadoi, S., Phan, P., Highton, D., Powell, S., Cooper, R. J., Hebden, J. C., Smith, M., Tachtsidis, I., Elwell, C. E. and Gibson, A. P. "Image reconstruction of oxidized cerebral cytochrome C oxidase changes from broadband near-infrared spectroscopy data". *Neurophotonics*, 4(2), 021105 (2017). [doi: 10.1117/1.NPh.4.2.021105].
- Bright, M. G., Tench, C. R. and Murphy, K. "Potential pitfalls when denoising resting state fMRI data using nuisance regression". *Neuroimage* 154, 159-168 (2016). [doi: 10.1016/j.neuroimage.2016.12.027].
- Brookes, M. J., Woolrich, M., Luckhoo, H., Price, D., Hale, J. R., Stephenson, M. C., Barnes, G. R., Smith, S. M. and Morris, P. G. "Investigating the electrophysiological basis of resting state networks using magnetoencephalography". *Proc. Natl. Acad. Sci.* 108(40), 16783-16788 (2011). [doi: 10.1073/pnas.1112685108].
- Bulgarelli, C., Blasi, A., de Clerk, C. C., Richards, J. E., Hamilton, A., and Southgate, V. "Frontotemporoparietal connectivity and self-awareness in 18-month-olds: A resting state fNIRS study". *Dev. Cogn. Neurosci.* 38, 100676 (2019). [doi: 10.1016/j.dcn.2019.100676].
- Bullmore, E. Brammer, M., Williams, S. C., Rabe-Hesketh, S., Janot, N., David, A., Mellers, J., Howard, R. and Sham, P. "Statistical methods of estimation and inference for functional MR image analysis". *Magn. Reson. Med.* 35(2), 261-277 (1996). [doi: 10.1002/mrm.1910350219].
- Burns, T. C., Yoshida, K. A., Hill, K., and Werker, J. F. "The development of phonetic representation in bilingual and monolingual infants". *Appl. Psycholinguist.* 28, 455-474 (2007). [doi: 10.1017/S0142716407070257].
- Buxton, R. B. "The elusive initial dip". *Neuroimage*, 13:953-958 (2001). [doi: 10.1006/nimg.2001.0814].

- Byers-Heinlein, K., Burns, T. C., and Werker, J. F. "The roots of bilingualism in newborns". *Psych. Science*, 21(3), 343-348 (2010). [doi: 10.1177/0956797609360758].
- Byers-Heinlein, K. "Parental language mixing: Its measurement and the relation of mixed input to young bilingual children's vocabulary size". *Biling. Lang. Cogn.* 16(1), 32-48 (2013). [doi: 10.1017/S1366728912000120P].
- Byers-Heinlein, K., and Fennell, C. T. "Perceptual narrowing in the context of increased variation: Insights from bilingual infants". *Dev. Psychobiol.* 56(2), 274-291 (2014). [doi: 10.1002/dev.21167].
- Caballero-Gaudes, C., Petridou, N., Francis, S. T., Dryden, I. L. and Gowland, P. A. "Paradigm free mapping with sparse regression automatically detects single-trial functional magnetic resonance imaging blood oxygenation level dependent responses". *Hum. Brain Mapp.* 34(3), 501-18 (2013). [doi: 10.1002/hbm.21452].
- Cai, L., Dong, Q., and Niu, H. "The development of functional network organization in early childhood and early adolescence: a resting-state fNIRS study". *Dev. Cogn. Neurosci.* 30, 223-235 (2018). [doi: 10.1016/j.dcn.2018.03.003].
- Calhoun, V. D., Adali, T., Pearson, G. D., and Pekar, J. J. "A method for making group inferences from functional MRI data using independent component analysis". *Hum. Brain Map.* 14(3), 140-151 (2001). [doi: https://doi.org/10.1002/hbm.1048].
- Cantlon, J. F., Brannon, E. M., Carter, E. J., and Pelpfrey, K. A. "Functional imaging of numerical processing in adults and 4-y-old children". *PLoS biology*, 4(5) (2006). [doi: 10.1371/journal.pbio.0040125].
- Chance, B., Zhuang, Z., UnAh, C., Alter, C., and Lipton, L. "Cognition-activated low-frequency modulation of light absorption in human brain". *P. Natl. Acad. Sci.* 90(8), 3770-3774 (1993). [doi: 10.1073/pnas.90.8.3770].
- Cheour, M., Martynova, O., Näätänen, R., Erkkola, R., Sillanpää, M., Kero, P., Raz, A., Kaipio, M.L., Hiltunen, J., Aaltonen, O., Savela, J. and Hämäläinen, H. "Speech sounds learned by sleeping newborns". *Nature*, 415(6872), 599-600 (2002). [doi: 10.1038/415599b].
- Chiarelli, A. M., Maclin, E. L., Fabiani, M., and Gratton, G. "A kurtosis-based wavelet algorithm for motion artifact correction of fNIRS data". *Neuroimage*, 112, 128-137 (2015). [doi: 10.1016/j.neuroimage.2015.02.057].
- Chitnis, D., Cooper, R. J., Dempsey, L., Powell, S., Quaggia, S., Highton, D., Elwell, C., Hebden, J. C., and Everdell, N. L. (2016). "Functional imaging of the human brain using a modular, fibre-less, high-density diffuse optical tomography system". *Biomed. Opt. Exp.* 7(10), 4275-4288 (2016).
- Christova, P., Lewis, S. M., Jerde, T. A., Lynch, J. K. and Georgopoulos, A. P. "True associations between resting fMRI time series based on innovations". *J. Neural Eng.* 8(4), 46025 (2011). [doi: 10.1088/1741-2560/8/4/046025].
- Comishen, K. J., Bialystok, E., and Adler, S. A. "The impact of bilingual environments on selective attention in infancy". *Developmental science*, 22(4), e12797 (2019). [doi: 10.1111/desc.12797].
- Conboy, B. T., and Mills, D. L. "Two languages, one developing brain: Event-related potentials to words in bilingual toddlers". *Dev. Sci.* 9(1), F1-F12 (2006). [doi: 10.1111/j.1467-7687.2005.00453.x].
- Cooper, R. J., Everdell, N. L., Enfield, L. C., Gibson, A. P., Worley, A., and Hebden, J. C. "Design and evaluation of a probe for simultaneous EEG and near-infrared imaging of cortical activation". *Physics Med. Biol.* 54(7), 2093 (2009). [doi: 10.1088/0031-9155/54/7/016].
- Cooper, R., Selb, J., Gagnon, L., Phillip, D., Schytz, H. W., Iversen, H. K., Ashina, M., and Boas, D. A. "A systematic comparison of motion artifact correction techniques for functional near-infrared spectroscopy". *Front. Neurosci.* 6, 147 (2012). [doi: 10.3389/fnins.2012.00147].
- Costa, A., and Sebastián-Gallés, N. "How does the bilingual experience sculpt the brain?". *Nat. Rev. Neurosci.* 15(5), 336 (2014). [doi: 10.1038/nrn3709].
- Cristia, A., Dupoux, E., Hakuno, Y., Lloyd-Fox, S., Schuetze, M., Kivits, J., Bergvelt, T., van Gelder M., Filippin, L., Charron, S., and Minagawa-Kawai, Y. "An online database of infant functional near infrared spectroscopy studies: a community-augmented systematic review". *PLoS one*, 8(3) (2013). [doi: 10.1371/journal.pone.0058906].

- Cristia, A., Minagawa-Kawai, Y., Egorova, N., Gervain, J., Filippin, L., Cabrol, D., and Dupoux, E. "Neural correlates of infant accent discrimination: an fNIRS study". *Dev. Sci.* 17(4), 628-635 (2014). [doi: 10.1111/desc.12160].
- Csibra, G., Henty, J., Volein, Á., Elwell, C., Tucker, L., Meek, J., and Johnson, M. H. "Near infrared spectroscopy reveals neural activation during face perception in infants and adults". *J. Ped. Neurol.* 2(02), 085-089 (2004). [doi: 10.1055/s-0035-1557198].
- Czisch, M., Wetter, T. C., Kaufmann, C., Pollmächer, T., Holsboer, F., and Auer, D. P. "Altered processing of acoustic stimuli during sleep: reduced auditory activation and visual deactivation detected by a combined fMRI/EEG study". *Neuroimage*, 16(1), 251-258 (2002). [doi: 10.1006/nimg.2002.1071].
- Czisch, M., Wehrle, R., Kaufmann, C., Wetter, T. C., Holsboer, F., Pollmächer, T., and Auer, D. P. "Functional MRI during sleep: BOLD signal decreases and their electrophysiological correlates". *Eur. J. Neurosci.* 20(2), 566-574 (2004). [doi: 10.1111/j.1460-9568.2004.03518.x].
- Cui, X., Bray, S., and Reiss, A. L. "Functional near infrared spectroscopy (NIRS) signal improvement based on negative correlation between oxygenated and deoxygenated hemoglobin dynamics". *Neuroimage*, 49(4), 3039-3046 (2010). [doi: 10.1016/j.neuroimage.2009.11.050].
- Cusack, R., Wild, C., Linke, A. C., Arichi, T., Lee, D. S., and Han, V. K. "Optimizing stimulation and analysis protocols for neonatal fMRI". *PLoS One*, 10(8) (2015). [doi: 10.1371/journal.pone.0120202].
- Damaraju, E., Phillips, J., Lowe, J. R., Ohls, R., Calhoun, V. D., and Caprihan, A. "Resting-state functional connectivity differences in premature children". *Front. Syst. Neurosci.* 4, 23 (2010). [doi: 10.3389/fnsys.2010.00023].
- Damaraju, E., Caprihan, A., Lowe, J. R., Allen, E. A., Calhoun, V. D. and Phillips, J. P. "Functional connectivity in the developing brain: a longitudinal study from 4 to 9 months of age". *Neuroimage* 84, 169-80 (2014). [doi: 10.1016/j.neuroimage.2013.08.038].
- Damoiseaux, J. S., Rombouts, S. A., Barkhof, F., Scheltens, P., Stam, C. J., Smith, S. M. and Beckmann, C. F. "Consistent resting-state networks across healthy subjects". *Proc. Natl. Acad. Sci. U. S. A.* 103(37), 13848-53 (2006). [doi: 10.1073/pnas.0601417103].
- Dehaene-Lambertz, G., and Houston, D. "Faster orientation latencies toward native language in two-month-old infants". *Lang. Speech*, 41(1), 21-43 (1998). [doi: 10.1177/002383099804100102].
- Dehaene-Lambertz, G., Dehaene, S., and Hertz-Pannier, L. "Functional neuroimaging of speech perception in infants". *Science*, 298(5600), 2013-2015 (2002). [doi: 10.1126/science.1077066].
- Dehaene, S., Piazza, M., Pinel, P., and Cohen, L. "Three parietal circuits for number processing". *Cogn. Neuropsych.* 20(3-6), 487-506 (2003). [doi: 10.1080/02643290244000239].
- Dehaene-Lambertz, G., and Gliga, T. "Common neural basis for phoneme processing in infants and adults". *J. Cogn. Neurosci.* 16(8), 1375-1387 (2004). [doi: 10.1162/0898929042304714].
- Dehaene-Lambertz, G., Hertz-Pannier, L., Dubois, J., Mériaux, S., Roche, A., Sigman, M., and Dehaene, S. "Functional organization of perisylvian activation during presentation of sentences in preverbal infants". *Proc. Natl. Acad. Sci. USA*, 103(38), 14240-14245 (2006). [doi: 10.1073/pnas.0606302103].
- Dehaene-Lambertz, G., Montavont, A., Jobert, A., Allirol, L., Dubois, J., Hertz-Pannier, L., and Dehaene, S. "Language or music, mother or Mozart? Structural and environmental influences on infants' language networks". *Brain Lang.* 114(2), 53-65 (2010). [doi: 10.1016/j.bandl.2009.09.003].
- De Luca, M., Beckmann, C. F., De Stefano, N., Matthews, P. M. and Smith, S. M. "fMRI resting state networks define distinct modes of long-distance interactions in the human brain". *Neuroimage* 29(4), 1359-1367 (2006). [doi: 10.1016/j.neuroimage.2005.08.035].
- deRegnier, R. A., Nelson, C. A., Thomas, K. M., Wewerka, S., and Georgieff, M. K. "Neurophysiologic evaluation of auditory recognition memory in healthy newborn infants and infants of diabetic mothers". *J. Pediatrics*, 137(6), 777-784 (2000). [doi: 10.1067/mpd.2000.109149].
- de Roever, I., Bale, G., Mitra, S., Meek, J., Robertson, N. J., and Tachtsidis, I. "Investigation of the pattern of the hemodynamic response as measured by functional near-infrared spectroscopy (fNIRS) studies in newborns, less than a month old: a systematic review". *Front. Hum. Neurosci.* 12, 371 (2018). [doi: 10.3389/fnhum.2018.00371].

de Souza Rodrigues, J., Ribeiro, F. L., Sato, J. R., Mesquita, R. C., and Júnior, C. E. B. "Identifying individuals using fNIRS-based cortical connectomes". *Biomed. Opt. Exp.* 10(6), 2889-2897 (2019). [doi: 10.1364/BOE.10.002889].

Di Lorenzo, R., Pirazzoli, L., Blasi, A., Bulgarelli, C., Hakuno, Y., Minagawa, Y., and Brigadoi, S. "Recommendations for motion correction of infant fNIRS data applicable to multiple data sets and acquisition systems". *Neuroimage*, 200, 511-527 (2019). [doi: 10.1016/j.neuroimage.2019.06.056].

Dinstein, I., Pierce, K., Eyler, L., Solso, S., Malach, R., Behrmann, M., and Courchesne, E. "Disrupted neural synchronization in toddlers with autism". *Neuron* 70(6), 1218-1225 (2011). [doi: 10.1016/j.neuron.2011.04.018].

Doria, V., Beckmann, C. F., Arichi, T., Merchant, N., Groppo, M., Turkheimer, F. E., Counsell, S. J., Murgasova, M., Aljabar, P., Nunes, R. G., Larkman, D. J., Rees, G. and Larkman, D. J. "Emergence of resting state networks in the preterm human brain". *Proc. Natl. Acad. Sci. USA*, 107(46), 20015-20020 (2010). [doi: 10.1073/pnas.1007921107].

Duncan, A., Meek, J. H., Clemence, M., Elwell, C. E., Tysczuk, L., Cope, M., and Delpy, D. "Optical pathlength measurements on adult head, calf and forearm and the head of the newborn infant using phase resolved optical spectroscopy". *Phys. Med. Biol.* 40(2), 295 (1995). [doi: 10.1088/0031-9155/40/2/007].

Duncan, A., Meek, J. H., Clemence, M., Elwell, C. E., Fallon, P., Tysczuk, L., Cope, M. and Delpy, D. T. "Measurement of cranial optical path length as a function of age using phase resolved near infrared spectroscopy". *Ped. Res.* 39(5), 889-894 (1996). [doi: 10.1203/00006450-199605000-00025].

Duyn, J. H., Ozbay, P. S., Chang, C., and Picchioni, D. "Physiological changes in sleep that affect fMRI inference". *Curr. Op. Behav. Sci.* 33, 42-50 (2020). [doi: 10.1016/j.cobeha.2019.12.007].

Eggebrecht, A. T., White, B. R., Ferradal, S. L., Chen, C., Zhan, Y., Snyder, A. Z., Dehghani, H., and Culver, J. P. "A quantitative spatial comparison of high-density diffuse optical tomography and fMRI cortical mapping". *Neuroimage*, 61(4), 1120-1128 (2012). [doi: 10.1016/j.neuroimage.2012.01.124].

Eggebrecht, A. T., Ferradal, S. L., Robichaux-Viehoever, A., Hassanpour, M. S., Dehghani, H., Snyder, A. Z., Hershey, T., and Culver, J. P. "Mapping distributed brain function and networks with diffuse optical tomography". *Nat. Photonics* 8(6), 448 (2014). [doi: 10.1038/NPHOTON.2014.107].

Elwell, C. E., and Cooper, C. E. "Making light work: illuminating the future of biomedical optics". *PHILOS. T. R. SOC. A.* 369(1955), (2011). [doi: 10.1098/rsta.2011.0302].

Emberson, L. L., Richards, J. E., and Aslin, R. N. "Top-down modulation in the infant brain: Learning-induced expectations rapidly affect the sensory cortex at 6 months". *P. Natl Acad. Sci.* 112(31), 9585-9590 (2015). [doi: 10.1073/pnas.1510343112].

Emberson, L. L., Crosswhite, S. L., Goodwin, J. R., Berger, A. J., and Aslin, R. N. "Isolating the effects of surface vasculature in infant neuroimaging using short-distance optical channels: a combination of local and global effects". *Neurophotonics*, 3(3), 031406 (2016). [doi: 10.1117/1.NPh.3.3.031406].

Emberson, L. L., Cannon, G., Palmeri, H., Richards, J. E., and Aslin, R. N. "Using fNIRS to examine occipital and temporal responses to stimulus repetition in young infants: Evidence of selective frontal cortex involvement". *Dev. Cogn. Neurosci.* 23, 26-38 (2017). [doi: 10.1016/j.dcn.2016.11.002].

Emerson, R. W., Adams, C., Nishino, T., Hazlett, H. C., Wolff, J. J., Zwaigenbaum, L., ... and Kandala, S. "Functional neuroimaging of high-risk 6-month-old infants predicts a diagnosis of autism at 24 months of age". *Sci. Transl. Med.* 9(393), eaag2882 (2017). [doi: 10.1126/scitranslmed.aag2882].

Essenpreis, M., Cope, M., Elwell, C. E., Arridge, S. R., Van der Zee, P., and Delpy, D. T. "Wavelength dependence of the differential pathlength factor and the log slope in time-resolved tissue spectroscopy". In *Optical Imaging of Brain Function and Metabolism* (pp. 9-20). Springer, Boston, MA (1993). [doi: 10.1007/978-1-4899-2468-1_2].

Fava, E., Hull, R., Baumbauer, K., and Bortfeld, H. "Hemodynamic responses to speech and music in preverbal infants". *Child Neuropsych.* 20(4), 430-448 (2014). [doi: 10.1080/09297049.2013.803524].

Fennell, C. T., Byers-Heinlein, K. and Werker, J. "Using speech sounds to guide word learning: the case of bilingual infants". *Child Dev.* 78:1510-1525 (2007). [doi: 10.1111/j.1467-8624.2007.01080.x].

Ferjan-Ramírez, N., Ramírez, R. R., Clarke, M., Taulu, S., and Kuhl, P. K. "Speech discrimination in 11-month-old bilingual and monolingual infants: a magnetoencephalography study". *Dev. Sci.* 20(1), e12427 (2017). [doi: 10.1111/desc.12427].

- Ferradal, S. L., Liao, S. M., Eggebrecht, A. T., Shimony, J. S., Inder, T. E., Culver, J. P., and Smyser, C. D. "Functional imaging of the developing brain at the bedside using diffuse optical tomography". *Cereb. Cortex* 26(4), 1558-1568 (2015). [doi: 10.1093/cercor/bhu320].
- Ferrari, M., and Quaresima, V. "A brief review on the history of human functional near-infrared spectroscopy (fNIRS) development and fields of application". *Neuroimage*, 63(2), 921-935 (2012). [doi: 10.1016/j.neuroimage.2012.03.049].
- Ferry, A. L., Fló, A., Brusini, P., Cattarossi, L., Macagno, F., Nespor, M., and Mehler, J. "On the edge of language acquisition: Inherent constraints on encoding multisyllabic sequences in the neonate brain". *Dev. Science*, 19(3), 488-503 (2016). [doi: 10.1111/desc.12323].
- Filippini, N., MacIntosh, B. J., Hough, M. G., Goodwin, G. M., Frisoni, G. B., Smith, S. M., Matthews, P. M., Beckmann, C. F. and Mackay, C. E. "Distinct patterns of brain activity in young carriers of the APOE-ε4 allele". *Proc. Natl. Acad. Sci. USA*, 106(17), 7209-7214 (2009). [doi: 10.1073/pnas.0811879106].
- Fishburn, F.A., Ludlum, R.S., Vaidya, C.J. and Medvedev, A.V., "Temporal derivative distribution repair (TDDR): a motion correction method for fNIRS". *Neuroimage*, 184, pp.171-179 (2019). [doi: 10.1016/j.neuroimage.2018.09.025].
- Fong, A. H. C., Yoo, K., Rosenberg, M. D., Zhang, S., Li, C. S. R., Scheinost, D., Constable, T. and Chun, M. M. "Dynamic functional connectivity during task performance and rest predicts individual differences in attention across studies". *Neuroimage*, 188, 14-25 (2019). [doi: 10.1016/j.neuroimage.2018.11.057].
- Fox, M. D., Snyder, A. Z., Vincent, J. L., Corbetta, M., Van Essen, D. C., and Raichle, M. E. "The human brain is intrinsically organized into dynamic, anticorrelated functional networks". *Proc. Natl. Acad. Sci.* 102(27), 9673-9678 (2005). [doi: 10.1073/pnas.0504136102].
- Fox, M. D. and Raichle, M. E. "Spontaneous fluctuations in brain activity observed with functional magnetic resonance imaging". *Nat. Rev. Neurosci.* 8(9), 700-711 (2007). [doi: 10.1038/nrn2201].
- Fox, M. D., Snyder, A. Z., Vincent, J. L. and Raichle, M. E. "Intrinsic fluctuations within cortical systems account for intertrial variability in human behavior". *Neuron* 56(1), 171-184 (2007). [doi: 10.1016/j.neuron.2007.08.023].
- Franceschini, M. A., Toronov, V., Filiaci, M. E., Gratton, E., and Fantini, S. "On-line optical imaging of the human brain with 160-ms temporal resolution". *Opt. Exp.* 6(3), 49-57 (2000). [doi: 10.1364/OE.6.000049].
- Frank, M. C., Vul, E., and Saxe, R. "Measuring the development of social attention using free-viewing". *Infancy*, 17(4), 355-375 (2011). [doi: 10.1111/j.1532-7078.2011.00086.x].
- Fransson, P., Krüger, G., Merboldt, K. D., and Frahm, J. "Temporal characteristics of oxygenation-sensitive MRI responses to visual activation in humans". *Magn. Res. Med.* 39(6), 912-919 (1998). [doi: 10.1002/mrm.1910390608].
- Fransson, P. "Spontaneous low-frequency BOLD signal fluctuations: An fMRI investigation of the resting-state default mode of brain function hypothesis". *Hum. Brain Mapp.* 26(1), 15-29 (2005). [doi: 10.1002/hbm.20113].
- Fransson, P., Skiöld, B., Horsch, S., Nordell, A., Blennow, H. L. and Aden, U. "Resting-state networks in the infant brain". *Proc. Natl. Acad. Sci.* 104(39), 15531-15536 (2007). [doi: 10.1073/pnas.0704380104].
- Fransson, P., Skiöld, B., Engstrom, M., Hallberg, B., Mosskin, M., Aden, U., Lagercrantz, H. and Blennow, M. "Spontaneous brain activity in the newborn brain during natural sleep—An fMRI study in infants born at full term". *Pediatr. Res.* 66(3), 301-5 (2009). [doi: 10.1203/PDR.0b013e3181b1bd84].
- Fransson P, Åden U, Blennow M and Lagercrantz H "The functional architecture of the infant brain as revealed by resting-state fMRI". *Cereb Cortex*, 21:145-154 (2010). [doi: 10.1093/cercor/bhq071].
- Friederici, A. D. "Towards a neural basis of auditory sentence processing". *Trends Cogn. Sci.* 6(2), 78-84 (2002). [doi: 10.1016/S1364-6613(00)01839-8].
- Friston, K. J., Josephs, O., Zarahn, E., Holmes, A. P., Rouquette, S. and Poline, J. "To smooth or not to smooth? Bias and efficiency in fMRI time-series analysis" *Neuroimage* 12(2), 196-208 (2000). [doi: 10.1006/nimg.2000.0609].
- Frostig, R. D., Lieke, E. E., Ts'o, D. Y., and Grinvald, A. "Cortical functional architecture and local coupling between neuronal activity and the microcirculation revealed by in vivo high-resolution optical imaging of intrinsic signals". *P. Natl. Acad. Sci.* 87(16), 6082-6086 (1990). [doi: 10.1073/pnas.87.16.6082].

- Fuchino, Y., Naoi, N., Shibata, M., Niwa, F., Kawai, M., Konishi, Y., Okanoya, K., and Myowa-Yamakoshi, M. "Effects of preterm birth on intrinsic fluctuations in neonatal cerebral activity examined using optical imaging". *PloS one*, 8(6) (2013). [doi: 10.1371/journal.pone.0067432].
- Fukui, Y., Ajichi, Y., and Okada, E. "Monte Carlo prediction of near-infrared light propagation in realistic adult and neonatal head models". *App. Opt.* 42(16), 2881-2887 (2003). [doi: 10.1364/AO.42.002881].
- Gagnon, L., Perdue, K., Greve, D. N., Goldenholz, D., Kaskhedikar, G., and Boas, D. A. "Improved recovery of the hemodynamic response in diffuse optical imaging using short optode separations and state-space modeling". *Neuroimage*, 56(3), 1362-1371 (2011). [doi: 10.1016/j.neuroimage.2011.03.001].
- Gagnon, L., Yücel, M. A., Boas, D. A., and Cooper, R. J. "Further improvement in reducing superficial contamination in fNIRS using double short separation measurements," *Neuroimage* 85(Pt 1), 127-135 (2014). [doi: 10.1016/j.neuroimage.2013.01.073].
- Gao, W., Zhu, H., Giovanello, K. S., Smith, J. K., Shen, D., Gilmore, J. H. and Lin, W. "Evidence on the emergence of the brain's default network from 2-week-old to 2-year-old healthy pediatric subjects". *Proc. Natl. Acad. Sci. USA*, 106(16) 6790-6795 (2009). [doi: 10.1073/pnas.0811221106].
- Gao, W., Alcauter, S., Elton, A., Hernandez-Castillo, C. R., Smith, J. K., Ramirez, J. and Lin, W. "Functional network development during the first year: relative sequence and socioeconomic correlations". *Cereb. Cortex* 25(9), 2919-2928 (2015). [doi: 10.1093/cercor/bhu088].
- Gao, W., Lin, W., Grewen, K., and Gilmore, J. H. "Functional connectivity of the infant human brain: plastic and modifiable". *Neuroscientist* 23(2), 169-184 (2017). [doi: 10.1177/1073858416635986].
- García-Pentón, L., Fernández, A. P., Iturria-Medina, Y., Gillon-Dowens, M., and Carreiras, M. "Anatomical connectivity changes in the bilingual brain". *Neuroimage* 84, 495-504 (2014). [doi: 10.1016/j.neuroimage.2013.08.064].
- García-Sierra, A., Rivera-Gaxiola, M., Percaccio, C. R., Conboy, B. T., Romo, H., Klarman, L., Ortiz, S., and Kuhl, P. K. "Bilingual language learning: An ERP study relating early brain responses to speech, language input, and later word production". *J. Phon.* 39(4), 546-557 (2011). [doi: 10.1016/j.wocn.2011.07.002].
- García-Sierra, A., Ramírez-Esparza, N., and Kuhl, P. K. "Relationships between quantity of language input and brain responses in bilingual and monolingual infants". *Int. J. Psychophys.* 110, 1-17 (2016). [doi: 10.1016/j.ijpsycho.2016.10.004].
- Geng, S., Liu, X., Biswal, B. B., and Niu, H. "Effect of resting-state fNIRS scanning duration on functional brain connectivity and graph theory metrics of brain network". *Front. Neurosci.* 11, 392 (2017). [doi: 10.3389/fnins.2017.00392].
- Gervain, J., Macagno, F., Cogoi, S., Peña, M., and Mehler, J. "The neonate brain detects speech structure. P. *Natl. Acad. Sci.* 105(37), 14222-14227 (2008). [doi: 10.1073/pnas.0806530105].
- Gervain, J., and Mehler, J. "Speech perception and language acquisition in the first year of life". *Annu. Rev. Psychol.* 61, 191-218 (2010). [doi: 10.1146/annurev.psych.093008.100408].
- Gervain, J., Mehler, J., Werker, J. F., Nelson, C. A., Csibra, G., Lloyd-Fox, S., Shukla, M. and Aslin, R. N. "Near-infrared spectroscopy: a report from the McDonnell infant methodology consortium". *Dev. Cogn. Neurosci.* 1(1), 22-46 (2011). [doi: 10.1016/j.dcn.2010.07.004].
- Gibson, A. P., Hebden, J. C., and Arridge, S. R. "Recent advances in diffuse optical imaging". *Phys. Med. Biol.* 50(4), R1 (2005). [doi: 10.1088/0031-9155/50/4/R01].
- Gitelman, D. R., Penny, W. D., Ashburner, J. and Friston, K. J. "Modeling regional and psychophysiologic interactions in fMRI: the importance of hemodynamic deconvolution". *Neuroimage* 19(1), 200-7 (2003). [doi: 10.1016/S1053-8119(03)00058-2].
- Golub, G. H., and Van Loan, C. F. (2012). Matrix computations (Vol. 3). JHU press.
- Grady, C. L., Luk, G., Craik, F. I., and Bialystok, E. "Brain network activity in monolingual and bilingual older adults". *Neuropsychologia* 66, 170-181 (2015). [doi: 10.1016/j.neuropsychologia.2014.10.042].
- Granger, C. W. J. and Newbold, P. "Spurious regressions in econometrics". *J. Econom.* 2(2), 111-120 (1974). [doi: 10.1016/0304-4076(74)90034-7].
- Graven, S. N., and Browne, J. V. "Auditory development in the fetus and infant". *Newborn Infant Nursing Rev.* 8(4), 187-193 (2008). [doi: 10.1053/j.nainr.2008.10.010].

- Grinvald A, Frostig RD, Siegel RM and Bartfeld RM. "High-resolution optical imaging of functional brain architecture in the awake monkey". Proc. Natl. Acad. Sci. USA, 1991;88:11559-11563 (1991). [doi: 10.1073/pnas.88.24.11559].
- Grossmann, T., Oberecker, R., Koch, S. P., and Friederici, A. D. "The developmental origins of voice processing in the human brain". Neuron, 65(6), 852-858 (2010). [doi: 10.1016/j.neuron.2010.03.001].
- Grossmann, T., Lloyd-Fox, S., and Johnson, M. H. "Brain responses reveal young infants' sensitivity to when a social partner follows their gaze". Dev. Cog. Neurosci. 6, 155-161 (2013). [doi: 10.1016/j.dcn.2013.09.004].
- Gullifer, J. W., Chai, X. J., Whitford, V., Pivneva, I., Baum, S., Klein, D., and Titone, D. (2018). "Bilingual experience and resting-state brain connectivity: Impacts of L2 age of acquisition and social diversity of language use on control networks". Neuropsychologia, 117, 123-134 (2018). [doi: 10.1016/j.neuropsychologia.2018.04.037].
- Hampson, M., Driesen, N., Roth, J. K., Gore, J. C., and Constable, R. T. "Functional connectivity between task-positive and task-negative brain areas and its relation to working memory performance". Magn. Reson. Imaging 28(8), 1051-1057 (2010).
- Harris, J. J., Reynell, C., and Attwell, D. "The physiology of developmental changes in BOLD functional imaging signals". Dev. Cogn. Neurosci. 1(3), 199-216 (2011). [doi: 10.1016/j.dcn.2011.04.001].
- Hassanpour, M. S., White, B. R., Eggebrecht, A. T., Ferradal, S. L., Snyder, A. Z., and Culver, J. P. "Statistical analysis of high density diffuse optical tomography". Neuroimage, 85, 104-116 (2014). [doi: 10.1016/j.neuroimage.2013.05.105].
- Hassanpour MS, Eggrebeck AT, Peele JE and Culver JP. "Mapping effective connectivity within cortical networks with diffuse optical tomography". Neurophotonics 4(4): 041402 (2017). [doi: 10.1117/1.NPh.4.4.041402].
- Hebden, J. C., and Delpy, D. T. "Enhanced time-resolved imaging with a diffusion model of photon transport". Opt. Lett. 19(5), 311-313 (1994). [doi: 10.1364/OL.19.000311].
- Hickok, G., and Poeppel, D. "The cortical organization of speech processing". Nat. Revs. Neurosci. 8(5), 393-402 (2007). [doi: 10.1038/nrn2113].
- Himberg, J., Hyvärinen, A., and Esposito, F. "Validating the independent components of neuroimaging time series via clustering and visualization". Neuroimage 22(3), 1214-1222 (2004). [doi: 10.1016/j.neuroimage.2004.03.027].
- Hocke, L. M., Oni, I. K., Duszynski, C. C., Corrigan, A. V., Frederick, B. D., and Dunn, J. F. "Automated processing of fNIRS data – a visual guide to the pitfalls and consequences". Algorithms, 11(5), 67 (2018). [doi: 10.3390/a11050067].
- Höhle, B., Bijeljac-Babic, R., and Nazzi, T. "Variability and stability in early language acquisition: Comparing monolingual and bilingual infants' speech perception and word recognition". Biling: Lang. Cogn. 23(1), 56-71 (2020). [doi: 10.1017/S1366728919000348].
- Holper, L., Scholkemann, F. and Seifritz, E., "Time-frequency dynamics of intra- and extracerebral hemodynamic functional connectivity during resting-state and respiratory challenges assessed by multimodal functional near-infrared spectroscopy". Neuroimage 120, 481- 492 (2015). [doi: 10.1016/j.neuroimage.2015.07.021].
- Homae, F., Watanabe, H., Nakano, T., Asakawa, K., and Taga, G. "The right hemisphere of sleeping infant perceives sentential prosody". J. Neurosci, Res. 54(4), 276-280 (2006). [doi: 10.1016/j.jneures.2005.12.006].
- Homae, F., Watanabe, H., Otobe, T., Nakano, T., Go, T., Konishi, Y. and Taga, G. "Development of global cortical networks in early infancy". J. Neurosci. 30(14), 4877-4882 (2010). [doi: 10.1523/JNEUROSCI.5618-09.2010].
- Homae, F., Watanabe, H., Nakano, T. and Taga, G. "Large-scale brain networks underlying language acquisition in early infancy". Front. Psychol. 2, 93 (2011). [doi: 10.3389/fpsyg.2011.00093].
- Honey, C.J., Sporns, O., Cammoun, L., Gigandet, X., Thiran, J. P., Meuli, R., and Hagmann, P. "Predicting human resting-state functional connectivity from structural connectivity". Proc. Natl. Acad. Sci. 106(6), 2035-2040 (2009). [doi: 10.1073/pnas.0811168106].
- Hoshi, Y., and Tamura, M. "Detection of dynamic changes in cerebral oxygenation coupled to neuronal function during mental work in man". Neurosci. Lett. 150(1), 5-8 (1993). [doi: 10.1016/0304-3940(93)90094-2].

- Hoshi, Y., Kohri, S., Matsumoto, Y., Cho, K., Matsuda, T., Okajima, S., and Fujimoto, S. "Hemodynamic responses to photic stimulation in neonates". *Ped. Neur.* 23(4), 323-327 (2000). [doi: 10.1016/S0887-8994(00)00195-8].
- Hu, X., Le, T. H., Ugurbil, K. "Evaluation of the early response in fMRI in individual subjects using short stimulus duration". *Magn. Reson. Med.* 37:877-884 (1997). [doi: 10.1002/mrm.1910370612].
- Hu, X. S., Arredondo, M. M., Gomba, M., Confer, N., DaSilva, A. F., Johnson, T. D., Shalinsky, M. and Kovelman, I. "Comparison of motion correction techniques applied to functional near-infrared spectroscopy data from children". *J. Biomed. Opt.* 20(12), 126003 (2015). [doi: 10.1117/1.JBO.20.12.126003].
- Huber, L. Handwerker, D. A., Jangraw, D. C., Chen, G., Hall, A., Stüber, C., Gonzalez-Castillo, J., Ivanov, D., Marrett, S., Guidi, M., Goense, J., Posner, B. A. and Bandettini, P. A. "High-Resolution CBV-fMRI allows mapping of laminar activity and connectivity of cortical input and output in human M1". *Neuron* 96(6), 1253-1263.e7 (2017). [doi: 10.1016/j.neuron.2017.11.005].
- Hull, R., and Vaid, J. "Bilingual language lateralization: A meta-analytic tale of two hemispheres". *Neuropsychologia*, 45(9), 1987-2008 (2007). [doi: 10.1016/j.neuropsychologia.2007.03.002].
- Huppert, T. J., Diamond, S. G., Franceschini, M. A. and Boas, D. A. "HomER: a review of time-series analysis methods for near-infrared spectroscopy of the brain". *Appl. Opt.* 48(10), D280-98 (2009). [doi: 10.1364/AO.48.00D280].
- Huppert, T. J. "Commentary on the statistical properties of noise and its implication on general linear models in functional near-infrared spectroscopy". *Neurophotonics* 3(1), 10401 (2016). [doi: 10.1117/1.NPh.3.1.10401].
- Hyde, D. C., Boas, D. A., Blair, C., and Carey, S. "Near-infrared spectroscopy shows right parietal specialization for number in pre-verbal infants". *Neuroimage*, 53(2), 647-652 (2010). [doi: 10.1016/j.neuroimage.2010.06.030].
- Hyvarinen, A. "Fast and robust fixed-point algorithms for independent component analysis". *IEEE Trans. Neural Netw.* 10(3), 626-634 (1999). [doi: 10.1109/72.761722].
- Imai, M., Watanabe, H., Yasui, K., Kimura, Y., Shitara, Y., Tsuchida, S., Takahashi, N. and Taga, G. "Functional connectivity of the cortex of term and preterm infants and infants with Down's syndrome". *Neuroimage* 85, 272-278 (2014). [doi: 10.1016/j.neuroimage.2013.04.080].
- Issard, C., and Gervain, J. "Variability of the hemodynamic response in infants: Influence of experimental design and stimulus complexity". *Dev. Cogn. Neurosci.* 33, 182-193 (2018). [doi: 10.1016/j.dcn.2018.01.009].
- Issard, C., and Gervain, J. "Adult-like processing of time-compressed speech by newborns: A NIRS study". *Dev. Cogn. Neurosci.* 25, 176-184 (2017). [doi: 10.1016/j.dcn.2016.10.006].
- Jahani, S., Setarehdan, S. K., Boas, D. A., and Yücel, M. A. "Motion artifact detection and correction in functional near-infrared spectroscopy: a new hybrid method based on spline interpolation method and Savitzky-Golay filtering". *Neurophotonics*, 5(1), 015003 (2018). [doi: 10.1117/1.NPh.5.1.015003].
- James, O., Park, H., and Kim, S. G. "Impact of sampling rate on statistical significance for single subject fMRI connectivity analysis". *Hum. Brain Mapp.* 40(11), 3321-3337 (2019). [doi: 10.1002/hbm.24600].
- Jardri, R., Pins, D., Houfflin-Debarge, V., Chaffiotte, C., Rocourt, N., Pruvo, J. P., Steinling, M., Delion, P., and Thomas, P. "Fetal cortical activation to sound at 33 weeks of gestation: a functional MRI study". *Neuroimage*, 42(1), 10-18 (2008). [doi: 10.1016/j.neuroimage.2008.04.247].
- Jasdzewski, G., Strangman, G., Wagner, J., Kwong, K. K., Poldrack, R. A., and Boas, D. A. "Differences in the hemodynamic response to event-related motor and visual paradigms as measured by near-infrared spectroscopy". *Neuroimage*, 20(1), 479-488 (2003). [doi: 10.1016/S1053-8119(03)00311-2].
- Jasper, H. H. "The ten-twenty electrode system of the International Federation". *Electroencephalogr. Clin. Neurophysiol.*, 10, 370-375 (1958).
- Jiang, P., Vuontela, V., Tokariev, M., Lin, H., Aronen, E. T., Ma, Y., and Carlson, S. "Functional connectivity of intrinsic cognitive networks during resting state and task performance in preadolescent children". *PLoS one*, 13(10) (2018). [doi: 10.1371/journal.pone.0205690].
- Jobsis, F. F. "Noninvasive, infrared monitoring of cerebral and myocardial oxygen sufficiency and circulatory parameters". *Science*, 198(4323), 1264-1267 (1977). [doi: 10.1126/science.929199].

- Kabdebon, C., Leroy, F., Simmonet, H., Perrot, M., Dubois, J., and Dehaene-Lambertz, G. "Anatomical correlations of the international 10-20 sensor placement system in infants". *Neuroimage*, 99, 342-356 (2014). [doi: 10.1016/j.neuroimage.2014.05.046].
- Kalashnikova, M., Pejovic, J., and Carreiras, M. (in press). "The effects of bilingualism on attentional processes in the first year of life". *Developmental Science*. [doi: <https://doi.org/10.1111/desc.13011>].
- Kao, M. H., Mandal, A., Lazar, N., and Stusken, J. "Multi-objective optimal experimental designs for event-related fMRI studies". *NeuroImage*, 44(3), 849-856 (2009). [doi: 10.1016/j.neuroimage.2008.09.025].
- Kato, T., Kamei, A., Takashima, S., and Ozaki, T. "Human visual cortical function during photic stimulation monitoring by means of near-infrared spectroscopy". *J. Cereb. Blood Flow Metab.* 13(3), 516-520 (1993). [doi: 10.1038/jcbfm.1993.66].
- Kamran, M. A., Naeem Mannan, M. M., and Jeong, M. Y. "Initial-dip existence and estimation in relation to DPF and data drift". *Front. Neuroinform.* 12, 96 (2018). [doi: 10.3389/fninf.2018.00096].
- Karahanoglu, F. I., Caballero-Gaudes, C., Lazeyras, F. and Van De Ville, D. "Total activation: fMRI deconvolution through spatio-temporal regularization". *Neuroimage* 73, 121-134 (2013). [doi: 10.1016/j.neuroimage.2013.01.067].
- Keehn, B., Wagner, J. B., Tager-Flusberg, H. and Nelson, C. A. "Functional connectivity in the first year of life in infants at-risk for autism: a preliminary near-infrared spectroscopy study". *Front. Hum. Neurosci.* 7, 444 (2013). [doi: 10.3389/fnhum.2013.00444].
- Kersey, A. J., and Emberson, L. L. "Tracing trajectories of audio-visual learning in the infant brain". *Dev. Sci.* 20(6), e12480 (2017). [doi: 10.1111/desc.12480].
- Keunen, K., Counsell, S. J., and Benders, M. J. "The emergence of functional architecture during early brain development". *Neuroimage*, 160, 2-14 (2017). [doi: 10.1016/j.neuroimage.2017.01.047].
- Keysers, C., Gazzola, V., and Wagenmakers, E. J. "Using Bayes factor hypothesis testing in neuroscience to establish evidence of absence". *Nat. Neurosci.* 23(7), 788-799 (2020). [doi: 10.1038/s41593-020-0660-4].
- Kirilina, E., Jelzow, A., Heine, A., Niessing, M., Wabnitz, H., Brühl, R., Itterman, B., Jacobs, A. M., and Tachtsidis, I. (2012). "The physiological origin of task-evoked systemic artefacts in functional near infrared spectroscopy". *Neuroimage*, 61(1), 70-81 (2012). [doi: 10.1016/j.neuroimage.2012.02.074].
- Kirilina, E., Yu, N., Jelzow, A., Wabnitz, H., Jacobs, A. M., and Tachtsidis, I. "Identifying and quantifying main components of physiological noise in functional near infrared spectroscopy on the prefrontal cortex". *Front. Hum. Neurosci* 7, 864 (2013). [doi: 10.3389/fnhum.2013.00864].
- Kotilahti, K., Nissilä, I., Näsi, T., Lipiäinen, L., Noponen, T., Meriläinen, P., Huotilainen, M., Fellman, V. (2010). "Hemodynamic responses to speech and music in newborn infants". *Hum. Brain Mapp.* 31(4), 595-603 (2010), [doi: 10.1002/hbm.20890].
- Kousaie, S., Chai, X. J., Sander, K. M., and Klein, D. "Simultaneous learning of two languages from birth positively impacts intrinsic functional connectivity and cognitive control". *Brain Cogn* 117, 49-56 (2017). [doi: 10.1016/j.bandc.2017.06.003].
- Kovács, Á. M., and Mehler, J. "Cognitive gains in 7-month-old bilingual infants". *Proc. Natl. Acad. Sci. USA*, 106(16), 6556-6560 (2009a). [doi: 10.1073/pnas.0811323106].
- Kovacs, A. M., and Mehler, J. "Flexible learning of multiple speech structures in bilingual infants". *Science*, 325, 611-612 (2009b). [doi: 10.1126/science.1173947].
- Kovács, Á. M. "Cognitive adaptations induced by a multi-language input in early development". *Curr. Opin. Neurobiol.* 35, 80-86 (2015). [doi: 10.1016/j.conb.2015.07.003].
- Kovacsova, Z., Bale, G., Mitra, S., de Roeck, I., Meek, J., Robertson, N., and Tachtsidis, I. "Investigation of confounding factors in measuring tissue saturation with NIRS spatially resolved spectroscopy". *Adv. Exp. Med. Biol.* 1072, 307-312 (2018). Springer, Cham. [doi: 10.1007/978-3-319-91287-5_49].
- Kozberg, M., and Hillman, E. "Neurovascular coupling and energy metabolism in the developing brain". *Progress in brain research*, 225 (ch. 10), 213-242 (2016). Elsevier. [doi: 10.1016/bs.pbr.2016.02.002].
- Krizman, J., Marian, V., Shook, A., Skoe, E., and Kraus, N. "Subcortical encoding of sound is enhanced in bilinguals and relates to executive function advantages". *Proc. Natl. Acad. Sci. USA*, 109(20), 7877-7881 (2012). [doi: 10.1073/pnas.1201575109].

- Kuhl, P. K., Stevens, E., Hayashi, A., Deguchi, T., Kiritani, S., and Iverson, P. "Infants show a facilitation effect for native language phonetic perception between 6 and 12 months". *Dev. Sci.* 9(2), F13-F21 (2006). [doi: 10.1111/j.1467-7687.2006.00468.x].
- Kuhl, P. K., Conboy, B. T., Coffey-Corina, S., Padden, D., Rivera-Gaxiola, M., and Nelson, T. "Phonetic learning as a pathway to language: new data and native language magnet theory expanded (NLM-e)". *Philos. T. R. Soc. B.* 363(1493), 979-1000 (2008). [doi: 10.1098/rstb.2007.2154].
- Kuhl, P. K. "Brain mechanisms underlying the critical period for language: Linking theory and practice". *Hum Neuroplast. Educ.* 27, 33 (2010a).
- Kuhl, P. K. "Brain mechanisms in early language acquisition". *Neuron*, 67(5), 713-727 (2010b). [doi: 10.1016/j.neuron.2010.08.038].
- Larraza, S., Molnar, M., and Samuel, A. G. "Phonemic contrasts under construction? Evidence from Basque". *Infancy*, 25(3), 304-318 (2020). [doi: 10.1111/infa.12330].
- Lee, C. W., Blanco, B., Dempsey, L., Chalia, M., Hebden, J. C., Caballero-Gaudes, C., Austin, T., and Cooper, R. J. "Sleep state modulates resting-state functional connectivity in neonates". *Front. Neurosci.* 14, 347 (2020). [doi: 10.3389/fnins.2020.00347].
- Lewkowicz, D. J., and Hansen-Tift, A. M. "Infants deploy selective attention to the mouth of a talking face when learning speech". *Proc. Natl. Acad. Sci. USA*, 109, 1431-1436 (2012). [doi: 10.1073/pnas.1114783109].
- Lin, W., Zhu, Q., Gao, W., Chen, Y., Toh, C. H., Styner, M., Gerig, G., Smith, J. K., Biswal, B. and Gilmore, J. H. "Functional connectivity MR imaging reveals cortical functional connectivity in the developing brain". *AJNR. Am. J. Neuroradiol.* 29(10), 1883-9 (2008). [doi: 10.3174/ajnr.A1256].
- Lindauer, U., Royl, G., Leithner, C., Kühl, M., Gold, L., Gethmann, J., Kohl-Bareis M., Villringer, A. and Dirnagl, U. "No evidence for early decrease in blood oxygenation in rat whisker cortex in response to functional activation". *Neuroimage*, 13(6), 988-1001 (2001). [doi: 10.1006/nimg.2000.0709].
- Lindquist, M. A., Geuter, S., Wager, T. D., and Caffo, B. S. "Modular preprocessing pipelines can reintroduce artifacts into fMRI data". *Hum. Brain Mapp.* 40(8), 2358-2376 (2019). [doi: 10.1002/hbm.24528].
- Linke, A. C., Wild, C., Zubiaurre-Elorza, L., Herzmann, C., Duffy, H., Han, V. K., Lee, D.S.C. and Cusack, R. "Disruption to functional networks in neonates with perinatal brain injury predicts motor skills at 8 months". *Neuroimage Clin.* 18, 399-406 (2018). [doi: 10.1016/j.nicl.2019.101670].
- Lloyd-Fox, S., Blasi, A., Volein, A., Everdell, N., Elwell, C. E., and Johnson, M. H. "Social perception in infancy: a near infrared spectroscopy study". *Child Dev.* 80(4), 986-999 (2009). [doi: 10.1111/j.1467-8624.2009.01812.x].
- Lloyd-Fox, S., Blasi, A., and Elwell, C. E. "Illuminating the developing brain: the past, present and future of functional near infrared spectroscopy". *Neurosci. Biobehav. Rev.* 34(3), 269-284 (2010). [doi: 10.1016/j.neubiorev.2009.07.008].
- Lloyd-Fox, S., Blasi, A., Everdell, N., Elwell, C. E., and Johnson, M. H. "Selective cortical mapping of biological motion processing in young infants". *J. Cogn. Neurosci.* 23(9), 2521-2532 (2011). [doi: 10.1162/jocn.2010.21598].
- Lloyd-Fox, S., Papademetriou, M., Darboe, M. K., Everdell, N. L., Wegmuller, R., Prentice, A. M., Moore, S. E., and Elwell, C. E. "Functional near infrared spectroscopy (fNIRS) to assess cognitive function in infants in rural Africa". *Sci. Rep.* 4, 4740 (2014). [doi: 10.1038/srep04740].
- Lloyd-Fox, S., Richards, J. E., Blasi, A., Murphy, D. G., Elwell, C. E., and Johnson, M. H. Coregistering functional near-infrared spectroscopy with underlying cortical areas in infants. *Neurophotonics*, 1(2), 025006 (2014). [doi: 10.1111/1.NPh.1.2.025006].
- Lloyd-Fox, S., Begus, K., Halliday, D., Pirazzoli, L., Blasi, A., Papademetriou, M., Darboe, M. K., Prentice, A.M., Johnson, M. H., Moore, S. E. and Elwell, C. E. "Cortical specialisation to social stimuli from the first days to the second year of life: A rural Gambian cohort". *Dev. Cog. Neurosci.* 25, 92-104 (2017). [doi: 10.1016/j.dcn.2016.11.005].
- Lloyd-Fox, S., Blasi, A., McCann, S., Rozhko, M., Katus, L., Mason, L., Austin, T., Moore, S. E., Elwell, C., and BRIGHT project team. (2019). "Habituation and novelty detection fNIRS brain responses in 5-and 8-month-old infants: The Gambia and UK". *Dev. Sci.* 22(5), e12817 (2019). [doi: 10.1111/desc.12817].

- Logothetis, N. K., Pauls, J., Augath, M., Trinath, T., and Oeltermann, A. "Neurophysiological investigation of the basis of the fMRI signal". *Nature*, 412(6843), 150-157 (2001). [doi: 10.1038/35084005].
- Lombardi, F., Herrmann, H. J. and de Arcangelis, L. "Balance of excitation and inhibition determines 1/f power spectrum in neuronal networks". *Chaos Interdiscip. J. Nonlinear Sci.* 27, 47402 (2017). [doi: 10.1523/JNEUROSCI.21-04-01370.2001].
- Lu, C. M., Zhang, Y. J., Biswal, B. B., Zang, Y. F., Peng, D. L., and Zhu, C. Z. "Use of fNIRS to assess resting state functional connectivity". *J. Neurosci. Methods* 186(2), 242-249 (2010). [doi: 10.1016/j.jneumeth.2009.11.010].
- Luk, G., Bialystok, E., Craik, F. I., and Grady, C. L. "Lifelong bilingualism maintains white matter integrity in older adults". *J. Neurosci.* 31(46), 16808-16813 (2011). [doi: 10.1523/JNEUROSCI.4563-11.2011].
- MacLeod, A. A., Stoel-Gammon, C., and Wassink, A. B. "Production of high vowels in Canadian English and Canadian French: A comparison of early bilingual and monolingual speakers". *J. Phonetics*, 37(4), 374-387. [doi: 10.1016/j.wocn.2009.07.001].
- Madsen, H. (2007). Time series analysis. CRC Press.
- Mahmoudzadeh, M., Dehaene-Lambertz, G., Fournier, M., Kongolo, G., Goudjil, S., Dubois, J., Grebe, R., and Wallois, F. "Syllabic discrimination in premature human infants prior to complete formation of cortical layers". *Proc. Natl. Acad. Sci. USA*, 110(12), 4846-4851 (2013). [doi: 10.1073/pnas.1212220110].
- Majeed, W., and Avison, M. J. "Robust data driven model order estimation for independent component analysis of fMRI data with low contrast to noise". *PLoS One*, 9(4): e94943 (2014). [doi: 10.1371/journal.pone.0094943].
- Malonek D and Grinvald A. "Interactions between electrical activity and cortical microcirculation revealed by imaging spectroscopy: implications for functional brain mapping". *Science*. 1996;272:551–554 (1996). [doi: 10.1126/science.272.5261.551].
- Mampe, B., Friederici, A. D., Christophe, A., and Wermke, K. "Newborns' cry melody is shaped by their native language". *Curr. Biol.* 19(23), 1994-1997 (2009). [doi: 10.1016/j.cub.2009.09.064].
- Mantini, D., Perrucci, M. G., Del Gratta, C., Romani, G. L. and Corbetta, M. "Electrophysiological signatures of resting state networks in the human brain". *Proc. Natl. Acad. Sci.* 104(32), 13170-13175 (2007). [doi: 10.1073/pnas.0700668104].
- Maris, E., and Oostenveld, R. "Nonparametric statistical testing of EEG-and MEG-data". *J. Neurosci. Methods*, 164(1), 177-190 (2007). [doi: 10.1016/j.jneumeth.2007.03.024].
- Matcher, S. J., Elwell, C. E., Cooper, C. E., Cope, M., and Delpy, D. T. "Performance comparison of several published tissue near-infrared spectroscopy algorithms". *Anal. Biochem.* 227(1), 54-68 (1995). [doi: 10.1006/abio.1995.1252].
- May, L., Byers-Heinlein, K., Gervain, J., and Werker, J. F. "Language and the newborn brain: does prenatal language experience shape the neonate neural response to speech?". *Front. Psychol.* 2, 222 (2011). [doi: 10.3389/fpsyg.2011.00222].
- May, L., Gervain, J., Carreiras, M., and Werker, J. F. "The specificity of the neural response to speech at birth". *Dev. Sci.* 21(3), e12564 (2017). [doi: 10.1111/desc.12564].
- McDonald, N. M., and Perdue, K. L. "The infant brain in the social world: Moving toward interactive social neuroscience with functional near-infrared spectroscopy". *Neurosci. Biobehav. Rev.* 87, 38-49 (2018). [doi: 10.1016/j.neubiorev.2018.01.007].
- Mechelli, A., Crinion, J. T., Noppeney, U., O'Doherty, J., Ashburner, J., Frackowiak, R. S., and Price, C. J. "Neurolinguistics: structural plasticity in the bilingual brain". *Nature* 431(7010), 757 (2004). [doi: 10.1038/431757a].
- Medvedev, A. V. "Does the resting state connectivity have hemispheric asymmetry? A near-infrared spectroscopy study". *Neuroimage* 85, 400-407 (2014). [doi: 10.1016/j.neuroimage.2013.05.092].
- Meek, J. H., Firbank, M., Elwell, C. E., Atkinson, J., Braddick, O., and Wyatt, J. S. "Regional hemodynamic responses to visual stimulation in awake infants". *Ped. Res.* 43(6), 840-843 (1998). [doi: 10.1203/00006450-199806000-00019].
- Mehler, J., Jusczyk, P., Lambertz, G., Halsted, N., Bertoni, J., and Amiel-Tison, C. "A precursor of language acquisition in young infants". *Cognition*, 29(2), 143-178 (1988). [doi: 10.1016/0010-0277(88)90035-2].

- Menon, R. S., Ogawa, S., Hu, X., Strupp, J. P., Anderson, P., and Uğurbil, K. "BOLD based functional MRI at 4 Tesla includes a capillary bed contribution: echo-planar imaging correlates with previous optical imaging using intrinsic signals". *Magn. Res. Med.* 33(3), 453-459 (1995). [doi: 10.1002/mrm.1910330323].
- Menon, V. "Large-scale brain networks and psychopathology: a unifying triple network model". *Trends Cogn. Sci.* 15(10), 483-506 (2011). [doi: 10.1016/j.tics.2011.08.003].
- Mensen, A., and Khatami, R. "Advanced EEG analysis using threshold-free cluster-enhancement and non-parametric statistics". *Neuroimage*, 67, 111-118 (2013). [doi: 10.1016/j.neuroimage.2012.10.027].
- Mercure, E., Evans, S., Pirazzoli, L., Goldberg, L., Bowden-Howl, H., Coulson-Thaker, K., ... and MacSweeney, M. "Language experience impacts brain activation for spoken and signed language in infancy: Insights from unimodal and bimodal bilinguals". *Neurobiol. Lang.* 1(1), 9-32 (2020). [doi: 10.1162/nol_a_00001].
- Mesquita, R. C., Franceschini, M. A. and Boas, D. A. "Resting state functional connectivity of the whole head with near-infrared spectroscopy". *Biomed. Opt. Express* 1(1), 324-336 (2010). [doi: 10.1364/BOE.1.000324].
- Meyer, M., Alter, K., Friederici, A. D., Lohmann, G., and von Cramon, D. Y. "fMRI reveals brain regions mediating slow prosodic modulations in spoken sentences". *Hum. Brain Mapp.* 17(2), 73-88 (2002). [doi: 10.1002/hbm.10042].
- Miao, X., Gu, H., Yan, L., Lu, H. Wang, D. J., Zhou, X. J., Zhuo, Y. and Yang, Y. "Detecting resting-state brain activity by spontaneous cerebral blood volume fluctuations using whole brain vascular space occupancy imaging". *Neuroimage* 84, 575-584 (2014). [doi: 10.1016/j.neuroimage.2013.09.019].
- Mills, D. L., Coffey-Corina, S. A., and Neville, H. J. "Language acquisition and cerebral specialization in 20-month-old infants". *J. Cogn. Neurosci.* 5(3), 317-334 (1993). [doi: 10.1162/jocn.1993.5.3.317].
- Mills, D. L., Coffey-Corina, S., and Neville, H. J. "Language comprehension and cerebral specialization from 13 to 20 months". *Dev. Neuropsychol.* 13(3), 397-445 (1997). [doi: 10.1080/87565649709540685].
- Minagawa-Kawai, Y., Mori, K., Hebden, J. C., and Dupoux, E. "Optical imaging of infants' neurocognitive development: recent advances and perspectives". *Dev. Neurobiol.* 68(6), 712-728 (2008). [doi: 10.1002/dneu.20618].
- Minagawa-Kawai, Y., Matsuoka, S., Dan, I., Naoi, N., Nakamura, K., and Kojima, S. "Prefrontal activation associated with social attachment: facial-emotion recognition in mothers and infants". *Cereb. Cortex*, 19(2), 284-292 (2009). [doi: 10.1093/cercor/bhm081].
- Minagawa-Kawai, Y., Van Der Lely, H., Ramus, F., Sato, Y., Mazuka, R., and Dupoux, E. "Optical brain imaging reveals general auditory and language-specific processing in early infant development". *Cereb. Cortex*, 21(2), 254-261 (2011). [doi: 10.1093/cercor/bhq082].
- Minka, T. P. "Automatic choice of dimensionality for PCA". *Adv. Neural Inf. Process Syst.* 598-604 (2001).
- Mohades, S. G., Struys, E., Van Schuerbeek, P., Mondt, K., Van De Craen, P., and Luypaert, R. "DTI reveals structural differences in white matter tracts between bilingual and monolingual children". *Brain Res.* 1435, 72-80 (2012). [doi: 10.1016/j.brainres.2011.12.005].
- Mohades, S. G., Van Schuerbeek, P., Rosseel, Y., Van De Craen, P., Luypaert, R., and Baeken, C. "White-matter development is different in bilingual and monolingual children: a longitudinal DTI study". *PloS one* 10(2), e0117968 (2015). [doi: 10.1371/journal.pone.0117968].
- Molavi, B., and Dumont, G. A. "Wavelet-based motion artifact removal for functional near-infrared spectroscopy". *Physiol. Meas.* 33(2), 259 (2012). [doi: 10.1088/0967-3334/33/2/259].
- Molavi, B., May, L., Gervain, J., Carreiras, M., Werker, J. F., and Dumont, G. A. "Analyzing the resting state functional connectivity in the human language system using near infrared spectroscopy". *Front. Hum. Neurosci.* 7, 921 (2014). [doi: 10.3389/fnhum.2013.00921].
- Molnar, M., Gervain, J., and Carreiras, M. "Within-rhythm class native language discrimination abilities of Basque-Spanish monolingual and bilingual infants at 3.5 months of age". *Infancy* 19(3), 326-337 (2014). [doi: 10.1111/infa.12041].
- Montero-Hernandez, S., Orihuela-Espina, F., Sucar, L., Pinti, P., Hamilton, A., Burgess, P., and Tachtsidis, I. "Estimating functional connectivity symmetry between oxy-and deoxy-haemoglobin: implications for fNIRS connectivity analysis". *Algorithms* 11(5), 70 (2018). [doi: 10.3390/a11050070].

- Moon, C., Cooper, R. P., and Fifer, W. P. "Two-day-olds prefer their native language. Infant behavior and development", 16(4), 495-500 (1993). [doi: 10.1016/0163-6383(93)80007-U].
- Murphy, K., and Fox, M. D. "Towards a consensus regarding global signal regression for resting state functional connectivity MRI". Neuroimage 154, 169-173 (2017). [doi: 10.1016/j.neuroimage.2016.11.052].
- Nácar-García, L., Guerrero-Mosquera, C., Colomer, M., and Sebastián-Gallés, N. "Evoked and oscillatory EEG activity differentiates language discrimination in young monolingual and bilingual infants". Sci. Rep. 8(1), 2770 (2018). [doi: 10.1038/s41598-018-20824-0].
- Nakano, T., Watanabe, H., Homae, F., and Taga, G. "Prefrontal cortical involvement in young infants' analysis of novelty". Cereb. Cortex, 19(2), 455-463 (2009). [doi: 10.1093/cercor/bhn096].
- Nakato, E., Otsuka, Y., Kanazawa, S., Yamaguchi, M. K., Watanabe, S., and Kakigi, R. "When do infants differentiate profile face from frontal face? A near-infrared spectroscopic study". Hum. Brain Mapp. 30(2), 462-472 (2009). [doi: 10.1002/hbm.20516].
- Nakato, E., Otsuka, Y., Kanazawa, S., Yamaguchi, M. K., and Kakigi, R. "Distinct differences in the pattern of hemodynamic response to happy and angry facial expressions in infants—A near-infrared spectroscopic study". Neuroimage, 54(2), 1600-1606. (2011a). [doi: 10.1016/j.neuroimage.2010.09.021].
- Nakato, E., Otsuka, Y., Kanazawa, S., Yamaguchi, M. K., Honda, Y., and Kakigi, R. "I know this face: Neural activity during mother/face perception in 7-to 8-month-old infants as investigated by near-infrared spectroscopy". Early Hum. Dev. 87(1), 1-7 (2011b). [doi: 10.1016/j.earlhummdev.2010.08.030].
- Nazzi, T., Flocchia, C., and Bertoni, J. "Discrimination of pitch contours by neonates". Inf. Behav. Dev. 21(4), 779-784 (1998). [doi: 10.1016/S0163-6383(98)90044-3].
- Nippert, A. R., Biesecker, K. R., and Newman, E. A. "Mechanisms mediating functional hyperemia in the brain". Neuroscientist, 24(1), 73-83 (2018). [doi: 10.1177/1073858417703033].
- Niu, H., and He, Y. "Resting-state functional brain connectivity: lessons from functional near-infrared spectroscopy". Neuroscientist, 20(2), 173-188 (2014). [doi: 10.1177/1073858413502707].
- Nourhashemi, M., Mahmoudzadeh, M., Goudjil, S., Kongolo, G., and Wallois, F. "Neurovascular coupling in the developing neonatal brain at rest". Hum. Brain Mapp. 41(2), 503-519 (2020). [doi: 10.1002/hbm.24818].
- Novi, S. L., Rodrigues, R. B., and Mesquita, R. C. "Resting state connectivity patterns with near-infrared spectroscopy data of the whole head". Biomed. Opt. Express. 7(7), 2524-2537 (2016). [doi: 10.1364/BOE.7.002524].
- Obrig, H., Neufang, M., Wenzel, R., Kohl, M., Steinbreik, J., Einhäupl, K. and Villringer, A. "Spontaneous low frequency oscillations of cerebral hemodynamics and metabolism in human adults". Neuroimage 12, 623-639 (2000). [doi: 10.1006/nimg.2000.0657].
- Obrig, H. and Villringer, A. "Beyond the visible - Imaging the human brain with light". J. Cereb. Blood Flow Metab. 23(1), 1-18 (2003). [doi: 10.1097/01.WCB.0000043472.45775.29].
- Obrig, H. "NIRS in clinical neurology—a 'promising' tool?". Neuroimage, 85, 535-546 (2014). [doi: 10.1016/j.neuroimage.2013.03.045].
- Orihuela-Espina, F., Leff, D. R., James, D. R., Darzi, A. W., and Yang, G. Z. "Quality control and assurance in functional near infrared spectroscopy (fNIRS) experimentation". Phys. Med. Biol. 55(13), 3701 (2010). [doi: 10.1088/0031-9155/55/13/009].
- Otsuka, Y., Nakato, E., Kanazawa, S., Yamaguchi, M. K., Watanabe, S., and Kakigi, R. "Neural activation to upright and inverted faces in infants measured by near infrared spectroscopy". Neuroimage, 34(1), 399-406 (2007). [doi: 10.1016/j.neuroimage.2006.08.013].
- Ouyang, M., Kang, H., Detre, J. A., Roberts, T. P., Huang, H. "Short-range connections in the developmental connectome during typical and atypical brain maturation". Neurosci Biobehav Rev, 83, 109-122 (2017). [doi: 10.1016/j.neubiorev.2017.10.007].
- Parker Jones, Ō., Green, D. W., Grogan, A., Pliatsikas, C., Filippopolitis, K., Ali, N., Lee, H. L., Ramsden, S., Gazarian, K., Prejawa, S., Seghier, M. L and Price, C. J. "Where, when and why brain activation differs for bilinguals and monolinguals during picture naming and reading aloud". Cereb. Cortex 22(4), 892-902 (2011). [doi: 10.1093/cercor/bhr161].

- Patel, A. X., Kundu, P., Rubinov, M., Jones, P. S., Vértes, P. E., Ersche, K. D., Suckling, J. and Bullmore, E. T. "A wavelet method for modeling and despiking motion artifacts from resting-state fMRI time series". *Neuroimage*, 95, 287–304 (2014). [doi: 10.1016/j.neuroimage.2014.03.012].
- Patel, A. X., and Bullmore, E. T. "A wavelet-based estimator of the degrees of freedom in denoised fMRI time series for probabilistic testing of functional connectivity and brain graphs". *Neuroimage*, 142, 14–26 (2016). [doi: 10.1016/j.neuroimage.2015.04.052].
- Peña, M., Maki, A., Kovacić, D., Dehaene-Lambertz, G., Koizumi, H., Bouquet, F., and Mehler, J. "Sounds and silence: an optical topography study of language recognition at birth". *Proc. Natl. Acad. Sci. USA*, 100(20), 11702-11705 (2003). [doi: 10.1073/pnas.1934290100].
- Peña, M., Pittaluga, E., and Mehler, J. "Language acquisition in premature and full-term infants". *Proc. Natl. Acad. Sci. USA*, 107(8), 3823-3828 (2010). [doi: 10.1073/pnas.0914326107].
- Peña, M., Werker, J. F., and Dehaene-Lambertz, G. "Earlier speech exposure does not accelerate speech acquisition". *J. Neurosci.* 32(33), 11159-11163 (2012). [doi: 10.1523/JNEUROSCI.6516-11.2012].
- Perani, D., Saccuman, M. C., Scifo, P., Anwander, A., Spada, D., Baldoli, C., Poloniato, A., Lohman, G. and Friederici, A. D. "Neural language networks at birth". *Proc. Natl. Acad. Sci. USA*, 108(38), 16056-16061 (2011). [doi: 10.1073/pnas.1102991108].
- Perdue, K. L., Jensen, S. K., Kumar, S., Richards, J. E., Kakon, S. H., Haque, R., ... and Nelson, C. A. "Using functional near-infrared spectroscopy to assess social information processing in poor urban Bangladeshi infants and toddlers". *Dev. Sci.* 22(5), e12839 (2019). [doi: 10.1111/desc.12839].
- Pernet, C. R., Latinus, M., Nichols, T. E., and Rousselet, G. A. "Cluster-based computational methods for mass univariate analyses of event-related brain potentials/fields: A simulation study". *J. Neurosci. Methods*, 250, 85-93 (2015). [doi: 10.1016/j.jneumeth.2014.08.003].
- Petitto, L. A., Berens, M. S., Kovelman, I., Dubins, M. H., Jasinska, K., and Shalinsky, M. "The "Perceptual Wedge Hypothesis" as the basis for bilingual babies' phonetic processing advantage: New insights from fNIRS brain imaging". *Brain Lang.* 121(2), 130-143 (2012). [doi: 10.1016/j.bandl.2011.05.003].
- Pfeifer, M. D., Scholkmann, F. and Labryère, R. "Signal processing in functional near-infrared spectroscopy (fNIRS): methodological differences lead to different statistical results". *Front. Hum. Neurosci.* 11, 641 (2018). [doi: 10.3389/fnhum.2017.00641].
- Phan, P., Highton, D., Lai, J., Smith, M., Elwell, C., and Tachtsidis, I. "Multi-channel multi-distance broadband near-infrared spectroscopy system to measure the spatial response of cellular oxygen metabolism and tissue oxygenation". *Biomed. Opt. Exp.* 7(11), 4424-4440 (2016). [doi: 10.1364/BOE.7.004424].
- Piazza, E. A., Hasenfratz, L., Hasson, U., and Lew-Williams, C. "Infant and adult brains are coupled to the dynamics of natural communication". *Psych. Sci.* 31(1), 6-17 (2020). [doi: 10.1177/0956797619878698].
- Pinti, P., Scholkmann, F., Hamilton, A., Burgess, P., and Tachtsidis, I. "Current status and issues regarding pre-processing of fNIRS neuroimaging data: an investigation of diverse signal filtering methods within a general linear model framework". *Front. Hum. Neurosci.* 12, 505 (2019). [doi: 10.3389/fnhum.2018.00505].
- Polka, L., and Werker, J. F. "Developmental changes in perception of nonnative vowel contrasts". *J. Exp. Psychol. Hum. Percept. Perform.* 20(2), 421 (1994). [doi: 10.1037/0096-1523.20.2.421].
- Pons, F., Bosch, L., and Lewkowicz, D. J. "Bilingualism modulates infants' selective attention to the mouth of a talking face". *Psych. Science*, 26(4), 490-498 (2015). [doi: 10.1177/0956797614568320].
- Portas, C. M., Krakow, K., Allen, P., Josephs, O., Armony, J. L., and Frith, C. D. "Auditory processing across the sleep-wake cycle: simultaneous EEG and fMRI monitoring in humans". *Neuron*, 28(3), 991-999 (2000). [doi: 10.1016/S0896-6273(00)00169-0].
- Poulin-Dubois, D., Bialystok, E., Blaye, A., Polonia, A. and Yott, J. "Lexical access and vocabulary development in very young bilinguals". *Int. J. Bilingual.* 17:57-70 (2013). [doi: 10.1177/1367006911431198].
- Pritchard, W. S. "The brain in fractal time: 1/F-like power spectrum scaling of the human electroencephalogram". *Int. J. Neurosci.* 66, 119-129 (1992). [doi: 10.3109/00207459208999796].
- Quaresima, V., Bisconti, S., and Ferrari, M. "A brief review on the use of functional near-infrared spectroscopy (fNIRS) for language imaging studies in human newborns and adults". *Brain Lang.* 121(2), 79-89 (2012). [doi: 10.1016/j.bandl.2011.03.009].

- Raichle, M. E., MacLeod, A. M., Snyder, A. Z., Powers, W. J., Gusnard, D. A., and Shulman, G. L. "A default mode of brain function". Proc. Natl. Acad. Sci. USA, 98(2), 676-682 (2001). [doi: 10.1073/pnas.98.2.676].
- Ramus, F., Hauser, M. D., Miller, C., Morris, D., and Mehler, J. "Language discrimination by human newborns and by cotton-top tamarin monkeys". Science (New York, N.Y.), 288(5464), 349-51 (2000). [doi: 10.1126/science.288.5464.349].
- Richards, J. E., Sanchez, C., Phillips-Meek, M., and Xie, W. "A database of age-appropriate average MRI template". Neuroimage 124(B): 1254-1259 (2016). [doi: 10.1016/j.neuroimage.2015.04.055].
- Rivera-Gaxiola, M., Silva-Pereyra, J., and Kuhl, P. K. "Brain potentials to native and non-native speech contrasts in 7-and 11-month-old American infants". Dev. Sci. 8(2), 162-172 (2005). [doi: 10.1111/j.1467-7687.2005.00403.x].
- Robertson, F. C., Douglas, T. S., and Meintjes, E. M. "Motion artifact removal for functional near infrared spectroscopy: a comparison of methods". IEEE Trans. Biomed. Eng. 57(6), 1377-1387 (2010). [doi: 10.1109/TBME.2009.2038667].
- Saager, R. B., and Berger, A. J. "Measurement of layer-like hemodynamic trends in scalp and cortex: implications for physiological baseline suppression in functional near-infrared spectroscopy". J. Biomed. Opt. 13(3), 034017 (2008). [doi: 10.1117/1.2940587].
- Saint-Exupéry, A. and Woods, K. "The little prince". Harcourt, Brace and World. (1943).
- Sakatani, K., Chen, S., Lichty, W., Zuo, H., and Wang, Y. P. "Cerebral blood oxygenation changes induced by auditory stimulation in newborn infants measured by near infrared spectroscopy". Early Hum. Dev. 55(3), 229-236 (1999). [doi: 10.1016/S0378-3782(99)00019-5].
- Santosa, H., Aarabi, A., Perlman, S. B. and Huppert, T. J. "Characterization and correction of the false-discovery rates in resting state connectivity using functional near-infrared spectroscopy". J. Biomed. Opt. 22(5), 55002 (2017). [doi: 10.1117/1.JBO.22.5.055002].
- Santosa, H., Fishburn, F., Zhai, X., and Huppert, T. J. "Investigation of the sensitivity-specificity of canonical- and deconvolution-based linear models in evoked functional near-infrared spectroscopy". Neurophotonics, 6(2), 025009 (2019). [doi: 10.1117/1.NPh.6.2.025009].
- Sasai, S., Homae, F., Watanabe, H., and Taga, G. "Frequency-specific functional connectivity in the brain during resting state revealed by NIRS". Neuroimage 56(1), 252-257 (2011). [doi: 10.1016/j.neuroimage.2010.12.075].
- Sasai, S., Homae, F., Watanabe, H., Sasaki, A. T., Tanabe, H. C., Sadato, N., and Taga, G. "A NIRS-fMRI study of resting state network". Neuroimage, 63(1), 179-193 (2012). [doi: 10.1016/j.neuroimage.2012.06.011].
- Sato, H., Yahata, N., Funane, T., Takizawa, R., Katura, T., Atsumori, H., Nishimura, Y., Kinoshita, A., Kiguchi, M., Koizumi, H., Fukuda, M. and Kasai, K. "A NIRS-fMRI investigation of prefrontal cortex activity during a working memory task". Neuroimage, 83, 158-173 (2013). [doi: 10.1016/j.neuroimage.2013.06.043].
- Sebastián-Gallés, N., and Bosch, L. "Developmental shift in the discrimination of vowel contrasts in bilingual infants: Is the distributional account all there is to it?". Dev. Sci. 12(6), 874-887 (2009). [doi: 10.1111/j.1467-7687.2009.00829.x].
- Sebastián-Gallés, N., Albareda-Castellot, B., Weikum, W. M., and Werker, J. F. "A bilingual advantage in visual language discrimination in infancy". Psychol. Sci. 23(9), 994-999 (2012). [doi: 10.1177/0956797612436817].
- Selesnick, I. W., Gruber, H. L., Ding, Y., Zhang, T., and Barbour, R. L. "Transient artifact reduction algorithm (TARA) based on sparse optimization". IEEE Trans. Sign. Proc. 62(24), 6596-6611 (2014). [doi: 10.1109/TSP.2014.2366716].
- Scholkmann, F., Spichtig, S., Muehlemann, T., and Wolf, M. "How to detect and reduce movement artifacts in near-infrared imaging using moving standard deviation and spline interpolation". Physiol. Meas. 31(5), 649 (2010). [doi: 10.1088/0967-3334/31/5/004].
- Scholkmann, F., Gerber, U., Wolf, M., and Wolf, U. "End-tidal CO₂: an important parameter for a correct interpretation in functional brain studies using speech tasks". Neuroimage, 66, 71-79 (2013). [doi: 10.1016/j.neuroimage.2012.10.025].

- Scholkmann, F., and Wolf, M. "General equation for the differential pathlength factor of the frontal human head depending on wavelength and age". *J. Biomed. Opt.* 18(10), 105004 (2013). [doi: 10.1117/1.JBO.18.10.105004].
- Scholkmann, F., Kleiser, S., Metz, A. J., Zimmermann, R., Pavia, J. M., Wolf, U., and Wolf, M. "A review on continuous wave functional near-infrared spectroscopy and imaging instrumentation and methodology". *Neuroimage*, 85, 6-27 (2014). [doi: 10.1016/j.neuroimage.2013.05.004].
- Schweiger M., and Arridge S. R., "The Toast++ software suite for forward and inverse modeling in optical tomography" *J. Biomed. Opt.* 19(4), 040801 (2014). [doi: 10.1117/1.JBO.19.4.040801].
- Shafer, V. L., Yan, H. Y., and Datta, H. "The development of English vowel perception in monolingual and bilingual infants: neurophysiological correlates". *J. Phonetics*, 39(4), 527-545 (2011). [doi: 10.1016/j.wocn.2010.11.010].
- Shafer, V. L., Yan, H. Y., and Garrido-Nag, K. "Neural mismatch indices of vowel discrimination in monolingually and bilingually exposed infants: Does attention matter?". *Neurosci. Lett.* 526(1), 10-14 (2012). [doi: 10.1016/j.neulet.2012.07.064].
- Shekhar, S., Maria, A., Kotilahti, K., Huotilainen, M., Heiskala, J., Tuulari, J. J., Hirvi, P., Karlsson, L., Karlsson, H., and Nissilä, I. "Hemodynamic responses to emotional speech in two-month-old infants imaged using diffuse optical tomography". *Sci. Rep.* 9(1), 1-15 (2019). [doi: 10.1038/s41598-019-39993-7].
- Shmuel, A., Yacoub, E., Pfeuffer, J., Van De Moortele, P. F., Adriany, G., Ugurbil, K., and Hu, X. "Negative BOLD response and its coupling to the positive response in the human brain". *Neuroimage*, 13(6), 1005 (2001). [doi: 10.1016/S1053-8119(01)92341-9].
- Shultz, S., Vouloumanos, A., Bennett, R. H., and Pelpfrey, K. "Neural specialization for speech in the first months of life". *Dev. Sci.* 17(5), 766-774 (2014). [doi: 10.1111/desc.12151].
- Singh, L., Fu, C. S., Rahman, A. A., Hameed, W. B., Sanmugam, S., Agarwal, P., ... and GUSTO Research Team. "Back to basics: a bilingual advantage in infant visual habituation". *Child Dev.* 86(1), 294-302 (2015). [doi: 10.1111/cdev.12271].
- Smith, S. M., Fox, P. T., Miller, K. L., Glahn, D. C., Mickle Fox, P., Mackay, C. E., Filippini, N., Watkins, K. E., Toro, R., Laird, A. R. and Beckmann, C. F. "Correspondence of the brain's functional architecture during activation and rest". *Proc. Natl. Acad. Sci.* 106(31), 13040-13045 (2009). [doi: 10.1073/pnas.0905267106].
- Smith, S. M., and Nichols, T. E. "Threshold-free cluster enhancement: addressing problems of smoothing, threshold dependence and localisation in cluster inference". *Neuroimage*, 44(1), 83-98 (2009). [doi: 10.1016/j.neuroimage.2008.03.061].
- Smith, S. M., Miller, K. L., Moeller, S., Xu, J., Auerbach, E. J., Woolrich, M. W., Beckmann, C. F., Jenkinson, M., Andersson, J., Glasser, M. F., Van Essen, D. C., Feinberg, D., A., Yacoub, E. S., and Ugurbil, K. "Temporally-independent functional modes of spontaneous brain activity". *Proc. Natl. Acad. Sci. USA*, 109(8), 3131-3136 (2012). [doi: 10.1073/pnas.1121329109].
- Smyser, C. D., Inder, T. E., Shimony, J. S., Hill, J. E., Degnan, A. J., Snyder, A. Z., and Neil, J. J. "Longitudinal analysis of neural network development in preterm infants". *Cereb. Cortex* 20(12), 2852-2862 (2010). [doi: 10.1093/cercor/bhq035].
- Smyser, C. D., Snyder, A. Z., Shimony, J. S., Mitra, A., Inder, T. E., and Neil, J. J. (2016). Resting-state network complexity and magnitude are reduced in prematurely born infants. *Cereb. Cortex*, 26(1), 322-333 (2016). [doi: 10.1093/cercor/bhu251].
- Steinbrink, J., Villringer, A., Kempf, F., Haux, D., Boden, S., and Obrig, H. "Illuminating the BOLD signal: combined fMRI-fNIRS studies". *Magn. Res. Imag.* 24(4), 495-505 (2006). [doi: 10.1016/j.mri.2005.12.034].
- Stoica, P., and Moses, R. L. (2005). Spectral analysis of signals.
- Strangman, G., Boas, D. A., and Sutton, J. P. "Non-invasive neuroimaging using near-infrared light. *Biol. Psych.* 52(7), 679-693 (2002a). [doi: 10.1016/S0006-3223(02)01550-0].
- Strangman, G., Culver, J. P., Thompson, J. H., and Boas, D. A. "A quantitative comparison of simultaneous BOLD fMRI and NIRS recordings during functional brain activation". *Neuroimage*, 17(2), 719-731 (2002b). [doi: 10.1006/nimg.2002.1227].

- Strangman, G. E., Li, Z., and Zhang, Q. "Depth sensitivity and source-detector separations for near infrared spectroscopy based on the Colin27 brain template". *PloS one*, 8(8) (2013). [doi: 10.1371/journal.pone.0066319].
- Sulpizio, S., Del Maschio, N., Del Mauro, G., Fedeli, D., and Abutalebi, J. "Bilingualism as a gradient measure modulates functional connectivity of language and control networks". *Neuroimage*, 205, 116306 (2020). [doi: 10.1016/j.neuroimage.2019.116306].
- Sundara, M., Polka, L., and Baum, S. "Production of coronal stops by simultaneous bilingual adults". *Biling: Lang. Cogn.* 9(1), 97-114 (2006). [doi: 10.1017/S1366728905002403].
- Sundara, M., Polka, L., and Molnar, M. "Development of coronal stop perception: Bilingual infants keep pace with their monolingual peers". *Cognition*, 108, 232- 242 (2008). [doi: 10.1016/j.cognition.2007.12.013].
- Suzuki, S., Takasaki, S., Ozaki, T., and Kobayashi, Y. "Tissue oxygenation monitor using NIR spatially resolved spectroscopy". *Proc. SPIE 3597, Optical Tomography and Spectroscopy of Tissue III* (582-592) (1999). [doi: 10.1117/12.356862].
- Tachtsidis, I. and Scholkemann, F. "False positives and false negatives in functional near-infrared spectroscopy: issues, challenges, and the way forward". *Neurophotonics* 3(3), 31405 (2016). [doi: 10.1117/1.NPh.3.3.031405].
- Taga, G., Konishi, Y., Maki, A., Tachibana, T., Fujiwara, M., and Koizumi, H. "Spontaneous oscillation of oxy-and deoxy-hemoglobin changes with a phase difference throughout the occipital cortex of newborn infants observed using non-invasive optical topography". *Neurosci. Lett.* 282(1-2), 101-104 (2000). [doi: 10.1016/S0304-3940(00)00874-0].
- Taga, G., Watanabe, H., and Homae, F. "Spatial variation in the hemoglobin phase of oxygenation and deoxygenation in the developing cortex of infants". *Neurophotonics*, 5(1), 011017 (2017). [doi: 10.1117/1.NPh.5.1.011017].
- Taga, G., Watanabe, H., and Homae, F. "Developmental changes in cortical sensory processing during wakefulness and sleep". *Neuroimage*, 178, 519-530 (2018). [doi: 10.1016/j.neuroimage.2018.05.075].
- Tak, S., and Ye, J. C. "Statistical analysis of fNIRS data: a comprehensive review". *Neuroimage*, 85, 72-91 (2014). [doi: 10.1016/j.neuroimage.2013.06.016].
- Tarullo, A. R., Balsam, P. D., and Fifer, W. P. "Sleep and infant learning". *Infant Child Dev.* 20(1), 35-46 (2011). [doi: 10.1002/icd.685].
- Tavor, I., Jones, O. P., Mars, R. B., Smith, S. M., Behrens, T. E., and Jbabdi, S. "Task-free MRI predicts individual differences in brain activity during task performance". *Science*, 352(6282), 216-220 (2016). [doi: 10.1126/science.aad8127].
- Tenenbaum, E. J., Shah, R. J., Sobel, D. M., Malle, B. F., and Morgan, J. L. "Increased focus on the mouth among infants in the first year of life: A longitudinal eye-tracking study". *Infancy*, 18, 534-553 (2013). [doi: 10.1111/j.1532-7078.2012.00135.x].
- Telkemeyer, S., Rossi, S., Koch, S.P., Nierhaus, T., Steinbrink, J., Poeppel, D., Obrig, H. and Wartenburger, I. "Sensitivity of newborn auditory cortex to the temporal structure of sounds". *J. Neurosci.* 29(47), pp.14726-14733 (2009). [doi: 10.1523/JNEUROSCI.1246-09.2009].
- Telkemeyer, S., Rossi, S., Nierhaus, T., Steinbrink, J., Obrig, H., and Wartenburger, I. "Acoustic processing of temporally modulated sounds in infants: evidence from a combined near-infrared spectroscopy and EEG study". *Front. Psych.* 2, 62 (2011). [doi: 10.3389/fpsyg.2011.00062].
- Torricelli, A., Contini, D., Pifferi, A., Caffini, M., Re, R., Zucchelli, L., and Spinelli, L. "Time domain functional NIRS imaging for human brain mapping". *Neuroimage*, 85, 28-50 (2014). [doi: 10.1016/j.neuroimage.2013.05.106].
- Tsang, T., Atagi, N., and Johnson, S. P. "Selective attention to the mouth is associated with expressive language skills in monolingual and bilingual infants". *J. Exp. Child Psychol.* 169, 93-109 (2018). [doi: 10.1016/j.jecp.2018.01.002].
- Tsui, A., and Fennell, C. "Do bilingual infants possess enhanced cognitive skills? PsyArxiv (2019). [doi: 10.31234/osf.io/dcn7y].
- Tzourio-Mazoyer, N., Landeau, B., Papathanassiou, D., Crivello, F., Etard, O., Delcroix, N., Mazoyer, B., and Joliot, M. "Automated anatomical labeling of activations in SPM using a macroscopic anatomical

parcellation of the MNI MRI single-subject brain". *Neuroimage* 15(1), 273-289 (2003). [doi: 10.1006/nimg.2001.0978].

Uddin, L. Q., Supekar, K. S., Ryali, S., and Menon, V. "Dynamic reconfiguration of structural and functional connectivity across core neurocognitive brain networks with development". *J. Neurosci.* 31(50), 18578-18589 (2011). [doi: 10.1523/JNEUROSCI.4465-11.2011].

Urakawa, S., Takamoto, K., Ishikawa, A., Ono, T., and Nishijo, H. "Selective medial prefrontal cortex responses during live mutual gaze interactions in human infants: an fNIRS study". *Brain Topog.* 28(5), 691-701 (2015). [doi: 10.1007/s10548-014-0414-2].

Vannasing, P., Florea, O., González-Frankenberger, B., Tremblay, J., Paquette, N., Safi, D., ... and Gallagher, A. "Distinct hemispheric specializations for native and non-native languages in one-day-old newborns identified by fNIRS". *Neuropsychologia*, 84, 63-69 (2016). [doi: 10.1016/j.neuropsychologia.2016.01.038].

Van de Ven, V. G., Formisano, E., Prvulovic, D., Roeder, C. H., and Linden, D. E. "Functional connectivity as revealed by spatial independent component analysis of fMRI measurements during rest". *Hum. Brain Mapp.* 22(3), 165-178 (2004). [doi: 10.1002/hbm.20022].

Vanderwert, R. E., and Nelson, C. A. "The use of near-infrared spectroscopy in the study of typical and atypical development". *Neuroimage*, 85, 264-271 (2014). [doi: 10.1016/j.neuroimage.2013.10.009].

Vanzetta, I., and Grinvald, A. "Evidence and lack of evidence for the initial dip in the anesthetized rat: implications for human functional brain imaging" 13(6), 959-967 (2001). [doi: 10.1006/nimg.2001.0843].

Villringer, A., Planck, J., Hock, C., Schleinkofer, L., and Dirnagl, U. "Near infrared spectroscopy (NIRS): a new tool to study hemodynamic changes during activation of brain function in human adults". *Neurosci. Lett.* 154(1-2), 101-104 (1993). [doi: 10.1016/0304-3940(93)90181-J].

Villringer, A., and Chance, B. "Non-invasive optical spectroscopy and imaging of human brain function". *Trends Neurosci.* 20(10), 435-442 (1997). [doi: 10.1016/S0166-2236(97)01132-6].

von Lühmann, A., Boukouvalas, Z., Müller, K.R. and Adali, T., "A new blind source separation framework for signal analysis and artifact rejection in functional Near-Infrared Spectroscopy". *Neuroimage*, 200, pp.7 (2019). [doi: 10.1016/j.neuroimage.2019.06.021].

von Lühmann, A., Li, X., Müller, K. R., Boas, D. A., and Yücel, M. A. "Improved physiological noise regression in fNIRS: A multimodal extension of the General Linear Model using temporally embedded Canonical Correlation Analysis". *NeuroImage*, 208, 116472 (2020). [doi: 10.1016/j.neuroimage.2019.116472].

Wallopis, F., Mahmoudzadeh, M., Patil, A., and Grebe, R. "Usefulness of simultaneous EEG-NIRS recording in language studies". *Brain Lang.* 121(2), 110-123 (2012). [doi: 10.1016/j.bandl.2011.03.010].

Wang, J., Dong, Q., and Niu, H. "The minimum resting-state fNIRS imaging duration for accurate and stable mapping of brain connectivity network in children". *Sci. Rep.* 7(1), 1-10 (2017). [doi: 10.1038/s41598-017-06340-7].

Ward, T. E. "Hybrid optical-electrical brain computer interfaces, practices and possibilities". In: Allison B., Dunne S., Leeb R., Del R. Millán J., Nijholt A. (eds) *Towards Practical Brain-Computer Interfaces. Biological and Medical Physics, Biomedical Engineering*. Springer, Berlin, Heidelberg 17-40 (2012). [doi: /10.1007/978-3-642-29746-5_2].

Watanabe, H., Homae, F., Nakano, T., and Taga, G. "Functional activation in diverse regions of the developing brain of human infants". *Neuroimage*, 43(2), 346-357 (2008). [doi: 10.1016/j.neuroimage.2008.07.014].

Watanabe, H., Homae, F., and Taga, G. "General to specific development of functional activation in the cerebral cortices of 2-to 3-month-old infants". *Neuroimage*, 50(4), 1536-1544 (2010). [doi: 10.1016/j.neuroimage.2010.01.068].

Watanabe, T., Kan, S., Koike, T., Misaki, M., Konishi, S., Miyauchi, S., Miyahsita, Y., Masuda, N. "Network-dependent modulation of brain activity during sleep". *Neuroimage* 98, 1-10 (2014). [doi: 10.1016/j.neuroimage.2014.04.079].

Watanabe, H., Shitara, Y., Aoki, Y., Inoue, T., Tsuchida, S., Takahashi, N. and Taga, G. "Hemoglobin phase of oxygenation and deoxygenation in early brain development measured using fNIRS". *P. Natl. Acad. Sci. USA*, 114(9), E1737-E1744 (2017). [doi: 10.1073/pnas.1616866114].

- Weikum, W. M., Vouloumanos, A., Navarra, J., Soto-Faraco, S., Sebastián-Gallés, N., and Werker, J. F. "Visual language discrimination in infancy". *Science* 316(5828), 1159-1159 (2007). [doi: 10.1126/science.1137686].
- Werker, J. F., and Tees, R. C. "Cross-language speech perception: Evidence for perceptual reorganization during the first year of life". *Inf. Behav. Dev.* 7(1), 49-63 (1984). [doi: 10.1016/S0163-6383(84)80022-3].
- Werker, J. "Perceptual foundations of bilingual acquisition in infancy". *Ann. NY Acad. Sci.* 1251(1), 50-61 (2012). [doi: 10.1111/j.1749-6632.2012.06484.x].
- Werker, J. F., and Hensch, T. K. "Critical periods in speech perception: new directions". *Annu. Rev. Psychol.* 66, 173-196 (2015). [doi: 10.1146/annurev-psych-010814-015104].
- Werker, J. F. "Perceptual beginnings to language acquisition". *Appl. Psycholinguist.* 39(4), 703-728 (2018). [doi: 10.1017/S0142716418000152].
- White, B. R., Snyder, A. Z., Cohen, A. L., Petersen, S. E., Raichle, M. E., Schlaggar, B. L., and Culver, J. P. "Resting-state functional connectivity in the human brain revealed with diffuse optical tomography". *Neuroimage* 47(1), 148-156 (2009). [doi: 10.1016/j.neuroimage.2009.03.058].
- White, B. R., and Culver, J. P. "Quantitative evaluation of high-density diffuse optical tomography: in vivo resolution and mapping performance". *J. Biomed. Opt.* 15(2), 026006 (2010). [doi: 10.1117/1.3368999].
- White, B. R., Liao, S. M., Ferradal, S. L., Inder, T. E. and Culver, J. P. "Bedside optical imaging of occipital resting-state functional connectivity in neonates". *Neuroimage* 59(3), 2529-2538 (2012). [doi: 10.1016/j.neuroimage.2011.08.094].
- Wilcox, T., Bortfeld, H., Woods, R., Wruck, E., Armstrong, J., and Boas, D.A., "Haemodynamic changes in the infant cortex during the processing of featural and spatiotemporal information". *Neuropsychology* 47, 657-662 (2009). [doi: 10.1016/j.neuropsychologia.2008.11.014]
- Wilcox, T., Haslup, J. A., and Boas, D. A. "Dissociation of processing of featural and spatiotemporal information in the infant cortex". *Neuroimage*, 53(4), 1256-1263 (2010). [doi: 10.1016/j.neuroimage.2010.06.064].
- Wilcox, T., Stubbs, J., Hirshkowitz, A., and Boas, D. A. "Functional activation of the infant cortex during object processing". *Neuroimage*, 62(3), 1833-1840 (2012). [doi: 10.1016/j.neuroimage.2012.05.039].
- Wilcox, T., Hawkins, L. B., Hirshkowitz, A., and Boas, D. A. "Cortical activation to object shape and speed of motion during the first year". *Neuroimage*, 99, 129-141 (2014). [doi: 10.1016/j.neuroimage.2014.04.082].
- Wolf, M., Wolf, U., Toronov, V., Michalos, A., Paunescu, L. A., Choi, J. H. and Gratton, E. "Different time evolution of oxyhemoglobin and deoxyhemoglobin concentration changes in the visual and motor cortices during functional stimulation: a near-infrared spectroscopy study". *Neuroimage* 16(3 Pt 1), 704-12 (2002). [doi: 10.1006/nimg.2002.1128].
- Wolf, M., Wolf, U., Choi, J. H., Gupta, R., Safanova, L. P., Paunescu, L. A., Michalos, A., and Gratton, E. "Functional frequency-domain near-infrared spectroscopy detects fast neuronal signal in the motor cortex". *Neuroimage*, 17(4), 1868-1875 (2002). [doi: 10.1006/nimg.2002.1261].
- Woolrich, M. W., Ripley, B. D., Brady, M. and Smith, S. M. "Temporal autocorrelation in univariate linear modeling of fMRI data". *Neuroimage* 14(6), 1370-1386 (2001). [doi: 10.1006/nimg.2001.0931].
- Yang, J., Kanazawa, S., Yamaguchi, M. K., and Kuriki, I. Cortical response to categorical color perception in infants investigated by near-infrared spectroscopy. *P. Natl. Acad. Sci.* 113(9), 2370-2375 (2016). [doi: 10.1073/pnas.1512044113].
- Ye, J. C., Tak, S., Jang, K. E., Jung, J., and Jang, J. "NIRS-SPM: statistical parametric mapping for near-infrared spectroscopy". *Neuroimage*, 44(2), 428-447 (2009). [doi: 10.1016/j.neuroimage.2008.08.036].
- Yücel, M. A., Selb, J., Cooper, R. J., and Boas, D. A. "Targeted principle component analysis: a new motion artifact correction approach for near-infrared spectroscopy". *J. Innov. Opt. Health Sci.* 7(02), 1350066 (2014). [doi: 10.1142/S1793545813500661].
- Yücel, M. A., Selb, J., Aasted, C. M., Lin, P. Y., Borsook, D., Becerra, L., and Boas, D. A. "Mayer waves reduce the accuracy of estimated hemodynamic response functions in functional near-infrared spectroscopy". *Biomed. Opt. Exp.* 7(8), 3078-3088 (2016). [doi: 10.1364/BOE.7.003078].
- Zalesky, A., Fornito, A., Bullmore, E. T. "Network-based statistic: identifying differences in brain networks". *Neuroimage*, 53(4), 1197-1207 (2010). [doi: 10.1016/j.neuroimage.2010.06.041].

- Zalesky, A., Cocchi, L., Fornito, A., Murray, M. M., and Bullmore, E. D. "Connectivity differences in brain networks". *Neuroimage*, 60(2), 1055-1062 (2012). [doi: 10.1016/j.neuroimage.2012.01.068].
- Zaramella, P., Freato, F., Amigoni, A., Salvadori, S., Marangoni, P., Supphei, A., Schiavo, B. and Chiandetti, L. "Brain auditory activation measured by near-infrared spectroscopy (NIRS) in neonates". *Ped. Res.* 49(2), 213-219 (2001). [doi: 10.1203/00006450-200102000-00014].
- Zhang, H., Zhang, Y.J., Lu, C. M., Ma, S. Y., Zang, Y. F., and Zhu, C. Z. "Functional connectivity as revealed by independent component analysis of resting-state fNIRS measurements". *Neuroimage* 51(3), 1150-1161 (2010). [doi: 10.1016/j.neuroimage.2010.02.080].
- Zhang, H., Duan, L., Zhang, Y.J., Lu, C. M., Liu, H., and Zhu, C. Z. "Test-retest assessment of independent component analysis-derived resting-state functional connectivity based on functional near-infrared spectroscopy". *Neuroimage* 55(2), 607-615 (2011). [doi: 10.1016/j.neuroimage.2010.12.007].
- Zhang, H., Shen, D., and Lin, W. "Resting-state functional MRI studies on infant brains: A decade of gap-filling efforts". *Neuroimage*, 185, 664-684 (2019). [doi: 10.1016/j.neuroimage.2018.07.004].
- Zhang, Y.J., Lu, C. M., Biswal, B. B., Zang, Y. F., Peng, D., and Zhu, C. Z. "Detecting resting-state functional connectivity in the language system using functional near-infrared spectroscopy". *J. Biomed. Opt.* 15(4), 047003 (2010). [doi: 10.1117/1.3462973].
- Zhao, H., and Cooper, R. J. "Review of recent progress toward a fiberless, whole-scalp diffuse optical tomography system". *Neurophotonics*, 5(1), 011012 (2017). [doi: 10.1117/1.NPh.5.1.011012].
- Zou, Q., Wu, C. W., Stein, E. A., Zang, Y. and Yang, Y. "Static and dynamic characteristics of cerebral blood flow during the resting state". *Neuroimage* 48(3), 515-24 (2009). [doi: 10.1016/j.neuroimage.2009.07.006].
- Zimeo-Morais, G. A., Scholkmann, F., Balardin, J. B., Furucho, R. A., de Paula, R. C. V., Biazoli, J. R. and Sato, J. R. "Non-neuronal evoked and spontaneous hemodynamic changes in the anterior temporal region of the human head may lead to misinterpretations of functional near-infrared spectroscopy signals". *Neurophotonics* 5(1), 1 (2017). [doi: 10.1117/1.NPh.5.1.011002].

